Processing Lignocellulosic Feedstock Using Ionic Liquids for Biorefinery Application

Ferrari, F.A.

DOI
10.4233/uuid:6acd402e-4436-440d-a5bf-fbd68c2bfdde

Publication date
2021

Document Version
Final published version

Citation (APA)
Ferrari, F. A. (2021). *Processing Lignocellulosic Feedstock Using Ionic Liquids for Biorefinery Application*. [Dissertation (TU Delft), Delft University of Technology]. https://doi.org/10.4233/uuid:6acd402e-4436-440d-a5bf-fbd68c2bfdde

Processing Lignocellulosic Feedstock Using Ionic Liquids for Biorefinery Application

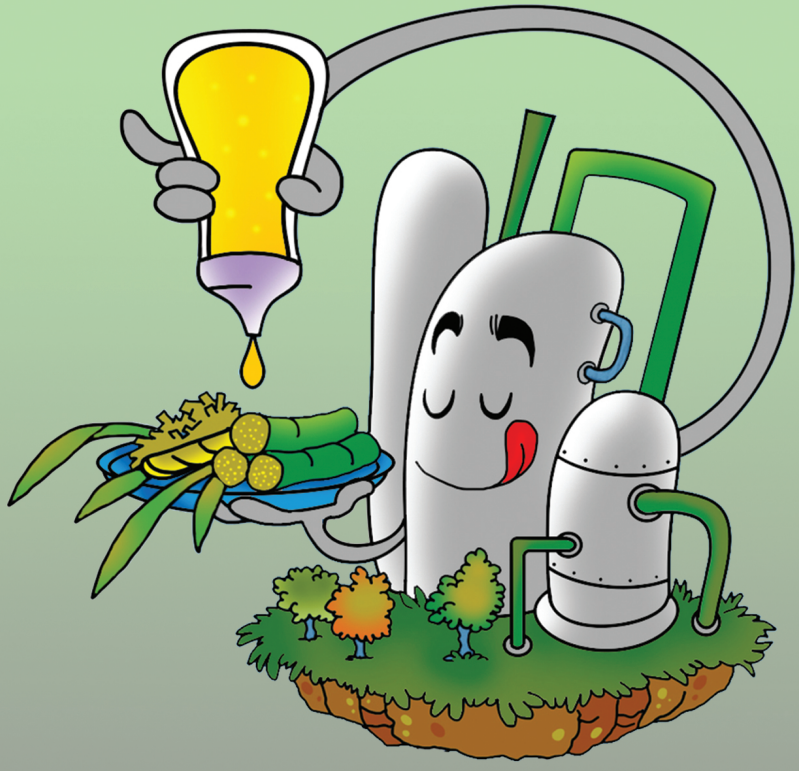

Felipe Augusto Ferrari

Processing Lignocellulosic Feedstock Using Ionic Liquids for Biorefinery Application

Dissertation

for the purpose of obtaining the degree of doctor
at Delft University of Technology
by the authority of the Rector Magnificus, prof.dr.ir. T.H.J.J. van der Hagen
chair of the Board for Doctorates
to be defended publicly on
Thursday 22 April 2021 at 12:30 o'clock

by

Felipe Augusto FERRARI

Master of Science in Chemical Engineering, University of Campinas, Brazil
Born in Campinas, Brazil

This dissertation has been approved by the promotors.

Composition of the doctoral committee:

Rector Magnificus,	chairperson
Prof.dr.ir. L.A.M. van der Wielen	Delft University of Technology, promotor
Prof.dr. M.B.S. Forte	University of Campinas, Brazil, promotor
Prof.dr. G.J. Witkamp	King Abdullah University of Science and Technology, Saudi Arabia, promotor

Independent members:

Prof.dr. P. Osseweijer	Delft University of Technology
Prof.dr. J.P. Hallett	Imperial College London, UK
Prof.dr. S.I. Mussatto	Technical University of Denmark, Denmark
Prof.dr. A.P. Mariano	University of Campinas, Brazil
Prof.dr.ir. M.C.M. van Loosdrecht	Delft University of Technology, reserve

The doctoral research has been carried out in the context of an agreement on joint doctoral supervision between University of Campinas, Brazil and Delft University of Technology, The Netherlands. The project was financed by the Be-Basic Foundation, The Netherlands, and CNPq, CAPES and FAPESP, Brazil.

This is a PhD thesis in the dual degree program as agreed between UNICAMP and TUDelft.

Esta é uma tese de doutorado de co-tutela conforme acordado entre UNICAMP e TUDelft.

ISBN: 978-94-6366-412-7

Cover: Cartoon – Feed the Biorefinery (A. Vasconcelos, 2020)

"The proper penalty of ignorance, which is of course that those who don't know should learn from those who do, which is the course I propose."

Plato – The Republic

Errata for Ph.D. dissertation

"Processing Lignocellulosic Feedstock Using Ionic Liquids for Biorefinery Application"

by Felipe Augusto Ferrari

- Incorrect language used on page ii:

The complete and correct institutions name are:

- São Paulo Research Foundation (FAPESP)

- National Council for Scientific and Technological Development (CNPq)

- Coordination for the Improvement of Higher Education Personnel (CAPES)

- Missing information on page ii:

Where it reads "The project was financed by the Be-Basic Foundation, The Netherlands, and CNPq, CAPES and FAPESP, Brazil" should read "The project was financed by São Paulo Research Foundation (FAPESP, São Paulo, Brazil; grant numbers 2015/50612-8, 2017/24520-4, 2019/19976-4, 2018/20173-0 and 2019/10439-6), National Council for Scientific and Technological Development (CNPq - Brazil), Coordination for the Improvement of Higher Education Personnel (CAPES – Brazil) and by the BE-BASIC Foundation, the Netherlands."

Table of Contents

Summary

The use of Lignocellulosic residues (LC) such as conventional food crop remains, for Bioenergy and Biorefinery applications is an attractive way to increase feedstock availability without the investment in additional land area. Moreover, it is noteworthy that biomolecules produced from LC, namely second generation (2G), has a potentially better greenhouse gases (GHG) emissions balance. One of the most economically successful lignocellulosic sources is the sugarcane crop, with a global production of about 1.7 gigatonnes in 2019. Although LC is rich in carbohydrates, 40 – 90 wt%, these sugars are not readily converted due to their molecular structure. Consequently, it must be treated, so that LC's molecular nature is changed into a more convenient arrangement favoring subsequent conversions. Such process is called pretreatment (PT) and is considered the most important step to obtain an efficient conversion of LC's constituents. Recently, ionic liquids (ILs) have emerged as an alternative technology for biomass pretreatment. ILs can break the H bonds which stabilize LC's molecular structure, improving components solubility and/or turning LC's structure more susceptible to further conversions, such as improving the enzymatic digestibility of pretreated solids.

The objective of this work was to use ionic liquids (ILs) for the pretreatment of a lignocellulosic (LC) residue in a Biorefinery concept. Sugarcane straw (SW), instead of bagasse, was chosen as model LC feedstock, and ethanol used as ultimate bio-based product to elaborate on experiments in order to answer the research question: "Are protic ionic liquids viable alternatives for biomass pretreatment in large scale Biorefineries, and which are the key parameters involved?" .

Two ILs were considered throughout this work, namely 2-hydroxyethylammonium acetate ([Mea][Ac]) and 2-hydroxyethylammonium hexanoate ([Mea][Hex]). The selection of ILs was based on literature review and experimental screening with respect to their efficiency to improve the enzymatic saccharification and decrease lignin concentration in pretreated solids. The temperature, water content, solid loading, agitation speed, ultrasonication, use of pure and ILs mixtures were considered during the PT setup, in order to assess their relevance on PT efficiency as a matter of scale-up.

The efficient recycle of ILs' streams is vital to sustain process's sustainability. In this work, two methods were explored for IL recovery, namely freeze concentration (FC) and aqueous biphasic system (ABS). The freezing point of several ILs solutions were assessed and, through thermodynamic correlations, used to calculate the water activity from each system. The ice wash ratio was

evaluated, and its influence in the mass balance stablished. The mass and energy balances were calculated considering the FC operating in a continuous regime.

Process setup and operating conditions have a direct impact on energy consumption, downstream efficiency, product price and environmental impact. The techno-economic and environmental analysis of the process was performed on a full scale Biorefinery perspective assuming ethanol as target product. The capital and operational expenditure, CAPEX and OPEX, respectively, and the environmental impact were assessed considering 8 different scenarios. Taken together, the sustainable metrics of the process were achieved, whereas recommendations to improve process' sustainability were given.

Structure

After a general introduction to the context, this work moves forward with 3 chapters presented in a scientific paper format. Each chapter will provide a relevant introduction, methodology, results and discussion and conclusions to the topic. The references are provided at the end of each chapter with the supplementary information. This first part addresses the matters related to the process design.

The final part of this work consists of two appendices which explore the physicochemical properties of the neat ILs and their mixtures in water. The combination of the Appendices is intended as a 4th publication from this thesis.

Results

In **Chapter 2** at lab scale flasks, a good enzymatic digestibility efficiency was obtained using a 1:1 (w/w) mixture of [Mea][Ac]/[Mea][Hex] at 13 % (w/w) solids loading and water content in the reaction medium. Under mild temperature conditions (90 °C), the [Mea][Ac]/[Mea][Hex] mixture increased delignification compared with pure ILs, 3-fold more. Although 1-ethyl-3-methylimidazolium acetate achieved the best enzymatic digestibility at initial conditions (dry biomass), it had the worst performance following water addition and solid loading increase. Two crucial parameters for scaling up. The effects of variables on residual solids enzymatic digestibility and delignification were assessed and the process scaled up from a 50 mL static flask to a 1 L impelled reactor. The most significant variables were found to be temperature, solid loading and water content. Enzymatic hydrolysis of residual solids after bench-scale pretreatment of SW for 3 h at 15% (w/w) solids loading and 20% (w/w) water content in the liquid phase resulted in 98% cellulose digestibility under non-optimized conditions.

Although interesting for their flexibility, ILs can have a carbon-intensive production background, may be toxic and expensive. Thereby, in **Chapter 3** the recycle of [Mea][Ac] [Mea][Hex] were explored. The aqueous biphasic system, using phosphate-based salts as phase separation promoters, was not efficient for the recycling of the tested ILs. On the other hand, the ILs were efficiently recycled whether pure or mixed, without mass loss by the freezing concentration process. The freezing point of the aqueous solutions were determined in the concentration range of 0.5% to 50 % (w/w) for both ILs. Water activities were satisfactory calculated from the water freezing point depression trough the Hildebrand and Scott's equation. [Mea][Hex] solutions showed a similar freezing curve as that found for an organic acid. The FC can be operated in continuous mode without waste generation and removing water as pure as desired.

The setup of the pretreatment step has a direct influence on the properties of the resulting solids, which in turn affects the yields of subsequent conversion steps, impacting the overall productivity. Apart from the residual solid quality, the pretreatment design will also affect the mass and energy balance within the hole Biorefinery, which were assessed in **Chapter 4**. Results showed that the solid loading and IL dilution have a direct effect for the reduction of steam consumption. Temperature also had a direct influence in the steam consumption, but with significant impact in the saccharification yield, consequently, in the overall ethanol productivity. Apart from product selling price, IL recycle is the dominant factor on economic and environmental impacts. Most of the process's parameters analyzed in this work had a significant impact on ethanol's environmental impact profile. The IL-based pretreatment feasibility was shown to be dependent on conditions that minimize the IL make-up.

During the process design study, the information regarding the physicochemical properties of the IL-based solutions reveled to be equally important and scarce. In the **Appendices** a systematic study of the physicochemical properties characterization of [Mea][Ac] and [Mea][Hex], and their mixture in water, was carried in the entire range of dilution between 278 K and 393 K. Density data was fitted to a polynomial for density predictions as function of temperature and IL concentration with the average deviation percentage (ADP) not exceeding 0.63%. The viscosities of the binary systems (IL+water) were studied considering 6 different models, and deviations between predicted and experimental data provided. The conductivity, water activity and surface tension data were summarized and the influence of both anions, i.e $[Ac]^-$ and $[Hex]^-$, evaluated. The mixture of ILs showed to be an interesting strategy to fine-tune system's properties.

In the outlook, the opinion of the author about the Bioenergy position on the path for a sustainable development is shared in short lines. Moreover, the

directions for broader use of ILs in improved biomass valorization and IL recycle are highlighted.

In a short conclusion, there is a bright future for ILs in Biorefinery application, with still many options for improved use.

Resumo

O emprego de resíduos lignocelulósicos (LC) como, por exemplo, os restos provenientes de culturas alimentícias, para fins energéticos e em Biorefinarias é uma alternativa interessante para obtenção de matéria-prima sem a necessidade de expansão da área agrícola cultivada. A produção de biomoléculas a partir de LC, ditas segunda geração (2G), são potencialmente favoráveis ao balanço de emissões de gases de efeito estufa (GHG). A cana-de-açúcar é uma das culturas mais bem estabelecidas fontes para obtenção de LC, com a produção mundial em 2019 a cerca de 1,7 giga toneladas. Em virtude de sua organização molecular, os açúcares contidos na LC, 40-90 % em massa, são resistentes às transformações bioquímicas. Desta forma, esses materiais são tratados, alterando sua estrutura rígida de modo conveniente às futuras etapas de conversão. Recentemente, os líquidos iônicos (ILs) surgiram como uma alternativa promissora para o pré-tratamento de biomassas. Os ILs atuam predominantemente quebrando as ligações de H que estabilizam a matriz lignocelulósica e/ou solubilizando seus componentes, o que torna o material mais susceptível à etapas de transformação como, por exemplo, a conversão enzimática.

O objetivo deste trabalho é utilizar ILs no pré-tratamento (PT) de LC no conceito e Biorefinaria. A palha de cana-de-açúcar (SW) foi escolhida como resíduo lignocelulósico modelo e o etanol como bio-produto para a concepção dos estudos a fim de responder a pergunta: "São os Líquidos iônicos uma alternativa viável para o pré-tratamento de biomassa em escala industrial, e quais são os parâmetros chave envolvidos?"

A escolha dos ILs e das condições de pré-tratamento são pontos fundamentais para a viabilidade do projeto em grande escala. Dois ILs em particular foram estudados ao longo dos capítulos, acetato de monoetanolamina ([Mea][Ac]) e hexanoato de monoetanolamina ([Mea][Hex]). Estes foram selecionados a partir da revisão de literatura e posterior screening experimental levanndo em consideração a eficiência da hidrólise enzimática e o teor de lignina nos sólidos pré-tratados. A temperatura, teor de água, proporção de sólidos, agitação, ultrassom e o uso de misturas de ILs foram estudados durante a etapa de pré-tratamento, a fim de identificar e entender a efetividade de cada variável para o desenvolvimento e aumento de escala dessa etapa.

O reciclo eficiente dos ILs é vital par a sustentabilidade do processo. Neste trabalho dois métodos de baixo consumo energético foram estudados, separação aquosa bifásica (ABS) e concentração por congelamento (FC). Os pontos de congelamento para diferentes composições de ILs em solução foram estabelecidos e, através de correlações termodinâmicas, utilizados no cálculo das atividades de água passa cada sistema. A "razão de lavagem", utilizada durante a recuperação,

foi avaliada quanto ao seu impacto nas perdas dos ILs e no balanço de massa. Os balanços de massa e energia foram calculados considerando o sistema de FC operando em modo contínuo.

As características operacionais do pré-tratamento e reciclo dos ILs, tem um impacto direto no consumo energético, eficiência nas etapas de downstream, custo do produto e impacto ambiental. A análise tecno-econômica e ambiental do processo foi realizada no âmbito de uma Biorefinaria completa, considerando o etanol como o bio-produto alvo. Os custos de capital empregado e operacional, CAPEX e OPEX, respectivamente, bem como os impactos ambientais foram avaliados para 8 cenários diferentes. As métricas e recomendações para otimização do processo foram estabelecidas e exploradas através da avaliação conjunta dos resultados.

Estrutura

Após um primeiro capítulo introdutório, este trabalho segue por 3 capítulos apresentados no formato de artigo científico. Cada capítulo proverá uma introdução, metodologia, resultados e discussão e as conclusões pertinentes ao tópico. As devidas referências serão fornecidas ao final, seguidas de material complementar quando cabível. Esta primeira parte diz respeito à concepção do processo.

A parte final deste trabalho consiste em um capítulo onde a perspectiva do autor sobre o tema é apresentada, seguido de dois apêndices, os quais exploram as propriedades e físico-químicas e caraterísticas moleculares dos ILs estudados neste trabalho quando puros e/ou misturados em água. A combinação desses apêndices pretende ser a 4ª publicação direta desta tese.

Resultados

No **capítulo 2**, foi observada que a mistura de [Mea][Ac]/[Mea][Hex], 1:1 em massa, teve uma resposta positiva, mantendo a eficiência na etapa de hidrólise enzimática mesmo com o amento do teor de água e proporção de sólidos durante o pré-tratamento. Em baixa temperature (90 °C), a mesma mistura apresentou melhor eficiência de deslignificação, 3 vezes mais, quando comparada aos ILs puros. Embora o acetato de 1-ethil-3-methilimidazolio tenha apresentado o melhor resultado para digestibilidade enzimática nas condições iniciais, este apresentou a pior performance quando acrescido de água e com o aumento da proporção de sólidos, parâmetros essenciais para o aumento de escala. O efeito conjunto das variáveis foi estudado e o processo de pré-tratamento escalonado à reator agitado de escala bancada, onde a temperatura, proporção de sólidos e teor de água foram as variáveis mais relevantes. Foi alcançada uma digestibilidade enzimática de 98

% para a celulose após 3 h de pré-tratamento com 15 % (massa) de sólidos e 20 % (massa) de água.

Embora interessantes por um lado, os ILs podem apresentar rotas produtivas carbono intensivas, e são um ponto de atenção ambiental e de custo para o processo. Desta forma, o reciclo dos ILs foi estudado no **capítulo 3**. A recuperação dos ILs não foi possível através do sistema aquoso bifásico. Entretanto, os ILs foram recuperados de forma eficiente através do processo FC, sendo determinado os pontos de congelamento no intervalo da concentração de IL 0,5 % - 50 % (massa). As atividades de água foram calculadas por meio da queda no ponto de fusão da água através da equação de Hildebrand e Scott. [Mea][Hex] apresentou um comportamento em solução próximo àquele observado para soluções de ácidos orgânicos. O processo de FC pode ser operado de forma contínua, sem a geração de resíduos e recuperando água com a pureza necessária.

As configurações usadas no pré-tratamento têm impacto direto nas características dos sólidos resultantes, o que por sua vez afeta as etapas de conversão seguintes e, consequentemente, a produtividade geral. Não obstante, o projeto do pré-tratamento também terá influência em todo balanço de massa e energia da Biorefinaria. Os quais foram estudados no **capítulo 4**. Foi observado que a proporção de sólidos e diluição do IL têm efeito direto no consumo de vapor da planta e, de forma substancial, nas eficiências de sacarificação, consequentemente, na produtividade em etanol. Ademais ao preço de venda do produto, o reciclo do IL é o fator dominante para o impacto econômico e ambiental do projeto. A maior parte dos parâmetros avaliados neste trabalho tiveram impacto relevante nos impactos ambientais na produção do etanol. A viabilidade do pré-tratamento baseado em IL mostrou-se dependente de condições que maximizem o reciclo desse.

Durante os estudos de desenvolvimento do processo, as informações a respeito das propriedades físico-químicas das soluções e misturas de ILs mostrara-se igualmente importantes e escassas. Um estudo sistemático das características de [Mea][Ac] e [Mea][Hex], bem como suas misturas em água, foi realizado por todo intervalo de diluição entre 278 K e 393 K, e apresentado nos **apêndices.** A predição da densidade das misturas de ILs em função de sua composição e temperatura foi realizada através de ajuste de um polinômio, obtendo um desvio médio percentual (ADP) máximo de 0,63 %. As viscosidades das misturas binárias (IL+H2O) foram avaliadas segundo 6 modelos diferentes, e os resultados apresentados. A condutividade, atividade de agua e tensão superficial são apresentadas avaliando a influência dos íons envolvidos. Os resultados mostraram que o ajusto das propriedades também pode ser realizado através da mistura entre diferentes ILs.

No **outlook**, o autor divide sua perspectiva em breves linhas obre a relevância da Bioenergia para um desenvolvimento sustentável. Ademais, as direções para um uso amplo dos ILs na valorização de biomassa são levantadas.

Em uma breve conclusão, existe um futuro promissor para o emprego dos ILs em Biorefinarias, mas ainda com muitas opções para sua melhoria.

Samenvatting

Translation: Danny de Graaff

Het gebruik van restproducten vanuit voedselgewassen is een aantrekkelijke optie voor toepassingen in bioenergie en bioraffinage. Lignocellulose residuen (LC) verbeteren de beschikbaarheid van grondstoffen, zonder dat extra landoppervlakte benodigd is. Hiernaast hebben de producten uit LC (tweede generatie biomoleculen) een betere balans aan broeikasgassen. Een van de meest succesvolle bronnen van lignocellulose is suikerriet, met een wereldwijde productie van nabij 1.7 gigaton in 2019. Hoewel LC rijk is in koolhydraten met 40-90wt%, zijn deze suikerpolymeren niet direct biologisch omzetbaar door hun moleculaire structuur. Deze koolhydraten moeten behandeld worden zodat deze omgezet worden in een meer geschikte structuur voor daaropvolgende omzettingen. Dit proces heet voorbehandeling (of pretreatement PT) en wordt gezien als de meest belangrijke stap om lignocellulose efficiënt te kunnen verwerken.

Recentelijk zijn ionische vloeistoffen (IL's) ontwikkeld als een alternatieve technologie voor dergelijke voorbehandeling. IL's kunnen de waterstofbruggen verbreken die de structuur van LC stabiliseren. Hiermee kan de oplosbaarheid van individuele onderdelen vergroot worden en/of wordt de LC-structuur meer toegankelijk voor omzettingen zoals enzymatische conversie van voorbehandelde vaste stoffen.

Het doel van dit onderzoek is om ionische vloeistoffen te gebruiken voor de voorbehandeling van lignocellulose residuen in een bioraffinage concept. Suikerrietstro (SW) is gekozen als het LC-grondstofmodel en ethanol als het eindproduct om de experimenten te ontwerpen en de onderzoeksvraag te beantwoorden: "Zijn protische ionische vloeistoffen levensvatbare alternatieven voor biomassa-voorbehandeling in grootschalige bioraffinage, en wat zijn de belangrijkste parameters?".

Twee IL's zijn gebruikt in dit werk, namelijk 2-hydroxyethylammonium acetaat ([Mea][Ac]) en 2-hydroxyethylammonium hexanoaat ([Mea][Hex]). De selectie van IL's was gebaseerd op literatuuronderzoek en experimentele screening van hun efficiëntie in enzymatische saccharificatie en van de afname van lignineconcentratie. Tijdens dit proces zijn meerdere parameters van belang geweest van de PT-opzet, namelijk temperatuur, watergehalte, stofgehalte, roersnelheid, ultrasonicatie en het gebruik van pure IL's dan wel mengsels.

Het efficiënt hergebruiken van IL-stromen is essentieel voor het duurzaam gebruik van het proces. In dit onderzoek zijn twee methodes gebruikt voor IL-terugwinning, namelijk vriesconcentratie (FC) en waterige tweefase systemen

(ABS). Het vriespunt van enkele IL-oplossingen is gebruikt om de wateractiviteit in elk systeem te bepalen met thermodynamische correlaties. De ijswasratio is geëvalueerd en haar invloed op de massabalans is bepaald. De massa- en energiebalansen zijn berekend met de FC in een continue operatie.

De opzet van het proces en operationele omstandigheden hebben een directe impact op energieconsumptie, downstream efficiëntie, prijs en milieu-impact. Techno-economische en milieukundige analyse van het proces is uitgevoerd op een volle schaal bioraffinage met ethanol als product. De kapitaaluitgaven (CAPEX), operationele uitgaven (OPEX) en de milieu-impact zijn beoordeeld in acht verschillende scenario's. De duurzaamheidseisen van het proces zijn behaald en adviezen zijn gegeven voor het verbeteren van deze duurzaamheid.

Structuur

Na een algemene introductie worden in dit proefschrift drie hoofdstukken gepresenteerd in het format van samenhangende wetenschappelijke papers. Elk hoofdstuk bevat een relevante introductie, methodologie, resultaten en discussie en een conclusie. Referenties zijn gegeven aan het einde van elk hoofdstuk in de appendices. Het eerste deel van dit proefschrift richt zich op het procesontwerp. Het tweede deel van het proefschrift bevat twee appendices waarin ingegaan wordt op de fysisch-chemische eigenschappen van de IL's in water. De combinatie van de bijlagen is bedoeld als een 4de publicatie uit dit proefschrift.

Resultaten

In **hoofdstuk 2** wordt een goede enzymatische omzetting behaald in maatkolven met een 1:1 (w/w) mengsel van [Mea][Ac]/[Mea][Hex] bij 13% (w/w) vaste stof en watergehalte in het reactiemedium. Onder milde condities (90 °C) verbeterde, 3 keer, het [Mea][Ac]/[Mea][Hex] mengsel de delignificatie in vergelijking met pure IL's. 1-ethyl-3-methylimidazolium acetaat had de beste enzymatische omzetting bij de initiële condities (droge biomassa), maar had de slechtste omzetting na toevoeging van water en verhoging van het vaste stofgehalte, wat twee cruciale factoren zijn voor opschaling. De effecten van variabelen op de enzymatische omzetting van residuele vaste stof en op delignificatie zijn hierna bepaald. Het proces is opgeschaald van een 50 mL maatkolf naar een 1 L geroerde reactor. De meeste belangrijke parameters waren temperatuur, vaste stofgehalte en watergehalte. Enzymatische hydrolyse van residuele vaste stof na bench-scale voorbehandeling van SW gedurende 3 uur met 15% (w/w) vaste stofgehalte en 20% (w/w) watergehalte resulteerde in 98% afbraak van cellulose onder niet-geoptimaliseerde condities.

Hoewel IL's interessant zijn door hun flexibiliteit, kan hun productie koolstofintensief zijn en daarnaast toxisch en duur. Hierom is in **hoofdstuk 3** het hergebruik van [Mea][Ac] en [Mea][Hex] onderzocht. Het waterige tweefasensysteem met fosfaatzouten als promotors van faseschеiding was niet efficiënt voor het hergebruiken van deze IL's. In parallel hiermee, werd een vriesconcentratieproces ontwikkeld voor efficiënt hergebruik van de IL's zowel in pure als gemengde vorm, zonder noemenswaardig massaverlies. Het vriespunt van de waterige oplossingen was bepaald in het concentratiebereik van 0.5% tot 50% (w/w) voor beide IL's. De wateractiviteit is berekend van de vriespuntdaling door de vergelijking van Hildebrand en Scott. [Mea][Hex] oplossingen lieten een gelijkaardige vriescurve zien als organische zuren. De FC kan zo worden uitgevoerd zonder afvalproductie en met verwijdering van puur water.

De opzet van de voorbehandelingsstap heeft een directe invloed op de eigenschappen van de vaste biomassarestanten. Dit kan vervolgens de opbrengst van vervolgstappen en de algemene productiviteit beïnvloeden. Naast de kwaliteit van de residuele vaste stof, zal het ontwerp van de voorbehandeling de massa- en energiebalans beïnvloeden binnen de gehele bioraffinaderij. Dit is onderzocht in **hoofdstuk 4**. Resultaten laten zien dat de vaste stof loading en IL-verdunning een direct effect hebben voor reductie van stoomconsumptie. Temperatuur heeft ook een directe invloed hierop, maar hiernaast ook op de algemene productiviteit van ethanol vanwege de significant invloed op de sacharificatie-opbrengst. Naast de verkoopprijs van het product is het hergebruiken van IL's de meest dominante factor voor de positieve impact op economie en milieu. De meeste van de procesparameters die in dit werk zijn geanalyseerd, hebben een significante impact op de milieu-invloed van ethanol. De haalbaarheid van de IL-gebaseerde voorbehandeling is afhankelijk van condities die de IL-samenstelling.

Tijdens de procesontwerpstudie bleek dat de informatie over de fysisch-chemische eigenschappen zowel belangrijk als schaars is. In de **appendices** is een systematische studie uitgevoerd voor de fysisch-chemische eigenschappen van [Mea][Ac] en [Mea][Hex] en een reeks aan mengsels in water tussen 278 K en 293 K. Dichtheidsdata is gefit op een polynoom voor voorspellingen als functie van temperatuur en IL-concentratie met een gemiddelde deviatie percentage dat niet hoger kwam dan 0.63%. De viscositeiten van de binaire systemen (IL en water) zijn bestudeerd met zes verschillende modellen met voorspellingen van deviaties en voorziening van data. De geleidbaarheid, wateractiviteit en oppervlaktespanning zijn samengevat en de invloed van beide anionen [Ac-] en [Hex-] is geëvalueerd. Het mengsel van IL's bleek een interessante strategie om de systeemeigenschappen te verfijnen.

In de vooruitzicht (**outlook)** is de mening van de auteur uiteengezet over de positie van bio-energie op het pad van duurzame ontwikkeling. Aanwijzingen worden gegeven voor breder gebruik van IL's in verbeterde biomassavalorisatie en IL-hergebruik.

Concluderend is er een veelbelovende toekomst voor IL's in bioraffinage toepassingen, met vele mogelijkheden voor verbeterd gebruik.

Chapter 1

General Introduction

1.1 Introduction

Humankind has counted significantly on chemical bonds as a reliable source of stored energy, firstly using natural wood and, then, relying mostly on fossil-based components. During the combustion of these energy carriers, useful heat is provided which in turn can be converted into mechanical work, then, mechanical work is either used directly on pumping engines or converted into electrical energy. Within the process there is an inevitably emission of particular gases, resulted from the oxidation, i.e., CO (carbon monoxide), CO_2 (carbon dioxide), NO_2 (nitrogen dioxide), and reduction reactions, i.e., CH_4 (methane), H_2O. Naturally present in our atmosphere, these molecules are essential for ecosystem homeostasis, crucial within the Carbon and Nitrogen cycles, and for the maintenance of global temperature acting as greenhouse gases (GHGs). However, the progressive accumulation of these molecules, due to intense use of fossil sources of energy, lead to unbalanced levels of GHGs, and, consequently, to undesired increase in global average temperatures.

The outcomes of our unsustainable relation with the environment are already noticeable, as successive top highest average global temperatures on record. Beyond to what is noticed by our body in a warm day, the increase in global temperatures have a direct and far-reaching effects on the dynamics of planet's atmosphere and biosystems. With the aim of ensure the prosperity of future generations – and ours –, countries have committed themselves to reduce GHG emissions, expressed as CO_2 equivalents, to minimize the increase in global temperature. The urge for technologies capable to meet our energy needs without compromising our relationship with environment is an essential subject within the 4th Industrial Revolution towards a sustainable development[1].

Renewable energy currently accounts for 20 % of total primary energy consumption globally, or 11 % if nuclear and traditional biomass are excluded [2]. Lately, significant investment has been done in wind and solar power, first and second most invested technologies for the renewable energy expansion in 2019 (excluding hydroelectric)[3]. Wind and solar represent an interesting strategy for electrification due to their low cost of operation and absence of emissions during energy production. However, they are greatly impacted by atmospheric conditions, which compromise their capacity to provide power uninterruptedly.

Apart from the renewable production of energy, new technologies must cope with the circular economy approach. Circular economy is conceived on the notion of an industrial metabolism and industrial ecology [4]. In contrast to the regular linear economy, it diminishes the accumulative environmental impact of production. The life cycle of a given product is remodeled so that the by-products

of the productive procedure and the end-of-life product itself serve as feedstocks for the same or another process within the industrial network. The reuse and recycle by the end-of-life of the technology are crucial for a circular economy. Wind turbines and solar panels life cycle is of major importance while considering their environmental implementation. The recycling and reuse of wind turbines and solar panels at the end-of-life is challenging due to the way the equipment are produced, as their current production relies on carbon intense, fossil industries[5,6]. These aspects, if not addressed, represent a mismatch with the sustainable development.

Bioenergy was the third highest investment in renewable energy capacity in 2019 with 9.7 US$ bn[3], and is currently the major source of renewable energy. A reasonable share of the total bioenergy production comes still from traditional biomass use, which is the combustion of natural feedstock, such as wood, in households. The most interesting strategy for energy production, however, is by means of the modern bioenergy, which uses higher density energy carriers such as liquid biofuels, reducing the negative impact of emissions. Drop-in biofuels are an interesting alternative to fossil fuels, that can be used directly in the transport sector, which accounts 32 % of the global total energy consumption[2]. Ethanol is a prime example of large-scale application of renewable energy. In 2019, United States of America and Brazil, first and second major ethanol producers respectively, produced approximately 49 Mtoe (million tons of oil equivalent) of ethanol[7,8]. To put into perspective, this corresponds to the total primary energy consumption of Norway in 2019.

Ethanol is mostly produced following the sugar platform, in which carbohydrates are converted to the desired molecule by means of microorganisms. Based on this general transformation concept, sugars can be transformed into any other molecule within the range of metabolism of a given microorganism[9]. The possibility to diversify products from ethanol-alone is of vital importance to fossil independence since plastic, pharmaceuticals, solvents, fine-chemicals – and so on – could be produced from bio-based and renewable sources. Such diversification increases the biorefinery potential from biomass to products and is one milestone for a prosperous Bioeconomy.

The bioeconomy is defined by the European Commission as the economic activities covering the production of different renewable biological resources and its conversion into value-added bio-based products such as food, feed, chemicals and fuel[10]. In 2017, the bioeconomy had a turnover of € 2.4 trillion in EU, accounting for 18.5 million jobs[11]. The conventional agricultural sector still contributes the largest share, even though , it has the lower labor productivity (€ per employed person) among the sectors of the bioeconomy[12]. It is expected that

efficient implementation of biorefineries can contribute to improve labor productivity, thus increasing bioeconomy contribution to GDP[12].

The use of Lignocellulosic residues (LC) such as conventional food crop remains, is an attractive way to increase feedstock availability without the investment in additional land area. Moreover, it is compatible with the circular economy principles, as this provides an answer to concerns around water and food security. It is estimated that the LC production potential, within limits of biodiversity, water and food security, could account for almost half of the total global energy demand by 2050[13]. One of the most economically successful lignocellulosic sources is the sugarcane crop, with a global production of about 1.7 gigatonnes in 2019[14]. This crop is especially important in Brazil, where the sector accounts for 2 % of GDP, and represents 18 % of the total primary energy supply [15,16]. In 2019/ 2020, Brazil harvesters processed 640 Mt of sugarcane stalks[17]. It is estimated that 280 kg of humid bagasse and 250 kg of straw (dry weight) are generated per ton of processed sugarcane[18]. Moreover, it is noteworthy that ethanol production from sugarcane residues, namely second generation (2G), has a potentially better greenhouse gases (GHG) emissions balance than other high production crops[19], as the same time that improves bio-based products productivity within the same agricultural area.

Although LC is rich in carbohydrates, 40 – 90 wt% [20], these sugars are not readily converted due to their molecular structure, as elaborated in the **Lignocellulose Material** section above. Consequently, it must be treated, so that LC's molecular nature is changed into a more convenient arrangement favoring subsequent conversions. Such process is called pretreatment (PT) and is considered the most important step to obtain an efficient conversion of LC's constituents[21,22]. Even though improvements have been achieved over the past years, to be effective and economical the PT still need to overcome some hurdles, such as: i) high power and energy consumption; ii) recovery and recycling of auxiliary materials such as catalysts and solvents, when applicable; iii) scale-up towards lower CAPEX and OPEX per unit of product [23]. These 3 aspects were the milestones and served as guidance during the elaboration of the "Research Questions" of this work.

Different pretreatment methods exist, as discussed in the **Pretreatment** section above, and a weighted approach is useful for selecting the most economically and environmentally sustainable strategy[21,24–26]. The pros and cons of each method need to be carefully analyzed in a project design phase. Recently, ionic liquids (ILs) have emerged as an alternative technology for biomass pretreatment. ILs can break the H bonds which stabilize LC's molecular structure, improving components solubility and/or turning LC's structure more susceptible to further conversions, for instance, improving the enzymatic digestibility of pretreated

solids. ILs are salts that are often molten at temperatures below 100 °C because of the large size, asymmetry, and conformational flexibility of their constituting ions [20,27]. Cation and anion groups can be designed to confer specific properties, such as low vapor pressure, high solubility of solutes, or high (or low) miscibility with other solvents [20,26,28,29]. ILs can be involved in different kinds of molecular interactions, for instance, H bonding, Coulomb, van de Waals, solvophobic and dipole-dipole interactions. The first three are considered the main contributors to the cation-anion interaction[30]. These features are important when addressing the selective recovery of the different components present in LC materials.

Lately, much attention has been given to lignin valorization since efficient valorization of this by-product as a potential source of revenue, has a direct positive impact in the biorefinery's profitability[31]. The application of lignin might be limited by its heterogeneous molecular structure which is largely dependent on its source. The choice of the pretreatment technology will also have an effect in the final properties of resulting lignin[32]. The tunable characteristic of ILs' systems could represent an advantage during pretreatment design to obtain lignin with desirable characteristics[33].

To date, imidazolium-based ILs are the most explored cations for LC pretreatment, mostly associated with acetate (Ac), chloride (Cl) and fluor-based (-F-) anions. Ac and Cl anions are commonly used in IL-based pretreatment studies, that when associated with imidazolium cation can lead to the dissolution of all LC's major components, i.e. cellulose, hemicellulose and lignin. Acetate is particularly noteworthy for its ability to promote H-bounding between the IL and LC matrix. The recovery of dissolved molecules is achieved by the addition of an anti-solvent, usually water, but it may vary depending on the IL involved[20].

Water has several roles in IL-based systems. Apart from its uses as anti-solvent, water has been also explored as a dilution agent, decreasing system viscosity and reducing the amount of IL used. The extension to which water can be added without compromising pretreatment efficiency is dependent on types of both cation and anion. The temperature and time conditions can vary greatly among studies, ranging from 25 °C to high as 180 °C, and from minutes to hours [20,34]. Usually, higher temperatures will contribute to reduced pretreatment residence times, and increased solid loadings[35]. Higher temperatures have also undesired effects, such as, enhanced carbohydrates degradation and IL decomposition[36]. To minimize material loss due to degradation, pretreatment temperatures and (decreasing) particle size need to be optimized. A significant number of different lignocellulosic materials was studied[37] with regard to IL pretreatment, while the most explored are cellulose (avicel), lignin, pine, poplar, eucalyptus, switchgrass, rice straw, miscanthus and sugarcane bagasse. In this work, sugarcane straw (SW)

was chosen as model feedstock due to sugarcane crop potential. The choice of SW rather than bagasse was mainly due to: i) it is a residue traditionally left on the field, being a readily source of extra LC; ii) far less information is available on straw pretreatment than bagasse.

Recently, protic ILs (PILs), characterized by a proton transfer between cation and anion, have emerged as an interesting option to aprotic ILs due to their lower cost, toxicity and easier synthesis [38,39]. Among PILs, ammonium-based cations are the most studied, especially choline ([Cho]). Quaternary ammonium-based cations are interesting options when objecting the enhancement of residual solids digestibility and delignification, not much efficient on cellulose dissolution though. Ethanolamine-based ILs have being reported as an efficient class of solvents for the valorization of agricultural residues [40,41]. In addition, at bulk scale production, this class of ILs might be as cost-effective as regular organic solvents[42]. Detailed information about existing IL-based pretreatment studies can be found elsewhere[34,37]

As with every new technology, there are challenges to be overcome in IL-based PT method for LC biomass. IL-based pretreatment methods must be improved for large scale applications in terms of conversion yield, energy consumption and IL recyclability, which will be addressed in further chapters.

1.1.1 Lignocellulose Material

LC materials are basically composed of three main constituents, namely cellulose, hemicellulose and lignin [43], and the use of each component may vary based on process needs. Cellulose is the most abundant organic compound in nature. It is a linear polymer with high molecular weight, composed of glucose molecules. The glucopyranosyl monomers are linked by β1-4 glycosidic bounds, which gives a stretched chain conformation for the molecule. Hydrogen bounds link those chains in a flat position, which differs from starch. The latter has α bounds in anomeric carbon, conferring it a helicoidally shape. The linear configuration enables cellulose chains to be packed in crystalline fibrils [44]. In natural cellulose, each glucosyl is linked with 3 hydrogen bounds, 2 intramolecular, and 1 intermolecular, with the neighbor lateral cellulose molecule [45]. Natural crystalline cellulose is very stable, hampering its conversion and molecular break, thus, transforming it into amorphous cellulose is desirable. In this later format, an additional intermolecular hydrogen bound occurs between cellulose chains, reducing fibril compaction [20]. Full chain of cellulose can vary from 1000 up to 50000 glucose units depending on vegetal source [20,43].

Although hemicellulose chains are smaller than cellulose, they have higher heterogeneity in composition. Hemicellulose has xylose and arabinose as major components, and mannose, galactose and glucose in lower proportion. The main chain is branched and added of functionalities such as glucuronic, galacturonic acids, and acetyl and methyl groups [20]. Hemicellulose binds to the cellulose surface through non-covalent interaction, putting together the fibrils. The addition of hydrophobic molecules, such as methyl and acetyl, enhances the affinity with lignin, binding the three major components together [46]. Unlikely cellulose, hemicellulose chain is majority amorphous which entails higher solubility in water and susceptibility to pretreatment.

Lignin is an amorphous polymer responsible for vegetal inert property, providing hardness, hydrophobicity and resistance to enzymatic and chemical attack. It is mainly present in old tissues in cellular middle lamella. The polymer can vary in composition and complexity depending on vegetal source: softwood, hardwood, grasses. Nevertheless, is polymerized from up three monomers: coni-feryl, sinapyl and pcoumaryl alcohols. In the molecule, each subunit is identified by the radicals' positions in the aromatic rings, as shown in Figure 1[20]. Hemicellulose and Lignin are both, entangled and covalently cross-linked in a complex, which in grasses, such as sugarcane, has ferulic acid, binding components through ester bounds [20,47,48].

Fig 1: Lignin molecular subunits. Adapted from Brandt et al., 2013

1.1.2 Pretreatment (PT)

Great part of LC molecular components is buildup of carbohydrates, these cannot be directly used, though. As mentioned, cellulose, hemicellulose and lignin interaction leads to a recalcitrant structure, depicted in Figure 2, limiting its conversion [20,25]. The overall objective of pretreatment is to destabilize the LC matrix, making it more susceptible to further conversion. Efficient pretreatment

processes should target: i) full carbohydrates recovery; ii) high yields on subsequent conversion steps, for instance during saccharification through enzymatic hydrolysis; iii) do not produce undesirable compounds from sugar and lignin decomposition decreasing overall yield of feedstock into products; iv) efficiently separate carbohydrate fractions and lignin; v) low energy demand; vi) low capital and operating costs [49].

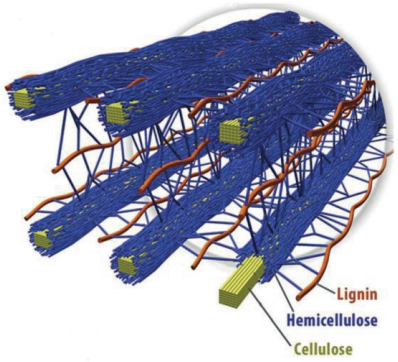

Fig 2: Lignocellulose polymer structure. U.S Department of Energy Genome Program image gallery (BRANDT et al., 2013)

Even though pulp and paper industry goes back to 19th century[50], some limitations and disadvantages still to be solved for Biorefinery applications. Moreover, some standards must be achieved within the process to make LC feasible as feedstock to biological conversion. Traditional methods are: mechanical, steam explosion, ammonia fiber explosion (AFEX), acid, organic solvent (Organosolv) and alkaline pre-treatment[24,25]. Those methods have some disadvantages, such as high thermal demand, use of toxic reagents and production of inhibitory compounds [24–26,49,51].

Mechanical pretreatment aims the reduction of particle size, increasing surface area and reducing the degree of polymerization. This effect can be achieved by chipping, grinding and milling processes, which can lead to particles ranging from 10 to 30 mm, until 0.2 to 2 mm [52]. Particles comminution or size reduction can be attained using different milling processes, such as: ball, hammer, two-roll and colloid milling [51]. The major drawback of this strategy is the high-energy

demand of the process, which could be reduced in consolidate processes where pretreatment and hydrolysis are performed simultaneously in the same reactor[53].

Steam explosion is one of the most widely used and known pretreatment. It relies on subjecting biomass to a pressurized steam stream in a range of time, varying from seconds to several minutes, and then it is suddenly depressurized. In this process, there are two mains mechanisms acting in biomass. First, the mechanical expansion of the fibrils, opening and fracturing the material. Second, the chemical hydrolysis of carbohydrates down to acid formed from released acetyl groups present in LC. Due to partial hemicellulose solubilization, lignin is partially removed, which is beneficial to enzyme activity. In addition, the partial hemicellulose solubilization exposes the cellulose fibrils, which also contribute to enhance the enzymatic digestibility of this component [54]. Steam explosion is mainly governed by particle size, temperature and resident time[55]. This method has some advantages, such as not using toxic substances and short resident time. Nevertheless, it generates inhibitory components, for example hydroxymethyl furfural, furfural and acetic acid, which have negative effect on biological conversion[25]. Moreover, the design and construction of pressure resistant equipment will lead to an increase in the capital expenditure (CAPEX).

In AFEX, biomass is pretreated with liquid ammonia under high pressure in temperatures ranging from 60 to 100 °C. The pressure is then released, provoking sudden expansion. Similarly to steam explosion, the expansion leads to mechanical disruption of LC fibrils. It is also reported that AFEX process acts on bounds between hemicellulose and lignin, and lowering cellulose crystallinity [56]. This method is not worryingly affected by inhibitors production; however has low efficiency with high lignin content feedstocks and high initial cost due to ammonia input[25]. Ammonia is also a component that demands attention due to its toxicity.

The main objective of acid strategies is to hydrolyze the carbohydrate portion of LC, and can be conducted with diluted or concentrated acid. The prior acts mainly in hemicellulose, and the latter in all carbohydrate quota. Due to acid costs and corrosion issues, the diluted strategy has been preferred. Usually, it is conducted between 120 to 180 °C, with the residence time dependent on the temperature used [24,25]. In the process, hemicellulose is extracted from LC, and can be solubilized in oligomers and monomers, depending on temperature and time conditions. This is one advantage of this process, which can convert hemicellulose into fermentable sugars without enzymatic conversion, while lignin is recovered by solid-liquid separation. Nevertheless, this strategy can generate undesirable concentration of inhibitors, negatively affecting fermentation. Acid strategy also

imply in use of more expensive steel to avoid corrosion, thus increasing CAPEX[24,25,49].

In Organosolv, biomass is treated using an aqueous solution with organic solvent, such as methanol, ethanol, glycerol, acetone and ethylene glycol. Some process also use acid to catalyze hemicellulose bound breaking, accelerating delignification and enhancing the process efficiency [24,25,49]. Acid addition is necessary in lower temperatures, under 180 °C, in higher temperatures acid is produced from LC matrix, thus acting as catalyst [57]. Temperature working range vary in between 100 °C and 250°C. Moreover, Organosolv acts mainly in three bounds level, hydrolyzing lignin internal linkages, between lignin and hemicellulose and breaking glycosidic bounds within hemicellulose [57]. Thus, resulting in high delignification and hemicellulose dissolution. On the other hand, residual solvent inhibits fermentation and enzymatic hydrolysis, so that efficient wash or removal is necessary. Additional drawback is solvent price and inflammability.

Alkaline pre-treatment acts swelling biomass, increasing internal surface of cellulose, decreasing crystallinity, thus disrupting lignin structure[51]. It enhances carbohydrates digestibility, being more effective on lignin solubilization though. The process can be conducted at room temperature or at higher temperatures, impacting on residence time. It produces less inhibitors in comparison to acid pretreatment; however it loses efficiency in materials with higher lignin content [24,25,49].

1.1.3 Ionic Liquids (IL)

Ionic liquids were initially introduced by Gabriel and Wiener (1888) [58]. Nevertheless, more detailed studies concerning its synthesis and water and air stability began in the early 90's [59]. Among IL, imidazole-based salts are widely studied. IL are molecules composed by and anion and cation, that are mainly, but not solely, linked by ionic bounds, from which came their names. Differently to NaCl, ILs have complex and usually not symmetric molecules, making difficult their arrangement in a full ordered way. Thus, conferring a lower molten point, which gave them the label of "room temperature molten salts". Additionally to ionic forces, anion and cation can also interact through hydrogen bounds [60,61] , that impacts ILs behavior in solution and is a crucial characteristic for LC solubilization, as discussed in further chapters.

Due to IL's common complex molecules, its nomenclature generally follows equation 1

$$\left[C_n\ C_m\ \left(C_o C_p\right) x\right]^+\ \left[A\right]^- \qquad \text{eq. 1}$$

where "C" refers to alkyl chain (up to four alkyl chains can by linked to cation's nucleus), and indices indicate the chain length (methyl units' number plus ending methyl). The "x" defines cation nucleus, such as "N" for ammonium salts, "im" for imidazole, "pyr" for pyridine and "pyrr" for pyrrolidine salts. "A" refers to anion.

Electric conductivity, low vapor pressure, ionic strength and thermal stability are some interesting properties regarding chemical catalysis and purification through phase equilibrium [20,62]. In addition, IL solvent property has been studied due to its capability to dissolve variously the different materials depending on ions involved. Such characteristic also imply that IL can interact with different materials according with its molecular configuration. Taken these features together, ILs are often addressed as tailored solvents.

From extraction perspective, IL are interesting to dissolve components specifically from a complex matrix. Using algae as an example to illustrate, the extraction of internal lipids demands at least three main actions: cell disruption; lipid extraction; purification[63]. The cell disruption lead to other components release which difficult the purification, such as proteins. IL have been addressed for lipid extraction from algae for disruption of cells and selectivity dissolve components. Thus, extracting not only the lipids, but also recovering proteins as a by-product[63]. IL facilitate the recovery of diverse compounds hence different anti-solvents can be applied specifically for each solute, such as ethanol for carbohydrates, water for lipids and salt for proteins [63–65].Another example of compound purification from complex matrix field is purifications of active compounds from vegetal tissue. Chowdhury and partners (2010)[66] used N,N-dimethylammonium N′-N′-dimethylcarbamate to extract hydrolysable tannin. Authors reported 85% of efficiency, which is higher than conventional methods.

We can classify ILs in two big families: protic and aprotic. The first group is characterized by the transfer of a proton from Brønsted acids to a base. The hydrogen bonding has a greater role in the interaction between cation and anion in protic than aprotic ILs, affecting the ionic bulk properties[30]. Hydrogen bound is also related to IL capability of solubilization [61,62,67,68]. In IL with non-functional cations,

hydrogen bonds basicity, related with solvent parameter Kamlet-Taft (β), has been pointed out as an important characteristic for solubilization. Kamlet-Taft model for linear solvation energy relates the capacity of both, solvent and solute donor hydrogen bound energy, acidity (α), and acceptor hydrogen bound energy, basicity (β)[69]. Considering that, LC is greatly stabilized by hydrogen bounds, protic ILs would act as efficient solvent for LC pretreatment. It was observed a direct relationship between the increase of β parameter and solubilization efficiency. Anion is the major responsible for hydrogen basicity character of an IL[29,62,67,70]. Although Kamlet-Taft solvation parameter can estimate IL efficiency on LC pre-treatment, cellulose dissolution is not only governed by such property. Indeed, cation play an important role in this sense. Taking the 1-ethyl-3-methylimidazolium cation to elaborate on this, the molecule has 4 characteristics impacting on cellulose dissolution: i) the presence of nitrogen heteroatom in 1-ethyl-3-methylimidazolium aromatic ring, which can delocalize the cation charge; ii) its ability to play a part in hydrogen bounds; iii) the cation geometry; iv) association with the acetate anion [71–74].

1.2 Scope and Thesis Outline

The objective of this work was to use ionic liquids (IL) for the pretreatment of a lignocellulosic (LC) residue in a Biorefinery concept. Sugarcane straw (SW) was chosen as model LC feedstock, and ethanol used as ultimate bio-based product to elaborate on process' parameters, such as productivity, yields and energy consumption. The present work addresses the main research question: "Are protic Ionic Liquids a viable alternative for LC pretreatment at large scale Biorefineries, and what are the key aspects for this application?". The overall structure is depicted in Figure 3.

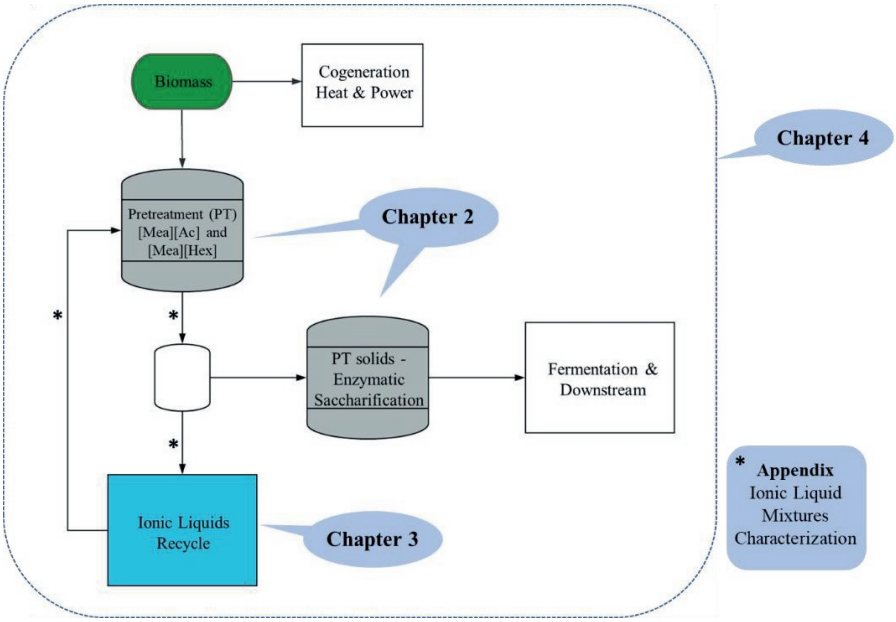

Fig 3: Schematic thesis outline.

Currently, PT is one major bottleneck for efficient LC processing in industrial scale. In short, PT must improve the conversion rates of LC' constituents, namely cellulose, hemicellulose and lignin, into target products by the subsequent steps. At the same time PT improves LC transformation, it must minimize the losses of its components due to decomposition and undesirable side-reactions, which would compromise process overall yield. The selection of the IL will have a direct effect on PT efficiency, in terms of conversion and chemical composition of residual solids. In **Chapter 2** the following question was addressed: *"What are the important characteristics of ILs for LC pretreatment? And, what are the settings conditions to be addressed during scale up?".* The selection of IL is carried out of potential ILs selected from literature and their effectiveness assessed considering criteria essential for industrial application. The PT's operational conditions will influence the performance and energy consumption of the process. Different operational conditions were selected based on literature and assessed in **Chapter 2** regarding the enzymatic digestibility and chemical composition of residual solids. Variables were explored in a bench-scale reactor set-up for scalable purposes.

After the PT, the resulting slurry is separated into solid and liquid phases. The solid stream is washed and destinated to further conversion steps, while the liquid stream is combined with the eluent from solid wash and is mostly comprised of water and IL, which must be recycled back to the process. The efficiency of IL

recycle is as important as the PT itself, as observed in **Chapter 4**. In **Chapter 3** the following question was addressed: "*Can ILs be recycled using alternative methods, for instance, by means of freeze concentration, lowering the energy consumption at the same time it reduces IL losses?".* In this chapter, IL recycle is investigated by means of freeze concentration (FC), which objective was the recovery of IL from aqueous stream without losses and residues generation. The freezing point of IL aqueous solution were determined as function of IL concentration, and the water activity calculated from the freezing point depression. The effectiveness of ice wash was studied avoiding IL losses and improving water end-use possibilities. The mass and energy balances were determined considering a starting IL-water mixture following the composition studied in **Chapter 2**.

From the results observed in **Chapters 2** and **4**, it was evident that the different ILs were influenced variously by the water content in the system and that the mixture of ILs could be an interesting strategy to improve IL solvent capacity and fine-tune system's physicochemical properties. In **Appendix** the physicochemical properties of the ILs mixtures and solutions were characterized and studied with respect to concentration and temperature influence, forwarding the following question: *"Can the mixture of ILs be used to adjust the properties of the system with regard to process necessities?"***.** The results were linked to molecular observations by means of FTIR and NMR techniques.

In **Chapter 4**, the IL-based PT was assessed with respect to a Biorefinery application. The results obtained in **Chapters 2** and **3**, were used for the design of a full process, from biomass to products, which was modeled in Aspen® in order to answer the following question: *"Will the best choice set-up for pretreatment also be the best choice for the Biorefinery design? What would be the sustainable metrics for the process?".* The mass and energy balance of 8 different scenarios were provided, and the environmental e economic evaluation given as function of PT conditions set-up. The life cycle assessment provided a valuable knowledge regarding IL's production background. From the environmental assessment, we quantify the potential of GHG emissions mitigation in comparison to a benchmark bioprocess and to that of a fossil-based alternative production.

Finally, **Chapter 5** summarizes the main outlook from this work. It is also highlighted the perspectives regarding this subject, questions raised that the author would appreciate to investigate if time was not a finite resource.

1.5 References

(1) Maynard, A. D. Navigating the Fourth Industrial Revolution. *Nat. Nanotechnol.* **2015**, *10* (12), 1005–1006. https://doi.org/10.1038/nnano.2015.286.

(2) REN21. *Renewables 2020 Global Status Report*; 2020.

(3) McCrone, Angus (BloombergNEF), Moslener Ulf (Frankfurt School), d'Estais, Francoise (UNEP), Grüning, Christine (Frankfurt School), Emmerich, M. (Frankfurt S. *Globar Trends in Renewable Energy Investment 2020*; 2020.

(4) Frosch, R. A.; Gallopoulos, N. E. Strategies for Manufacturing the Impact of Industry on the Environment. *Sci. Am.* **1989**, *261* (September), 144–153.

(5) Xu, Y.; Li, J.; Tan, Q.; Peters, A. L.; Yang, C. Global Status of Recycling Waste Solar Panels: A Review. *Waste Management*. Elsevier Ltd May 1, 2018, pp 450–458. https://doi.org/10.1016/j.wasman.2018.01.036.

(6) Jensen, J. P. Evaluating the Environmental Impacts of Recycling Wind Turbines. *Wind Energy* **2019**, *22* (2), 316–326. https://doi.org/10.1002/we.2287.

(7) ANP Brazil. Biofuels Production http://www.anp.gov.br/conteudo-do-menu-superior/31-dados-abertos/5537-producao-de-biocombustiveis (accessed Sep 7, 2020).

(8) EIA. Fuel Ethanol Overview https://www.eia.gov/totalenergy/data/browser/?tbl=T10.03 (accessed Aug 7, 2020).

(9) Enriquez, J. GENOMICS:Genomics and the World's Economy. *Science (80-.).* **1998**, *281* (5379), 925–926. https://doi.org/10.1126/science.281.5379.925.

(10) European Commission. *A Sustainable Bioeconomy for Europe: Strengthening the Connection between Economy, Society and the Environment*; 2018. https://doi.org/10.2777/478385.

(11) Porc, O.; Hark, N.; Carus, M.; Dammer, L.; Carrez, D. *European Bioeconomy in Figures 2008-2017*; Hürth, 2020.

(12) Ronzon, T.; Piotrowski, S.; Tamosiunas, S.; Dammer, L.; Carus, M.; M'barek, R. Developments of Economic Growth and Employment in Bioeconomy Sectors across the EU. *Sustain.* **2020**, *12* (11), 1–13. https://doi.org/10.3390/su12114507.

(13) EIA projects nearly 50% increase in world energy usage by 2050, led by growth in Asia - Today in Energy - U.S. Energy Information Administration (EIA) https://www.eia.gov/todayinenergy/detail.php?id=41433 (accessed Oct 29, 2020).

(14) The Statistics Portal. Sugar cane production worldwide - forecast 2016-2026 https://www.statista.com/statistics/249679/total-production-of-sugar-worldwide/ (accessed Sep 7, 2020).

(15) UNICA. Sugarcane Share in The Brazilian Energy Generation https://unica.com.br/noticias/cresce-participacao-da-cana-de-acucar-na-geracao-de-energia/ (accessed Sep 7, 2020).

(16) Popp, J.; Lakner, Z.; Harangi-Rákos, M.; Fári, M. The Effect of Bioenergy Expansion: Food, Energy, and Environment. *Renew. Sustain. Energy Rev.* **2014**, *32*, 559–578. https://doi.org/10.1016/j.rser.2014.01.056.

(17) Observatório da cana. Hisórico de produção e moagem https://observatoriodacana.com.br/historico-de-producao-e-moagem.php?idMn=32&tipoHistorico=4&acao=visualizar&idTabela=2449&safra=2019%2F2020&estado=RS%2CSC%2CPR%2CSP%2CRJ%2CMG%2CES%2CMS%2CMT%2CGO%2CDF%2CBA%2CSE%2CAL%2CPE%2CPB%2CRN%2CCE%2CPI%2CMA%2CTO%2CPA (accessed Nov 26, 2020).

(18) Chandel, A. K.; da Silva, S. S.; Carvalho, W.; Singh, O. V. Sugarcane Bagasse and Leaves:

Foreseeable Biomass of Biofuel and Bio-Products. *J. Chem. Technol. Biotechnol.* **2012**, *87* (1), 11–20. https://doi.org/10.1002/jctb.2742.

(19) Wang, M.; Han, J.; Dunn, J. B.; Cai, H.; Elgowainy, A. Well-to-Wheels Energy Use and Greenhouse Gas Emissions of Ethanol from Corn, Sugarcane and Cellulosic Biomass for US Use. *Environ. Res. Lett.* **2012**, *7* (4), 045905. https://doi.org/10.1088/1748-9326/7/4/045905.

(20) Brandt, A.; Gräsvik, J.; Hallett, J. P.; Welton, T. Deconstruction of Lignocellulosic Biomass with Ionic Liquids. *Green Chem.* **2013**, *15* (3), 550–583. https://doi.org/10.1039/c2gc36364j.

(21) Mussatto, S. I.; Dragone, G. M. Biomass Pretreatment, Biorefineries, and Potential Products for a Bioeconomy Development. In *Biomass Fractionation Technologies for a Lignocellulosic Feedstock Based Biorefinery*; Elsevier, 2016; pp 1–22. https://doi.org/10.1016/B978-0-12-802323-5.00001-3.

(22) Stark, A. Ionic Liquids in the Biorefinery: A Critical Assessment of Their Potential. *Energy Environ. Sci.* **2011**, *4* (1), 19–32. https://doi.org/10.1039/c0ee00246a.

(23) Soltanian, S.; Aghbashlo, M.; Almasi, F.; Hosseinzadeh-Bandbafha, H.; Nizami, A. S.; Ok, Y. S.; Lam, S. S.; Tabatabaei, M. A Critical Review of the Effects of Pretreatment Methods on the Exergetic Aspects of Lignocellulosic Biofuels. *Energy Convers. Manag.* **2020**, *212* (April), 112792. https://doi.org/10.1016/j.enconman.2020.112792.

(24) Agbor, V. B.; Cicek, N.; Sparling, R.; Berlin, A.; Levin, D. B. Biomass Pretreatment: Fundamentals toward Application. *Biotechnol. Adv.* **2011**, *29* (6), 675–685. https://doi.org/10.1016/j.biotechadv.2011.05.005.

(25) Alvira, P.; Tomás-Pejó, E.; Ballesteros, M.; Negro, M. J. Pretreatment Technologies for an Efficient Bioethanol Production Process Based on Enzymatic Hydrolysis: A Review. *Bioresour. Technol.* **2010**, *101* (13), 4851–4861. https://doi.org/10.1016/j.biortech.2009.11.093.

(26) Wang, H.; Gurau, G.; Rogers, R. D. Ionic Liquid Processing of Cellulose. *Chem. Soc. Rev.* **2012**, *41* (4), 1519. https://doi.org/10.1039/c2cs15311d.

(27) Laher, T. M.; Hussey, C. L. Copper(I) and Copper(II) Chloro Complexes in the Basic Aluminum Chloride-1-Methyl-3-Ethylimidazolium Chloride Ionic Liquid. *Inorg. Chem.* **1983**, *22* (22), 3247–3251. https://doi.org/10.1021/ic00164a016.

(28) Elgharbawy, A. A.; Alam, M. Z.; Moniruzzaman, M.; Goto, M. Ionic Liquid Pretreatment as Emerging Approaches for Enhanced Enzymatic Hydrolysis of Lignocellulosic Biomass. *Biochem. Eng. J.* **2016**, *109*, 252–267. https://doi.org/10.1016/J.BEJ.2016.01.021.

(29) da Costa Lopes, A. M.; João, K. G.; Morais, A. R. C.; Bogel-Łukasik, E.; Bogel-Łukasik, R. Ionic Liquids as a Tool for Lignocellulosic Biomass Fractionation. *Sustain. Chem. Process.* **2013**, *1* (1), 3. https://doi.org/10.1186/2043-7129-1-3.

(30) Nagi, D.; Thummuru, R.; Mallik, B. S. Structure and Dynamics of Hydroxyl-Functionalized Protic Ammonium Carboxylate Ionic Liquids. **2017**, 8097–8107. https://doi.org/10.1021/acs.jpca.7b05995.

(31) Konda, N. M.; Shi, J.; Singh, S.; Blanch, H. W.; Simmons, B. A.; Klein-Marcuschamer, D. Understanding Cost Drivers and Economic Potential of Two Variants of Ionic Liquid Pretreatment for Cellulosic Biofuel Production. *Biotechnol. Biofuels* **2014**, *7* (1), 1–11. https://doi.org/10.1186/1754-6834-7-86.

(32) Liu, E.; Li, M.; Das, L.; Pu, Y.; Frazier, T.; Zhao, B.; Crocker, M.; Ragauskas, A. J.; Shi, J. Understanding Lignin Fractionation and Characterization from Engineered Switchgrass Treated by an Aqueous Ionic Liquid. *ACS Sustain. Chem. Eng.* **2018**, *6* (5), 6612–6623. https://doi.org/10.1021/acssuschemeng.8b00384.

(33) Pin, T. C.; Nascimento, V. M.; Costa, A. C.; Pu, Y.; Ragauskas, A. J.; Rabelo, S. C. Structural Characterization of Sugarcane Lignins Extracted from Different Protic Ionic Liquid Pretreatments. *Renew. Energy* **2020**, *161*, 579–592. https://doi.org/10.1016/j.renene.2020.07.078.

(34) Usmani, Z.; Sharma, M.; Gupta, P.; Karpichev, Y.; Gathergood, N.; Bhat, R.; Gupta, V. K. Ionic Liquid Based Pretreatment of Lignocellulosic Biomass for Enhanced Bioconversion. *Bioresour. Technol.* **2020**, *304* (February), 123003. https://doi.org/10.1016/j.biortech.2020.123003.

(35) Brandt-Talbot, A.; Gschwend, F. J. V.; Fennell, P. S.; Lammens, T. M.; Tan, B.; Weale, J.; Hallett, J. P. An Economically Viable Ionic Liquid for the Fractionation of Lignocellulosic Biomass. *Green Chem.* **2017**, *19* (13), 3078–3102. https://doi.org/10.1039/c7gc00705a.

(36) Wu, B.; Liu, W. W.; Zhang, Y. M.; Wang, H. P. Do We Understand the Recyclability of Ionic Liquids? *Chem. - A Eur. J.* **2009**, *15* (8), 1804–1810. https://doi.org/10.1002/chem.200801509.

(37) Halder, P.; Kundu, S.; Patel, S.; Setiawan, A.; Atkin, R.; Parthasarthy, R.; Paz-Ferreiro, J.; Surapaneni, A.; Shah, K. Progress on the Pre-Treatment of Lignocellulosic Biomass Employing Ionic Liquids. *Renew. Sustain. Energy Rev.* **2019**, *105* (February), 268–292. https://doi.org/10.1016/j.rser.2019.01.052.

(38) Baaqel, H.; Díaz, I.; Tulus, V.; Chachuat, B.; Guillén-Gosálbez, G.; Hallett, J. P. Role of Life-Cycle Externalities in the Valuation of Protic Ionic Liquids – a Case Study in Biomass Pretreatment Solvents. *Green Chem.* **2020**. https://doi.org/10.1039/d0gc00058b.

(39) Tzani, A.; Elmaloglou, M.; Kyriazis, C.; Aravopoulou, D.; Kleidas, I.; Papadopoulos, A.; Ioannou, E.; Kyritsis, A.; Voutsas, E.; Detsi, A. Synthesis and Structure-Properties Relationship Studies of Biodegradable Hydroxylammonium-Based Protic Ionic Liquids. *J. Mol. Liq.* **2016**, *224*, 366–376. https://doi.org/10.1016/j.molliq.2016.09.086.

(40) Pin, T. C.; Nakasu, P. Y. S.; Mattedi, S.; Rabelo, S. C.; Costa, A. C. Screening of Protic Ionic Liquids for Sugarcane Bagasse Pretreatment. *Fuel* **2019**, *235* (July 2018), 1506–1514. https://doi.org/10.1016/j.fuel.2018.08.122.

(41) Dias, R. M.; da Costa Lopes, A. M.; Silvestre, A. J. D.; Coutinho, J. A. P.; da Costa, M. C. Uncovering the Potentialities of Protic Ionic Liquids Based on Alkanolammonium and Carboxylate Ions and Their Aqueous Solutions as Non-Derivatizing Solvents of Kraft Lignin. *Ind. Crops Prod.* **2020**, *143* (November 2019), 111866. https://doi.org/10.1016/j.indcrop.2019.111866.

(42) Chen, L.; Sharifzadeh, M.; Mac Dowell, N.; Welton, T.; Shah, N.; Hallett, J. P. Inexpensive Ionic Liquids: [HSO4]--Based Solvent Production at Bulk Scale. *Green Chem.* **2014**, *16* (6), 3098–3106. https://doi.org/10.1039/c4gc00016a.

(43) Chandel, A. K.; Singh, O. V. Weedy Lignocellulosic Feedstock and Microbial Metabolic Engineering: Advancing the Generation of "Biofuel." *Appl. Microbiol. Biotechnol.* **2011**, *89* (5), 1289–1303. https://doi.org/10.1007/s00253-010-3057-6.

(44) O'SULLIVAN, A. C. Cellulose: The Structure Slowly Unravels. *Cellulose* **1997**, *4* (3), 173–207. https://doi.org/10.1023/A:1018431705579.

(45) Qian, X.; Ding, S.-Y.; Nimlos, M. R.; Johnson, D. K.; Himmel, M. E. Atomic and Electronic Structures of Molecular Crystalline Cellulose Iβ: A First-Principles Investigation. *Macromolecules* **2005**, *38* (25), 10580–10589. https://doi.org/10.1021/ma051683b.

(46) Hansen, C. M.; Björkman, A. The Ultrastructure of Wood from a Solubility Parameter Point of View. *Holzforschung* **1998**, *52* (4), 335–344. https://doi.org/10.1515/hfsg.1998.52.4.335.

(47) Hsu, T. C.; Guo, G. L.; Chen, W. H.; Hwang, W. S. Effect of Dilute Acid Pretreatment of Rice Straw on Structural Properties and Enzymatic Hydrolysis. *Bioresour. Technol.* **2010**, *101* (13), 4907–4913. https://doi.org/10.1016/j.biortech.2009.10.009.

(48) Li, C.; Knierim, B.; Manisseri, C.; Arora, R.; Scheller, H. V.; Auer, M.; Vogel, K. P.; Simmons, B. A.; Singh, S. Comparison of Dilute Acid and Ionic Liquid Pretreatment of Switchgrass: Biomass Recalcitrance, Delignification and Enzymatic Saccharification. *Bioresour. Technol.* **2010**, *101* (13), 4900–4906. https://doi.org/10.1016/j.biortech.2009.10.066.

(49) Galbe, M.; Zacchi, G. Pretreatment of LignocellulosicMaterials for Efficient Bioethanol

Production. *Adv. Biochem. Eng. Biotechnol.* **2007**, *19* (July), 41–65. https://doi.org/10.1002/abio.370190215.

(50) Britt, K. K. Papermaking https://www.britannica.com/technology/papermaking#ref82429 (accessed Dec 23, 2020).

(51) Taherzadeh, M.; Karimi, K. Pretreatment of Lignocellulosic Wastes to Improve Ethanol and Biogas Production: A Review. *Int. J. Mol. Sci.* **2008**, *9* (9), 1621–1651. https://doi.org/10.3390/ijms9091621.

(52) Sun, Y.; Cheng, J. Hydrolysis of Lignocellulosic Materials for Ethanol Production: A Review. *Bioresour. Technol.* **2002**, *83* (1), 1–11. https://doi.org/10.1016/S0960-8524(01)00212-7.

(53) Balch, M. L.; Holwerda, E. K.; Davis, M. F.; Sykes, R. W.; Happs, R. M.; Kumar, R.; Wyman, C. E.; Lynd, L. R. Lignocellulose Fermentation and Residual Solids Characterization for Senescent Switchgrass Fermentation by: Clostridium Thermocellum in the Presence and Absence of Continuous in Situ Ball-Milling. *Energy Environ. Sci.* **2017**, *10* (5), 1252–1261. https://doi.org/10.1039/c6ee03748h.

(54) Pan, X.; Xie, D.; Gilkes, N.; Gregg, D. J.; Saddler, J. N. Strategies to Enhance the Enzymatic Hydrolysis of Pretreated Softwood with High Residual Lignin Content. *Appl. Biochem. Biotechnol.* **2005**, *124* (1–3), 1069–1080. https://doi.org/10.1385/ABAB:124:1-3:1069.

(55) Alfani, F.; Gallifuoco, A.; Saporosi, A.; Spera, A.; Cantarella, M. Comparison of SHF and SSF Processes for the Bioconversion of Steam-Explode Wheat Straw. *J. Ind. Microbiol. Biotechnol.* **2000**, *25* (4), 184–192. https://doi.org/10.1038/sj.jim.7000054.

(56) Laureano-Perez, L.; Teymouri, F.; Alizadeh, H.; Dale, B. E. Understanding Factors That Limit Enzymatic Hydrolysis of Biomass: Characterization of Pretreated Corn Stover. *Appl. Biochem. Biotechnol.* **2005**, *124* (1–3), 1081–1100. https://doi.org/10.1385/ABAB:124:1-3:1081.

(57) Duff, S. J. B.; Murray, W. D. Bioconversion of Forest Products Industry Waste Cellulosics to Fuel Ethanol: A Review. *Bioresour. Technol.* **1996**, *55* (1), 1–33. https://doi.org/10.1016/0960-8524(95)00122-0.

(58) Gabriel, S.; Weiner, J. Ueber Einige Abkömmlinge Des Propylamins. *Berichte der Dtsch. Chem. Gesellschaft* **1888**, *21* (2), 2669–2679. https://doi.org/10.1002/cber.18880210288.

(59) Wilkes, J. S.; Zaworotko, M. J. Air and Water Stable 1-Ethyl-3-Methylimidazolium Based Ionic Liquids. *J. Chem. Soc. Chem. Commun.* **1992**, *04* (13), 965. https://doi.org/10.1039/c39920000965.

(60) Sánchez, P. B.; García, J.; Pádua, A. A. H. Structural Effects on Dynamic and Energetic Properties of Mixtures of Ionic Liquids and Water. *J. Mol. Liq.* **2017**, *242*, 204–212. https://doi.org/10.1016/j.molliq.2017.06.109.

(61) Shi, J.; Balamurugan, K.; Parthasarathi, R.; Sathitsuksanoh, N.; Zhang, S.; Stavila, V.; Subramanian, V.; Simmons, B. A.; Singh, S. Understanding the Role of Water during Ionic Liquid Pretreatment of Lignocellulose: Co-Solvent or Anti-Solvent? *Green Chem.* **2014**, *16* (8), 3830–3840. https://doi.org/10.1039/c4gc00373j.

(62) Holbrey, J. D.; Seddon, K. R. Ionic Liquids. *Clean Technol. Environ. Policy* **1999**, *1* (4), 223–236. https://doi.org/10.1007/s100980050036.

(63) Orr, V. C. A.; Rehmann, L. Ionic Liquids for the Fractionation of Microalgae Biomass. *Current Opinion in Green and Sustainable Chemistry*. Elsevier October 1, 2016, pp 22–27. https://doi.org/10.1016/j.cogsc.2016.09.006.

(64) Quental, M. V.; Caban, M.; Pereira, M. M.; Stepnowski, P.; Coutinho, J. A. P.; Freire, M. G. Enhanced Extraction of Proteins Using Cholinium-Based Ionic Liquids as Phase-Forming Components of Aqueous Biphasic Systems. *Biotechnol. J.* **2015**, *10* (9), 1457–1466. https://doi.org/10.1002/biot.201500003.

(65) Lan, W.; Liu, C. F.; Sun, R. C. Fractionation of Bagasse into Cellulose, Hemicelluloses,

and Lignin with Ionic Liquid Treatment Followed by Alkaline Extraction. *J. Agric. Food Chem.* **2011**, *59* (16), 8691–8701. https://doi.org/10.1021/jf201508g.

(66) Chowdhury, S. A.; Vijayaraghavan, R.; MacFarlane, D. R. Distillable Ionic Liquid Extraction of Tannins from Plant Materials. *Green Chem.* **2010**, *12* (6), 1023–1028. https://doi.org/10.1039/b923248f.

(67) Brandt, A.; Ray, M. J.; To, T. Q.; Leak, D. J.; Murphy, R. J.; Welton, T. Ionic Liquid Pretreatment of Lignocellulosic Biomass with Ionic Liquid-Water Mixtures. *Green Chem.* **2011**, *13* (9), 2489–2499. https://doi.org/10.1039/C1GC15374A.

(68) Lu, B.; Xu, A.; Wang, J. Cation Does Matter: How Cationic Structure Affects the Dissolution of Cellulose in Ionic Liquids. *Green Chem.* **2014**, *16* (3), 1326–1335. https://doi.org/10.1039/c3gc41733f.

(69) Taft, R. W.; Abboud, J.-L. M.; Kamlet, M. J.; Abraham, M. H. Linear Solvation Energy Relations. *J. Solution Chem.* **1985**, *14* (3), 153–186. https://doi.org/10.1007/BF00647061.

(70) Sun, J.; Konda, N. V. S. N. M.; Parthasarathi, R.; Dutta, T.; Valiev, M.; Xu, F.; Simmons, B. A.; Singh, S. One-Pot Integrated Biofuel Production Using Low-Cost Biocompatible Protic Ionic Liquids. *Green Chem.* **2017**, *19* (13), 3152–3163. https://doi.org/10.1039/C7GC01179B.

(71) Kuo, C.-H.; Lee, C.-K. Enhancement of Enzymatic Saccharification of Cellulose by Cellulose Dissolution Pretreatments. *Carbohydr. Polym.* **2009**, *77* (1), 41–46. https://doi.org/10.1016/j.carbpol.2008.12.003.

(72) Fort, D. a.; Remsing, R. C.; Swatloski, R. P.; Moyna, P.; Moyna, G.; Rogers, R. D. Can Ionic Liquids Dissolve Wood? Processing and Analysis of Lignocellulosic Materials with 1-n-Butyl-3-Methylimidazolium Chloride. *Green Chem.* **2007**, *9* (1), 63. https://doi.org/10.1039/b607614a.

(73) Pinkert, A.; Marsh, K. N.; Pang, S. Reflections on the Solubility of Cellulose. *Ind. Eng. Chem. Res.* **2010**, *49* (22), 11121–11130. https://doi.org/10.1021/ie1006596.

(74) Haykir, N. I.; Bahcegul, E.; Bicak, N.; Bakir, U. Pretreatment of Cotton Stalk with Ionic Liquids Including 2-Hydroxy Ethyl Ammonium Formate to Enhance Biomass Digestibility. *Ind. Crops Prod.* **2013**, *41*, 430–436. https://doi.org/10.1016/J.INDCROP.2012.04.041.

Chapter 2[1]

Which Variables Matter for Process Design and Scale-Up? A Study of Sugarcane Straw Pretreatment Using Low-Cost and Easily Synthesizable Ionic Liquids

Ionic liquids (ILs) have great potential as solvents and catalysts for pretreatment of lignocellulosic biomass. However, process scale-up necessitates that IL-based pretreatment methods be optimized in terms of cost and sustainability. In this study, low-cost and easily synthesizable ethanolammonium-based ILs were prepared and used in the pretreatment of sugarcane straw (SW). The effects of ILs, IL mixtures, pretreatment temperature, water content, solids loading, ultrasonication, and agitation speed on residual solids enzymatic digestibility and delignification were systematically assessed, and the process was scaled up from a 50 mL static flask to a 1 L impelled reactor. IL mixtures improved enzymatic digestibility at higher solids loading and water addition in the reaction medium under mild temperature conditions (90 °C). Enzymatic hydrolysis of residual solids after bench-scale pretreatment of SW for 3 h at 15% (w/w) solids loading and 20% (w/w) water content in the liquid phase resulted in 98% cellulose digestibility under non-optimized conditions. This study pro-vides a practical review of IL-based pretreatment methods, discusses the selection of variables for process design and scale-up, and presents empirical results.

[1] This chapter was published as: Ferrari, F. A.; Pereira, J. F. B.; Witkamp, G. J.; Forte, M. B. S. Which Variables Matter for Process Design and Scale-up? A Study of Sugar Cane Straw Pretreatment Using Low-Cost and Easily Synthesizable Ionic Liquids. ACS Sustain. Chem. Eng. 2019, 7 (15), 12779–12788.

2.1 Introduction

Climate change and environmental degradation are a major concern for all sectors of society, from governmental agencies to industries and consumers. This awareness of environmental issues motivates the search for sustainable energy production technologies. The society demands sustainability not only in electricity generation and fuel production [1,2] but also in the manufacture of chemicals and starting materials [1,3,4]. One solution to the environmental problems associated with the large energy demands of modern society is to invest in sustainable biorefineries to convert lignocellulosic biomass into electricity, fuel, and chemicals [3,5].

Lignocellulosic residues are low cost and abundant. These materials may vary in composition depending on their origin but are typically composed of 40–80% cellulose, 10–40% hemicellulose, and 5–36% lignin [6,7]. Some of the most economically interesting lignocellulosic sources are sugarcane residues. The global production of sugarcane, estimated at 1.9 gigatonnes in 2017, is on the rise [8]. Only about one-third of the sugarcane weight is turned into sugar and first-generation ethanol. The other two-thirds are bagasse and straw, that is, lignocellulosic biomass. Sugarcane residues can be burned for electricity generation or used as lignocellulosic feedstock in the production of chemicals and second-generation biofuels. It is noteworthy that ethanol production from sugarcane residues has better greenhouse gas balance than from other high production crops [9].

However, because it is recalcitrant to hydrolysis, lignocellulosic biomass must be pretreated before it can be converted to biomolecules. Pretreatment reactions disrupt the cellulose–hemicellulose–lignin matrix, facilitating the release of sugars, such as glucose and xylose. Pretreatment optimization is a crucial step in the implementation of a biorefinery: it directly affects the price of the final product [10] and, consequently, the project's viability.

Different pretreatment methods exist, and a weighted approach is useful for selecting the most economically and environmentally sustainable strategy. Several criteria should be taken into account, including energy consumption, prices of reagents and starting materials, use of toxic chemicals (such as organic solvents, alkaline solutions, and inorganic acids), implementation and operating costs, and process yield [11–14]. The pros and cons of each method need to be carefully analyzed in the project design phase.

Recently, ionic liquids (ILs) have emerged as a solution to the problems of biomass pretreatment. ILs are salts that are usually molten at temperatures below

100 °C because of the large size, asymmetry, and conformational flexibility of their ions [15,16]. Cation and anion groups can be designed to confer specific properties, such as low vapor pressure, specific solubility of solutes, or high miscibility with other solvents [14,16–18].

As with every new technology, there are challenges to be overcome in IL-based pretreatment methods for lignocellulosic biomass. Improvements in the design and synthesis of IL molecules are required to reduce costs and make their production less laborious. IL-based pretreatment methods must be improved in terms of conversion yield and energy consumption. The state-of-the-art in IL pretreatment is illustrated by the benchmark IL 1-ethyl-3-methylimidazolium acetate ([Emim][Ac])[16]. Although an efficient pretreatment agent, [Emim][Ac] has to be completely removed from residual solids because of its negative impacts on microbial cells and enzymes in downstream steps [19]. Cholinium-based ILs are interesting alternatives to [Emim][Ac], as they lead to good delignification efficiency and enzymatic digestibility with reduced inhibitory effects on enzymes and fermentative microorganisms [19]. However, cholinium-based ILs must be synthesized under a nitrogen atmosphere to avoid oxidation and are, therefore, expensive. ILs containing other ammonium groups, such as triethylammonium and 2-hydroxyethylammonium ($[Mea]^+$), have been used with success for lignocellulosic biomass pretreatment [20–22]. At the time this article is being written, monoethanolamine, used in the synthesis of $[Mea]^+$-based ILs, is quoted about 40 times less expensive than choline hydroxide, used in the synthesis of cholinium-based ILs (Sigma–Aldrich website). Taken together, these reports suggest that $[Mea]^+$-based ILs may be cheaper and yet effective alternatives to [Emim][Ac] and cholinium-based ILs.

Process setup and operating conditions have a direct impact on energy consumption, downstream efficiency, and product price [23–25]. For instance, temperature has a large influence on process efficiency and other indicators. Although high temperature may lead to high yields, it can break down cellulose and hemicellulose molecules into single sugars, which is undesirable at the pretreatment stage. Temperature acts predominantly in two manners: *i*) by lowering IL viscosity and thereby favoring dynamic interactions between IL and biomass and *ii*) by increasing the energy level of the system [16,18,26]. Ultrasound irradiation enhances process performance through sonochemical and sonophysical effects: the first generates radicals that attack the internal bonds of the lignocellulosic matrix and the second disrupts the lignocellulosic structure through the mechanical impact of sound waves [27]. Other important factors affecting process efficiency and energy

consumption are solids loading, agitation speed, and water content in the reaction medium [14,16,26]. Aung et al. (2018)[28] studied the effect of solid loading increase on lignocellulosic biomass pretreatment and observed a dependent relationship between this parameter and temperature. Agitation will affect system homogeneity, and at higher solid loading it will lead to more frequent contact between biomass particle and IL [26]. Nevertheless, agitation of lignocellulosic biomass at large scale is very energy consuming, impacting on process energy efficiency [29].

The effects of pretreatment parameters were assessed separately in previous studies [19,23,28,30]. This study aimed to synthesize low-cost ILs using a simple chemical route and investigate the combined effects of temperature, water content, solids loading, agitation speed, ultrasonication, pure ILs, and IL mixtures on the pretreatment of sugarcane straw (SW) using a Plackett–Burman type factorial design.

2.2 Material and Methods

2.2.1 Biomass characterization

SW was kindly provided by the Brazilian Bioethanol Science and Technology Laboratory (CTBE). Dry leaves and tops were milled and passed through a set of sieves. The material retained between 16- and 24-mesh sieves (0.7–1.19 mm in diameter) was used for the experiments. Moisture content was determined gravimetrically by oven drying (Fanen) the samples overnight at 105 °C. The chemical composition of untreated SW and the residual solids remaining after pretreatment of SW was determined according to National Renewable Energy Laboratory (NREL) methods [31].

2.2.2 Chemicals, synthesis of synthetized ILs

[Emim][Ac] (98% pure) was purchased from Iolitec (Germany) and used as received. All other chemicals and standards were purchased from Sigma–Aldrich (Germany) and used as received. 2-Hydroxyethylammonium acetate ([Mea][Ac]) and 2-hydroxyethylammonium hexanoate ([Mea][Hex]) were synthesized respectively in 100 mL and 500 mL Schott flasks by a one-step, acid–base exothermic neutralization method, in which a proton (H^+) is transferred to the NH_2 group of an amino alcohol reagent, conferring a positive charge to the molecule (NH_3^+). First, ethanolamine was weighed into a flask. The flask was closed with a silicone septum and placed in a cold-water bath. An equimolar quantity of either acetic acid or hexanoic acid was slowly added through the septum using a syringe.

The reaction was carried out overnight at room temperature under agitation. The formation of [Mea][Ac] or [Mea][Hex] was confirmed by proton nuclear magnetic resonance (^{1}H NMR), as detailed in Appendix. The water content (measured by Karl Fischer titration) was 0.53 % and 0.58 % (m/m) for [Mea][Ac] and [Mea][Hex], respectively. The viscosity, glass-transition temperature, density and other physic-chemical properties are detailed in the Appendix. Cholinium acetate ([Cho][Ac]) was synthesized from choline hydroxide and acetic acid under the same conditions but under a N_2 atmosphere and with an additional washing step using ethyl acetate.

2.2.3 Enzymatic hydrolysis and digestibility efficiency

Assays were performed in 1.5 mL plastic tubes using Cellic CTec2 (Novozymes) at 10 filter-paper units (FPU) of enzyme per gram of biomass and a solids loading of 5% (w/w). Hydrolysis was carried out in citrate buffer (pH 4.8) for 48 h in a thermoblock (Loccus Biotecnologia) at 50 °C and 1500 rpm. Upon completion of the hydrolysis reaction, the supernatant was filtered through a 0.22 µm syringe filter (Millipore), and its composition determined by high-performance liquid chromatography (HPLC). The enzymatic digestibility of cellulose and hemicellulose was calculated according to the relationship between the initial mass of these components and sugar concentration in the supernatant of pretreated samples, eqs. 1 and 2, adapted from NREL LAP TP-510-43630 [31,32].

$$Y_{Cell} = \frac{\mathrm{m}_{Glu} + 1.053\ \mathrm{m}_{Cello}}{1.111\ f\ \mathrm{m}_{sw}} x\ 100 \quad (1)$$

$$Y_{Hem} = \frac{\mathrm{m}_{Xyl}\ 0.9 + \ 0.9\ \mathrm{m}_{Arab}}{1.111\ f\ \mathrm{m}_{sw}} x100 \quad (2)$$

where m_{Glu}, mass of glucose; 1.053, multiplication factor to converts cellobiose into glucose; m_{Cello}, mass of cellobiose; f, mass fraction of cellulose or hemicellulose in the biomass; m_{SW}, initial mass of SW; m_{Xyl}, mass of xylose; m_{Arab}, mass of arabinose.

2.2.4 Biomass pretreatment

Preliminary pretreatment assays were performed in triplicate in 50 mL glass flasks closed with a silicone stopper. Dried SW (0.6 g) was mixed with different volumes of IL and water at different ratios to obtain predefined solids loadings. Flasks were incubated in a convection oven at 90 °C for 12 h. After the

pretreatment, 10 g of water was added to each sample, and solid and liquid fractions were separated using a 125 μm nylon filter. Residual solid fractions were washed three times with 10 g of water and then dried overnight at 105 °C.

The pretreatment process was scaled up from 50 ml glass container (referred to here as lab scale) to 1 L (referred to here as bench scale). Bench-scale pretreatments were carried out in a stainless-steel reactor consisting of a jacketed vessel with a maximum operating pressure of 10 bar, an anchor impeller, and a 300 W and 19 kHz ultrasound probe, depicted in Figure 1. All experiments were carried out using 37.24 g of SW at 8.7% (w/w) moisture content. Different quantities of IL and water were added to obtain the solids loading and water contents described in Table 1 (Results section). After 4 h of pretreatment, 300 g of water was added to the samples, and solid and liquid fractions were separated using a 125 μm nylon filter. Solid fractions were washed twice with 300 g of water and then dried overnight at 105 °C. The influence of solids loading (S), water content (H_2O), temperature (T), agitation speed (N), ultrasonication (U), and [Mea][Ac]/[Mea][Hex] ratio ($IL_{1/2}$) on pretreatment efficiency was assessed using DOE (design of experiments) strategy by a Plackett–Burman matrix, in which multiple conditions are varied simultaneously. The codified variables are summarized in Table 1. The design consisted of 12 runs with the independent variables at the low (−1) or high (+1) level and 3 repetitions of the center point (0), totaling 15 experiments (Table 2). Center point runs were used to estimate process reproducibility [33]. Pretreatment efficiency was evaluated in terms of enzymatic digestibility and lignin content of residual solids. Data were analyzed using the on-line software Protimiza Experimental Design (https://experimental-design.protimiza.com.br).

Table 1: Table of Variables range used to design experiments of section IV of Results and Discussion.

Variables	Levels		
	- 1	**0**	**+1**
T (°C)	80	110	130
H_2O/IL % (w/w)	10	35	60
Loading % (w/w)	10	15	20
Ultrasound (W)	0	60	120
Agitation (rpm)	3	15	30
ILs Mixture % ([Mea][Ac]/[Mea][Hex])	25	50	75

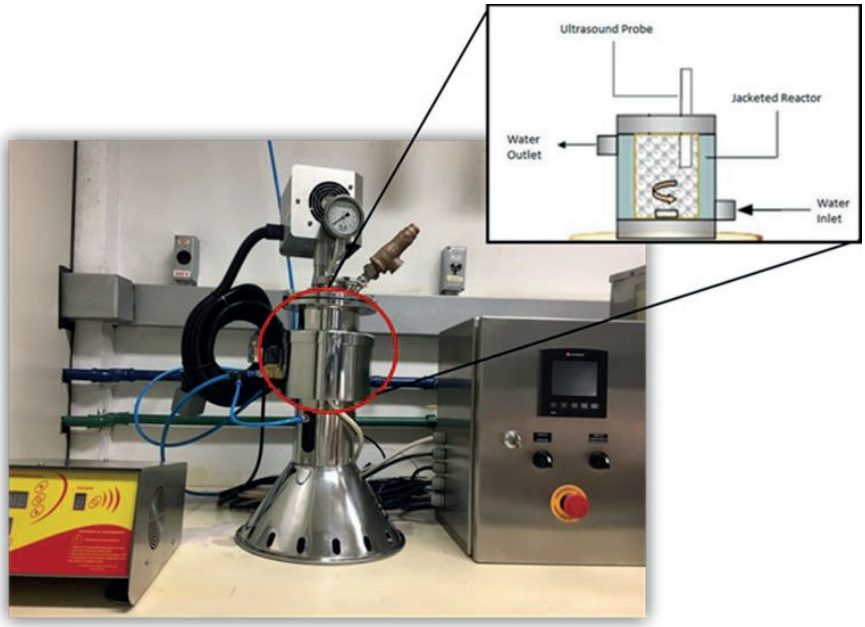

Fig 1: Bench Scale Reactor.

2.2.5 HPLC quantification

The contents of sugars, organic acids, furfural (FUR), and hydroxymethyl furfural (HMF) were determined using an HPLC system (Thermo Fisher Scientific) equipped with a refractive index detector. The column oven was kept at 35 °C. Samples were eluted using a 0.01 M aqueous solution of H_2SO_4 (pH 2.6) at a flow rate of 0.6 mL min^{-1} and separated using an Aminex HPX-87H (300 × 78 mm) column. Concentrations were calculated from calibration curves of standard compounds. Sugar contents ranged from 0.01 to 10 g L^{-1}, organic acid contents ranged from 0.01 to 5 g L^{-1}, and FUR and HMF contents ranged from 0.001 to 1.0 g L^{-1}.

2.2.6 Attenuated total reflection Fourier transform infrared spectroscopy

Infrared spectroscopic measurements were performed on neat samples using an ALPHA attenuated total reflectance Fourier transform infrared (ATR-FTIR) spectrometer (Bruker, Banner Lane). Spectra were acquired in the wavenumber range of 400–4000 cm^{-1}.

2.3 Results and Discussion

2.3.1 Effect of water content and solids loading on pretreatment efficiency at lab scale

It is necessary to select ILs that act efficiently on lignocellulosic biomass and satisfy economic and environmental sustainability criteria, such as wide availability, low price, and low toxicity. However, this is not enough to develop a sustainable pretreatment method. It is also crucial to understand how operating conditions affect biomass pretreatment. This section describes the steps taken to evaluate pretreatment efficiency and reports the experimental results obtained with four ILs, [Emim][Ac], [Cho][Ac], [Mea][Ac], and [Mea][Hex].

First, the performance of the protic ILs [Mea][Ac] and [Mea][Hex] was tested under standard pretreatment conditions: 90 °C, 6% (w/w) solids loading, no water addition, 12 h, no agitation. The efficiency of protic ILs was then compared with that of [Cho][Ac] and [Emim][Ac], as depicted in Figure 2. As expected, [Emim][Ac] was the most efficient pretreatment agent, achieving 100% of glucose release from cellulose in the enzymatic hydrolysis step. [Mea][Ac], [Mea][Hex], and [Cho][Ac] resulted in a glucose release of 69, 46, and 26%, respectively. [Cho][Ac] was much less efficient than expected from previous studies [34,35], probably because of its residual moisture content (4.1% w/w), as [Cho][Ac] is highly sensitive to water [36]. Although biomass pretreatment with acetate-based ILs commonly affords good results, the association of acetate with different cations may produce diverse effects [37–40].

[Emim][Ac]-treated biomass showed the highest enzymatic digestibility, which was expected as [Emim][Ac] can solubilize cellulose. The ability to dissolve cellulose of [Emim][Ac] is likely due to *i*) the presence of a nitrogen heteroatom in the 1-ethyl-3-methylimidazolium cation, which delocalizes the positive charge; *ii*) its ability to form hydrogen bonds; *iii*) the cation geometry; and *iv*) the association of the cation with an acetate anion [41–44].

[Mea][Ac] and [Emim][Ac]-treated samples showed similar hemicellulose digestibilities (Figure 3). This result is attributed to their similar delignification efficiencies. During delignification, ester bonds between hemicellulose and lignin are broken, and lignin is redistributed on the molecule surface or released, facilitating the access of hydrolytic enzymes [45,46]. Interestingly, [Mea][Ac] pretreatment was 40 and 87% more efficient in increasing cellulose and hemicellulose digestibility, respectively, than [Mea][Hex], which contains the same cation. The small size of acetate compared with that of hexanoate improves the

molecular diffusion of [Mea][Ac] into the lignocellulosic matrix. At longer pretreatment time (24 h, data not shown) the efficiency of [Mea][Hex] process came closer to that obtained from [Mea][Ac], regarding enzymatic hydrolysis. The difference on their efficiencies is time dependent, what suggests that under the tested process conditions, IL diffusivity at molecular levels impacts on pretreatment performance.

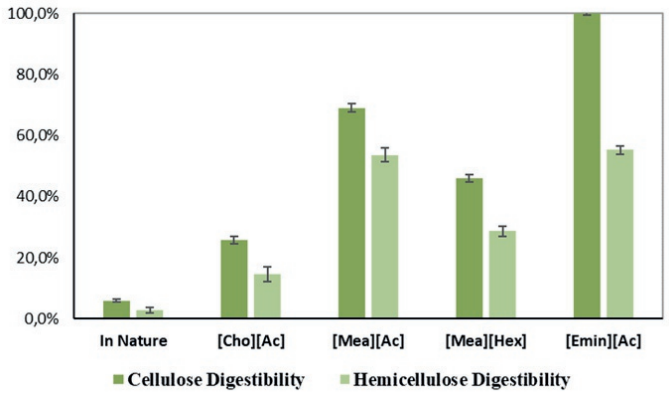

Fig 2: Enzymatic digestibility from residual solid after pre-treatment using different ILs at 90 °C for 12 h. Results expressed as percentage of released sugars from theoretical. Enzymatic hydrolysis using 5 % (w/w) of solid loading in acetate buffer pH 4.8, 50 °C, stirred for 48 h using 10 FPU CellicCtec2 (Novozymes®) per gram of dry biomass

Other important aspects regarding the choice of ILs for biomass pretreatment are related to scalability. Solids loading and water content influence process scale-up and costs. Lignocellulosic residues are highly hydrophilic, and the addition of water can reduce process costs and environmental impacts. Higher solids loading reduce capital and operating expenditures and increase productivity [24,25]. Therefore, ILs that perform well in the presence of water and high solids loadings are desirable. The effectiveness of [Emim][Ac], [Mea][Ac], and [Mea][Hex] in the presence of water and high solids loading was evaluated.

Acetate-based ILs were greatly affected by the presence of water, resulting in low cellulose and hemicellulose yields: 52 and 57% for [Mea][Ac] and 53 and 41% for [Emim][Ac], respectively. In contrast, [Mea][Hex] was positively influenced by the addition of water: enzymatic digestion of cellulose was improved in 49% and of hemicellulose in 89%. These results can be explained by an overall reduction in viscosity, increasing system's dynamics. Although the increase on

systems' dynamics holds true for all tested ILs, only [Mea][Hex] was positively affected. Water influence is very dependent on IL's components, entailing in different consequences on system's properties, i.e. viscosity, density, diffusivity [47]. Up to a limit, water can also enhance the interaction of IL with lignocellulose. Cations and anions interact with each other through electrostatic and also hydrogen bonds, which can limit the formation of hydrogen bonds with the lignocellulosic matrix. Therefore, water might hinder cation–anion hydrogen bonding, making them more available to interact with lignocellulosic sources [36,48]. However, water-IL interaction is also dependent on IL composition. Sanchez et al. (2017) studied the solvation profile and the hydrogen bonds energy between water and ILs for two different cations groups, namely cholinium and N-ethylpiridinium, concluding different patterns dependence on IL's cation and anion. It seems that in the [Mea][Hex] system, the positive effects on system dynamics were greater than the negative consequences due to water addition, and the opposite for the others ILs. Moreover, water generally interacts closely with ionic region [36,49]. Consequently, long nonpolar alkyl chains of anions interact preferentially with the biomass instead of water. Long alkyl chains increase the hydrophobic binding sites [50] of the IL molecule, promoting hydrophobic interactions between [Mea][Hex] and the biomass, mainly with lignin, explaining the superior performance of [Mea][Hex] compared to [Mea][Ac].

The increase in solids loading from 6 to 13% (w/w) at 30% water content led to a 20% and 23% decrease in cellulose and hemicellulose digestibility, respectively, in biomass pretreated with [Emim][Ac] compared with $[Mea]^+$-based ILs. Under these conditions, the effectiveness of [Mea][Hex] on cellulose digestibility was not affected, but an 18% reduction in hemicellulose digestibility was observed, attributed to lower delignification. [Mea][Ac] had the best performance at high solids loading, increasing cellulose and hemicellulose yields by 66 and 49%, respectively.

2.3.2 Effect of ILs and IL mixtures on pretreatment efficiency at lab scale

Although [Mea][Ac] resulted in a 14-fold increase in cellulose digestibility compared with untreated SW, it did not cause a significant increase in delignification. [Mea][Hex] reduced acid-insoluble lignin content by 11%, whereas [Mea][Ac] gave a reduction of only 9%. Acid-insoluble lignin was quantified instead of total lignin (soluble + insoluble) because compounds not derived from lignin, such as wax, may lead to unreliable results in soluble lignin determination,

and because acid-insoluble lignin has a direct impact on enzymatic hydrolysis efficiency [45].

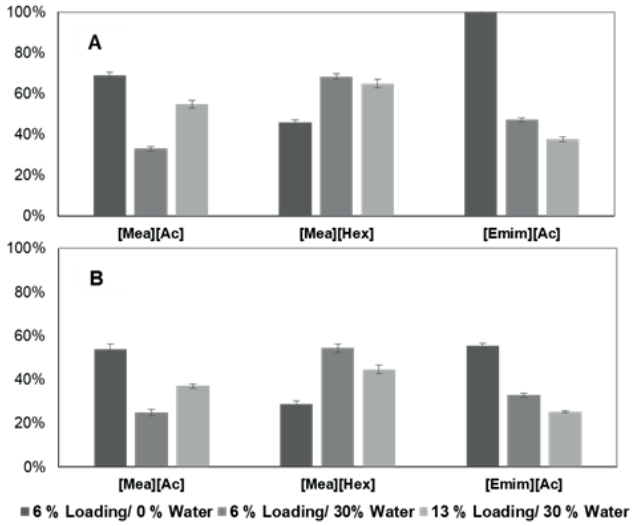

Fig 3: Enzymatic digestibility of cellulose (A) and hemicellulose (B) in residual solids obtained after pretreatment with different ionic liquids at lab scale. Experimental conditions: 90 °C, 12 h, no agitation.

As [Mea][Ac] and [Mea][Hex] reacted differently in the presence of water, a second set of experiments was carried out using a 1:1 (w/w) mixture of [Mea][Ac]/[Mea][Hex] to investigate their combined effects on pretreatment efficiency. First, SW was pretreated under standard conditions [6% (w/w) solids loading, no agitation, no water addition, 90 °C, and 12 h]. The mixture increased delignification by 2-fold (25% reduction in insoluble lignin) compared with pure ILs (Figure 4). Cellulose digestibility did not differ from that obtained using pure [Mea][Ac]. These results suggest that the acetate anion plays a major role in cleaving intermolecular hydrogen bonds. Hemicellulose digestibility did not differ between biomass treated with pure ILs or the IL mixture, suggesting that treatment with the IL mixture did not increase the cleavage of ester bonds between lignin and structural carbohydrates. The higher delignification observed in biomass pretreated with [Mea][Ac]/[Mea][Hex] than in biomass pretreated with pure ILs is probably a result of the increase in hydrophobic interactions with the hexanoate anion and cleavage of ester and hydrogen bonds from acetate, which prevents released lignin from redepositing on the lignocellulosic matrix.

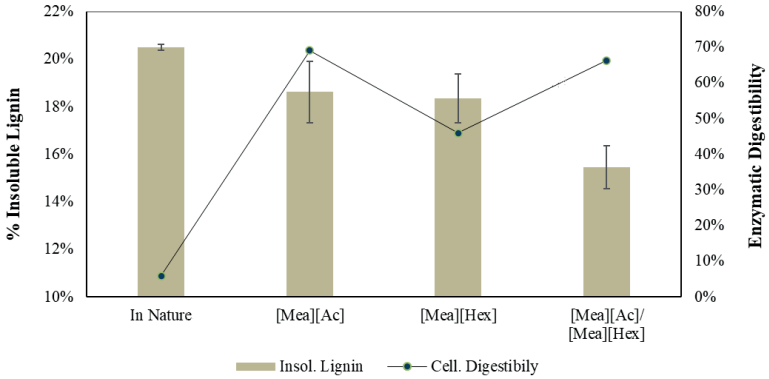

Fig 4: Enzymatic digestibility and delignification of residual solids after pretreatment of sugarcane straw with pure ionic liquids (ILs) and an IL mixture at lab scale. Experimental conditions: 6% (w/w) solids loading, 90 °C, 12 h, no water addition, no agitation. Standard deviation bars for enzymatic digestibility may appear smaller than graphic marker.

Water content and solids loading were varied to assess their effect on the efficiency of IL mixtures. In addition to pure ILs and the [Mea][Ac]/[Mea][Hex] mixture, a 1:1 (w/w) mixture of [Emim][Ac]/[Mea][Ac] was tested. Results are presented in Figure 5.

An increase in solids loading from 6 to 13% (w/w) did not affect cellulose digestibility in biomass pretreated with IL mixtures, different from the observed with pure ILs. The results of enzymatic digestibility showed that the hexanoate anion contributed positively to digestibil-ity performance in the presence of water. As expected, water negatively affected delignification. The best result in the presence of water (12% w/w lignin removal) was obtained using [Mea][Ac]/[Mea][Hex]. [Mea][Ac] was more effective than [Emim][Ac] at high solids loadings, which is probably due to their different interactions with the water–lignocellulose complex. Hydrogen bonds between water and $[Emim]^+$ seem to be more stable than those between water and $[Mea]^+$. Consequently, water is more likely to bind to hydrophilic cellulosic regions of the lignocellulosic matrix than to [Mea][Ac], allowing the IL to act on the lignocellulosic matrix. This effect becomes more evident at high solids loadings.

The fact that [Emim][Ac] is extremely sensitive to the presence of water is a limiting factor for industrial application. For instance, about 4 MJ/kg of water is necessary to dry lignocellulosic residues, whose moisture content typically varies from 30 to 60% (w/w). Thus, the use of [Emim][Ac] increases capital expenditure,

lowers energy efficiency, and increases the risk of combustion due to dry material [51]. Furthermore, solids loadings higher than 10% (w/w) are necessary to achieve cost-effectiveness [25]. As such, $[Mea]^+$-based ILs are promising alternatives for industrial-scale processes.

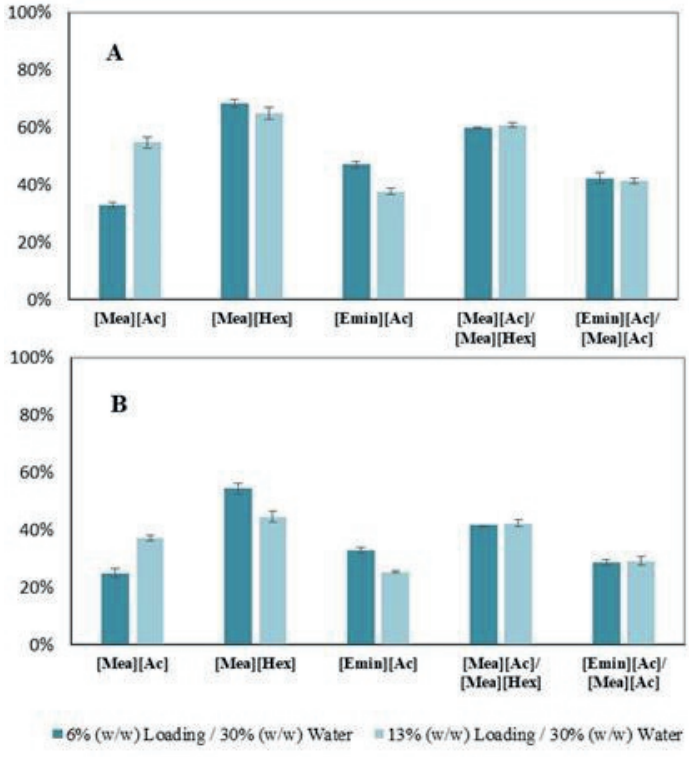

Fig 5: Enzymatic digestibility of cellulose (A) and hemicellulose (B) in the solids remaining after pretreatment of sugarcane straw with pure ionic liquids (ILs) and IL mixtures at lab scale. Experimental conditions: 90 °C, 12 h, no agitation.

2.3.3 Scale-up: effect of process conditions at bench scale

Process scale-up is a mandatory stage for any new technology during which bottlenecks and challenges not observed at small scale will likely appear. In addition to the type and composition of IL mixtures, operating conditions (such as solids loading and liquid phase water content) strongly influence biomass pretreatment efficiency. Pretreatment experiments were carried out on a 1 L bench-scale reactor, increasing the volume of pretreated biomass by 60 fold. The effects

of process variables were assessed, aiming to facilitate further scale-up. In all experiments, SW was used without drying (8.7% w/w moisture content) to reduce the number of steps in the process.

As shown in Table 2, delignification and cellulose digestibility varied greatly according to process conditions, from 2 to 56% and 17.6 to 100%, respectively. Variables were analyzed statistically at 90% confidence level ($p < 0.10$) to identify significant effects on enzymatic digestibility, lignin removal, and hemicellulose removal (not desirable). According Rodrigues and Iemma (2014) [33] this is the recommended confidence level for this type of DOE. In this set of experiments, cellulose removal was not determined, as [Mea][Ac]/[Mea][Hex] does not hydrolyze cellulose efficiently [20]. The effects are summarized in table 3, the detailed effects and Pareto Chart is shown in Figure 6.

The results of experiments conducted in the 1 L reactor were similar to those obtained at small scale. Li et al. (2013)[52] and Li et al. (2015)[53] scaled up the pretreatment of lignocellulosic feedstock with [Emin][Ac] from 10 mL to 6 L without compromising residual solids recovery and enzymatic digestibility. The authors reported that process scale-up was effective because of efficient homogenization (using an anchor impeller) and heat transfer. According to the authors, a homogenization after pretreatment is necessary to separate IL from residual solids. Li et al. (2013)[52] reported that the formation of a gel phase following the addition of water can affect solids recovery if homogenization is not performed. In the current study, post-pretreatment homogenization was not necessary, as no gel phase was formed and no solid agglomerates were observed. Residual solids were washed three times with water, and solid–liquid separation was achieved using a bag filter.

Ninomiya et al. (2015) [19] applied ultrasound during sugarcane bagasse pretreatment to enhance process efficiency. In the present study, sonication showed no significant effect on lignin removal or enzymatic digestibility. Sonochemical and sonophysical effects of ultrasound depend on system characteristics and operating conditions, such as viscosity, chemical components, agitation speed, solids loading, and particle size [27,54,55].

Velmurugan et al. (2011)[56] observed that ultrasound and alkali pretreatment of sugarcane bagasse were three times more efficient when combined than when applied individually. The authors concluded that ultrasound promoted radical formation in the NaOH solution, increasing lignin oxidation. Bussemaker et al. (2013)[27] observed that sonochemical and sonophysical effects are dependent on

solids loading and particle size and that high solids loadings (above 5% v/w) hamper the propagation of ultrasonic waves. Accordingly, in the current study, high solids loadings (above 10% w/w) and low ultrasound frequency (19 kHz), which favors sonophysical effects, resulted in the lack of significant effects of ultrasonication.

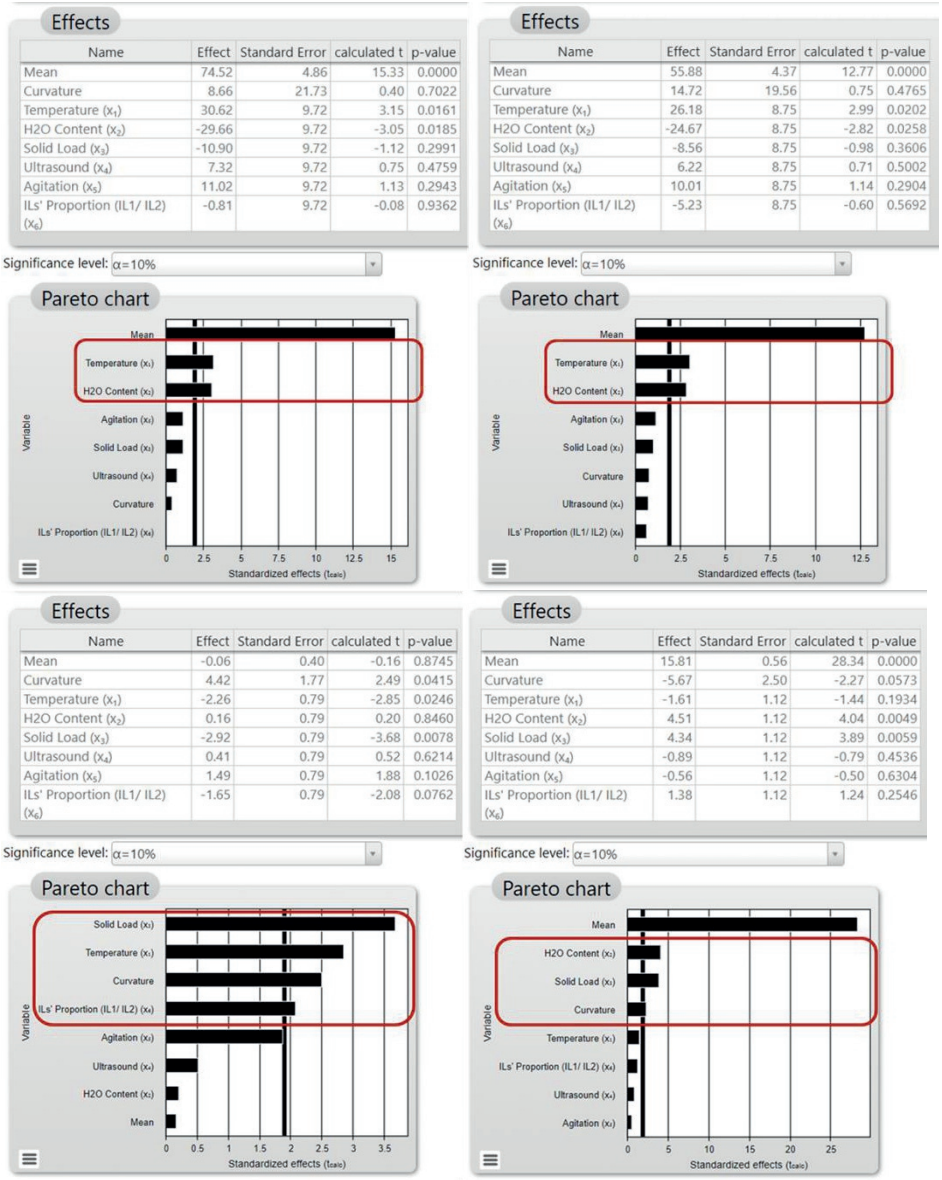

Fig 6: Table of effects and Pareto Chart. Top left: Cellulose enzymatic digestibility. Top right: Hemicellulose enzymatic digestibility. Bottom left: Hemicellulose content. Bottom right: Insoluble Lignin content.

Tab 2: Chemical composition and enzymatic digestibility of residual solids after pretreatment of sugarcane straw under different conditions

	Experimental Set Up						Residual Solid Composition			Enzymatic Digestibility [a]	
Essay	T (°C)	H_2O (%)	S (%)	U (W)	N (rpm)	$IL_{1/2}$ (%)	Cel. (% w/w)	Hem. (% w/w)	Ins. Lign. (% w/w)	Y Cel (%)	Y Hem (%)
nature	-	-	-	-	-	-	38.8	30.1	21.8	5.9	2.7
1	130	10	20	0	3	25	49.0	27.4	16.4	88.8	69.4
2	130	60	10	120	3	25	48.2	32.1	15.5	78.5	55.8
3	80	60	20	0	30	25	41.3	30.3	20.1	17.6	11.2
4	130	10	20	120	3	75	50.4	24.3	14.8	83.3	63.4
5	130	60	10	120	30	25	53.2	30.9	12.4	90.5	77.4
6	130	60	20	0	30	75	45.8	28.3	21.3	96.2	72.8
7	80	60	20	120	3	75	42.4	29.5	19.9	42.6	28.4
8	80	10	20	120	30	25	47.3	31.8	15.4	86.0	64.3
9	80	10	10	120	30	75	47.5	33.0	14.2	88.2	64.6
10	130	10	10	0	30	75	53.3	30.6	9.7	100	74.9
11	80	60	10	0	3	75	42.8	29.7	10.1	32.8	15.5
12	80	10	10	0	3	25	49.3	32.8	10.9	88.1	72.7
13	110	35	15	60	16	50	45.2	32.9	11.8	81.8	58.7
14	110	35	15	60	16	50	49.5	31.3	12.1	81.9	68.4
15	110	35	15	60	16	50	49.3	32.6	15.1	72.8	62.6

[a] Calculated according to Eqs. 1 and 2

The fact that mass and energy transfer are crucial for conversion processes must be taken into account when optimizing IL-based pretreatments. ILs usually have high viscosity, which compromises mass transfer and diffusion in solids, and lignocellulose has poor heating properties, resulting in the formation of a temperature gradient in the reactor. For these reasons, the effect of agitation was evaluated in the 3–30 rpm range. As the system is connected to a heat source via a lateral jacket and temperature is measured at the center of the reactor, agitation was necessary to avoid overheating. Thus, a minimal of 3 rpm was used. Surprisingly, agitation speed did not significantly affect delignification and enzymatic digestibility, but a small effect was observed on hemicellulose extraction. Despite the lack of significance observed in this study, homogeneous heat and mass distributions during biomass pretreatment should always be viewed as essential.

The effect of IL ratio was only significant for hemicellulose removal. High acetate/hexanoate ratios had a negative impact on this parameter. This result might be associated with the ability of acetate anions to cleave hydrogen bonds within the lignocellulosic matrix [16], favoring the separation of hemicellulose from the cellulosic fraction. The effect of solids loading was significant on all responses.

Higher solids loading lead to lower delignification and, consequently, lower percentage of carbohydrates in residual solids. The studied ILs promote lignin dissolution and increasing the proportion of solids entails in higher amounts of lignin to be dissolved. Consequently, a greater redeposition of released lignin on the lignocellulosic matrix may occur because of the presence of high quantities of lignin molecules not completely solvated by ILs. However, the increase in solids loading from 10 to 20% (w/w) did not affect biomass enzymatic digestibility. A similar result was observed by Rocha et al. (2017) [20]. The authors increased solids loading from 5 to 10% (w/w) in the pretreatment of sugarcane bagasse with [Mea][Ac] and obtained similar enzymatic hydrolysis efficiencies under both conditions.

Tab 3: Summary of the effects of process variables on enzymatic digestibility, lignin removal, and hemicellulose removal. Statistical significance was set at $p < 0.10$.

	Removal (residual Solid)		Enz. Digestibility (%)	
Variable	**Hemi.**	**Ins. Lig.**	**Y Cel**	**Y Hemi**
Temp.	++		**+++**	**+++**
H2O		+++++	**+++**	**+++**
Loading	+++	++++		
Ultrasound				
Agitation	+			
IL1/2	++			

Delignification and enzymatic hydrolysis were negatively influenced by a water content of 60% (w/w) in the liquid phase, mainly at lower temperatures (80 °C). However, at high water contents, enzymatic hydrolysis and delignification increased with temperature (runs 2, 5, and 6; Table 2). Lignin removal was lower at a high solids loading (run 6). In general, the increase in temperature had a positive effect on enzymatic digestibility and delignification. Nevertheless, high digestibility yields, above 85% for cellulose and 64% for hemicellulose, were achieved at low temperatures and water content (runs 8, 9, and 12). High delignification values (>35%) were obtained at low temperature (80 °C), low water content, and low solids loading (runs 9 and 12).

The FTIR spectra of residual solids obtained after enzymatic pretreatment were compared with those of untreated SW to investigate changes at the molecular

level. In Figure 7, three spectra are compared: those of raw SW, residual solids obtained in run 3 (worst result), and residual solids obtained in run 10 (best result). Four regions were noticeably altered by pretreatment. The peaks at 900 and 1098 cm^{-1} correspond to amorphous and crystalline cellulose, respectively. The sharper peak at 900 cm^{-1} indicates that intermolecular linkages were affected by the pretreatment, resulting in a higher proportion of amorphous cellulose [48,57,58], i.e., an increase in enzymatic digestibility. The peaks at 1235 and 1733 cm^{-1} are attributed respectively to C–O stretching in hemicellulose–lignin and stretching of C=O ester bonds between hemicellulose and lignin [58,59]. Lower absorbance at these regions indicates the breakage of hemicellulose and lignin bonds. Note that absorbance gradually decreases from the spectrum of raw SW to that of run 10.

The reaction kinetics was evaluated under the conditions of run 10, with modifications (solids loading of 15% w/w and water content of 20% w/w). Ultrasound was not used and agitation speed was fixed at 3 rpm to avoid the formation of a temperature gradient, as previously discussed. Samples were taken at 0.5, 1, 2, 4, 16, and 24 h for determination of chemical composition and enzymatic digestibility.

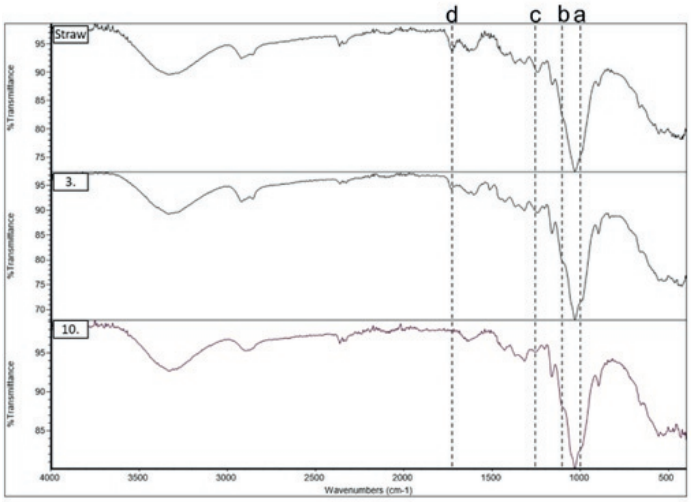

Fig 7: FTIR spectra of untreated sugarcane straw and residual solids obtained in runs 3 and 10 (Table 1). a, 900 cm^{-1}; b, 1098 cm^{-1}; c, 1235 cm^{-1}; and d, 1733 cm^{-1}.

Enzymatic digestibility increased exponentially after 30 min of reaction and reached maximum values in 2 h (Figure 8). The cellulose yield was 93.2%, and hemicellulose yield was 71.1% (12- and 19-fold higher than that of untreated SW, respectively). After 4 h, enzymatic digestibility decreased slightly, which can be

attributed to the redeposition of non-carbohydrate material on exposed fibrils [46,60]. Although biomass particle size was not quantitatively determined, qualitative analysis showed that particle size decreased with the increase in time; the most noticeable changes were seen after 1, 2, and 4 h of treatment, Figure 9. Delignification occurred mainly in the first 2 h, during which 49.5% of insoluble lignin was extracted. In the remaining 22 h, only 20.6% of insoluble lignin was extracted. A total delignification of 70.1% was achieved in 24 h. These results are in accordance with those observed by other authors, who reported that delignification occurs mainly within the first 3 h of pretreatment with protic ILs [20,60]. A significant hemicellulose loss was observed after 4 h of pretreatment. Rocha et al. (2017) used [Mea][Ac] for the pretreatment of biomass and detected a shift in the delignification curve at the same time that a shift in hemicellulose solubilization occurred. This result suggests that after reaching a limit, delignification will only occur with further hemicellulose solubilization. In other words, complete delignification can only be achieved following hemicellulose extraction.

An additional experiment was conducted under the same conditions of the kinetic assay to determine the recovery of residual solids. After 3 h of processing, residual solids were collected and washed. Then, samples were dried and weighed. The material separated by washing was filtered using an analytical paper filter to recover solid particles smaller than 125 μm. A total of 71.2% of initial solids was recovered, 65.2% of which were larger; and 6.6%, smaller than 125 μm. Small particles had higher hemicellulose (38.3%) and lignin (24.2%) contents than large particles (33.8 and 10.7%, respectively). On the other hand, large solids were 72% richer in cellulose than small particles. A schematic flow chart of the process showing the mass balance is presented in Figure 10. Investigation of particle size distribution after pretreatment is an important step to avoid miscalculation of the mass balance (small particles are not to be considered dissolved material) and to better design downstream processes.

Cellulose and hemicellulose yields of 98 and 88%, respectively, were achieved in this last experiment. These good results show that protic ILs are promising for the pretreatment of biomass feedstock [20,60]. The objective of the current study was to identify and understand the impact of each variable on the pretreatment of SW using mixtures of ILs. In future studies, operating conditions must be optimized. Gschwend et al. (2018) optimized the operating conditions for pretreatment of *Miscanthus* using protic IL at lab scale and estimated a reduction on reactor cost around 93%. Optimization of process parameters may lead to a

reduction in processing times and energy consumption and an increase in solids loading, resulting in a more cost-effective process ready for further scale-up.

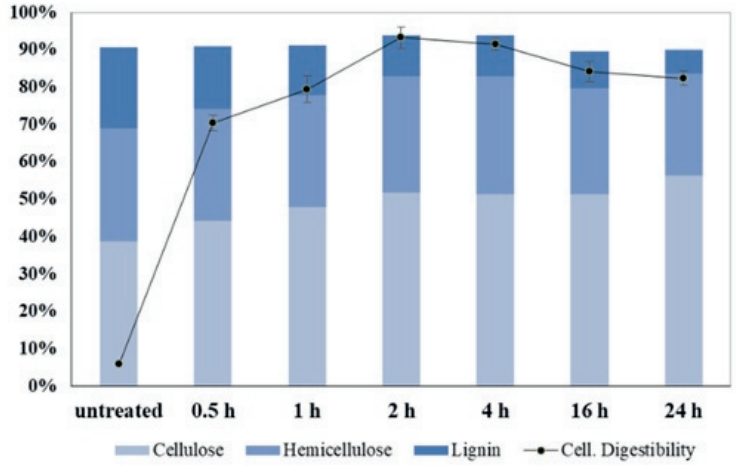

Fig 8: Chemical composition (weight percentage) and cellulose enzymatic digestibility of sugarcane straw residual solids after 0.5, 1, 2, 4, 16, and 24 h of pretreatment. Experimental conditions: 130 °C, 20% (w/w) water content, 15% (w/w) solids loading, no ultrasound, agitation speed of 3 rpm and rate [Mea][Ac]/[Mea][Hex] of 75%/25%.

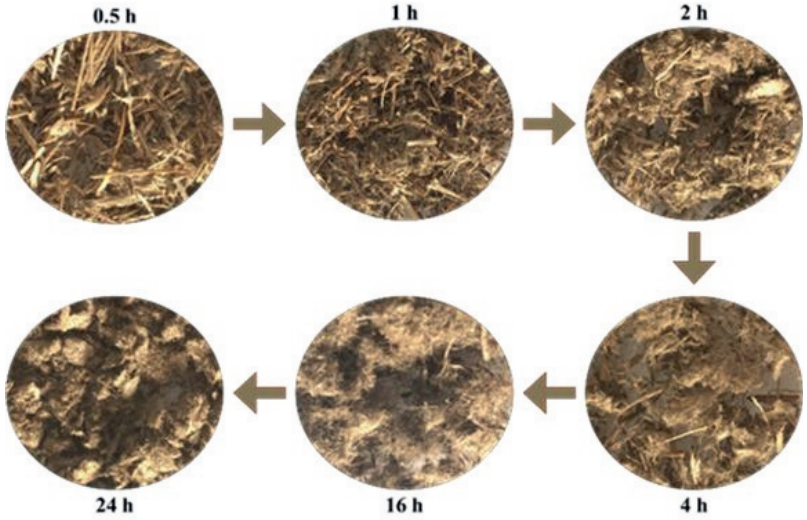

Fig 9: Pre-treated SW at respective process times. Dry material.

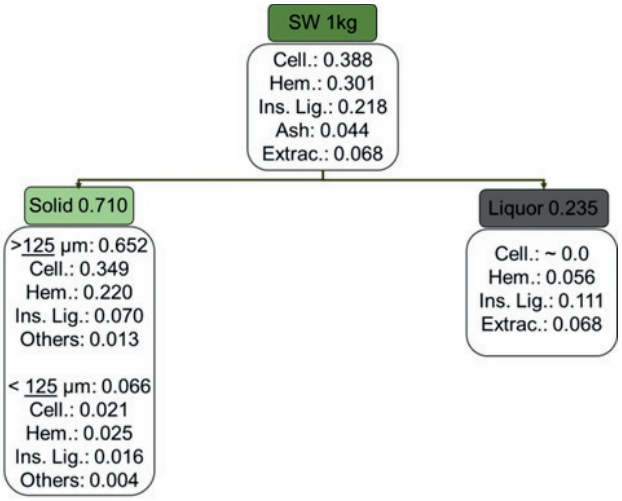

Fig 10: Schematic flow chart showing the mass balance of sugarcane straw pretreatment with a mixture of ionic liquids. Values correspond to the mass fraction starting with 1 kg of biomass.

2.4 Conclusions

The tested ILs exhibited great potential as SW pretreatment agents. Good enzymatic digestibility efficiency was obtained using a 1:1 (w/w) mixture of [Mea][Ac]/[Mea][Hex] at 13 % (w/w) solids loading and water content in the reaction medium at lab scale. Under mild temperature conditions (90 °C), the [Mea][Ac]/[Mea][Hex] mixture increased delignification compared with pure ILs. Although [Emim][Ac] achieved the best enzymatic digestibility at initial conditions (dry material), it had the worst performance following water addition and solid loading increase. Two crucial parameters for scaling up. As such, $[Mea]^+$-based ILs are promising alternatives for industrial-scale processes. The addition of water changed completely the performance of all tested ILs. The screening of ILs, for pretreatment purposes, must address water presence on its assessments, not only dry material. [Mea][Hex] was the only IL that had better performance after water addition regarding enzymatic digestibility.

Ultrasound and agitation speed had no significant effect on delignification, hemicellulose removal, or enzymatic digestibility in the bench scale reactor experiments. The increase in solids loading affected delignification and hemicellulose removal. On the other hand, an increase in solids loading from 10 to 20% (w/w) did not negatively influence enzymatic hydrolysis. A liquid phase water

content of 60% (w/w) reduced delignification and enzymatic digestibility. The increase in temperature had a positive effect on enzymatic digestibility. Water content, temperature and solid loading must be further investigated to improve pretreatment setups. It was noticed that the [Mea][Ac]/[Mea][Hex] mixture is benefit to the process.

Complete delignification is not likely to be achieved without hemicellulose dissolution, even under optimized conditions. The highest enzymatic digestibility was achieved within 2 h of pretreatment. The effect of operating parameters on SW pretreatment using protic ILs was satisfactorily assessed. Temperature, solids loading, water content, and IL ratios must be optimized to reduce process time and energy consumption.

2.5 References

(1) Nejat, P.; Jomehzadeh, F.; Taheri, M. M.; Gohari, M.; Abd. Majid, M. Z. A Global Review of Energy Consumption, CO2 Emissions and Policy in the Residential Sector (with an Overview of the Top Ten CO2 Emitting Countries). *Renew. Sustain. Energy Rev.* **2015**, *43*, 843–862. https://doi.org/10.1016/J.RSER.2014.11.066.

(2) Bilgen, S. Structure and Environmental Impact of Global Energy Consumption. *Renew. Sustain. Energy Rev.* **2014**, *38*, 890–902. https://doi.org/10.1016/J.RSER.2014.07.004.

(3) Dias, M. O. S.; Junqueira, T. L.; Cavalett, O.; Pavanello, L. G.; Cunha, M. P.; Jesus, C. D. F.; Maciel Filho, R.; Bonomi, A. Biorefineries for the Production of First and Second Generation Ethanol and Electricity from Sugarcane. *Appl. Energy* **2013**, *109*, 72–78. https://doi.org/10.1016/J.APENERGY.2013.03.081.

(4) Cherubini, F. The Biorefinery Concept: Using Biomass Instead of Oil for Producing Energy and Chemicals. *Energy Convers. Manag.* **2010**, *51* (7), 1412–1421. https://doi.org/10.1016/J.ENCONMAN.2010.01.015.

(5) Fatih Demirbas, M. Biorefineries for Biofuel Upgrading: A Critical Review. *Appl. Energy* **2009**, *86*, S151–S161. https://doi.org/10.1016/J.APENERGY.2009.04.043.

(6) Singh, S.; Simmons, B. A.; Vogel, K. P. Visualization of Biomass Solubilization and Cellulose Regeneration during Ionic Liquid Pretreatment of Switchgrass. *Biotechnol. Bioeng.* **2009**, *104* (1), 68–75. https://doi.org/10.1002/bit.22386.

(7) Yang, D.; Zhong, L. X.; Yuan, T. Q.; Peng, X. W.; Sun, R. C. Studies on the Structural Characterization of Lignin, Hemicelluloses and Cellulose Fractionated by Ionic Liquid Followed by Alkaline Extraction from Bamboo. *Ind. Crops Prod.* **2013**, *43* (1), 141–149. https://doi.org/10.1016/j.indcrop.2012.07.024.

(8) The Statistics Portal. Sugar cane production worldwide - forecast 2016-2026 https://www.statista.com/statistics/445636/global-sugar-cane-production-forecast/ (accessed Sep 12, 2018).

(9) Wang, M.; Han, J.; Dunn, J. B.; Cai, H.; Elgowainy, A. Well-to-Wheels Energy Use and Greenhouse Gas Emissions of Ethanol from Corn, Sugarcane and Cellulosic Biomass for US Use. *Environ. Res. Lett.* **2012**, *7* (4), 045905. https://doi.org/10.1088/1748-9326/7/4/045905.

(10) Efe, C.; Straathof, a. J. J.; Van der Wielen, L. a. M. *Technical and Economical Feasibility of Production of Ethanol from Sugar Cane and Sugar Cane Bagasse*; 2005.

(11) Agbor, V. B.; Cicek, N.; Sparling, R.; Berlin, A.; Levin, D. B. Biomass Pretreatment: Fundamentals toward Application. *Biotechnol. Adv.* **2011**, *29* (6), 675–685. https://doi.org/10.1016/j.biotechadv.2011.05.005.

(12) Alvira, P.; Tomás-Pejó, E.; Ballesteros, M.; Negro, M. J. Pretreatment Technologies for an Efficient Bioethanol Production Process Based on Enzymatic Hydrolysis: A Review. *Bioresour. Technol.* **2010**, *101* (13), 4851–4861. https://doi.org/10.1016/j.biortech.2009.11.093.

(13) Mussatto, S. I.; Dragone, G. M. Biomass Pretreatment, Biorefineries, and Potential Products for a Bioeconomy Development. *Biomass Fractionation Technol. a Lignocellul. Feed. Based Biorefinery* **2016**, 1–22. https://doi.org/10.1016/B978-0-12-802323-5.00001-3.

(14) Wang, H.; Gurau, G.; Rogers, R. D. Ionic Liquid Processing of Cellulose. *Chem. Soc. Rev.* **2012**, *41* (4), 1519. https://doi.org/10.1039/c2cs15311d.

(15) Laher, T. M.; Hussey, C. L. Copper(I) and Copper(II) Chloro Complexes in the Basic Aluminum Chloride-1-Methyl-3-Ethylimidazolium Chloride Ionic Liquid. *Inorg. Chem.* **1983**, *22* (22), 3247–3251. https://doi.org/10.1021/ic00164a016.

(16) Brandt, A.; Gräsvik, J.; Hallett, J. P.; Welton, T. Deconstruction of Lignocellulosic Biomass with Ionic Liquids. *Green Chem.* **2013**, *15* (3), 550–583. https://doi.org/10.1039/c2gc36364j.

(17) Elgharbawy, A. A.; Alam, M. Z.; Moniruzzaman, M.; Goto, M. Ionic Liquid Pretreatment as Emerging Approaches for Enhanced Enzymatic Hydrolysis of Lignocellulosic Biomass. *Biochem. Eng. J.* **2016**, *109*, 252–267. https://doi.org/10.1016/J.BEJ.2016.01.021.

(18) da Costa Lopes, A. M.; João, K. G.; Morais, A. R. C.; Bogel-Łukasik, E.; Bogel-Łukasik, R. Ionic Liquids as a Tool for Lignocellulosic Biomass Fractionation. *Sustain. Chem. Process.* **2013**, *1* (1), 3. https://doi.org/10.1186/2043-7129-1-3.

(19) Ninomiya, K.; Kohori, A.; Tatsumi, M.; Osawa, K.; Endo, T.; Kakuchi, R.; Ogino, C.; Shimizu, N.; Takahashi, K. Ionic Liquid/Ultrasound Pretreatment and in Situ Enzymatic Saccharification of Bagasse Using Biocompatible Cholinium Ionic Liquid. *Bioresour. Technol.* **2015**, *176*, 169–174. https://doi.org/10.1016/j.biortech.2014.11.038.

(20) Rocha, E. G. A.; Pin, T. C.; Rabelo, S. C.; Costa, A. C. Evaluation of the Use of Protic Ionic Liquids on Biomass Fractionation. *Fuel* **2017**, *206*, 145–154. https://doi.org/10.1016/j.fuel.2017.06.014.

(21) Chambon, C. L.; Mkhize, T. Y.; Reddy, P.; Brandt-Talbot, A.; Deenadayalu, N.; Fennell, P. S.; Hallett, J. P. Pretreatment of South African Sugarcane Bagasse Using a Low-Cost Protic Ionic Liquid: A Comparison of Whole, Depithed, Fibrous and Pith Bagasse Fractions. *Biotechnol. Biofuels* **2018**, *11* (1), 247. https://doi.org/10.1186/s13068-018-1247-0.

(22) Chambon, C. L.; Chen, M.; Fennell, P. S.; Hallett, J. P. Efficient Fractionation of Lignin- and Ash-Rich Agricultural Residues Following Treatment With a Low-Cost Protic Ionic Liquid. *Front. Chem.* **2019**, *7* (April), 1–13. https://doi.org/10.3389/fchem.2019.00246.

(23) George, A.; Brandt, A.; Tran, K.; Zahari, S. M. S. N. S.; Klein-Marcuschamer, D.; Sun, N.; Sathitsuksanoh, N.; Shi, J.; Stavila, V.; Parthasarathi, R.; et al. Design of Low-Cost Ionic Liquids for Lignocellulosic Biomass Pretreatment. *Green Chem.* **2015**, *17* (3), 1728–1734. https://doi.org/10.1039/C4GC01208A.

(24) Klein-Marcuschamer, D.; Simmons, B. A.; Blanch, H. W. Techno-Economic Analysis of a Lignocellulosic Ethanol Biorefinery with Ionic Liquid Pre-Treatment. *Biofuels, Bioprod. Biorefining* **2011**, *5* (5), 562–569. https://doi.org/10.1002/bbb.303.

(25) Konda, N. M.; Shi, J.; Singh, S.; Blanch, H. W.; Simmons, B. A.; Klein-Marcuschamer, D. Understanding Cost Drivers and Economic Potential of Two Variants of Ionic Liquid Pretreatment for Cellulosic Biofuel Production. *Biotechnol. Biofuels* **2014**, *7* (1), 1–11. https://doi.org/10.1186/1754-6834-7-86.

(26) Elgharbawy, A. A.; Alam, M. Z.; Moniruzzaman, M.; Goto, M. Ionic Liquid Pretreatment as Emerging Approaches for Enhanced Enzymatic Hydrolysis of Lignocellulosic Biomass. *Biochemical Engineering Journal*. Elsevier May 15, 2016, pp 252–267. https://doi.org/10.1016/j.bej.2016.01.021.

(27) Bussemaker, M. J.; Xu, F.; Zhang, D. Manipulation of Ultrasonic Effects on Lignocellulose by Varying the Frequency, Particle Size, Loading and Stirring. *Bioresour. Technol.* **2013**, *148*, 15–23. https://doi.org/10.1016/j.biortech.2013.08.106.

(28) Aung, E. M.; Endo, T.; Fujii, S.; Kuroda, K.; Ninomiya, K.; Takahashi, K. Efficient Pretreatment of Bagasse at High Loading in an Ionic Liquid. *Ind. Crops Prod.* **2018**, *119*, 243–248. https://doi.org/10.1016/j.indcrop.2018.04.006.

(29) Liu, Y.; Chen, J.; Lu, X.; Ji, X.; Wang, C. Reducing the Agitation Power Consumption in Anaerobic Digestion of Corn Straw by Adjusting the Rheological Properties. *Energy Procedia* **2019**, *158*, 1267–1272. https://doi.org/10.1016/J.EGYPRO.2019.01.314.

(30) Parthasarathi, R.; Sun, J.; Dutta, T.; Sun, N.; Pattathil, S.; Murthy Konda, N. V. S. N.; Peralta, A. G.; Simmons, B. A.; Singh, S. Activation of Lignocellulosic Biomass for Higher Sugar Yields Using Aqueous Ionic Liquid at Low Severity Process Conditions. *Biotechnol. Biofuels* **2016**, *9* (1), 1–13. https://doi.org/10.1186/s13068-016-0561-7.

(31) Sluiter, A.; Hames, B.; Ruiz, R.; Scarlata, C.; Sluiter, J.; Templeton, D.; Nrel, D. C. Determination of Structural Carbohydrates and Lignin in Biomass Determination of Structural Carbohydrates and Lignin in Biomass. *Contract* **2010**, *2011* (June).

(32) Qiu, Z.; Aita, G. M.; Walker, M. S. Effect of Ionic Liquid Pretreatment on the Chemical Composition, Structure and Enzymatic Hydrolysis of Energy Cane Bagasse. *Bioresour. Technol.* **2012**, *117*, 251–256. https://doi.org/10.1016/J.BIORTECH.2012.04.070.

(33) Rodrigues, M. I.; Iemma, A. F. *Experimental Design and Process Optimization*, 1 st Editi.; CRC Press: São Paulo, 2014.

(34) Ninomiya, K.; Omote, S.; Ogino, C.; Kuroda, K.; Noguchi, M.; Endo, T.; Kakuchi, R.; Shimizu, N.; Takahashi, K. Saccharification and Ethanol Fermentation from Cholinium Ionic Liquid-Pretreated Bagasse with a Different Number of Post-Pretreatment Washings. *Bioresour. Technol.* **2015**, *189*, 203–209. https://doi.org/10.1016/j.biortech.2015.04.022.

(35) An, Y. X.; Zong, M. H.; Wu, H.; Li, N. Pretreatment of Lignocellulosic Biomass with Renewable Cholinium Ionic Liquids: Biomass Fractionation, Enzymatic Digestion and Ionic Liquid Reuse. *Bioresour. Technol.* **2015**, *192*, 165–171. https://doi.org/10.1016/j.biortech.2015.05.064.

(36) Sánchez, P. B.; García, J.; Pádua, A. A. H. Structural Effects on Dynamic and Energetic Properties of Mixtures of Ionic Liquids and Water. *J. Mol. Liq.* **2017**, *242*, 204–212. https://doi.org/10.1016/j.molliq.2017.06.109.

(37) Lateef, H.; Grimes, S.; Kewcharoenwong, P.; Feinberg, B. Separation and Recovery of Cellulose and Lignin Using Ionic Liquids: A Process for Recovery from Paper-Based Waste. *J. Chem. Technol. Biotechnol.* **2009**, *84* (12), 1818–1827. https://doi.org/10.1002/jctb.2251.

(38) Sun, J.; Konda, N. V. S. N. M.; Parthasarathi, R.; Dutta, T.; Valiev, M.; Xu, F.; Simmons, B. A.; Singh, S. One-Pot Integrated Biofuel Production Using Low-Cost Biocompatible Protic Ionic Liquids. *Green Chem.* **2017**, *19* (13), 3152–3163. https://doi.org/10.1039/C7GC01179B.

(39) Lee, S. H.; Doherty, T. V.; Linhardt, R. J.; Dordick, J. S. Ionic Liquid-Mediated Selective Extraction of Lignin from Wood Leading to Enhanced Enzymatic Cellulose Hydrolysis. *Biotechnol. Bioeng.* **2009**, *102* (5), 1368–1376. https://doi.org/10.1002/bit.22179.

(40) Lu, B.; Xu, A.; Wang, J. Cation Does Matter: How Cationic Structure Affects the Dissolution of Cellulose in Ionic Liquids. *Green Chem.* **2014**, *16* (3), 1326–1335. https://doi.org/10.1039/c3gc41733f.

(41) Kuo, C.-H.; Lee, C.-K. Enhancement of Enzymatic Saccharification of Cellulose by Cellulose Dissolution Pretreatments. *Carbohydr. Polym.* **2009**, *77* (1), 41–46. https://doi.org/10.1016/j.carbpol.2008.12.003.

(42) Fort, D. a.; Remsing, R. C.; Swatloski, R. P.; Moyna, P.; Moyna, G.; Rogers, R. D. Can Ionic Liquids Dissolve Wood? Processing and Analysis of Lignocellulosic Materials with 1-n-Butyl-3-Methylimidazolium Chloride. *Green Chem.* **2007**, *9* (1), 63. https://doi.org/10.1039/b607614a.

(43) Pinkert, A.; Marsh, K. N.; Pang, S. Reflections on the Solubility of Cellulose. *Ind. Eng. Chem. Res.* **2010**, *49* (22), 11121–11130. https://doi.org/10.1021/ie1006596.

(44) Haykir, N. I.; Bahcegul, E.; Bicak, N.; Bakir, U. Pretreatment of Cotton Stalk with Ionic Liquids Including 2-Hydroxy Ethyl Ammonium Formate to Enhance Biomass Digestibility. *Ind. Crops Prod.* **2013**, *41*, 430–436. https://doi.org/10.1016/J.INDCROP.2012.04.041.

(45) Li, H.; Pu, Y.; Kumar, R.; Ragauskas, A. J.; Wyman, C. E. Investigation of Lignin Deposition on Cellulose during Hydrothermal Pretreatment, Its Effect on Cellulose Hydrolysis, and Underlying Mechanisms. *Biotechnol. Bioeng.* **2014**, *111* (3), 485–492. https://doi.org/10.1002/bit.25108.

(46) Driemeier, C.; Oliveira, M. M.; Curvelo, A. A. S. Lignin Contributions to the Nanoscale Porosity of Raw and Treated Lignocelluloses as Observed by Calorimetric Thermoporometry. *Ind. Crops Prod.* **2016**, *82*, 114–117. https://doi.org/10.1016/j.indcrop.2015.11.084.

(47) Ma, C.; Laaksonen, A.; Liu, C.; Lu, X.; Ji, X. The Peculiar Effect of Water on Ionic Liquids and Deep Eutectic Solvents. *Chem. Soc. Rev.* **2018**, *47* (23), 8685–8720. https://doi.org/10.1039/C8CS00325D.

(48) Shi, J.; Balamurugan, K.; Parthasarathi, R.; Sathitsuksanoh, N.; Zhang, S.; Stavila, V.; Subramanian, V.; Simmons, B. A.; Singh, S. Understanding the Role of Water during Ionic Liquid Pretreatment of Lignocellulose: Co-Solvent or Anti-Solvent? *Green Chem.* **2014**, *16* (8), 3830–3840. https://doi.org/10.1039/c4gc00373j.

(49) Canongia Lopes, J. N.; Costa Gomes, M. F.; Pádua, A. A. H. Nonpolar, Polar, and Associating Solutes in Ionic Liquids. *J. Phys. Chem. B* **2006**, *110* (34), 16816–16818. https://doi.org/10.1021/jp063603r.

(50) Canongia Lopes, J. N. A.; Pádua, A. A. H. Nanostructural Organization in Ionic Liquids. *J. Phys. Chem. B* **2006**, *110* (7), 3330–3335. https://doi.org/10.1021/jp056006y.

(51) Fagernäs, L.; Brammer, J.; Wilén, C.; Lauer, M.; Verhoeff, F. Drying of Biomass for Second Generation Synfuel Production. *Biomass and Bioenergy* **2010**, *34* (9), 1267–1277. https://doi.org/10.1016/J.BIOMBIOE.2010.04.005.

(52) Li, C.; Tanjore, D.; He, W.; Wong, J.; Gardner, J. L.; Sale, K. L.; Simmons, B. A.; Singh, S. Scale-up and Evaluation of High Solid Ionic Liquid Pretreatment and Enzymatic Hydrolysis of Switchgrass. *Biotechnol. Biofuels* **2013**, *6* (1), 154. https://doi.org/10.1186/1754-6834-6-154.

(53) Li, C.; Tanjore, D.; He, W.; Wong, J.; Gardner, J. L.; Thompson, V. S.; Yancey, N. A.; Sale, K. L.; Simmons, B. A.; Singh, S. Scale-Up of Ionic Liquid-Based Fractionation of Single and Mixed Feedstocks. **2015**, 982–991. https://doi.org/10.1007/s12155-015-9587-0.

(54) Velmurugan, R.; Muthukumar, K. Ultrasound-Assisted Alkaline Pretreatment of Sugarcane Bagasse for Fermentable Sugar Production: Optimization through Response Surface Methodology. *Bioresour. Technol.* **2012**, *112*, 293–299. https://doi.org/10.1016/j.biortech.2012.01.168.

(55) García, A.; Alriols, M. G.; Llano-Ponte, R.; Labidi, J. Ultrasound-Assisted Fractionation of the Lignocellulosic Material. *Bioresour. Technol.* **2011**, *102* (10), 6326–6330. https://doi.org/10.1016/j.biortech.2011.02.045.

(56) Velmurugan, R.; Muthukumar, K. Utilization of Sugarcane Bagasse for Bioethanol Production: Sono-Assisted Acid Hydrolysis Approach. *Bioresour. Technol.* **2011**, *102* (14), 7119–7123. https://doi.org/10.1016/j.biortech.2011.04.045.

(57) Yoon, L. W.; Ngoh, G. C.; May Chua, A. S.; Hashim, M. A. Comparison of Ionic Liquid, Acid and Alkali Pretreatments for Sugarcane Bagasse Enzymatic Saccharification. *J. Chem. Technol. Biotechnol.* **2011**, *86* (10), 1342–1348. https://doi.org/10.1002/jctb.2651.

(58) Li, C.; Knierim, B.; Manisseri, C.; Arora, R.; Scheller, H. V.; Auer, M.; Vogel, K. P.; Simmons, B. A.; Singh, S. Comparison of Dilute Acid and Ionic Liquid Pretreatment of Switchgrass: Biomass Recalcitrance, Delignification and Enzymatic Saccharification. *Bioresour. Technol.* **2010**, *101* (13), 4900–4906. https://doi.org/10.1016/j.biortech.2009.10.066.

(59) Hsu, T. C.; Guo, G. L.; Chen, W. H.; Hwang, W. S. Effect of Dilute Acid Pretreatment of Rice Straw on Structural Properties and Enzymatic Hydrolysis. *Bioresour. Technol.* **2010**, *101* (13), 4907–4913. https://doi.org/10.1016/j.biortech.2009.10.009.

(60) Brandt-Talbot, A.; Gschwend, F. J. V.; Fennell, P. S.; Lammens, T. M.; Tan, B.; Weale, J.; Hallett, J. P. An Economically Viable Ionic Liquid for the Fractionation of Lignocellulosic Biomass. *Green Chem.* **2017**, *19* (13), 3078–3102. https://doi.org/10.1039/c7gc00705a.

Chapter 3[2]

Complete Continuous Ionic Liquid Recycle From Aqueous Streams through Freeze Concentration

Ionic Liquids (ILs) can be designed by combining a diverse number of molecules, tuning desired properties for specific applications. The extensive possible applications range from gas adsorption to complex matrix dissolution, such as lignocellulosic materials. Although interesting for their flexibility, ILs can have a carbon-intensive production background, may be toxic and expensive. Thereby, it is essential to efficiently recycle them. This work presents a process scheme for ILs recycling, and their mixtures, from aqueous streams, without mass loss, by means of freeze concentration (FC). Process examples using 2-hydroxyethylammonium acetate ([Mea][Ac]) and 2-hydroxyethylammonium hexanoate ([Mea][Hex]) were explored. Their freezing point in aqueous solutions were determined in the concentration range of 0.5% to 50 % (w/w). The water activity and IL aggregation were investigated within the range. Water from [Mea][Hex] solutions crystallized at higher temperatures than [Mea][Ac]. [Mea][Hex] showed a similar freezing curve as that from an organic acid. The ILs were efficiently recycled whether pure or mixed, without mass loss by the FC process. The FC can be operated in continuous mode without waste generation and removing water as pure as desired.

[2] Chapter submitted to Separation and Purification Technology as: Ferrari, F. A., Wielen, L. A. M., Forte, M. B. S., Witkamp, G. J. Complete Continuous Ionic Liquid Recycle From Aqueous Streams through Freeze Concentration

3.1 Introduction

The expansion in the number of studies involving Ionic Liquids (IL) in the past 20 years is partly due to the vast range of possible applications of ILs. Based on process requirements, one can design ILs by combining different cations and anions, tuning desired properties, such as conductivity, vapor pressure, H bonding potential, density and catalytic sites [1–3].

Such diversity accredits ILs application as solvent for a wide range of applications from catalysis to gas adsorption [4]. Referred to as tailored solvents, ILs have been considered due to their capability to selectively dissolve different materials depending on ions involved [5,6]. The processing of lignocellulosic material (LC) is a good example to illustrate ILs' solvent character. LC's composition encompasses a range of different biopolymers, clustered in 3 main constituents, which vary according to LC's origin: i) 40-80% cellulose; ii) 10-40% hemicellulose; iii) 5- 36% lignin [5]. ILs can be solvents for LC processing in biorefineries, where LC is dissolved and then can be converted into valuable chemicals, fuel, and electricity. The initial step in which IL and LC come together is called pretreatment (PT)[7]. Moreover, ILs are commonly addressed as possible green solvents due to their potential to present low vapor pressure, non-flammability and recycle possibility. However, it is important to make clear that ILs can have a carbon-intensive production background, equal or exceeding those of regular solvents, incompatible with a sustainable development strategy [8]. Besides, certain ILs may present toxicity levels comparable to that from commercial bactericides[9]. Finally, price is a key factor for IL large-scale application [10]. Therefore, an efficient IL recycle is not only desirable but mandatory for industrial applications.

Considering the vast use possibilities, several IL recycling methods have been reported, such as evaporation, liquid-liquid extraction, pervaporation and electrodialysis [4,11–13]. Strategies based on membrane separation usually are limited by IL high viscosity and membrane fouling; additionally, some IL may demand more expensive material for membranes to avoid degradation, which might affect process' operational costs [12,14]. Evaporating the solvent from IL-aqueous streams is energy consuming due to the high heat of water evaporation. Besides, acid-based IL will add the corrosion hurdle to equipment, and some IL may degrade due to heating and chemical reactions, even at low temperatures [12,14,15]. Liquid-liquid extraction using organic solvents is also possible, but the use of organic solvents is incompatible with the "green" appeal and adds the combustion risks to the process [14]. Alternatively, aqueous biphasic system (ABS) by the addition of kosmotropic salts could be an easy way to recovery IL from an aqueous stream [16]. Nevertheless, salt must be also recycled considering process sustainability.

A recent study demonstrated the feasibility to crystallize water out of IL-water mixtures by cooling down the system [17]. Consequently, crystallized water could be removed as ice from the bulk, recycling the IL in a more concentrated stream. Freeze crystallization has been considered as an alternative strategy for water desalination [18], which accredits the method for large-scale applications. Moreover, energy costs can be significantly reduced, van der Ham et al [19] studied the crystallization of $CuSO_4$ from aqueous stream, reducing in 70 % in the total energy costs by means of freeze crystallization in comparison to traditional multiple-effect evaporation. Operating at low temperatures would also prevent IL degradation, and could be used as a strategy for systems containing thermo-sensitive molecules.

Therefore, the present work assesses the freeze concentration (FC) process as a strategy for IL recycle from aqueous streams. The study considers two ethanolamine based ILs and their mixtures, namely 2-hydroxyethylammonium acetate ([Mea][Ac]) and 2-hydroxyethylammonium hexanoate ([Mea][Hex]). ILs designed from ethanolamine cations and organic acids anions are remarked as efficient solvents in biomass applications [7,20]. Besides, at bulk scale production, ammonium based ILs might be a cost-effective alternative to regular organic solvents, [21]. The outputs from this study are organized in 4 parts: i) salt addition as phase promoters for the ILs recycle in ABS; ii) assessment of freezing points temperatures of various IL-water compositions; iii) water removal and purity using model solutions and a LC pretreated liquor; iv) process flowchart, mass balance, and energy consumption. During the present work, we also highlight limitations and alternatives for the hurdles found.

3.2 Material And Method

3.2.1 Chemicals and Synthesis of ILs

Kraft lignin, chemicals for IL synthesis and standards were purchased from Sigma−Aldrich (Germany) and used as received. 2-Hydroxyethylammonium acetate ([Mea][Ac]) and 2-hydroxyethylammonium hexanoate ([Mea][Hex]), as shown in Figure 1, were synthesized in 500 mL Schott flasks by a one-step, acid−base exothermic neutralization method, in which a proton (H^+) is transferred to the NH_2 group of an amino alcohol reagent, conferring a positive charge to the molecule (NH_3^+).

First, ethanolamine was weighed into a flask. The flask was closed with a silicone septum and placed in a cold-water bath. An equimolar quantity of either acetic acid or hexanoic acid was slowly added through the septum using a syringe. The reaction was carried out overnight at room temperature under agitation. The

formation of [Mea][Ac] or [Mea][Hex] was confirmed by proton nuclear magnetic resonance (^{1}H NMR), as detailed in the Appendix. The water content, measured by Karl Fischer titration, for [Mea][Ac] or [Mea][Hex] was 0.53 and 0.58 % (w/w), respectively.

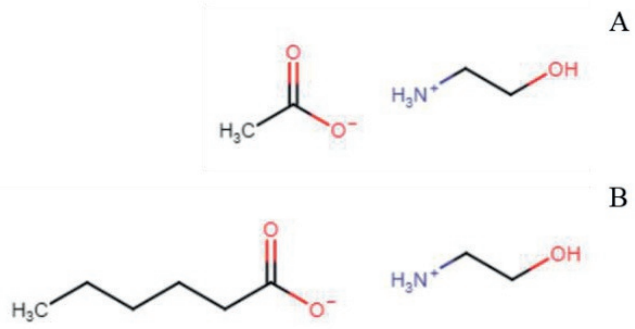

Fig 1: A- 2-hydroxyethylammonium acetate ([Mea][Ac]); B - 2-hydroxyethylammonium hexanoate ([Mea][Hex])

3.2.2 Freezing Process

Freezing point determination and FC experiments were conducted in a triple-layered glass reactor (Laboratory Glass Specialists, Assen, The Netherlands), as shown in Figure 2, equipped with an anchor impeller with silicon scrapers on edges. The triple layer was comprised of an internal cooling jacket, and an external vacuum insulation chamber. The temperature was monitored using a calibrated pt 100 thermometer with a precision of ± 0.01 °C. The reactor was connected to a Proline RP4090 CW Kryomat® (LAUDA, Germany) low-temperature thermostat and the coolant fluid used was the silicone oil Kryo 90 ® (LAUDA, Germany). The system was connected to a computer and data acquired in real-time.

The freezing point was determined of IL and MilliQ water mixtures, and the concentration calculated based on the weight of each component. The serial composition was achieved from both sides, by sequential addition of water to the IL and IL to the water solutions, respectively. The temperature was lowered until ice was observed upon seeding. The freezing point was determined by visual observation and confirmed by the presence of the corresponding exothermic peak in temperature. After each point, the temperature was raised until no ice was observed anymore, then IL or water was added for the next measurement. In order

to avoid underestimation of the freezing point, the system was let stabilize for 10 min before temperature changes. The reverse experiment where also conducted, where the freezing point was assessed by the melting point while increasing the temperature. The hysteresis was observed to be within the range between 0.5 -7 K, with the higher differences, between melting and freezing, found at lower temperatures.

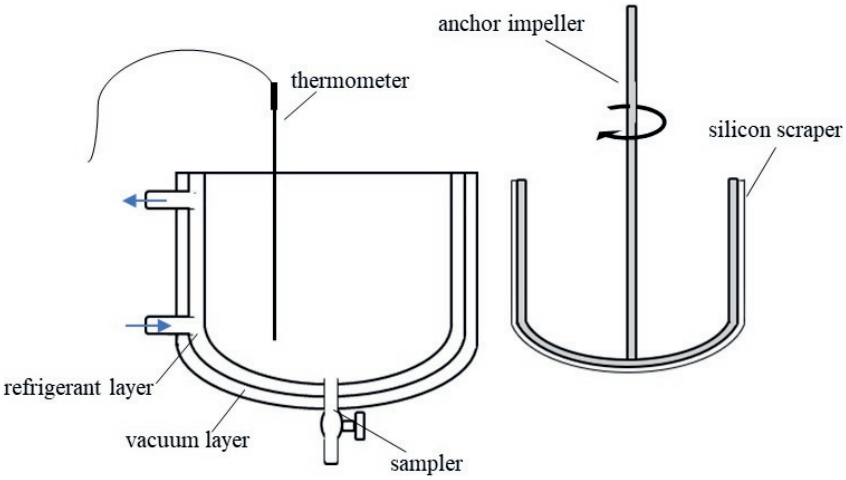

Fig 2: Freeze crystallization reactor

3.2.3 Ice Wash

Ice was harvested from the top of crystallizer, Figure 3, using a stainless-steel sieve, kept in freezer at -18 °C before each use. The ice mass was set to not exceed 10 % (w/w) of total batch and by the complete filling of the stainless-steel sieve during the sampling, the excess of liquid was drained, the ice fraction weighted, and the of 50 ± 1,3 g of ice was standardized after multiple repetitions. Therefore, ice was harvested and directly used in the wash experiments to prevent melting while weighing. The collected ice was disposed in a jacked glass filter kept at -5 °C, then, 15 ml of ice bath cooled MilliQ water were added, followed by vacuum filtration, without complete reslurrying the ice crystal cake. The retained ice and the liquid permeated were collected after each wash step for analysis.

3.2.4 Lignocellulosic Pretreated Liquor

For the pre-treatment, we assumed the best choice design described in a previous work (Chapter 2)[7], which assessed different conditions for the pre-treatment of sugarcane straw. Approximately 37 g of sugarcane straw was pretreated in a stainless-steel reactor using a mixture of 10 %(w/w) H_2O, 68 %(w/w) [Mea][Ac] and 22 %(w/w) [Mea][Hex], at 20 %(w/w) of solid loading and 130 °C (Ferrari et al, 2019). After 4 h of reaction, pretreated biomass was washed with demineralized water, solid and liquid were separated using a 125 μm pore size bag filter. IL concentration in liquor was about 20 %(w/w).

3.2.5 Analytical Method

IL concentrations were determined by acetate and hexanoate quantified in HPLC with an Aminex HPX-87H column from Biorad, coupled to a RI and UV detector, using 0.01M phosphoric acid as eluent at a flow rate of 0.6 $ml.min^{-1}$. Concentrations were calculated from calibration curves of [Mea][Ac] and [Mea][Hex]. Lignin concentration was determined by spectrophotometer absorbance at 280 nm and calculated from the calibration curve of kraft lignin.

3.3 Results And Discussion

3.3.1 Water-IL separation by Salting Out

Kosmotropic salts, such as phosphate-based, can be used as phase separation promoters in aqueous biphasic systems containing IL [22]. This principle could be used to concentrate ILs from aqueous streams by salting out, for instance [Mea][Ac], from water. Then, the salt could be recycled, for example, by eutectic freeze crystallization (EFC). Thereby, to determine the phase diagram of [Mea][Ac] and [Mea][Hex] in water, a 50 %(w/w) K_3PO_4 solution was slowly added to the IL/ H_2O mixture (50 % w/w) , following the cloud point procedure described elsewhere [23]. In addition to PO_4^{3-}, K_2HPO_4 was also tried for phase separation. However, no phase separation was observed in any tested condition, suggesting that these ILs cannot be salted out from water and, consequently, ABS using salts is not a feasible strategy for [Mea][Ac] and [Mea][Hex] recycle.

The absence of phase formation might be explained by the presence of OH and NH_3^+ groups in [Mea] and COO^- group in the anions, remarked for H-bonding, which stabilize the IL-H_2O bulk structure. In addition, the pH influence on proton transfer between the carboxylic acid and the ethanolamine might also play a role.

After measuring different solutions pH (data not shown), it was observed that K_3PO_4 solution did cause more pH change than K_2HPO_4 while increasing [Mea][Ac] concentration. Taking into consideration the pKa values of the species involved, i.e. NH_3^+ (9.55), HPO_4^{2-} (6.95) and PO_4^{3-} (12.9), it is possible to infer that K_3PO_4 might affect the proton transfer between the carboxylic acid and ammonia in [Mea][Ac]. It is valid to mention that if it holds true that K_3PO_4 influences the proton transfer in [Mea][Ac] it would also impact the IL formation, affecting the system's properties and functionalities.

Taken together the aforementioned, the IL-H_2O stream was directed to Freeze Concentration (FC) step, without prior concentration by salt addition.

3.3.2 Water-IL separation by Freeze concentration (FC)

First, the freezing point of water was determined for several concentrations for both IL-species, namely [Mea][Ac] and [Mea][Hex]. Results from chapter 2[7] show that both ILs have great potential for lignocellulose pre-treatment (PT) and that their combination can be used as a strategy to improve PT efficiency according to process' necessities. Therefore, a mixture of [Mea][Ac] and [Mea][Hex] in a molar fraction of 0.75:0.25, respectively, was also included in this study. The freezing points of water for ethanolamine (Mea) and acetic acid (HAc) solutions were incorporated for comparison.

In Figure 1, the freezing point of water is plotted against the solute concentration (as wt% and as molal) for the different systems. The freezing point curves of almost all solutions follow the same trend when expressed as function of solute mass fraction, within the reported range. The exception concerns [Mea][Hex], exhibiting water freezing at higher temperatures. When plotted against molality, as shown in Figure 1-B, the differences in the freezing point drop among solutions are more evident, especially above 2 molal. Under 2 molal, the highest difference within the freezing point did not exceed 1.5 °C. The freezing point depression curve of [Mea][Ac] lies in between those of its precursors Mea and HAc. Conversely, [Mea][Hex] showed a freezing curve profile similar to that from small organic acids, such as acetic and butyric[24]. In a closer look to Figure 1-B, it is possible to note that the slopes of the [Mea][Hex] and H.Ac freezing curves from about 6 molal becom less negative. Converting these into molar fraction, the slope change from both components happens close to 0.9 water molar fraction. Using the data from Noshadi and Sadehi [24] for propionic acid and doing the same calculation, the shift happens at 0.87 water molar fraction. The freezing point of [Mea][Hex] aqueous solution should be assessed in more concentrated regions to investigate a

possible eutectic point for this component. [Mea][Ac] aqueous solution might not reach the eutectic point. The increase in viscosity, which lead to the increase in the observed standard deviation in temperature measurements, due to worse heat transfer not compensated by agitation, and the glass appearance of the material (Figure 2) observed in the lowest temperature, suggest that [Mea][Ac]-water system is more likely to exhibit a glass transition instead of the eutectic point.

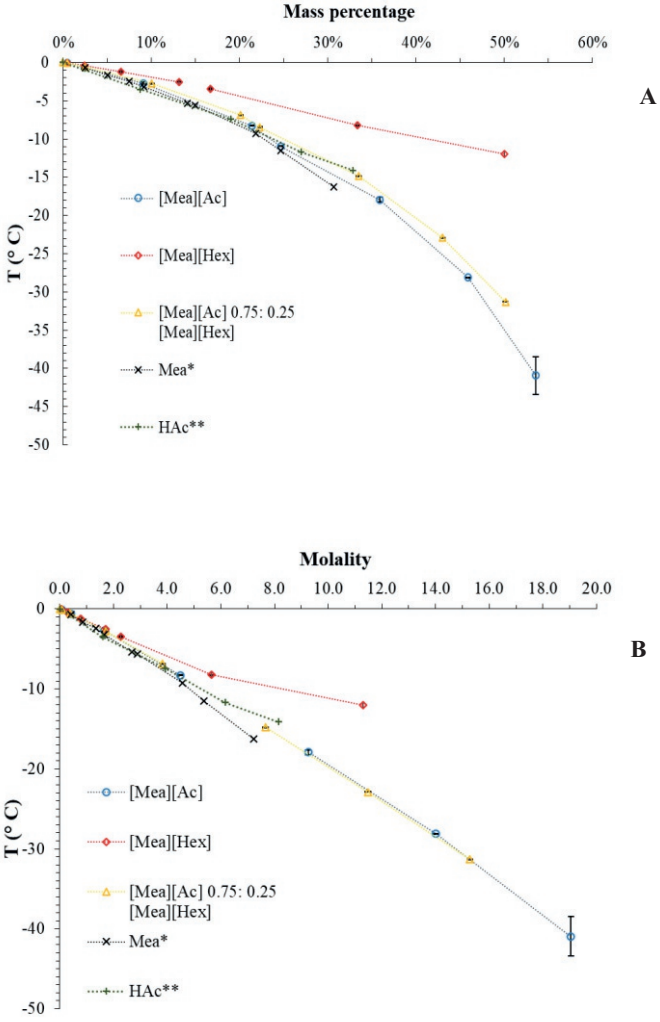

Fig 1: Freezing point of water as a function of solution composition expressed in A as mass percentage and B as molality. Molality assumes IL dissociation into cation and anion. Lines plotted for guidance. *Data from Louldrup et al. [25]. ** Data from Noshadi and Sadehi [24].

Fig 2: [Mea][Ac] in detail at the lowest tested temperature (– 45 °C)

Freezing point depression is a colligative property dependent on the solvent and proportional to solute molality, expressed according to equation 1 for ideal systems:

$$\Delta T_f = -\mathrm{k}_f . m \qquad \text{eq. 1}$$

where ΔT_f is the variation in freezing point, k_f is the cryoscopic constant of the solvent (1.858 K.kg.mol^{-1}, for water) and m is solute molality considering IL dissociation into anion and cation. Ma *et al* [26] proposed a framework to model the IL-water systems, suggesting a level of IL association dependent on its concentration. Therefore, the results of freezing point depression were considered in terms of Bjerrum's osmotic coefficient "Φ", relating the observed to the theoretical freezing point depression, according to equation 2. Values between 0 and 1 indicate a smaller freezing point depression than that assuming complete dissociation. Since the number of solute particles mostly determines ΔT_f, Φ would indicate, to a first approximation, an average degree of IL association.

$$\Phi = \frac{\Delta T_f}{\mathrm{k}_f . m} \qquad \text{eq. 2}$$

From the results of Φ in Table 1 it is possible to observe that systems with [Mea][Ac] behave closely to ideality. The increase in Φ beyond 4.5 molal and 3.8 molal, pure [Mea][Ac] and mixture respectively, could be occasioned by small differences between the temperature measured and initial crystallization, due to increasing viscosity. [Mea][Hex]-water system, in turn, seems to exhibit a certain degree of association progressively to molality increase. While Φ relates to the solute's degree of aggregation, water activity (a_w) expresses the ratio between partial vapor pressure of water in a substance and the standard vapor pressure of pure water. In other words, how easy the water content may be utilized. For IL-water separation, a_w is an important parameter, since the higher a_w the lower is the energy consumed, per mole of pure water, during the freezing process. The value of a_w can be accurately calculated from the freezing point, assuming a_w at to the solid-liquid equilibrium during the freezing process, the change in standard state enthalpy (273.15 K) with temperature, and applying the Hildebrand and Scott's equation[27,28].

Considering the equilibrium at the freezing point:

$$H_2O_{(S)} \leftrightarrow H_2O_{(l)} \qquad \text{eq.3}$$

water and ice coexist in equilibrium, so that the tendency of ice melts is the same as that to water solidifies. In terms of chemical potential,

$$\mu_{w(s)} = \mu_{w(l)} \qquad \text{eq.4}$$

where μ_w stands for the chemical potential of water, subscripts (l) and (s) for liquid and solid states, respectively. The addition of ionic liquid in the solution will affect the aforementioned equilibrium by changing the chemical potential of liquid water. In ideal solutions, the change in chemical potential is given by equation 5,

$$\mu_{w(l)} = \mu_w^* + RTln\, x_w \qquad \text{eq.5}$$

where μ_w^* is the chemical potential of pure liquid water, R is the gas constant (8.314 J.mol-1K-1), x_w is the water mol fraction and T the absolute temperature. The introduction of an extra term is necessary to cope with deviations from ideality, the activity coefficient γ_w. The γ_w times the molar fraction of water (x_w) gives the water activity, thus eq.5 is better represented as,

$$\mu_{w(l)} = \mu_w^* + RTln\, a_w \qquad \text{eq.6}$$

at the freezing point and isolating the activity term, one finds,

$$ln\ a_w = \frac{\left(\mu_{w(s)} - \mu_w^*\right)}{RT} \qquad \text{eq.7}$$

the derivative of both sides with respect to T results,

$$\frac{dln\ a_w}{dT} = -\frac{\left(\mu_{w(s)} - \mu_w^*\right)}{RT^2} + \frac{\left(\frac{d\mu_{w(s)}}{dT} + \frac{d\mu_w^*}{dT}\right)}{RT} \qquad \text{eq.8}$$

at the equilibrium there is no assignment for temperature and pressure change so that μ= G = H- TS. At constant pressure$\left(\frac{d\mu}{dT}\right)_P = -S$, from the thermodynamics first law and Gibbs - Duhem relation $Vdp - SdT + \sum_i \mu_i dN_i = 0$ [(equilibrium)], then, eq.8 can be reduced to,

$$\frac{ln\ a_w}{dT} = -\frac{\left(H_{w(s)} - H_w^*\right)}{RT^2} = \frac{\Delta H_f}{RT^2} \qquad \text{eq.9}$$

the integration of eq.9 from T to the melting point To, then,

$$lna_w = -\frac{\Delta H_f}{R} . \frac{T_o - T}{T.T_o} \qquad \text{eq.10}$$

the difference of heat capacity of solid water and liquid is ΔC_p, and $\Delta H_f = \Delta H^* - \Delta C_p$, where ΔH^* is water enthalpy of fusion, then, the integration of eq.10 gives the Hildebrand and Scott's equation, eq. 11,

$$ln\ a_{w(f)} = -\frac{\Delta H^*}{R}\left(\frac{1}{T_f} - \frac{1}{273.15}\right) - \frac{\Delta C_p}{R}\left[\frac{T_f - (273.15)}{T_f} - ln\left(\frac{T_f}{273.15}\right)\right] \qquad \text{eq. 11}$$

where, ΔH^* is water enthalpy of fusion (6009.5 $J.mol^{-1}$), R is the universal gas constant (8.314 $J.mol^{-1}.K^{-1}$), T_f is the freezing point in K and ΔC_p is water specific heat capacity change (37.87 $J.mol^{-1}.K^{-1}$). Correspondingly, the a_w values also indicate a distinguished profile between [Mea][Hex] and [Mea][Ac]. The longer alkyl chain from hexanoate increases the number of hydrophobic binding sites [29] and favors IL clustering, thus increasing water activity, which leads to higher freezing temperatures. Interestingly, the IL mixture did not follow a middle term

outline between that of [Mea][Ac] and [Mea][Hex], it exhibited fairly the same pattern observed on [Mea][Ac] solutions instead.

It is valid to mention that for a process in which it is essential to have [Mea][Ac] at lower water concentration than 50 %(w/w), one must incorporate an additional step for further water removal. The choice of strategies to remove water involving heating, such as distillation, must address potential IL decomposition and energy costs.

Table 1: Freezing point depression, molality, Bjerrum's osmotic coefficient Φ and water activity a_w for studied IL-water systems

[Mea][Ac]				[Mea][Hex]				[Mea][Ac]:[Mea][Hex]			
ΔT_f* (K)	Molality ($mol.kg_{H2O}^{-1}$)	Φ	a_w	ΔT_f* (K)	Molality ($mol.kg_{H2O}^{-1}$)	Φ	a_w	ΔT_f* (K)	Molality ($mol.kg_{H2O}^{-1}$)	Φ	a_w
0	0	-	1.000	0	0	-	1.000	0	0	-	1.000
-0.15	0.08	0.98	0.999	-0.12	0.06	-	1.000	-0.13	0.08	0.92	0.999
-0.74	0.41	0.96	0.994	-0.5	0.28	0.95	0.996	-0.65	0.40	0.88	0.995
-2.79	1.65	0.91	0.974	-1.29	0.79	0.88	0.988	-2.86	1.70	0.90	0.973
-8.36	4.50	1.00	0.923	-2.62	1.71	0.83	0.976	-6.95	3.83	0.98	0.935
-18.02	9.25	1.05	0.839	-3.55	2.27	0.84	0.967	-14.91	7.66	1.05	0.865
-28.22	14.01	1.08	0.759	-8.32	5.65	0.79	0.923	-22.99	11.48	1.08	0.799
-41.03	19.04	1.16	0.668	-12.07	11.30	0.57	0.890	-31.37	15.28	1.10	0.736

*calculated from measured temperatures; - values not considered

3.3.3 Ice Slurry Wash

After crystallization of water, ice is removed from the top of IL concentrated bulk, as seen in Figure 3. However, the ice fraction still has contaminants from the bulk that, if not enclosed inside during crystallization, can be washed out. IL entrainment in the ice stream would lead to IL losses and environmental restrictions concerning removed water end-use, as shown in figure 4.

To assess the level of IL contamination and the efficiency of wash, 50 g of ice was harvested from the crystallizer top after half an hour from the freezing point begin. The starting solution was composed of 25 % (w/w) of an IL molar mixture, [Mea][Ac] 0.75: [Mea][Hex] 0.25, in water. The model solution considers the characteristics described in chapter 2 for a post-PT stream [7]. The ice sampled from

the crystallizer without previous the wash process is labeled as the step “0”. Then, 15 ml of demineralized water, previously cooled in ice, were added, without complete reslurrying. Water was removed by vacuum in glass filters kept at -5 °C, and the process repeated in “n” wash steps. IL concentrations in melted ice, after each wash step, are presented in Figure 5.

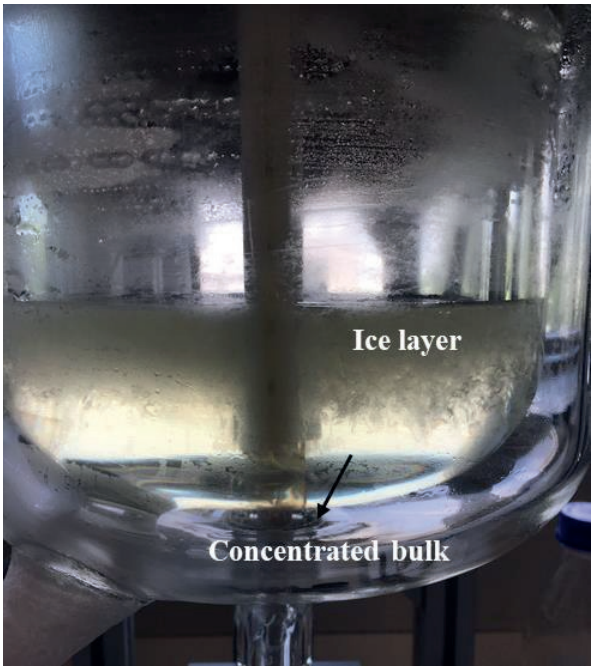

Fig 3: Reactor during Freeze Concentration of [Mea][Ac]. Ice layer on top and concentrated bulk on the bottom

From figure 5-A, 86 % of IL was removed in the very first trial and 99 % of the total in the second step. By mass balance calculation, approximately 10 %(w/w) of the ice sample consists of adhering mother liquor. Considering the log of IL concentration against wash steps, Figure 5-B, more or less linear correlation is observed. These indicate that the IL present in ice is probably prevenient from adhering bulk liquor. Therefore, it is possible to remove water as pure as desired by tuning wash process design [30]. The ratio between the concentrations of $[Ac]^-$ and $[Hex]^-$ anions measured in all streams during the wash process was the same as that from the initial solution, indicating that no preferential remove, or partition, happened in the tested conditions.

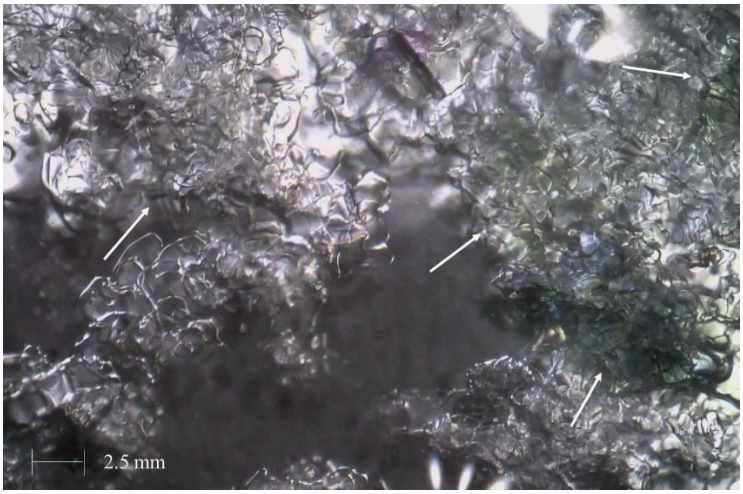

Fig 4: Colored shades indicating IL contamination, white arrows, in melting ice harvested from crystallizer. Difference in coloring was not observed in washed ice melting.

In the just mentioned experiment, pure water is added in every step, so that in a closed process all percolated liquid coming from each wash must be combined, resulting in a single stream to be recycled to the crystallizer. From now on, this strategy will be addressed as crossflow wash (CF). To investigate an alternative approach, a counter-current (CC) strategy was assessed. In the CC process, the percolated liquid from step "n" was used to wash a more contaminated ice slurry, step "n-1". Then, the resulting stream was used for step "n-2", and on. The objective was to reduce water volume by using pure water only in the final wash step. Experiments were conducted using the same starting solution and wash method already described. Results comparing CF and CC performance are depicted in Figure 6.

Both strategies removed IL from ice slurry almost in its totality after 3 washes, carrying away 99.6 % and 98.6 % of initial concentration, CF and CC respectively. As expected, the reduction profile from CF has a steeper slope than CC, nevertheless, the final differences tend to fade considering more efficient washing designs than the manual method employed during the experiments. The water volume used in three steps wash was 3 times smaller for CC than CF, consequently, higher IL concentration was obtained in the resulting percolated stream.

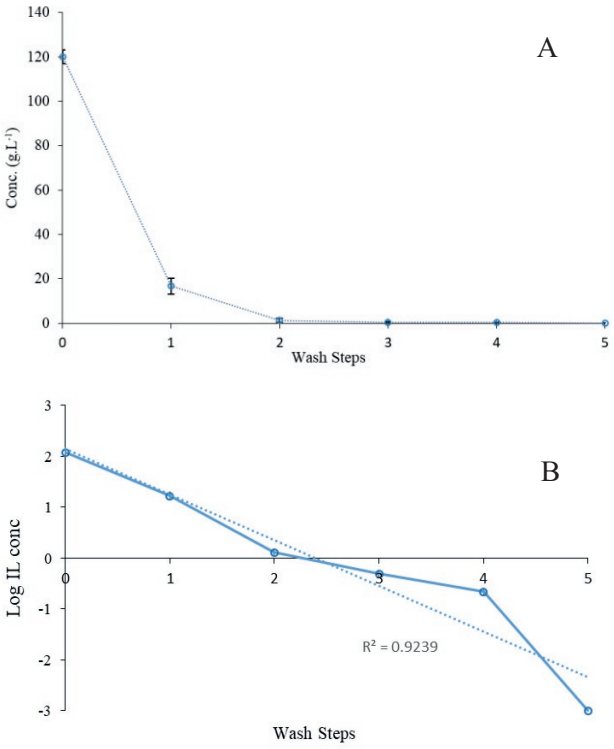

Fig 5: IL Impurity in melted ice fraction after each wash step: A- concentration in g.L-1,line plotted for guidance; B- log of concentration, doted line represent the linear regression, solid line plotted for guidance.

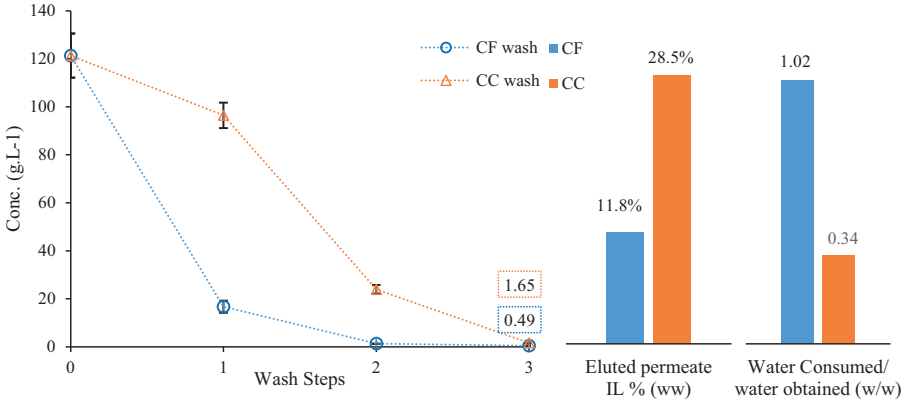

Fig 6: IL's concentration after successive washes. The dots and lines represent the residual concentration in ice. On right-sided bars, the final concentration in the eluted permeate and the amount of water consumed per L o water obtained: crossflow (CF) and counter-current (CC) wash.

The use of IL as a solvent for complex matrix dissolution, such as lignocellulosic feedstock, entails in many potential contaminants to be washout from ice slurry using the CC strategy. After good results with a model solution, a real PT stream was used to assess the viability of water removal by freeze concentration and CC wash. The aqueous solution used is prevenient from sugarcane straw pre-treatment. In short, it has in composition 20 % (w/w) of IL molar mixture, [Mea][Ac] 0.75: 0.25 [Mea][Hex], 3 %(w/w) of lignin and other minor contaminants, such as sugars, water accounts approximately 75 %(w/w). A more detailed composition and PT conditions were described in chapter 2^7. The starting solution froze at -4.5 °C, a little bit higher than the expected -6.8 °C observed with the model solution at the same IL concentration. In order to assess the accuracy of freezing point the melting point was checked by increasing temperature experiment, then followed by the freezing point repetition, where -4.5 °C is the average of freezing experiments. The difference might be due to IL decomposition during PT, contaminants bonded to IL hindering IL-water interaction, or a combination of both. The freezing process was kept for 15 min until enough ice available for harvesting and wash followed the CC process already described. The efficiency of wash was measured in terms of lignin removal. Lignin was chosen to evaluate wash quality due to 3 aspects: i) is the major component in the solution after IL; ii) it is a complex material, a potential source of different size molecules contaminants; iii) it is easy and reliably quantified using a spectrophotometer. The results of CC efficiency are depicted in Figure 7.

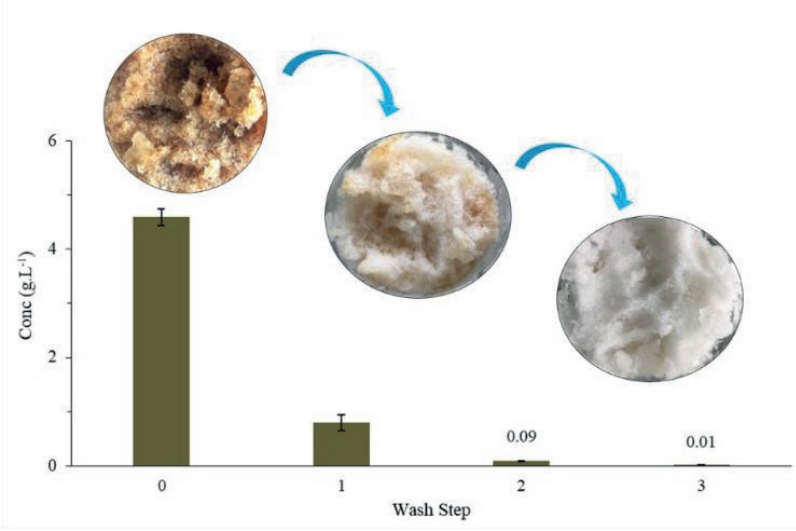

Fig 7: Lignin concentration in melted ice (bars) after sequential CC wash. Pictures were taken from ice during washing cycles.

Lignin was removed in almost its totality, 99.7 % of initial concentration after 3 washes. Lignin was easier washed out than IL in the very first wash step. Probably the higher water-IL affinity led to a greater exclusion of lignin out of the surrounding film on ice surface. Lignin precipitation was not observed on the reactor bottom during the cooling process at -5 °C.

3.3.4 Freeze Concentration Process

In the FC process, by cooling down the system an initial IL aqueous stream will originate three others, to be precise, concentrated IL, ice and the recycle stream. It will require a certain amount of work (W), which is dependent, for instance, on the amount of heat removed from the system, working temperature and the thermodynamic work of separation, and, then, reject to the environment, namely, cooling duty (Q_{duty}). The work is performed following the Carnot cycle, where a gas refrigerant is vaporized subtracting heat from the system in the crystallizer. The heat transferred from crystallizer plus the heat produced during the gas compression are rejected in a condenser. The ratio of Q_{duty} to the power required gives the system coefficient of performance (COP). One way to increase the COP is by improving the heat recovery. There are two ways of doing so. The first one is to use the ice produced to cool down the feed stream reducing Q_{duty}. The second one is to use ice to cool down the condenser after the crystallizer so that the compression power is considerably reduced. Whether using strategy one or two is dependent on process conditions and necessities and must be addressed considering one's system. The gain by reducing the compression power in strategy 2 must compensate the increase in Q_{duty} due to a larger temperature gradient between the feed stream and crystallizer, then, strategy 2 which is more likely to happen at higher temperatures of crystallization [31].

The energy requirements assumed in the present work consider the values from Ham [31] for the eutectic freezing crystallization of $MgCl_2$. It is a reasonable assumption given the proximity between the operation temperature, -36 °C for $MgCl_2$ and -31° C for the present work. In this system, ice heat of melting is used to cool down the feed stream, following strategy 1 for heat recovery. The process' theoretical flowchart is depicted in Figure 8. For the mass and energy calculations an IL-water stream is assumed. Therefore, the lignin would be removed in previous steps, for example, by means of precipitation and adsorption [32–34].

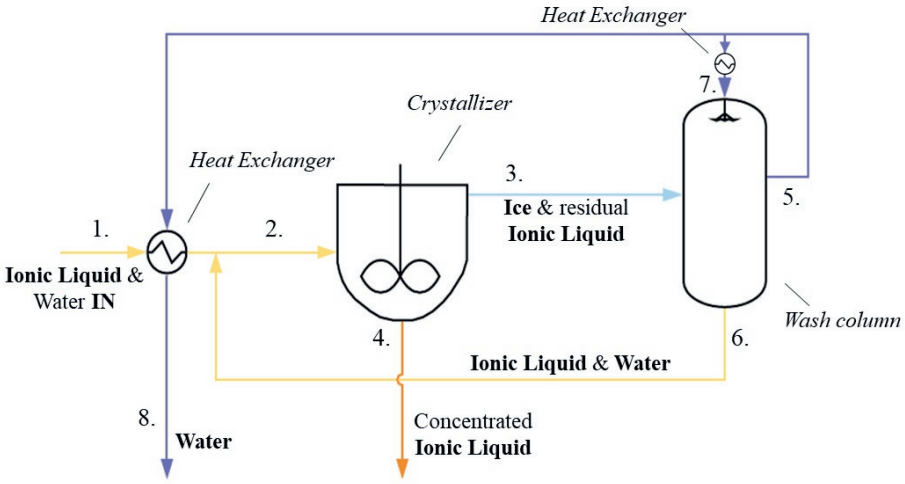

Fig 8: FC process flowchart. The numbers indicate independent streams.

The FC is a closed process demanding only electricity and the feed stream (1) to operate. The water necessary for wash, stream 7, comes from molten ice from stream 5. During the wash, cooler ice from crystallizer (3) is heated by part of water liquid in 7, which in turns solidify. The net mass of liquid in pure water flow 7 that solidifies during wash can be calculated by water mass and energy balance in the wash column according to equation 12.

$$m_s \,.\, \Delta H_{ice} = m_{2ice} \,.\, C_{Pice} \,.\, \Delta T \qquad \text{eq. 12}$$

where m_s is the mass of solidified water, ΔH_{ice} is the latent heat of ice (334 $kJ.kg^{-1}$), m_{2ice} is the mass of ice in 3, C_{Pice} is the heat capacity of ice (2.08 $kJ.kg^{-1}.K^{-1}$) and ΔT is the temperature difference between streams 3 (-31 °C) and 7 (0 °C).

The amount of water for washing is especially important for the process; too little would not wash ice crystals properly or be solidified due to heat transfer in the wash column. On the other hand, too much would generate a large volume in recycle flow 6, consequently, increasing significantly stream 2. A large recycle volume rises investment cost due to larger equipment requirements, especially the crystallizer, an expensive unit due to its complexity, which might accounts for

almost 50% of the capital expenditure (CAPEX) [31]. It would also increase operational costs since equipment would consume more energy. The size of 7 is, then, dependent on the amount of ice to be washed in 3 and is calculated as the mass ratio between stream 7 and ice in 3, namely wash ratio. Therefore, mass balances were considered, and the increase in feed stream (2) was calculated as a function of the wash ratio, depicted in Figure 9.

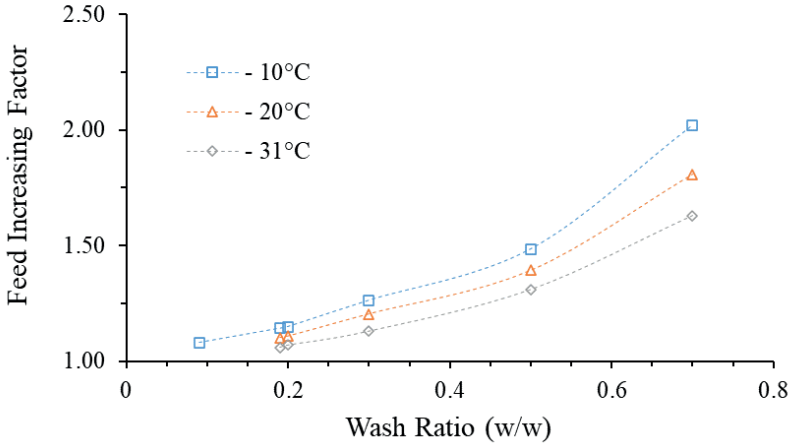

Fig 9: The increasing factor in feed stream 2 as a function of the wash ratio. The washing stream was calculated as a mass percent of the ice entering the wash column. See Figure 7 for labels.

In Figure 9, an increasing factor of 1 means that the mass entering the crystallizer (2) is the same as that from stream 1 (see Figure 8). A factor of 2 means that a mass two times greater than that coming from the upstream process in entering the crystallizer. Although it is possible to find in the literature that the wash ratio might be as low as 0.09 (w/w) [31] this value is not applicable to the present work; hence all water would be solidified due to heat transfer with ice. Thereby, the wash ratio is temperature dependent. The calculated minimum value for the wash ratio is 0.19 (w/w).

Considering above mentioned, the wash ratio was set in 0.20 (w/w). The mass balance was calculated considering a feed stream of 1 ton of 23 % (w/w) IL mixture, 0.75 [Mea][Ac]: 0.25 [Mea][Hex] molar fraction, in water. According to Figure 8, the increasing factor in feed stream for a wash ratio of 20 % is 1.08 and results are presented in Table 2.

Table 2: Streams' composition and mass balance for FC process. Labels are depicted in Figure 8.

Stream	Components (ton)		
	Water	[Mea][Ac]	[Mea][Hex]
1.	0.770	0.155	0.075
2.	0.778	0.202	0.098
3.	0.548	0.047	0.023
4.	0.230	0.155	0.075
5.	0.650	-	-
6.	0.008	0.047	0.023
7.	0.110	-	-
8.	0.540	-	-
Energy consumption: 40 kWh.t_{feed}^{-1} / equivalent to 74 kWh.t_{ice}^{-1}			

-: not present in that stream

3.4 Conclusions

Diluted [Mea][Ac] and [Mea][Hex] aqueous streams were efficiently concentrated to 50 % (w/w), without IL loss. After concentration, anions' proportion of [Mea][Ac]: [Mea]Hex] 0.75:0.25 molar mixture, respectively, was the same of that from initial solution. [Mea][Hex] might be further concentrated, beyond 50 %(w/w), using the FC method, additional experiments are needed though. It is possible to remove water as pure as wanted by tuning the wash process design, which increases water end-use possibilities.

The wash ratio will directly affect wash efficiency and the increasing factor. Lower volumes must consider wash methods more efficient, such as centrifuges and belt filters to separate and wash ice crystals, which in turn consumes more energy. Higher volumes will increase operational dimensions, increasing the capital expenditure. This tradeoff must be addressed by a techno-economic assessment.

FC is a promising method for IL recycling, since it increases IL concentration without losses.

3.5 References

(1) Albert, J.; Müller, K. A Group Contribution Method for the Thermal Properties of Ionic Liquids. *Ind. Eng. Chem. Res.* **2014**, *53* (44), 17522–17526. https://doi.org/10.1021/ie503366p.

(2) Bastos, J. C.; Carvalho, S. F.; Welton, T.; Canongia Lopes, J. N.; Rebelo, L. P. N.; Shimizu, K.; Araújo, J. M. M.; Pereiro, A. B. Design of Task-Specific Fluorinated Ionic Liquids: Nanosegregation versus Hydrogen-Bonding Ability in Aqueous Solutions. *Chem. Commun.* **2018**, *54* (28), 3524–3527. https://doi.org/10.1039/C8CC00361K.

(3) Brooks, N. J.; Castiglione, F.; Doherty, C. M.; Dolan, A.; Hill, A. J.; Hunt, P. A.; Matthews, R. P.; Mauri, M.; Mele, A.; Simonutti, R.; Villar-Garcia, I. J.; Weber, C. C.; Welton, T. Linking the Structures, Free Volumes, and Properties of Ionic Liquid Mixtures. *Chem. Sci.* **2017**, *8* (9), 6359–6374. https://doi.org/10.1039/C7SC01407D.

(4) Wang, B.; Qin, L.; Mu, T.; Xue, Z.; Gao, G. Are Ionic Liquids Chemically Stable? *Chem. Rev.* **2017**, *117* (10), 7113–7131. https://doi.org/10.1021/acs.chemrev.6b00594.

(5) Brandt, A.; Gräsvik, J.; Hallett, J. P.; Welton, T. Deconstruction of Lignocellulosic Biomass with Ionic Liquids. *Green Chem.* **2013**, *15* (3), 550–583. https://doi.org/10.1039/c2gc36364j.

(6) Orr, V. C. A.; Rehmann, L. Ionic Liquids for the Fractionation of Microalgae Biomass. *Current Opinion in Green and Sustainable Chemistry*. Elsevier October 1, 2016, pp 22–27. https://doi.org/10.1016/j.cogsc.2016.09.006.

(7) Ferrari, F. A.; Pereira, J. F. B.; Witkamp, G. J.; Forte, M. B. S. Which Variables Matter for Process Design and Scale-up? A Study of Sugar Cane Straw Pretreatment Using Low-Cost and Easily Synthesizable Ionic Liquids. *ACS Sustain. Chem. Eng.* **2019**, *7* (15), 12779–12788. https://doi.org/10.1021/acssuschemeng.9b01385.

(8) Wu, B.; Dai, C.; Chen, B.; Yu, G.; Liu, N.; Xu, R. Ionic Liquid versus Traditional Volatile Organic Solvent in the Natural Gas Dehydration Process: A Comparison from a Life Cycle Perspective. *ACS Sustain. Chem. Eng.* **2019**, *7* (23), 19194–19201. https://doi.org/10.1021/acssuschemeng.9b05194.

(9) Oliveira, M. V. S.; Vidal, B. T.; Melo, C. M.; de Miranda, R. de C. M.; Soares, C. M. F.; Coutinho, J. A. P.; Ventura, S. P. M.; Mattedi, S.; Lima, Á. S. (Eco)Toxicity and Biodegradability of Protic Ionic Liquids. *Chemosphere* **2016**, *147*, 460–466. https://doi.org/10.1016/j.chemosphere.2015.11.016.

(10) Konda, N. M.; Shi, J.; Singh, S.; Blanch, H. W.; Simmons, B. A.; Klein-Marcuschamer, D. Understanding Cost Drivers and Economic Potential of Two Variants of Ionic Liquid Pretreatment for Cellulosic Biofuel Production. *Biotechnol. Biofuels* **2014**, *7* (1), 1–11. https://doi.org/10.1186/1754-6834-7-86.

(11) Shukla, S. K.; Pandey, S.; Pandey, S. Applications of Ionic Liquids in Biphasic Separation: Aqueous Biphasic Systems and Liquid–Liquid Equilibria. *J. Chromatogr. A* **2018**, *1559*, 44–61. https://doi.org/10.1016/J.CHROMA.2017.10.019.

(12) Sun, J.; Shi, J.; Murthy Konda, N. V. S. N.; Campos, D.; Liu, D.; Nemser, S.; Shamshina, J.; Dutta, T.; Berton, P.; Gurau, G.; Rogers, R. D.; Simmons, B. A.; Singh, S. Efficient Dehydration and Recovery of Ionic Liquid after Lignocellulosic Processing Using Pervaporation. *Biotechnol. Biofuels* **2017**, *1* (1), 1–14. https://doi.org/10.1186/s13068-017-0842-9.

(13) Ninomiya, K.; Kohori, A.; Tatsumi, M.; Osawa, K.; Endo, T.; Kakuchi, R.; Ogino, C.; Shimizu, N.; Takahashi, K. Ionic Liquid/Ultrasound Pretreatment and in Situ Enzymatic Saccharification of Bagasse Using Biocompatible Cholinium Ionic Liquid. *Bioresour. Technol.* **2015**, *176*, 169–174. https://doi.org/10.1016/j.biortech.2014.11.038.

(14) Wu, B.; Liu, W. W.; Zhang, Y. M.; Wang, H. P. Do We Understand the Recyclability of Ionic Liquids? *Chem. - A Eur. J.* **2009**, *15* (8), 1804–1810. https://doi.org/10.1002/chem.200801509.

(15) Chhotaray, P. K.; Gardas, R. L. Thermophysical Properties of Ammonium and Hydroxylammonium Protic Ionic Liquids. *J. Chem. Thermodyn.* **2014**, *72*, 117–124. https://doi.org/10.1016/j.jct.2014.01.004.

(16) Shill, K.; Padmanabhan, S.; Xin, Q.; Prausnitz, J. M.; Clark, D. S.; Blanch, H. W. Ionic Liquid Pretreatment of Cellulosic Biomass: Enzymatic Hydrolysis and Ionic Liquid Recycle. *Biotechnol. Bioeng.* **2011**, *108* (3), 511–520. https://doi.org/10.1002/bit.23014.

(17) Liu, Y.; Meyer, A. S.; Nie, Y.; Zhang, S.; Zhao, Y.; Fosbøl, P. L.; Thomsen, K. Freezing Point Determination of Water–Ionic Liquid Mixtures. *J. Chem. Eng. Data* **2017**, *62* (8), 2374–2383. https://doi.org/10.1021/acs.jced.7b00274.

(18) Kalista, B.; Shin, H.; Cho, J.; Jang, A. Current Development and Future Prospect Review of Freeze Desalination. *Desalination* **2018**, *447*, 167–181. https://doi.org/10.1016/j.desal.2018.09.009.

(19) van der Ham, F.; Witkamp, G. J.; de Graauw, J.; van Rosmalen, G. M. Eutectic Freeze Crystallization: Application to Process Streams and Waste Water Purification. *Chem. Eng. Process. Process Intensif.* **1998**, *37* (2), 207–213. https://doi.org/10.1016/S0255-2701(97)00055-X.

(20) Pin, T. C.; Nakasu, P. Y. S.; Mattedi, S.; Rabelo, S. C.; Costa, A. C. Screening of Protic Ionic Liquids for Sugarcane Bagasse Pretreatment. *Fuel* **2019**, *235* (July 2018), 1506–1514. https://doi.org/10.1016/j.fuel.2018.08.122.

(21) Chen, L.; Sharifzadeh, M.; Mac Dowell, N.; Welton, T.; Shah, N.; Hallett, J. P. Inexpensive Ionic Liquids: [HSO4]--Based Solvent Production at Bulk Scale. *Green Chem.* **2014**, *16* (6), 3098–3106. https://doi.org/10.1039/c4gc00016a.

(22) Dupont, D.; Depuydt, D.; Binnemans, K. Overview of the Effect of Salts on Biphasic Ionic Liquid/Water Solvent Extraction Systems: Anion Exchange, Mutual Solubility, and Thermomorphic Properties. *J. Phys. Chem. B* **2015**, *119* (22), 6747–6757. https://doi.org/10.1021/acs.jpcb.5b02980.

(23) Trindade, J. R.; Visak, Z. P.; Blesic, M.; Marrucho, I. M.; Coutinho, J. A. P.; Canongia Lopes, J. N.; Rebelo, L. P. N. Salting-out Effects in Aqueous Ionic Liquid Solutions: Cloud-Point Temperature Shifts. *J. Phys. Chem. B* **2007**, *111* (18), 4737–4741. https://doi.org/10.1021/jp067022d.

(24) Noshadi, S.; Sadeghi, R. Differential Scanning Calorimetry Determination of Phase Diagrams and Water Activities of Aqueous Carboxylic Acid Solutions. *Thermochim. Acta* **2018**, *663*, 46–52. https://doi.org/10.1016/j.tca.2018.03.002.

(25) Fosbøl, P. L.; Pedersen, M. G.; Thomsen, K. Freezing Point Depressions of Aqueous MEA, MDEA, and MEA-MDEA Measured with a New Apparatus. *J. Chem. Eng. Data* **2011**, *56* (4), 995–1000. https://doi.org/10.1021/je100994v.

(26) Ma, C.; Laaksonen, A.; Liu, C.; Lu, X.; Ji, X. The Peculiar Effect of Water on Ionic Liquids and Deep Eutectic Solvents. *Chem. Soc. Rev.* **2018**, *47* (23), 8685–8720. https://doi.org/10.1039/C8CS00325D.

(27) Arrad, M.; Kaddami, M.; Sippola, H.; Taskinen, P. Determination of Pitzer Parameters for Ferric Nitrate from Freezing Point and Solubility of Ice. **2015**, No. 1, 1–5. https://doi.org/10.1021/acs.jced.5b00822.

(28) Hildebrand, J. H.; Scott, R. L. *Regular Solutions*; Prentice Hall: Englewood Cliffs, 1962.

(29) Canongia Lopes, J. N.; Costa Gomes, M. F.; Pádua, A. A. H. Nonpolar, Polar, and Associating Solutes in Ionic Liquids. *J. Phys. Chem. B* **2006**, *110* (34), 16816–16818. https://doi.org/10.1021/jp063603r.

(30) Vaessen, R.; Seckler, M.; Witkamp, G. J. Eutectic Freeze Crystallization with an Aqueous KNO3-HNO 3 Solution in a 100-L Cooled-Disk Column Crystallizer. *Ind. Eng. Chem. Res.* **2003**, *42* (20), 4874–4880. https://doi.org/10.1021/ie020946c.

(31) Van der Ham, F. Eutectic Freeze Crystallization, Delft University of Technology, 1999, Vol. 1.

(32) Dias, R. M.; da Costa Lopes, A. M.; Silvestre, A. J. D.; Coutinho, J. A. P.; da Costa, M. C. Uncovering the Potentialities of Protic Ionic Liquids Based on Alkanolammonium and Carboxylate Ions and Their Aqueous Solutions as Non-Derivatizing Solvents of Kraft Lignin. *Ind. Crops Prod.* **2020**, *143* (November 2019), 111866. https://doi.org/10.1016/j.indcrop.2019.111866.

(33) Montané, D.; Nabarlatz, D.; Martorell, A.; Torné-Fernández, V.; Fierro, V. Removal of Lignin and Associated Impurities from Xylo-Oligosaccharides by Activated Carbon Adsorption. *Ind. Eng. Chem. Res.* **2006**, *45* (7), 2294–2302. https://doi.org/10.1021/ie051051d.

(34) Francisco, M.; Mlinar, A. N.; Yoo, B.; Bell, A. T.; Prausnitz, J. M. Recovery of Glucose from an Aqueous Ionic Liquid by Adsorption onto a Zeolite-Based Solid. *Chem. Eng. J.* **2011**, *172* (1), 184–190. https://doi.org/10.1016/j.cej.2011.05.087.

Chapter 4[3]

The Role of Ionic Liquid Pretreatment Design in the Sustainability of a Biorefinery: a Sugarcane to Ethanol Example

Lignocellulosic (LC) feedstocks are a promising alternative to fossil- based production of fuels, power and chemicals with its significant global warming potential (GWP). The balanced utilization of LC residues, such as food crop remains, is of great importance as an effective way to improve utilization from the same cultivated land. The conversion of LC`s carbohydrates into useful sugars which in turn are converted into desirable molecules by microbial or chemical conversion is dependent on the pretreatment (PT) efficiency. Ionic liquids (IL) have been explored as tailored solvents for the solubilization of the LC complex matrix to overcome the existing hurdles of the PT process. This work assesses the impact of variables` set up, associated to IL-based pretreatment, using the production of ethanol as an example. The influence of temperature, solid loading and IL dilution in water were systematically studied with respect to mass and energy balance, CAPEX, yields, profitability and environmental impact. Life cycle analysis (LCA) was employed in a cradle-to-gate approach. Results showed that solid loading and IL dilution have a direct effect for the reduction of steam consumption during the PT and IL recycle and are critical to improve IL utilization, reducing the negative impacts associated to IL production background and costs, for the environmental and economic assessment, respectively. Temperature had a direct influence in the steam consumption and in the saccharification yield, consequently, in the overall ethanol productivity. Apart from product selling price, IL recycle is the dominant factor on economic and environmental impacts. The IL-based pretreatment feasibility was shown to be dependent on conditions that minimize the IL make-up. This work was conceived on IL-based pretreatment and ethanol production, but the outcomes provided are valuable for the design of Biorefineries in a broader sense.

[3] This chapter is based in a prepared paper to be submitted in the *Green Chemistry* as: Ferrari, F.A., Pessoa, G., Franco, T.T., C.K., Witkamp, G.J., Dias, M., Cavaliero, van der Wielen, L.A.M., Forte, M.B.S. The Role of Ionic Liquid Pretreatment and Recycle Design in the Sustainability of a Biorefinery: a Sugarcane to Ethanol Example

4.1 Introduction

The transition towards a low-carbon approach has already moved from intention to implementation. The environmental arguments are complemented by economic drivers. Governmental investments on renewable technologies can potentially generate more jobs than spending on fossil solutions[1,2]. Among the diverse possibilities, one must consider the best mix of technologies, fitting resources to the energy consumption profile. Biofuels are an interesting alternative to fossil fuels for the transport sector, which accounts 32 % of the global total energy consumption[3]. Ethanol is a prime example of large-scale application of renewable energy. In 2019, United States of America and Brazil, first and second major ethanol producers respectively, produced approximately 49 Mtoe (million tons of oil equivalent) of ethanol[4,5], which corresponds to the total energy consumption of Norway, to put into perspective.

Most of ethanol production follows the sugar platform, in which carbohydrates are converted to the desired molecule by means of microorganism cultivation. Based on this transformation concept, sugars can be, ideally, transformed into any other molecule within the range of metabolites of a given microorganism. Such diversification brings about the biorefinery potential, from sugars to products, similarly to from oil to products, in the old-fashioned refineries. In this sense, any source of carbohydrates is a feedstock. Lignocellulosic (LC) residues are abundant and globally available. Moreover, LC residues, for instance crop remains, are a valuable source of carbohydrates that are generated as a by-product of food production, without the investment in the land area expansion. Although rich in carbohydrates at 40 – 90 %w [6], these sugars are not readily available for conversion. Consequently, LC must be treated, thus converting potential carbohydrates into useful sugars, in a process namely pretreatment (PT) and saccharification. Pretreatment is considered the most important step for obtaining an efficient conversion of LC's constituents[7,8]. Although improvements have been achieved over the past years, to be effective and economical the PT still need to overcome some hurdles, for instance: i) high power and energy consumption; ii) input costs; ii) recovery and recycling of catalyst and solvent, when applicable; iii) scale-up towards lower CAPEX and OPEX [9]. In this paper, we study the outcomes of pretreatment design from the Biorefinery perspective.

One of the most economically successful lignocellulosic sources is the sugarcane crop, with a global production of about 1.7 gigatonnes in 2019[10]. This crop is especially important in Brazil, where the sector accounts for 2 % of GDP, and represents 18 % of the total energy offer [11]. Moreover, it is noteworthy that

ethanol production from sugarcane residues, namely second generation, has a potentially better greenhouse gases (GHG) emissions balance than other high production crops[12], and can improve biofuel productivity within the same agricultural area.

Recently, ionic liquids (ILs) have emerged as a solution to the hurdles of biomass pretreatment. Due to the size, asymmetry, and conformational flexibility of their ions, ILs have lower melting points than regular salts, in some cases at temperatures below 100 °C. The design of IL structure, by combining different cations and anions, determine distinct properties, such as conductivity, vapor pressure, H bonding potential, density, catalytic sites and dissolution potential[8,13]. Significant research was focused on the screening of potential ILs and assessment of PT conditions concerning LC's component solubilization and the effect on subsequent enzymatic saccharification[14–16] of resulting solids. The influence of solid loading, temperature and IL dilution in water during PT are reported in literature, and may vary dependent on ions involved[14,17–19].

Nevertheless, it is crucial to elaborate on techno-economic analysis of potential large-scale applications when developing new technologies, identifying and understanding process' driving forces and economics. In this sense, it is known that ILs' price and recycle have an important and direct effect in process profitability [8,20,21]. Usually, price and availability are pointed out as the limiting factor of IL large-scale application. Process intensification towards high solid density are also described as good strategies to improve PT economic feasibility [21,22].

The environmental assessment provides critical criteria for renewable energy technology development. The Life Cycle Assessment (LCA) tool is widely applied to identify potential environmental impacts of a given product, by considering not only the production process itself, but also the background activities and disposal of every relevant input and output. Historically, LCA studies regarding sugarcane for first-generation ethanol manufacturing point the agricultural phase as the main emissions hotspot in the life cycle [23,24]. In second-generation, where different chemicals and inputs are introduced, there are more process bound emission contributions to be expected, which can change the aforementioned convention. Nevertheless, the efficiency of second-generation process in mitigate GHG emissions is usually also dependent on the agricultural phase, being the choice of the feedstock of great importance[25]. For ionic liquids, the embedded environmental burden can be traced back to the IL precursors and also IL reuse efficiency, and can be as important in the overall process sustainability

as the economic costs [26].

Through rigorous process simulation and previous work experimental data, the effect of solid loading (SL), temperature (T) and water proportion (H_2O_{liq}) were analyzed and the mass and energy balance provided for eight different scenarios. The CAPEX and OPEX are discussed and linked to the different PT variables, as well as potential strategies to improve project economic feasibility, energy consumption and IL recyclability. The environmental impact for the different operational conditions is addressed by the means of LCA, highlighting potential emission hotspots and proposing mitigation alternatives in terms of GHG emissions. The focus is to understand and quantify the impacts of PT using IL in the overall project rather than testify the economic feasibility of ionic liquid PT technology, thus identifying set ups and concepts worth changing.

4.2 Method

4.2.1 Overview

The study relates to a Biorefinery project considering sugarcane crop as feedstock and ethanol as the ultimate product. The ethanol synthesis is based on biological conversion from carbohydrates. Sugars are available from both sugarcane juice, basically sucrose (C12), and from the hydrolysis of the lignocellulose's (LC) constituents, namely cellulose into C6- sugars and hemicellulose into C5 sugars. The fermentation of C12 and C6/C5 will be addressed as first (1G) and second generation (2G) processes, respectively. The C12 stream starts in the biomass reception and preparation block, depicted in Figure 1, after sugarcane stalks milling and crushing. The extracted juice is treated and used in 1G fermentation, the residual bagasse combusted for combined heat and power generation.

The 1G process runs exclusively on stalk derivatives, in another words, sugarcane juice and bagasse. The 2G process starts with the reception of sugarcane straw bales. The straw is cleaned and crushed, and subsequently mixed with the surplus bagasse not burned in boilers. Consequently, the 2G facility is mostly bolted on straw, accounting for 60 – 70 wt% of total LC. The LC stream is divided since the 2G process runs for 200 days during the season simultaneously with 1G, and as a stand-alone unit for 130 days in the off-season period. The LC is, then, destinated to ionic liquid based (IL) pretreatment (PT). PT was simulated varying 3 key parameters, namely temperature (T = 80, 110 and 130 °C), solid loading (SL = 10, 20 and 30 %w/w) and water content in the liquid phase (H_2O_{liq} = 20, 30 and 60

%w/w). In total, 8 different PT scenarios were considered:7 assessing parameters' effects, and 1 considering the best design regarding economic feasibility and environmental impact. Changes in PT conditions impact the subsequent enzymatic hydrolysis and, consequently, the production of fermentable sugars destined to 2G fermentation. Variables will also influence hemicellulose and lignin dissolution during PT. The specifications for each scenario are summarized in the "Process' Parameters" section and are based on results from a previous work [14]. After PT, the IL is washed out from the residual solids. The liquid stream goes to the IL recycle section, where the IL concentration is performed by a freezing concentration (FC) process, followed by a multiple stage evaporation, as shown in Figure 2. The water content in the recycled IL stream was dependent on the SL and H_2O_{liq} assumed in the PT. The pretreated solids are subjected to enzymatic conversion into sugars, then fermented to ethanol. The fermented streams from 1G and 2G facilities are distilled together during the season, and 2G alone during off-season. All common structures and equipment were dimensioned according to 1G+2G demand.

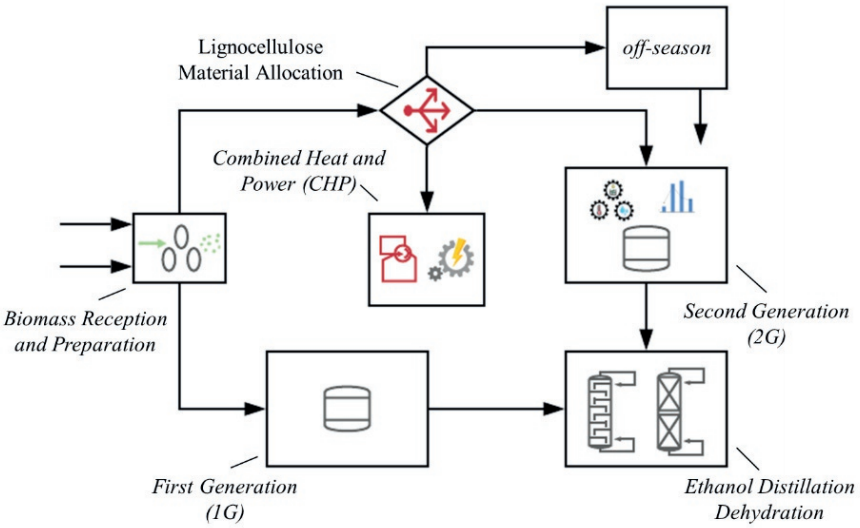

Fig 1: Process' simulation overview.

4.2.2 The Modeling

Simulations were carried using The Virtual Sugarcane Biorefinery (VSB)[23,27] established by the National Laboratory of Biorenewables (LNBR), former CTBE. The VSB is a virtual facility developed to evaluate new technologies

in biomass conversion platforms, providing useful information for academia, investors, and decision makers.

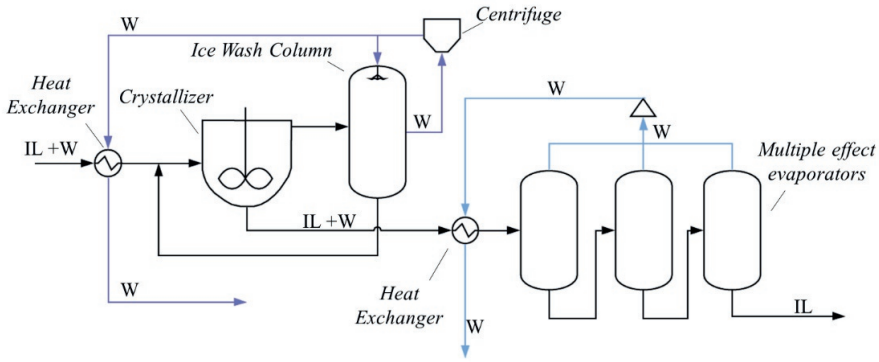

Fig 2: IL recycle process. W: water streams; IL: Ionic Liquid streams

The industrial modeling was designed in AspenPlus®, and the main property method used was NRTL. Redlich–Kwong equation of state, and Hayden O'Connell (NRTL-HOC) equation also took place depending on pressure and concentration of sugars and acids. For boilers and cogeneration, RKS-BM (RKS—Redlich–Kwong– Soave and BM-Boston-Mathias alpha function) was used, and steam tables (Steam NBS) for pure water streams.

Results obtained for the first-generation simulation using the VSB were validated by its developers against industrial bulletins provided by local Sugarcane Mills. The deviations between the industrial data and the simulation were 0.24 % for the ethanol production and 4.2% for the steam generation. The complete information and description about the model, inventory and VSB can be found elsewhere [23,27].

4.2.3 Process' Parameters

The simulation was performed following an iterative process for energy and mass convergence. A portion of the LC (solid residues after enzymatic hydrolysis), bagasse and straw are burned in the cogeneration system to meet the thermal energy demanded in the process, while the remaining part is diverted to the 2G facility, which, consequently, alters the energy demand. The convergence is achieved when the LC estimated for 2G is equal to the calculated LC surplus. The model also considers the off-season operation, meaning that the surplus LC must

converge with the estimated demand of season's 2G and off-season's 2G and cogeneration.

The refinery runs for anhydrous ethanol production. Although electricity accounts as an input and/or output for the process, it is only produced as consequence of process' demand for heat, while expanding high pressure steam in steam turbines. The lack or excess of electricity did not impact the simulation and was accounted as demand or supply to the electrical grid. The main overall parameters are summarized in Table 1.

Tab 1: Overall industrial parameters.

Stalks Processed (Mt/yr)	4.00
Dry Straw Processed (Mt/yr)	0.18
Boiler Efficiency (LHV basis)	87.70%
Turbine Isentropic Efficiency	85%
Generator Efficiency	98%
Air Excess in Boilers	30%
Energy Demand for the Process, excluding Straw Processing (kWh/ t stalks)	30.0
Electricity Demand for Straw Processing (kWh/t)	8.2
Sugar extraction efficiency	96%
Conversion of sugars to Ethanol (1G)	89.50%
Anhydrous Ethanol Purity (w/w)	99.60%

The PT was simulated according to results from chapter 2, where mixtures of 2-hydroxyethylammonium acetate ([Mea][Ac]) and 2-hydroxyethylammonium hexanoate ([Mea][Hex]) were used to pretreat sugarcane straw. In the mentioned work, the authors assessed PT efficiency, in terms of residual solids enzymatic digestibility, for several PT designs, from which the variables were selected for the study carried in the present work. Each set up led to different yields in the enzymatic hydrolysis step, changed in the simulations according to Table 2. Likewise, solubilization of LC's constituents were also adjusted according to PT conditions. After variables assessment, an additional simulation was carried

considering the best performing scenario. The Aspen simulation of 2G hierarchyare depicted in Figures 3 and 4.

The IL recovery, as depicted in Figure 2, considers that the major share of water is removed from IL recycling streams by freezing crystallization (FC), reducing the energy demand and avoiding IL loss, chapter 3. Because FC could not achieve the water level necessary for all PT conditions, a multiple effect evaporator was considered as well. The mass balance in the FC process was calculated separately, based on results from chapter 3. An extra scenario in the best design was used to depict how the process would behave if the crystallization step on the ionic liquid recycle presented different electricity demand, of 74 kWh/ton (Chapter 3), as opposed to the initial assumption of 12 kWh/ton[28], per ton of ice produced. The difference on energy consumption is regarded to the distinct operation temperatures during ice formation, -4.5 °C (12 kwh) and -31 °C (74 kWh).

Tab 2: Summary of pre-treatment and enzymatic hydrolysis conditions assumed in each scenario.

Pretreatment		**Enzymatic Hydrolysis**	
Temperature (T °C)	80, 110, 130	Temperature / Residence Time	50 °C / 48 h
Solid Loading (SL - % w/w)	10, 20, 30	Solid Loading	15 % w/w
Water Content in Liquid Fraction (H_2O_{liq} - % w/w)	20, 30 60	Enzyme Loading	5.8 $g.kg^{-1}$ cellulose

Scenarios T - H_2O_{liq} - SL	**Component Solubilization during Pretreatment [a] Xylose / Lignin (% w/w)**	**Yield Enzymatic Conversion [a,b] (%)**
130-30-20*	18.6 / 24.2	96
80-30-20	10.0 / 24.2	70
110-30-20	12.0 / 24.2	82
130-20-20	18.6 / 24.4	96
130-60-20	18.6 / 12.2	88
130-30-10	18.6 / 30.0	96
130-30-30	18.6 / 12.2	96
130-60-30	18.6 / 12.2	88
Sugars conversion to Ethanol	1G (C12 and C6) – 88%	2G (C6 and C5) – 80 %

* base case scenario; [a] value assumed based on experimental results from Ferrari et al (2019); [b] cellulose and hemicellulose hydrolysis.

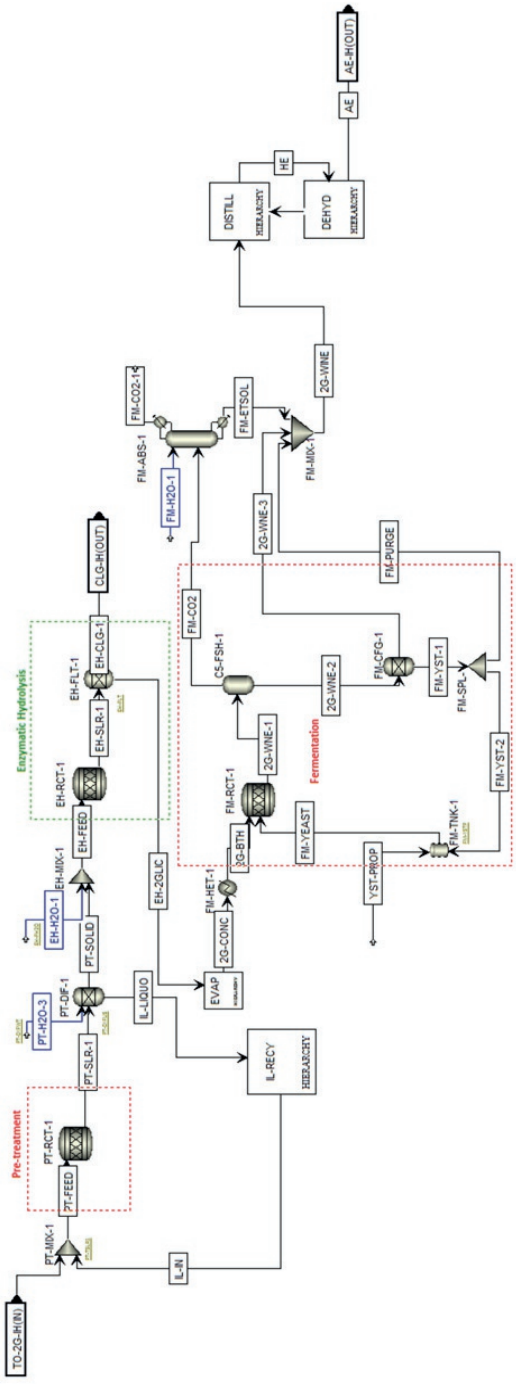

Fig 3: 2G facility used in simulations

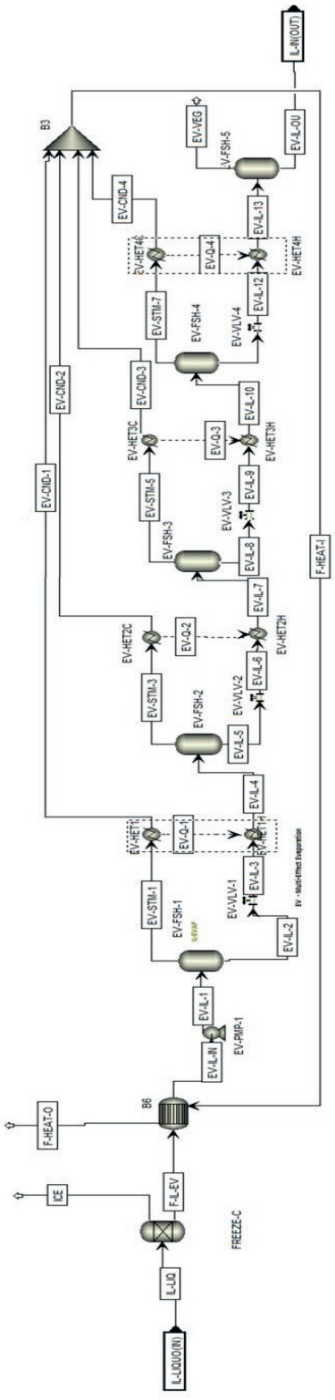

Fig 4: IL recycle hierarchy.

IL losses occur predominantly during PT and IL recycle. It was found that 84 % of the ethanolammonium in [Mea][Ac] can be converted to acetamide after the 6th pretreatment cycle, if the proportion of acid and base are not adjusted [29,30]. The reasons and quantities of IL losses are not on the scope of this work, therefore, an overall make up of 5 % in mass is assumed.

4.2.4 Economic

Equipment and installations capital expenditures (CAPEX) were calculated based on the literature, especially on VSB's values [23,27]. For the PT reactor and FC process the costs were based on BARAL; SHAH (2016)[31] and VAN DER HAM (1999)[32], respectively. The FC process encompasses a crystallizer, two wash columns, a centrifuge and a cooling machine. The equipment's size was adjusted using the Six-Tenths rule, and values adjusted by the Chemical Engineering Plant Cost Index (CEPCI). As this study considers a project based on Brazil, a localization factor of 1.35 and an exchange of 3.88 R$/ US$ were assumed. The main economic assumptions are summarized in Table 3. The electricity selling price was based on values provided by local sugarcane mills, and electricity purchase price based on the Brazilian National Agency of Electric Energy (ANEEL) tariff [33]. The production cost associated to sugarcane stalks and straw were obtained using CanaSoft spreadsheet-based model, developed by the LNBR in the Virtual Sugarcane Biorefinery context[27].

Ionic liquid price was calculated according to equation 1, established by CHEN et al. (2014).

$$IL_{price} = \frac{M_1 P_1 + M_2 P_2}{M_1 + M_2} \qquad \text{eq. 1}$$

where, M_1 and M_2 are the molecular weight of starting materials, while P_1 and P_2 the price of the two starting materials. The price estimation assumes an IL mixture of 75% [Mea][Ac] and 25% [Mea][Hex].

The Internal rate of return (IRR) was calculated based on a greenfield project (1G + 2G). In the sensitivity analysis, a variation of ± 20% was considered on the prices of ethanol, IL, sugarcane stalks and straw, ± 40% on 2G CAPEX, and an IL make up of 1% and 10% for the optimistic and pessimistic scenarios, respectively, to evaluate their impact on the IRR.

Tab 3: Main Economic Parameters

Economic Parameters	
Equity	100%
Depreciation	10%, 10 yrs linear
Lifespan	25 yrs
Income Tax	34% /yr
Discount Rate	12% /yr
IL Price ($/t)	1460.00
Stalks Cost (US$/t)	21.26
Straw Cost (US$/t)	24.48
Ethanol Price (US$/kg)	0.49
Electricity Selling Price (US$/MWh)	54.03
Electricity Buying Price (US$/MWh)	122.68
Maintenance	3 % CAPEX/ yr
Staff	301
Cost/ Staff	$ 1194.34

4.2.5 Environmental

The Life Cycle Inventories (LCI) for each scenario were built on SimaPro v9, using EcoInvent 3.5 as the main database for background information. The APOS (allocation at point-of-substitution) were the datasets of choice, with the "market for" inventories being used, to better represent the market share for different manufacturers and processes with the same output. When available, inventories regionalized for Brazil (BR) were preferred, but otherwise, "Rest of the World" (RoW) and "Global" (GLO) data sets were used.

To better represent Brazilian sugarcane agricultural activities, with straw as coproduct, the LCI published by the former CTBE [34] was adapted. Straw-to-stalk proportion and allowed retrieval fraction followed the work of Menandro *et al.* (2017)[35]. ReCiPe 2016 was selected as the impact assessment (LCIA) method, since

it presents characterization factors and normalization standards applicable on a global scale [36]. Three impact categories were considered: global warming potential (GWP), marine ecotoxicity, and water consumption.

The Life Cycle Assessment (LCA) adopted a "cradle-to-gate" approach, with 1 kg of ethanol as functional unit. Coproduction of electricity was accounted as an avoided product, using the Brazilian electricity matrix as reference, available on EcoInvent. Minor products such as low-grade ethanol, fuse oil and filter cake had no allocation of burden.

Even though the ionic liquid adopted in this study is a mixture of [Mea][Ac] and [Mea][Hex], this input was simplified as pure [Mea][Ac] in the LCI. This is due to the lack of data on hexanoic acid production on EcoInvent and other LCIs published in the literature. Acetic acid and monoethanolamine were used instead, in stoichiometric proportions. The effect of recycling water from the crystallization step was also explored on the water consumption impact category. IL losses are sent along with the other aqueous process' streams to a generic wastewater treatment unit, represented by the inventory "wastewater treatment (RoW), market for", on EcoInvent, assuming ILs biodegradation in this process [37,38]. Thus, IL's environmental impact is mostly arising from its production background.

For the initial scenario screening, the LCIs for off-season operation were used, since the operational aspects related to the ionic liquid are more apparent. The first generation sugarcane mill, used as baseline on the LCIA, was based on the Virtual Sugarcane Biorefinery (VSB) Autonomous Optimized [23], with minor adjustments to match the first generation plant's operating conditions, present in the Aspen simulations.

To display the ionic liquid process' decarbonization potential, the Brazilian RenovaBio certificate (CBio) was used. Gasoline was adopted as the fossil counterpart, with an emission factor of 93 $gCO_{2eq}.MJ^{-1}$. Anhydrous ethanol energy content is of 27 $MJ.kg^{-1}$ [39]. All vehicular carbon emissions from ethanol were assumed as biogenic and were not accounted for.

4.3 Results And Discussion

The simulations reflect the impact of PT set up on the mass and energy balance. Therefore, the impact of variables T, SL and H_2O_{liq} were assessed considering the whole biorefinery perspective, and are disclosed as: a) process' implications: mass flow, energy consumption and yields; b) economy: equipment

size and CAPEX implications; c) environmental: life cycle analysis. The PT set up in base case is 130 °C (T), 30 % (H_2O_{liq}) and 20 % (SL).

4.3.1 Pretreatment conditions impact on process streams.

Although a combined 1G and 2G plant was simulated, the impacts of T, SL and H_2O_f will be discussed concerning the 2G facility, schematized in Figure 5. Table 4 summarizes the yields of anhydrous ethanol and residual solids on biomass base, and process steam and IL consumption.

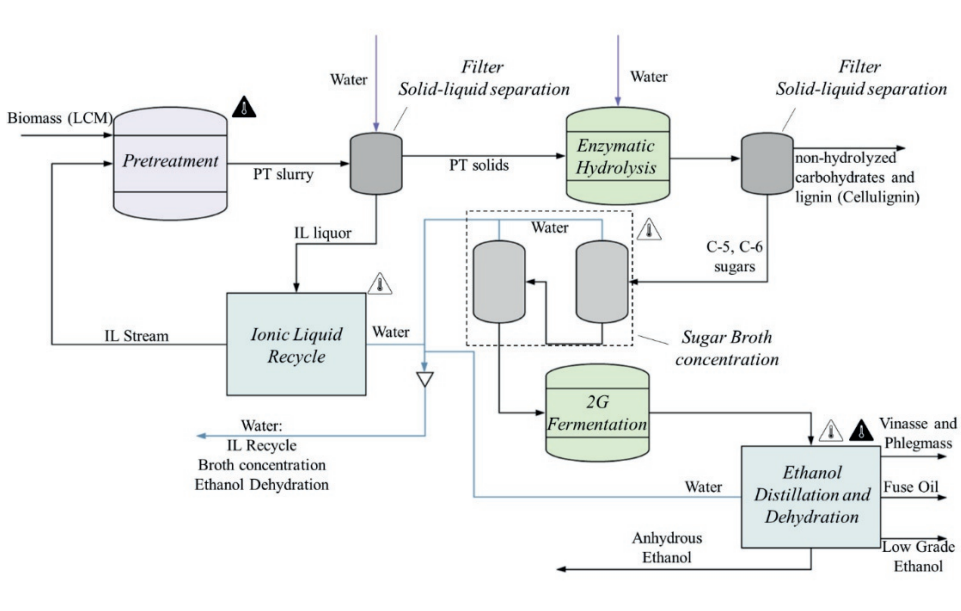

Fig 5: 2G plant scheme. Triangles identify relevant steam consumption processes: 6 bar (black); 2 bar (white).

The increase in temperature during pretreatment has a direct and, usually, positive effect on the enzymatic digestibility of residual solids. On the other hand, higher temperatures demand more steam, consequently, higher amounts of LC will be burned in the boilers to compensate for it. Therefore, both pretreatment and steam production affect LC consumption, competing for it. The decrease in temperature from 130 °C to 110 °C reduced in 32 % the steam consumption to pretreat 1 kg of biomass and, at 80 °C the reduction reached 74 %. However, during enzymatic hydrolysis, solids pretreated at 130 °C have a higher conversion yield (96 %) than those pretreated at 80 °C and 110 °C (70 % and 82 %, respectively). Differences in enzymatic conversion have a direct effect on sugars' concentration,

which must be adjusted to maximize ethanol productivity. Therefore, the stream from enzymatic hydrolysis is, concentrated in a multiple-effect evaporator, as shown in Figure 3. Higher enzymatic conversions lead to more concentrated streams after hydrolysis, and, consequently, lower amounts of steam consumed to reach the appropriate sugar composition. Although some energy was spared during pretreatment at 80 °C and 110 °C, steam consumed in multiple effect evaporators were 70 % and 127 % higher than the base case, respectively. Considering the overall steam balance in 2G ethanol production, the process with pretreatment at 130 °C exhibited better energy efficiency than at 80 °C and 110 °C, improving the ethanol yield in 9% and 4 %, respectively, mainly due to the higher enzymatic conversion. Besides the lower steam consumption, a higher enzymatic conversion is crucial to improve the relation between ethanol produced and IL consumed: scenario with pretreatment at 130 ºC was 13 % more effective in terms of IL utilized than the scenario at lower T (80 °C).

Tab 4: Yields of ethanol and cellulignin as function of the mass of biomass consumed, steam and Ionic Liquid used in the second generation (2G) facility. Results from simulations.

	$Y_{E/Btt}$ (w/w)	$Y_{E/Bpt}$ (w/w)	$Y_{E/Steam}$ (w/w)	$Y_{E/IL}$ (w/w)	$Y_{CL^c/Btt}$ (w/w)	$Y_{CL^c/Bpt}$ (w/w)	**Lignin CL^c** (w/w)
T- **130** °C/ H_2O_f- **30** %w/ SL- **20** %w (Base case)	0.216	0.283	0.095	1.78	0.16	0.21	0.81
T- **80** °C/ H_2O_f- **30** %w/ SL- **20** %w	0.197	0.214	0.086	1.55	0.36	0.39	0.47
T- **110** °C/ H_2O_f- **30** %w/ SL- **20** %w	0.210	0.249	0,091	1.77	0.26	0.31	0.59
T- **130** °C/ H_2O_f- **20** %w/ SL- **20** %w	0.219	0.283	0.095	1.69	0.17	0.22	0.83
T- **130** °C/ H_2O_f- **60** %w/ SL- **20** %w	0.237	0.261	0.112	3.29	0.27	0.30	0.71
T- **130** °C/ H_2O_f- **30** %w/ SL- **10** %w	0.200	0.283	0.080	0.84	0.15	0.21	0.81
T- **130** °C/ H_2O_f- **30** %w/ SL- **30** %w	0.252	0.284	0.124	3.82	0.22	0.25	0.85

$Y_{E/Btt}$: Anhydrous Ethanol/ total dry biomass pretreated and consumed for energy purpose; $Y_{E/Bpt}$: Anhydrous Ethanol/ dry biomass pretreated; $Y_{E/Steam}$: Anhydrous Ethanol/ steam produced (2G); $Y_{CL^c/Btt}$: Cellulignin after hydrolysis/ dry biomass pretreated and burned in boilers $Y_{CL^c/Bpt}$: Cellulignin after hydrolysis/ dry biomass pretreated; $^{CL:}$ dry solids after enzymatic hydrolysis.

Biomass pretreatment in water diluted solutions reduce the amount of IL consumed, decreasing process operational costs. Regardless of IL savings, water addition generally affects pretreatment's efficiency in IL process [14,40], decreasing sugar yielded from residual solids during hydrolysis. In the present work, water content in the pretreatment reactor lower than 20 %(w/w) could not be achieved considering the LC's initial moisture, approximately 50 %(w/w), at a SL of 20 %(w/w). The relationship between SL, moisture and H_2O_{liq} is depicted in Figure 6. As expected, the increase in water content reduced in almost 50% the amount of IL consumed per unit of ethanol produced.The reduction in enzymatic conversion from 96% to 88% due to water addition during pretreatment had a negative effect on ethanol yield from pretreated biomass. However, at higher H_2O_{liq} less water had to be removed from IL recycling stream, which in turn consumed less energy. The increase in H_2O_{liq} from 30 to 60 % decreased in 18% the total steam consumption and improved in 13 % the overall ethanol yield. For scenarios with H_2O_{liq} 60 %, IL was concentrated exclusively by the freeze concentration process (FC).

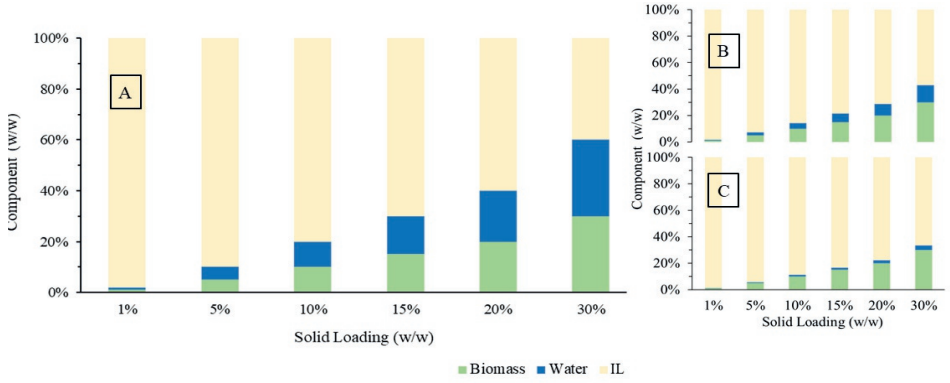

Fig 6: Mass proportion of the three main components during pretreatment at several solid loadings, considering three different biomass moisture,e.g., 50 %w (A), 30 %w (B) and 10 %w (C), and assuming an anhydrous ionic liquid.

It is evident that the SL direct impacts the amount of IL consumed during pretreatment. The highest SL (30) scenario presented an IL consumption 48 % lower than that from SL at 20 %. Moreover, the lowest SL (10) scenario revealed the worst energy balance and ethanol productivity, 16 % and 10% lower than that from base case scenario, respectively. Changing SL had a direct and substantial effect on the energy consumed during pretreatment. The reduction from 20 to 10% in SL increased in 77 % the amount of steam (6 bar) consumed to pretreat the equivalent mass of biomass, while a reduction of 20 % was observed at the highest

SL (30). SL set up was also relevant for lignin. The lowest percentage of lignin loss, 16 % (w/w), was observed in the scenario with the highest SL (30), which also originated the residual solid, after hydrolysis (cellulignin), with higher lignin concentration, 85 %(w/w), as summarized in Table 4.

4.3.2 Economics

The PT design impacted the CAPEXof almost all units from the 2G facility, summarized on Table 5. Among them, enzymatic hydrolysis, pretreatment and IL recycle were affected the most. The IL recycle facility accounted for approximately half of 2G CAPEX, mainly due to the high cost of the FC unit. Even that FC unit represents a significant share of CAPEX, it might be an efficient way to avoid IL losses during recycling.

The breakdown of 2G anhydrous ethanol production in its major cost drivers is depicted in Figure 7.

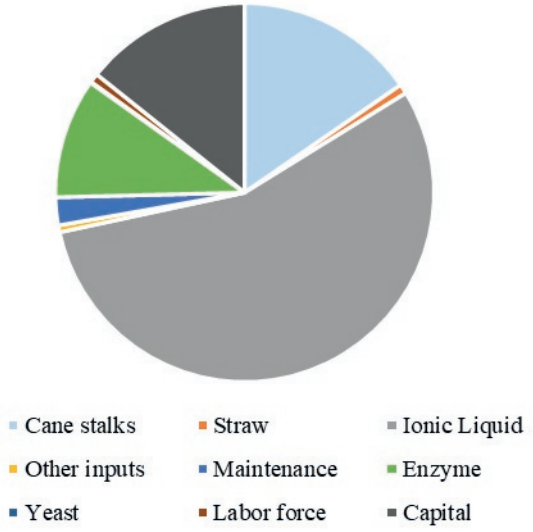

Fig 7: Breakdown of 2G anhydrous ethanol production cost, considering the base case scenario with 5 % of IL make up. Production cost of 1 L ethanol (2G) US$ 1.18. Total yearly production cost for 2G ethanol 111.7 Mi US$.

Although the decrease in pretreatment temperatures was beneficial to increase LC surplus, it did not compensate for the decrease in enzymatic conversion, leading to a reduction in the annual profit, 4.3 % and 21.8 % for the pretreatments at 110 ºC and 80ºC scenarios, respectively, in comparison with that

from the base case. Conversely, the reduction in hydrolysis efficiency, due to water increase in pretreatment, was compensated by the increment in LC surplus due to energy savings and reflected by the growth in ethanol production. The increase in H_2O_{liq} was also responsible for a substantial decrease in IL consumption. Thereby, the annual net profit was boosted in 64.5 % (H_2O_{liq} 60 %), compared to base case.

The SL was even more critical for process economic feasibility. The lower the solid density is, the bigger is the reactor volume to keep mass productivity during pretreatment. Likewise, bigger is the IL recycle system due to the higher liquid volume. Nevertheless, the most important consequences about SL were related to ethanol productivity and IL consumption; therefore, increasing SL from 20 to 30 % led to an increase of 82% in the annual net profit.

Table 5: Capital Expenditure, ethanol production and Ionic Liquid expenses from the different scenarios.

CAPEX 2G (Mi US$)	T **130** °C H_2O_{liq} **30** %w SL **20** %w	T **80** °C H_2O_{liq} **30** %w SL **20** %w	T **110** °C H_2O_{liq} **30** %w SL **20** %w	T **130** °C H_2O_{liq} **20** %w SL **20** %w	T **130** °C H_2O_{liq} **60** %w SL **20** %w	T **130** °C H_2O_{liq} **30** %w SL **10** %w	T **130** °C H_2O_{liq} **30** %w SL **30** %w
Pretreatment	20.185	23.113	22.055	20.917	22.886	29.817	16.788
Solid-Liquid Separation After Pretreatment	9.753	11.198	10.638	9.826	11.144	9.020	10.565
Enzymatic Hydrolysis	19.148	23.330	22.121	19.148	23.330	17.939	22.121
Solid-Liquid Separation After Hydrolysis	4.323	9.441	7.642	4.379	7.676	4.209	5.978
C-5 and C-6 Sugars Concentration	0.719	1.623	1.202	0.763	1.228	0.635	0.940
Fermentation 2G	16.266	16.266	16.266	16.266	16.266	16.266	16.266
Yeast Propagation	1.076	0.530	0.530	1.076	1.076	0.530	1.076
Sub-Total	*71.473*	*85.504*	*80.458*	*72.377*	*83.608*	*78.419*	*73.737*
IL Freeze Concentration	70.963	80.882	77.198	72.695	80.019	82.617	69.706
IL Evaporation	10.459	14.406	13.099	12.825	0.000	6.935	14.058
TOTAL 2G	*152.894*	*180.792*	*170.756*	*157.897*	*163.627*	*167.972*	*157.501*
2G Anhydrous Ethanol Production/ year (Mi L)*	94.3	88.4	93.3	93.2	106.8	85.1	107.0
Increment in Total Ethanol production*	+ 27.6 %	+ 25. 9 %	+ 27.3 %	+ 27.3 %	+ 31.3 %	+ 24.9 %	+ 31.3 %
Net Profit/ year (Mi US$) [a]	28.3	22.1	26.8	24.0	46.6	- 23.8	51.6

[a]: considering 5% of IL make up. * The production of 1G anhydrous ethanol was the same for all scenarios, 341.5 Mi L year.

4.3.3 Best Scenario Configuration

In the light of what has been discussed, an additional set up was simulated considering the best choice design. An extra scenario in the best design was used to depict how the process would behave if the crystallization step on the ionic liquid recycle presented an electricity demand of 74 kWh/ton, chapter 3, as opposed to the initial assumption of 12 kWh/ton [28], per ton of water crystalized. Results are summarized in Table 6.

Table 6: Economic and Process metrics from Scenario T **130 °C**/ H_2O_f **60 %**w/ SL **30 %**.

CAPEX 1G millions of US$		**CAPEX 2G** millions of US$		**Expenses** millions of US$/ year	
Auxiliary Buildings and Urbanization	46.2	**Pretreatment**	18.3	**Sugarcane**	85.1
Sugarcane Reception and Broth Extraction	33.1	**Solid-Liquid Separation After Pretreatment**	11.3	**Ionic Liquid** [a]	24.1
Straw Processing	11.6	**Enzymatic Hydrolysis**	24.5	**Enzymes**	14.5
Broth Treatment and Concentration	17.0	**Solid-Liquid Separation After Hydrolysis**	7.7	**Maintenance**	13.3
1G Fermentation	17.2	**Hydrolyzed Sugars Concentration**	1.3	**Straw**	4.5
Ethanol Facility	58.2	**Fermentation 2G**	16.3	**Labor**	4.3
Steam Production and Distribution	62.8	**Yeast Propagation**	1.1	**Other Inputs**	3.2
Electricity Production and Distribution	24.6	***Sub-Total***	*80.5*	**Yeast**	0.6
Water System and Compressed Air	18.6	**IL Crystallization**	75.1	**Revenue** (Mi US$/ year)	
Total 1G	289.2	**IL Evaporation**	0.0	**Electricity*** (FC: 12 hWh / 74 kWh)	12.6/ 3.6
		Total 2G	*155.6*	**Ethanol 1G**	167.8
TOTAL 1G + 2G = 444.8				**Ethanol 2G**	*54.6*

2G Process Yield Parameters (w/w)					
$Y_{E/Btt}$	0.250	$Y_{E/Steam}$	0.129	$Y_{CL^c/Btt}$	0.29
$Y_{E/Bpt}$	0.261	$Y_{E/IL}$	5.83	$Y_{CL^c/Bpt}$	0.30
				Lignin in CL	0.71

[a]: considering 5% of IL make up; $Y_{E/Btt}$: Anhydrous Ethanol/ dry biomass pretreated and burned in boilers; $Y_{E/Bpt}$: Anhydrous Ethanol/ dry biomass pretreated; $Y_{E/Steam}$: Anhydrous Ethanol/ steam produced; $Y_{CL^c/Btt}$: Cellulignin after hydrolysis/ dry biomass pretreated and burned in boilers $Y_{CL^c/Bpt}$: Cellulignin after hydrolysis/ dry biomass pretreated; [CL]: dry solids after enzymatic hydrolysis.*: electricity revenue considering FC electricity consumption of 12 kWh/ton and 74 kWh/ton.

Although temperature reduction was beneficial in terms of energy demand, the resulted surplus in LCM was not sufficient to compensate the reduction in enzymatic conversion yield, leading to a lower ethanol productivity thus. Nevertheless, it is important to highlight that any reduction in PT temperature without significant loss in the subsequent enzymatic step is highly desirable. Based

on scenarios considered in this work, the process would be benefitted in terms of ethanol production when the reduction in enzymatic hydrolysis, due to reduction in PT temperature, does not exceed 15 %. Besides decreasing energy demand, T reduction might also be beneficial for particular ILs, avoiding undesirable reactions [29]. In a system where the IL make up is benefited by milder PT's conditions, lower temperatures should be considered, even if they lead to a decrease in enzymatic conversion yield. To elaborate on that, if an IL make up of 2.5 % was assumed for the lowest T (80 °C) scenario, in contrast with 5 % for the base case, owing to a reduction in pretreatment temperature that would have doubled the economic performance in terms of investment return, (IRR), even with an enzymatic conversion 40 % lower. IL decomposition during PT is out of scope from the present study, thereby, it was assumed the same IL make-up in all scenarios and, the T of 130 ºC was assumed in the best scenario. The H_2O_{liq} 60 % was considered due to the reduction in IL consumption, decrease in energy demand and avoidance of IL drying by evaporation step, which might be a potential spot for IL loss. The SL 30% was assumed; since, it had the best performance on IL and energy consumption. The increase in process power demand decreased 3.5 fold the revenue prevenient from electricity commercialization, impacting directly on overall profitability. Major impacts were also observed in the environmental assessment, as discussed later.

Although the best scenario was set to minimize IL make up, the IL recycle remains one of the major economic cost drivers, as shown by the sensitivity analysis depicted in Figure 8, which illustrates the effect of key variables from the process in the Internal rate of Return (IRR) for both scenarios of electric demand (12 kWh and 74 kWh). The analysis assumes a green field project, in which the total CAPEX (1G + 2G) is considered. The 1G plant corresponds to 65 % of the total CAPEX investment, the 2G facility can represent weather a benefit or disadvantage for the overall economics depending on how it is designed, as discussed further on. The given numbers observed in the scenario considering lower electric consumption are dislocated towards larger IRR values due to the extra revenue accounted by greater electricity commercialization, which also decreased the negative effect of inputs' costs.

The IL recycle, rather than its price, should be tackled, even considering more expensive methods, such as FC, towards process' economic feasibility. Even with higher CAPEX, the FC process can considerably reduce the energy consumption related IL recycle per mass of pretreated biomass, considering distillation, 91% of reduction, based on values reported in Chapter 3 and

literature[41]. Moreover, the complete IL recovery is even more relevant in the light of environmental sustainability. Sun et al (2017) efficiently recycled IL using pervaporation, beyond 99%. Nevertheless, the results showed a low cost-effectiveness of this technique in comparison with vacuum distillation at high rates of IL recovery and lower IL prices, due to increased operational costs, despite the higher energy efficiency[42]. The advantage of the FC process relies on the efficiency of IL recovery, low energy consumption and operational costs.

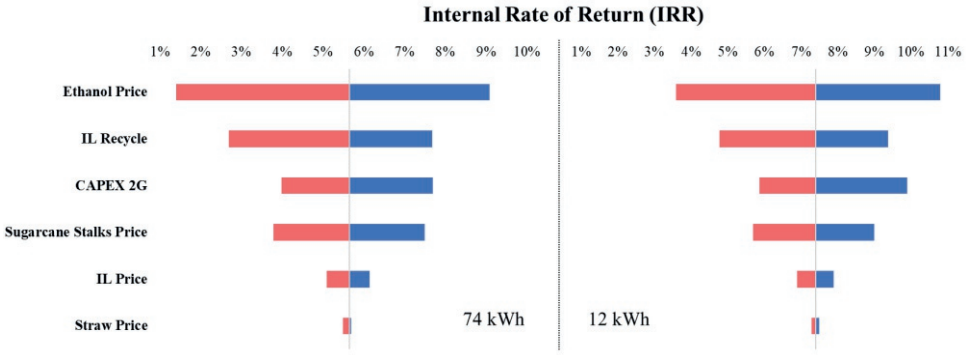

Fig 8: Economic sensitivity analysis depicted as tornado chart. The effects of variations are expressed in terms of Internal Rate of Return (IRR, % per yr) for both electric consumption figures assumed during the freeze concentration process. IRR considering 1G + 2G.

The most relevant factor from Figure 8, as expected, was the product price. The 2G ethanol corresponded to approximately 25 % of total ethanol production, and accounts for 24 % of the total annual revenue. One strategy to improve the average ethanol selling price is to go for markets inclined to pay more for advanced fuels, such as the 2G cellulosic ethanol.

A second way could rely on diversification, similarly to an oil refinery. Including different value-added molecules in the Biorefinery's portfolio would help 2G valorization and reduce risks endured from market fluctuations. The revenue breakdown from the 74 kWh scenario, and IRR as a function of 2G CAPEX and 2G product selling price, are depicted in Figure 9, which also remarks three potential molecules for 2G production with higher market selling prices than ethanol. Besides the attractiveness of selling value, these chemicals were selected based on global market size and mature technology readiness level (TRL 8- 9), thus having a near-term deployment potential [43].

In order to elaborate on molecules diversification, a hypothetical production of lactic acid (LA) was included in the 2G facility, adjusting CAPEX, average product selling price and IRR as function of the fraction of biomass diverted to LA production rather to ethanol, based on values found in literature [44]. The additional capital for LA's facility was calculated from the CAPEX of production and purification sections, assuming a constant relationship between cost and ton of LA produced. In a scenario where 20 % of pretreated biomass is diverted to LA production, and remaining 80 % to ethanol, the IRR would be 33 % higher than that achieved by only producing ethanol. The same strategy could be applied for other molecules. Nevertheless, it is important to mention that the ethanol production is crucial to keep in place the economy of scale, and the choice of product diversification must consider other arguments further than IRR, for instance, process intensification, beyond the scope of this work.

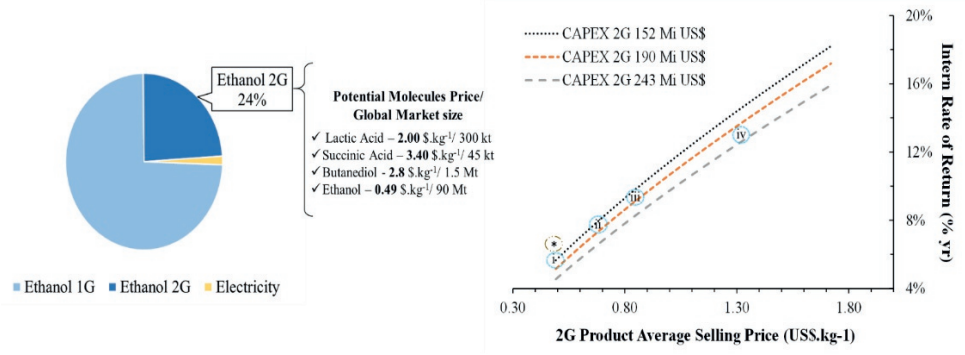

Fig 9: On the left-hand side, best scenario revenue profile, and examples of potential molecules. On the right, calculated Intern Rate of Return (IRR %yr) as a function of different values of 2G CAPEX and 2G product selling price. Labels represent the 2G CAPEX, 2G product average selling price and IRR for a production mix when in "i" 0 %, "ii" 10 %, "iii" 20% and "iv" 50% of the biomass is destinated to Lactic acid production rather than ethanol in the 2G facility. The "*" represents the scenario considering 12 kWh during FC, all others consider the 74 kWh scenario. Market and price data: NREL, 2016[43]. Lactic acid production: Gezae Daful *et al.* (2018)[44].

4.3.4 Environmental Assessment

In the overall perspective, the IL background production played a major role in three impact categories, as shown in Figures 10: (A) marine ecotoxicity, (B) water consumption and (C) GWP. On the initial LCIA run, with all of ReCiPe impact categories, five emerged as hotspots after normalization: terrestrial, freshwater and marine ecotoxicities; and carcinogenic and non-carcinogenic human

toxicities. Among the five, marine ecotoxicity was the most prominent and was, then, selected for further analysis. On the remaining four, sugarcane straw, ionic liquid and enzymes were identified as the main contributors. The IL is produced by a mass proportion of 49.6% acetic acid and 50.4% monoethanolamine. This trend proportion is followed into the LCIA, whereas in GWP, monoethanolamine has a bigger share (62.5%).

Process design decisions that minimize the make up of IL led to smaller marks on the three selected impact categories. By coupling specific scenarios it is possible to verify the positive effect of increasing: water loading on pretreatment (130-20-20, 130-30-20 and 130-60-20) , temperature on pretreatment (80-30-20, 110-30-20 and 130-30-20) and solids loading on the hydrolysis (130-30-10, 130-30-20 and 130-30-30).

The best configuration on all three impact categories combines the aforementioned design choices: T130 °C, H_2O_{liq} 60 and SL30, where IL make up is the lowest. Without optimization, ionic liquid production background can represent a significant share of the environmental burden, surpassing all other inputs and process steps in most scenarios in GWP and marine ecotoxicity. In water consumption, on the other hand, the process activity emerges as a new hotspot. This water demand can be traced to the boiler water make-up, pretreated biomass washing, and water loading in the hydrolysis. By comparing to the 1G baseline scenario, where the last two demands are absent, this difference becomes apparent.

It is important to remark, however, that the increased ethanol production in the 1G baseline compared to all 2G off-season scenarios, generates a dilution effect on all three impact categories. So, in order to mitigate this perception, both season and off-season operations were segregated and contrasted for the subsequent analysis, as shown in Figure 11. For scenario 130-60-30 (74 kWh), operation in the off-season negatively affects the whole-year performance on all categories, with the opposite happening with 130-60-30. This shows the effect of generating electricity surplus as opposed to using it from the grid in the overall performance. Now considering the whole-year operation for both scenarios compared to 1G baseline, 130-60-30 only succeeds in improving over the benchmark in GWP, with a potential reduction of 13.7%. For both scenarios, off-season appears as the offset, bringing the whole-year impact up and above the 1G baseline marks, on marine ecotoxicity and water consumption.

As mentioned before, IL make up was identified as a hotspot, so efforts towards improvements on IL recycle may have a strong effect on the overall

environmental performance. Addressing this, a sensitivity analysis was carried out on the IL make up, Figure 12. GWP and marine ecotoxicity indicators could be reduced by 40%, and water consumption by 28%, by reducing IL make-up from 5% to 1%. While the latter two impact categories are, still, superior to 1G baseline, they could be further improved by addressing other hotspots, such as enzyme consumption and water usage in the process.

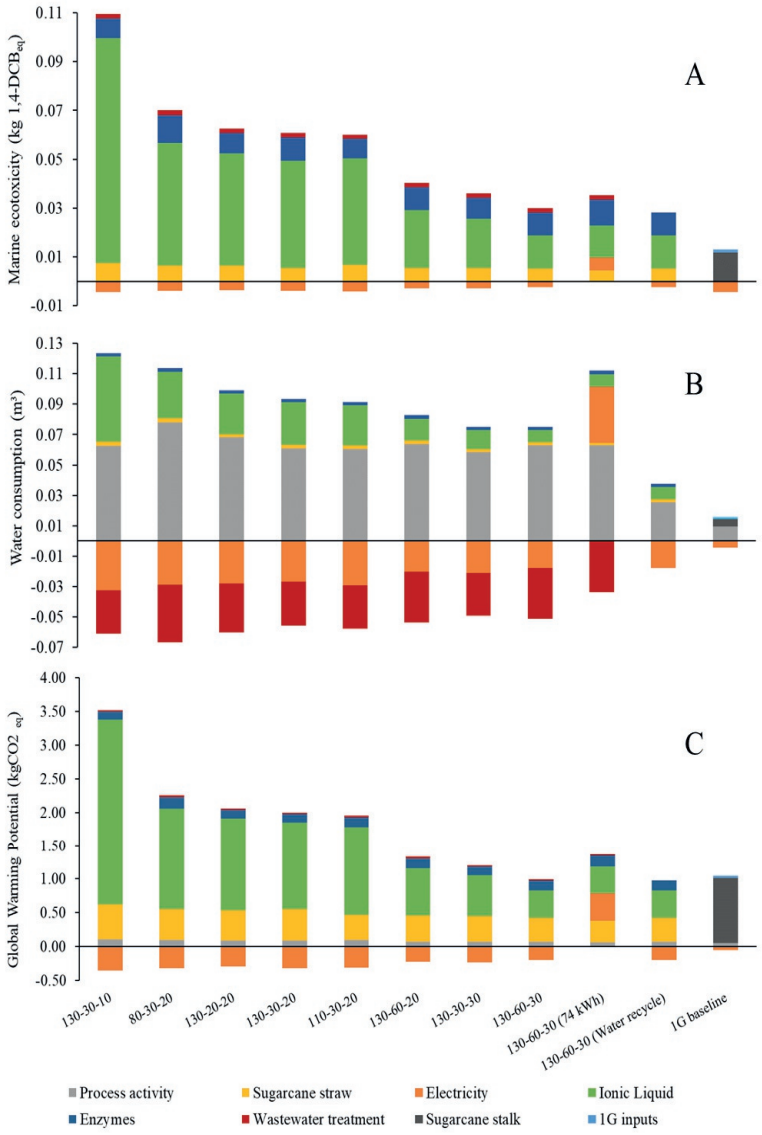

Fig 10: Scenario comparison for: (A) marine ecotoxicity, (B) water consumption and (C) Global Warming Potential (GWP). (T-H_2O_{liq}- SL)

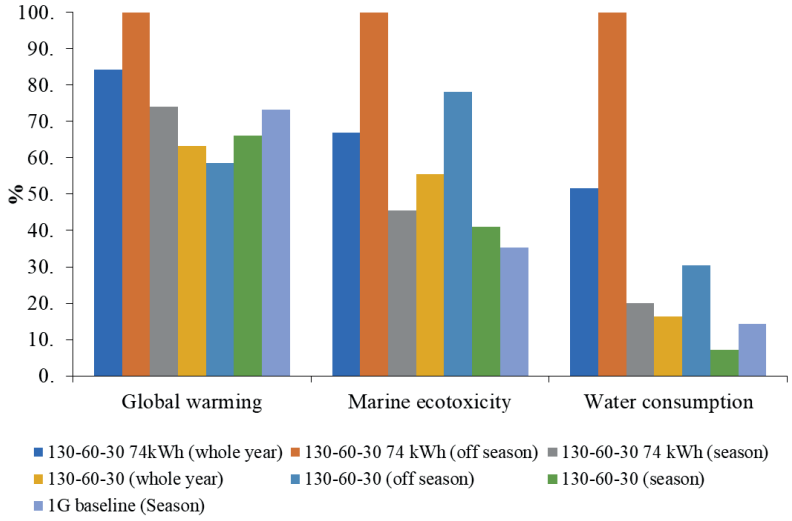

Fig 11: LCIA comparison for different operational periods (T – H_2O_{liq} – SL)

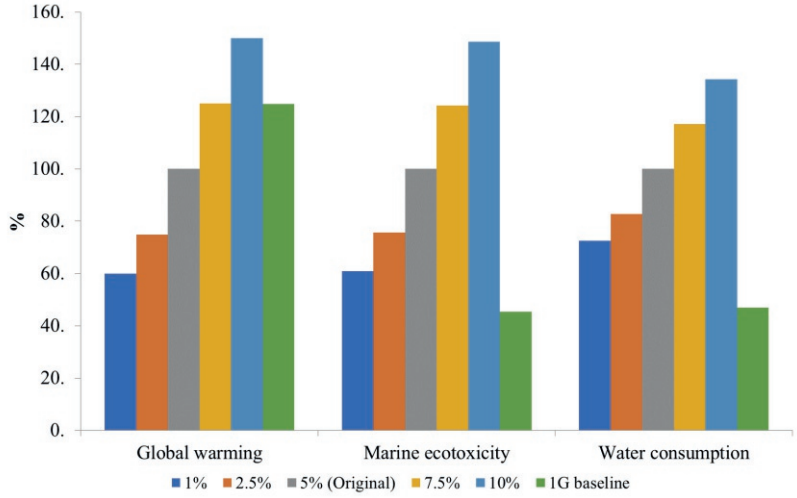

Fig 12: Ionic liquid make-up sensibility analysis (Off-Season operation)

In order to show the process potential for carbon emission mitigation the net avoided emissions in greenhouse gases were accounted for considering gasoline as the fossil counterpart, Figure 13. While in scenario 130-60-30 (74 kWh), the whole-year operation presents a bigger GWP indicator than 1G baseline, the increase in ethanol production, using the same sugarcane stalk crushing capacity in the mill, results in a boost of 23% in avoided emissions. For 130-60-30 (12kWh), 48%. In

the end, even with a larger GWP, in the 74 kWh's case, compared to 1G baseline, the net avoided emissions can be increased. And the boost in ethanol production, using the same sugarcane stalk crushing capacity and, consequently, the same agricultural land, can improve the amount of avoided GHG emissions.

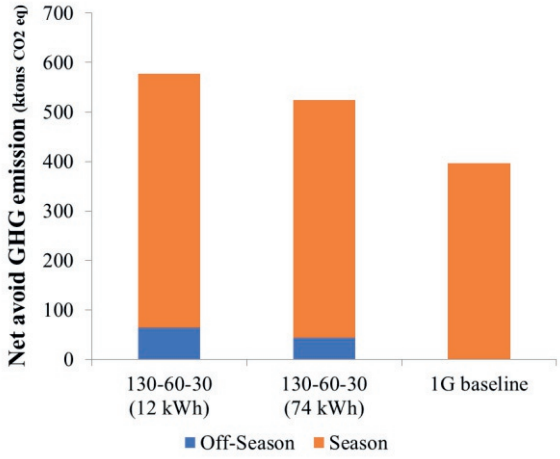

Fig 13: Global warming mitigation capacity for the same sugarcane stalk crushing capacity

4.4 Conclusions

The influence of the pretreatment (PT) design using ionic liquid (IL) for production of ethanol from sugarcane was systematically assessed on a Biorefinery perspective. The decrease in PT temperature reduced considerably the energy expended during PT, but the generated lignocellulose surplus did not compensate for the reduction in enzymatic hydrolysis conversion, resulting in a decreased ethanol productivity. Nevertheless, if the IL make up is positively affected by lower PT temperatures, the economic performance of the plant may overcome even lower enzymatic conversions.

The increase in water concentration during PT from 20% to 60% reduced in 96 % the IL consumption. At the higher water content, IL was recycled from water exclusively by the FC process. The SL had the highest impact on ethanol productivity, yield and on IL consumption among the assessed parameters.

PT design had a relevant and direct effect on PT reactor and IL recycle CAPEX, and an indirect effect on enzymatic hydrolysis reactor CAPEX. Among the assessed variables, SL had the highest impact on CAPEX. The project's economic feasibility, expressed as IRR, was most sensible to product selling price

variation, followed by IL make up, 2G CAPEX, sugarcane stalks price, IL price and straw price. Diversification is an efficient strategy to increase the average product selling price, and, consequently, improve process' economic attractiveness.

The efficient IL recycle, reduction in energy consumption and unnecessary use of consumables are the strengths of the FC process, resulting in low OPEX, supporting its economic feasibility despite to account for 48 % of total 2G CAPEX.

Most of the process parameters analyzed on this work had a significant impact on ethanol's environmental impact profile. This effect translates into the necessary make up for ionic liquid, the main contributor for the most significant impact categories, by normalization.

IL make up, rather than its price, is the most urgent aspect to be improved in an ionic liquid pretreatment based Biorefinery. Beyond economic arguments, improving IL recycle is crucial to consider it a green solvent. The increase in CAPEX is justified by the reduction of OPEX and, therefore, should not be the limiting aspect.

4.5 References

(1) Garrett-Peltier, H. Green versus Brown: Comparing the Employment Impacts of Energy Efficiency, Renewable Energy, and Fossil Fuels Using an Input-Output Model. *Econ. Model.* **2017**, *61* (November 2016), 439–447. https://doi.org/10.1016/j.econmod.2016.11.012.

(2) Hauke Engel, Alastair Hamilton, Solveigh Hieronimus, Tomas Nauclér, David Fine, Dickon Pinner, Matt Rogers, Sophie Bertreau, Peter Cooper, S. L. How a Post-Pandemic Stimulus Can Both Create Jobs and Help the Climate. *McKinsey Co.* **2020**, No. May, 1–10.

(3) REN21. *Renewables 2020 Global Status Report*; 2020.

(4) ANP Brazil. Biofuels Production http://www.anp.gov.br/conteudo-do-menu-superior/31-dados-abertos/5537-producao-de-biocombustiveis (accessed Sep 7, 2020).

(5) EIA. Fuel Ethanol Overview https://www.eia.gov/totalenergy/data/browser/?tbl=T10.03 (accessed Aug 7, 2020).

(6) Brandt, A.; Gräsvik, J.; Hallett, J. P.; Welton, T. Deconstruction of Lignocellulosic Biomass with Ionic Liquids. *Green Chem.* **2013**, *15* (3), 550–583. https://doi.org/10.1039/c2gc36364j.

(7) Mussatto, S. I.; Dragone, G. M. Biomass Pretreatment, Biorefineries, and Potential Products for a Bioeconomy Development. In *Biomass Fractionation Technologies for a Lignocellulosic Feedstock Based Biorefinery*; Elsevier, 2016; pp 1–22. https://doi.org/10.1016/B978-0-12-802323-5.00001-3.

(8) Stark, A. Ionic Liquids in the Biorefinery: A Critical Assessment of Their Potential. *Energy Environ. Sci.* **2011**, *4* (1), 19–32. https://doi.org/10.1039/c0ee00246a.

(9) Soltanian, S.; Aghbashlo, M.; Almasi, F.; Hosseinzadeh-Bandbafha, H.; Nizami, A. S.; Ok, Y. S.; Lam, S. S.; Tabatabaei, M. A Critical Review of the Effects of Pretreatment Methods on the Exergetic Aspects of Lignocellulosic Biofuels. *Energy Convers. Manag.* **2020**, *212* (April), 112792. https://doi.org/10.1016/j.enconman.2020.112792.

(10) The Statistics Portal. Sugar cane production worldwide - forecast 2016-2026 https://www.statista.com/statistics/249679/total-production-of-sugar-worldwide/ (accessed Sep 7, 2020).

(11) UNICA. Sugarcane Share in The Brazilian Energy Generation https://unica.com.br/noticias/cresce-participacao-da-cana-de-acucar-na-geracao-de-energia/ (accessed Sep 7, 2020).

(12) Wang, M.; Han, J.; Dunn, J. B.; Cai, H.; Elgowainy, A. Well-to-Wheels Energy Use and Greenhouse Gas Emissions of Ethanol from Corn, Sugarcane and Cellulosic Biomass for US Use. *Environ. Res. Lett.* **2012**, *7* (4), 045905. https://doi.org/10.1088/1748-9326/7/4/045905.

(13) Brooks, N. J.; Castiglione, F.; Doherty, C. M.; Dolan, A.; Hill, A. J.; Hunt, P. A.; Matthews, R. P.; Mauri, M.; Mele, A.; Simonutti, R.; Villar-Garcia, I. J.; Weber, C. C.; Welton, T. Linking the Structures, Free Volumes, and Properties of Ionic Liquid Mixtures. *Chem. Sci.* **2017**, *8* (9), 6359–6374. https://doi.org/10.1039/C7SC01407D.

(14) Ferrari, F. A.; Pereira, J. F. B.; Witkamp, G. J.; Forte, M. B. S. Which Variables Matter for Process Design and Scale-up? A Study of Sugar Cane Straw Pretreatment Using Low-Cost and Easily Synthesizable Ionic Liquids. *ACS Sustain. Chem. Eng.* **2019**, *7* (15), 12779–12788. https://doi.org/10.1021/acssuschemeng.9b01385.

(15) Pin, T. C.; Nakasu, P. Y. S.; Mattedi, S.; Rabelo, S. C.; Costa, A. C. Screening of Protic Ionic Liquids for Sugarcane Bagasse Pretreatment. *Fuel* **2019**, *235* (July 2018), 1506–1514. https://doi.org/10.1016/j.fuel.2018.08.122.

(16) Zhang, Q.; Hu, J.; Lee, D.-J. Pretreatment of Biomass Using Ionic Liquids: Research Updates. *Renew. Energy* **2017**, *111*, 77–84. https://doi.org/10.1016/J.RENENE.2017.03.093.

(17) Ma, C.; Laaksonen, A.; Liu, C.; Lu, X.; Ji, X. The Peculiar Effect of Water on Ionic Liquids and Deep Eutectic Solvents. *Chem. Soc. Rev.* **2018**, *47* (23), 8685–8720. https://doi.org/10.1039/C8CS00325D.

(18) Li, C.; Tanjore, D.; He, W.; Wong, J.; Gardner, J. L.; Sale, K. L.; Simmons, B. A.; Singh, S. Scale-up and Evaluation of High Solid Ionic Liquid Pretreatment and Enzymatic Hydrolysis of Switchgrass. *Biotechnol. Biofuels* **2013**, *6* (1), 154. https://doi.org/10.1186/1754-6834-6-154.

(19) Gschwend, F. J. V.; Malaret, F.; Shinde, S.; Brandt-Talbot, A.; Hallett, J. P. Rapid Pretreatment of: Miscanthus Using the Low-Cost Ionic Liquid Triethylammonium Hydrogen Sulfate at Elevated Temperatures. *Green Chem.* **2018**, *20* (15), 3486–3498. https://doi.org/10.1039/c8gc00837j.

(20) Konda, N. M.; Shi, J.; Singh, S.; Blanch, H. W.; Simmons, B. A.; Klein-Marcuschamer, D. Understanding Cost Drivers and Economic Potential of Two Variants of Ionic Liquid Pretreatment for Cellulosic Biofuel Production. *Biotechnol. Biofuels* **2014**, *7* (1), 1–11. https://doi.org/10.1186/1754-6834-7-86.

(21) Xu, F.; Sun, J.; Konda, N. V. S. N. M.; Shi, J.; Dutta, T.; Scown, C. D.; Simmons, B. A.; Singh, S. Transforming Biomass Conversion with Ionic Liquids: Process Intensification and the Development of a High-Gravity, One-Pot Process for the Production of Cellulosic Ethanol. *Energy Environ. Sci.* **2016**, *9* (3), 1042–1049. https://doi.org/10.1039/c5ee02940f.

(22) Baral, N. R.; Kavvada, O.; Mendez-Perez, D.; Mukhopadhyay, A.; Lee, T. S.; Simmons, B. A.; Scown, C. D. Techno-Economic Analysis and Life-Cycle Greenhouse Gas Mitigation Cost of Five Routes to Bio-Jet Fuel Blendstocks. *Energy Environ. Sci.* **2019**, *12* (3), 807–824. https://doi.org/10.1039/c8ee03266a.

(23) Bonomi, A.; Cavalett, O.; Pereira, M.; Cunha, D.; Lima Editors, M. A. P. *Virtual Biorefinery An Optimization Strategy for Renewable Carbon Valorization*; Bonomi, A., Cavalett, O., Pereira da Cunha, M., Lima, M. A. P., Eds.; Green Energy and Technology; Springer International Publishing: Cham, 2016. https://doi.org/10.1007/978-3-319-26045-7.

(24) Cavalett, O.; Chagas, M. F.; Seabra, J. E. A.; Bonomi, A. Comparative LCA of Ethanol versus Gasoline in Brazil Using Different LCIA Methods. *Int. J. Life Cycle Assess.* **2013**, *18* (3), 647–658. https://doi.org/10.1007/s11367-012-0465-0.

(25) Garlapati, V. K.; Tewari, S.; Ganguly, R. *Life CYCLE ASSESSMENT OF FIRST-, SECOND-GENERATION, AND MICROALGAE BIOFUELS*; Elsevier Inc., 2019. https://doi.org/10.1016/B978-0-12-817937-6.00019-9.

(26) Baaqel, H.; Díaz, I.; Tulus, V.; Chachuat, B.; Guillén-Gosálbez, G.; Hallett, J. P. Role of Life-Cycle Externalities in the Valuation of Protic Ionic Liquids – a Case Study in Biomass Pretreatment Solvents. *Green Chem.* **2020**. https://doi.org/10.1039/D0GC00058B.

(27) Junqueira, T. L.; Cavalett, O.; Bonomi, A. The Virtual Sugarcane Biorefinery—A Simulation Tool to Support Public Policies Formulation in Bioenergy. *Ind. Biotechnol.* **2016**, *12* (1), 62–67. https://doi.org/10.1089/ind.2015.0015.

(28) Rane, M. V.; Uphade, D. B. Energy Efficient Jaggery Making Using Freeze Pre-Concentration of Sugarcane Juice. *Energy Procedia* **2016**, *90*, 370–381. https://doi.org/10.1016/J.EGYPRO.2016.11.204.

(29) Wu, B.; Liu, W. W.; Zhang, Y. M.; Wang, H. P. Do We Understand the Recyclability of Ionic Liquids? *Chem. - A Eur. J.* **2009**, *15* (8), 1804–1810. https://doi.org/10.1002/chem.200801509.

(30) Nakasu, P. Y. S.; Nakasu, P. Y. S.; Clarke, C. J.; Rabelo, S. C.; Costa, A. C.; Brandt-Talbot, A.; Hallett, J. P. Interplay of Acid-Base Ratio and Recycling on the Pretreatment Performance of the Protic Ionic Liquid Monoethanolammonium Acetate. *ACS Sustain. Chem. Eng.* **2020**, *8* (21), 7952–7961. https://doi.org/10.1021/acssuschemeng.0c01311.

(31) Baral, N. R.; Shah, A. Techno-Economic Analysis of Cellulose Dissolving Ionic Liquid Pretreatment of Lignocellulosic Biomass for Fermentable Sugars Production. *Biofuels, Bioprod. Biorefining* **2016**, *10* (1), 70–88. https://doi.org/10.1002/bbb.1622.

(32) Van der Ham, F. Eutectic Freeze Crystallization, Delft University of Technology, 1999, Vol. 1.

(33) ANEEL. Electric Energy National Agency - Tariff https://www.aneel.gov.br/dados/tarifas.

(34) Cavalett, O.; Chagas, M. F.; Erguy, N. R.; Sugawara, E. T.; Cardoso, T. F.; Bonomi, A. *Sugarcane Life Cycle Inventory*; Campinas, 2012.

(35) Menandro, L. M. S.; Cantarella, H.; Franco, H. C. J.; Kölln, O. T.; Pimenta, M. T. B.; Sanches, G. M.; Rabelo, S. C.; Carvalho, J. L. N. Comprehensive Assessment of Sugarcane Straw: Implications for Biomass and Bioenergy Production. *Biofuels, Bioprod. Biorefining* **2017**, *11* (3), 488–504. https://doi.org/10.1002/bbb.1760.

(36) Huijbregts, M. A. J.; Steinmann, Z. J. N.; Elshout, P. M. F.; Stam, G.; Verones, F.; Vieira, M.; Zijp, M.; Hollander, A.; van Zelm, R. ReCiPe2016: A Harmonised Life Cycle Impact Assessment Method at Midpoint and Endpoint Level. *Int. J. Life Cycle Assess.* **2017**, *22* (2), 138–147. https://doi.org/10.1007/s11367-016-1246-y.

(37) Gjineci, N.; Boli, E.; Tzani, A.; Detsi, A.; Voutsas, E. Separation of the Ethanol/Water Azeotropic Mixture Using Ionic Liquids and Deep Eutectic Solvents. *Fluid Phase Equilib.* **2016**, *424*, 1–7. https://doi.org/10.1016/j.fluid.2015.07.048.

(38) Deng, Y.; Beadham, I.; Ghavre, M.; Costa Gomes, M. F.; Gathergood, N.; Husson, P.; Légeret, B.; Quilty, B.; Sancelme, M.; Besse-Hoggan, P. When Can Ionic Liquids Be Considered Readily Biodegradable? Biodegradation Pathways of Pyridinium, Pyrrolidinium and Ammonium-Based Ionic Liquids. *Green Chem.* **2015**, *17* (3), 1479–1491. https://doi.org/10.1039/c4gc01904k.

(39) Kumar, S.; Singh, N.; Prasad, R. Anhydrous Ethanol: A Renewable Source of Energy. *Renew. Sustain. Energy Rev.* **2010**, *14* (7), 1830–1844. https://doi.org/10.1016/j.rser.2010.03.015.

(40) Usmani, Z.; Sharma, M.; Gupta, P.; Karpichev, Y.; Gathergood, N.; Bhat, R.; Gupta, V. K.

Ionic Liquid Based Pretreatment of Lignocellulosic Biomass for Enhanced Bioconversion. *Bioresour. Technol.* **2020**, *304* (February), 123003. https://doi.org/10.1016/j.biortech.2020.123003.

(41) Shiflett, M. B. *Commercial Applications of Ionic Liquids*; 2020.

(42) Sun, J.; Shi, J.; Murthy Konda, N. V. S. N.; Campos, D.; Liu, D.; Nemser, S.; Shamshina, J.; Dutta, T.; Berton, P.; Gurau, G.; Rogers, R. D.; Simmons, B. A.; Singh, S. Efficient Dehydration and Recovery of Ionic Liquid after Lignocellulosic Processing Using Pervaporation. *Biotechnol. Biofuels* **2017**, *1* (1), 1–14. https://doi.org/10.1186/s13068-017-0842-9.

(43) Biddy, M. J.; Scarlata, C.; Kinchin, C. *Chemicals from Biomass: A Market Assessment of Bioproducts with Near-Term Potential*; Golden, CO (United States), 2016. https://doi.org/10.2172/1244312.

(44) Gezae Daful, A.; Görgens, J. F. Techno-Economic Analysis and Environmental Impact Assessment of Lignocellulosic Lactic Acid Production. *Chem. Eng. Sci.* **2017**, *162*, 53–65. https://doi.org/10.1016/j.ces.2016.12.054.

Chapter 5

Bioenergy and Thesis Outlook

In 2020, we experienced how the decrease in the human activity had a positive effect in the reduction of greenhouse gases emissions. International Energy Agency estimated 10 -25% reduction in energy demand subject to severity of lockdown regime, and approximately 8% reduction in GHG emissions relative to 2019[1]. But there is no reason to celebrate, since such reduction was caused by a global pandemic disease, the Covid-19, which led to the deaths and impoverishment of millions. Even though improvement in the human development index (HDI) has been shown to directly relate to the increase in the energy consumption[2], it illustrated that the economic growth is not the only criterion for society prosperity.

Although the reduction in consumption would be an efficient strategy to decrease environmental impact of human activities [3], it is unlikely to continue in the next, post-pandemic years at a global scale. Even if highly industrialized and developed countries are effective in reducing their relative energy consumption, the development of Africa, Asia and Latin America will inevitably lead to an increase in their energy consumption, boosting global demand for energy and resources[4].

The deployment of bioenergy as a major player for energy transition is often questioned. The threats to biodiversity and food security are hot topics under the debate around the feasibility of bioenergy expansion. Dealing with such criticism should not be avoided but embraced to guide the development of sustainable technologies and public policies instead. The vulnerabilities concerning food security and biodiversity are a heritage from unsustainable business-as-usual. The new technologies, such as underpinning modern bioenergy development, are an opportunity to tackle these issues which are a consequence of our unsustainable economic development.

It is estimated that biomass –done right- can supply almost 50 % of global total energy demand by 2050 without compromising biodiversity, water and food security[5]. As a matter of fact, the development of a sustainable bioenergy sector has been claimed to support secure and sustainable food production[6]. The necessary technical effort to improve agricultural productivity is common for combined energy and food crops. From a Brazilian perspective, the knowledge and infrastructure created due to the expansion of bioenergy in 70's and 80's were extensively used for the intensification of food production. It is expected that the agricultural productivity increases between 0.6% - 0.8% yearly[5]. Carefully selected, multi-annual biomass production in marginal and degraded areas can be used to reestablish the soil fertility, improving and expanding agricultural

productivity[7]. Improving the fertility of marginal lands is even more relevant if we consider the clime-change effect on food production.

Apart from environmental aspect, the investment in renewable energy can potentially generate almost two times more[8] jobs compared to the more capital intensive fossil solutions. Bioenergy is an interdependent sector, involving multiple stakeholders and can play an important role for the development of vulnerable areas, thus promoting inclusive growth[9,10]. The use of agricultural and forestry residues, such as food crop remains, is a fundamental strategy to increase bioenergy capacity and increase the value added to the feedstock without land area expansion, as observed in **Chapter 4**.

In this thesis, Ionic Liquids' (ILs) solvent character was explored for the pretreatment of lignocellulosic (LC) residues, which are saccharified and, then, biologically converted into desirable molecules. In **chapter 2**, it was understood that ILs efficient on solubilizing LC's components might not be as efficient on pretreating LC. The use of ILs mixtures is a promising strategy to improve the solubilization of complex components, for instance, lignin, without the expense of heat. Moreover, mixtures can be used as strategy to overcome the negative effect of IL dilution in water. The homogenization during pretreatment, by means of agitation, should be considered only in case of temperature gradient. Temperature, solid loading and IL dilution are the key operational parameters for scale up, and should be optimized while varying them simultaneously. In **chapter 3**, its was observed that IL aggregation in water was favored by the increase in the hydrophobic region of IL's molecule, which will direct impact the energy consumption during the recycle. The proposed method (FC) was efficient to recycle the studied ILs, without losses and with low energy consumption (74 kWh/ ton water removed). The FC process would be also indicated where water end-use is a limiting factor. In **chapter 4**, it was highlighted that the best pretreatment set up was not the best choice set up with regard to the whole Biorefinery performance. A less effective pretreatment can have a positive effect on the overall productivity due to energy savings during pretreatment, streams concentration and IL recycle steps, and one must consider this tradeoff during the process design. The FC process was a key aspect for the economic and environmental outputs found, decreasing the energy consumption, water footprint and for potentially reduce IL makeup. IL recycle, rather than its price is the limiting aspect for its deployment at large scale. Finally, in **appendices** it was highlighted that ILs mixtures are an efficient strategy to adjust the properties of ILs' systems. Density and viscosity are satisfactory predicted by mathematical models. The H-bonding, and solvophobic interactions

are major forces influencing ionic molecular bulk and, consequently, the changes in such interactions had a direct affect in the viscosity, density, surface tension, chemical activity and thermal and rheological properties.

5.1 Directions for broader use of Ionic Liquids in improved biomass valorization

Nevertheless, further investigation is needed regarding the use of multiple and mixed feedstock. Feedstock diversification is a key aspect for the sustainable expansion of bioenergy, which cooperate with the crop rotation management, benefiting soil fertility[7]. An efficient multiple feedstock pretreatment is an opportunity to expand the potential sources of biomass for biorefinery application[5]. Moreover, it will particularly benefit the inclusion of small producers into the bioenergy sector, favoring wealth distribution and local development[11].

Therefore, it is important that pretreatment sustains its efficiency either working with single or multiple LC sources. The work from Oke et al[12] underlined the benefits of working with mixed as opposed to single feedstock. Apart from the economic and environmental benefits, the use of mixed feedstock showed to be beneficial for some biological conversion process; however, authors highlight the necessary development of flexible technologies, capable to handle changing feedstock characteristics.

Although ILs are generally efficient solvents for LC, some specific pretreatment strategies have already proven their feasibility when one's desire is to turn LC's constituents into fermentable sugars. Design and process strategies for ILs-based solvents were discussed in **Chapters 2, 3** and **4**. They provide great advantages compared to more traditional pretreatment strategies. The use of ILs should, however, also be further investigated as a purification method in Biorefineries in the downstream part. Examples are the recovery of by-products of LC feedstock and from microorganism biomass. This includes the potential to fractionate complex mixtures related to intracellular biomolecules purification, such as polyhydroxyalkanoates. The recovery of useful products from biomass of production organisms is a promising step for bio-based chemical and pharmaceutical production[13,14].

Regarding the recovery of LC constituents, ILs should be further explored for the non-carbohydrate components of biomass, such as proteins and lignin[15,16]. For the proteins, an initial study could focus on the screening of potential ILs considering the chemical reactions involved in pre-existing methods for the

fractionation of protein from ruminant feeds[17]. Another strategy could rely on the selection of ILs following a literature review contemplating the solubilization of other molecules analogous to proteins. The design of the IL-based system for protein purification will need to cope with particular properties throughout the process, for instance pH, surface tension, H bonding donor sites. Apart from the physicochemical properties, IL could be also designed with respect to the introduction of specific groups to the ILs, such as phosphate[17], which might improve protein recovery.

In **Chapter 2** the influence of IL and pretreatment design on delignification of residual solids were assessed. Although the efficiency of lignin removal was studied, the purity and structure characterization of the recovered lignin material were not addressed. The complex and heterogeneous nature of lignin is a limiting aspects for its large scale application[18], thus assessing the influence of ILs composition and pretreatment design on the characteristics of recovered lignin might provide relevant information to determine the possible applications of the resulting material [18,19]. This study is even more important considering mixed feedstock, since lignin structure is highly dependent on the LC source[20].

Lignin valorization may vary depending on its application. It can follow though lignin derivatization to aromatic chemicals[18]. Or, lignin can be explored in its original form, such as an additive for polymers reinforcement. ILs solvent capability can be used for both applications, improving lignin fractionation and purity. Moreover, the dissolution of lignin with ILs could be used to combine the physicochemical flexibility of IL-based systems to the specific properties of lignin. For example, the possibility to bind lignin-based composites to active surfaces could be the starting point to explore the inherent lignin electrochemical and photochemical properties, interesting for energy applications[21].

5.2 Directions in IL recycling

The IL recycle is one of the major limitations for its large-scale application, as evidenced by the findings in **Chapter 4**. In **Chapter 3,** the recovery of IL was studied by means of a freeze concentration process, promoting the continuous and complete IL recuperation. During the experiments it was observed that [Mea][Hex] exhibited a favorable phase behavior from what was observed for [Mea][Ac]. The IL recycle of [Mea][Hex], and other more hydrophobic ILs, should be further investigated considering the freeze concentration process. Hydrophobic regions might favor IL aggregation resulting in improved phase separation.

On the other hand, [Mea][Ac] is not likely to crystalize, thus removing the carbohydrates and aromatic contaminations from the pretreatment is required prior to the IL concentration process. Although not explored in this thesis, the purification of diluted aqueous IL streams by means of column adsorption should be further investigated[22,23].

From a Biorefinery perspective, diversification would be key to be considered in a smart, and efficient design. The diversification from a product perspective can improve process economic feasibility and protect it from market price fluctuation. The choice of product diversification must follow a techno-economic feasibility study in which one must consider the thermodynamic advantages based on feedstock characteristics and necessary steps to reach the desirable product, in order to potential for increased mass yield [24]. The selection must also consider the best options for process integration, minimizing CAPEX and OPEX expenditures, and focus on non-carbohydrates portions of biomass. Another option of diversification would rely on adopting technologies to valorize all possible waste streams, improving overall conversion yield (atom efficiency). Taking the example of a sugarcane mill to illustrate it, expand the traditional juice to ethanol/ sugar pathways to: i) lignocellulosic-based products; ii) capture and use the released CO_2 for synthesis and/or microorganism cultivation[25]; iii) biogas production from vinasse[26]; iv) use the solid residues, such as tart (mixture of sugarcane juice impurities) for agricultural use or energy and chemicals production. It is valid to mention, however, that the effectiveness of the choice is also influenced by the market acceptance.

The best design strategies using ILs in this context is far beyond the scope of this short text. It would demand an integral study, which could be structured as follows: i) identification of available feedstocks and screening of target market products; ii) assess the mass and energy profile of related production technologies, and understand the driving forces ruling the processes; iii) identify the hotspots for energy integration and potential by-products streams; iv) classify the technologies regarding OPEX and CAPEX; v) risk assessment related to each technology, which involve the technology readiness level and might be divided into installation, manufacture and operation[15,24,27]. The outcomes would provide a "matrix of correlation" tool, where potential combinations would be identified and then, validated by simulation. The socio-environmental assessment would also follow the engineering study. Further on, the recent advances in genetic engineering represents an opportunity where the feedstock and bio-catalyst, for instance

enzymes and microorganisms, can be designed to improve process' efficiencies, and should be considered whenever possible[15,28].

5.3 Directions beyond use of ILs in biomass processing

Energy transition is an integrated effort which encompasses industry, academia, the public sector and, at some extension, consumers. It is substantial that policy makers introduce initiatives to foster and guide sustainable development, such as with carbon pricing. In this sense, it is meaningful that new technologies are placed on the scope of such programs, making them tangible for other stakeholders. Moreover, policies like that can mitigate economic disadvantages present in new technologies for a sustainable development. Carbon pricing is a strategy to account for the effects of Carbon related emission into the market dynamics. It is supported by the market failure theory, which can be explained by the Coase Theorem of market externalities[29]. In short, the emissions associated to the production and consumption of a given product, such as gasoline, will affect a common space, atmosphere, which in turn will change the way that other goods must be produced, such as food. The food production will then absorb the extra costs due to additional watering and fertilization to sustain the production in a changed atmosphere, which is driven by the gasoline trade. The carbon pricing aims to account for the additional costs related to HGH emissions and assign it to its respective sources.

RenovaBio is the Brazilian alternative for carbon pricing The CBio is the monetary unit from RenovaBio and is equivalent to the avoided emission of 1 ton of CO_{2eq}. Based on the Cap-and-Trade strategy, it addresses the transport sector, which accounts for 43 % of total emissions. Considering the results from **Chapter 4** and assuming that 1 CBio is traded for US$12.89[30], the carbon pricing policy could add 7.6 M US$ in the Biorefinery annual income, representing a relevant contribution to its economic performance.

5.4 In Conclusion

ILs are a promising alternative for lignocellulose utilization, but still many options for improved use, as evinced by this work. The versatility of IL-based systems represents a great advantage for process design. There is a bright future for ILs in Biorefinery application, whereas minimizing their make-up for sustainable deployment at commercial scale.

5.5 References

(1) International Energy Agency. *Global Energy Review 2020*; 2020. https://doi.org/10.1787/a60abbf2-en.

(2) Ouedraogo, N. S. Energy Consumption and Human Development: Evidence from a Panel Cointegration and Error Correction Model. *Energy* **2013**, *63*, 28–41. https://doi.org/10.1016/j.energy.2013.09.067.

(3) D'Alessandro, S.; Cieplinski, A.; Distefano, T.; Dittmer, K. Feasible Alternatives to Green Growth. *Nat. Sustain.* **2020**, *3* (4), 329–335. https://doi.org/10.1038/s41893-020-0484-y.

(4) Marques, L. *Capitalismo e o Colapso Ambiental (Captalism and the Environmental Colapse)*, 2nd ed.; UNICAMP Publisher: Campinas, 2016.

(5) Popp, J.; Lakner, Z.; Harangi-Rákos, M.; Fári, M. The Effect of Bioenergy Expansion: Food, Energy, and Environment. *Renew. Sustain. Energy Rev.* **2014**, *32*, 559–578. https://doi.org/10.1016/j.rser.2014.01.056.

(6) Souza, G. M.; Victoria, R. L.; Joly, C. A.; Verdade, L. M. *Bioenergy & Sustainability: Bridging the Gaps*; São Paulo, 2015.

(7) Souza, G. M.; Ballester, M. V. R.; de Brito Cruz, C. H.; Chum, H.; Dale, B.; Dale, V. H.; Fernandes, E. C. M.; Foust, T.; Karp, A.; Lynd, L.; Maciel Filho, R.; Milanez, A.; Nigro, F.; Osseweijer, P.; Verdade, L. M.; Victoria, R. L.; Van der Wielen, L. The Role of Bioenergy in a Climate-Changing World. *Environ. Dev.* **2017**, *23* (February), 57–64. https://doi.org/10.1016/j.envdev.2017.02.008.

(8) Hauke Engel, Alastair Hamilton, Solveigh Hieronimus, Tomas Nauclér, David Fine, Dickon Pinner, Matt Rogers, Sophie Bertreau, Peter Cooper, S. L. How a Post-Pandemic Stimulus Can Both Create Jobs and Help the Climate. *McKinsey Co.* **2020**, No. May, 1–10.

(9) Maishanu, S. M.; Sambo, A. S.; Garba, M. M. *Sustainable Bioenergy Development in Africa: Issues, Challenges, and the Way Forward*; Elsevier Inc., 2019. https://doi.org/10.1016/B978-0-12-817654-2.00003-4.

(10) Kouton, J. The Impact of Renewable Energy Consumption on Inclusive Growth: Panel Data Analysis in 44 African Countries. *Econ. Chang. Restruct.* **2020**, No. 0123456789. https://doi.org/10.1007/s10644-020-09270-z.

(11) Sakai, P.; Afionis, S.; Favretto, N.; Stringer, L. C.; Ward, C.; Sakai, M.; Neto, P. H. W.; Rocha, C. H.; Gomes, J. A.; de Souza, N. M.; Afzal, N. Understanding the Implications of Alternative Bioenergy Crops to Support Smallholder Farmers in Brazil. *Sustain.* **2020**, *12* (5), 1–22. https://doi.org/10.3390/su12052146.

(12) Oke, M. A.; Suffian, M.; Annuar, M.; Simarani, K. Mixed Feedstock Approach to Lignocellulosic Ethanol Production — Prospects and Limitations. *BioEnergy Res.* **2016**, 1189–1203. https://doi.org/10.1007/s12155-016-9765-8.

(13) Kiss, A. A.; Lange, J. P.; Schuur, B.; Brilman, D. W. F.; van der Ham, A. G. J.; Kersten, S. R. A. Separation Technology–Making a Difference in Biorefineries. *Biomass and Bioenergy* **2016**, *95*, 296–309. https://doi.org/10.1016/j.biombioe.2016.05.021.

(14) Sadhukhan, J.; Ng, K. S.; Hernandez, E. M. *Biorefineries and Chemical Processes*; 2014. https://doi.org/10.1002/9781118698129.

(15) Dragone, G.; Kerssemakers, A. A. J.; Driessen, J. L. S. P.; Yamakawa, C. K.; Brumano, L. P.; Mussatto, S. I. Innovation and Strategic Orientations for the Development of Advanced Biorefineries. *Bioresour. Technol.* **2020**, *302* (December 2019), 122847. https://doi.org/10.1016/j.biortech.2020.122847.

(16) Solati, Z.; Manevski, K.; Jørgensen, U.; Labouriau, R.; Shahbazi, S.; Lærke, P. E. Crude Protein Yield and Theoretical Extractable True Protein of Potential Biorefinery Feedstocks. *Ind.*

Crops Prod. **2018**, *115* (January), 214–226. https://doi.org/10.1016/j.indcrop.2018.02.010.

(17) Licitra, G.; Hernandez, T. M.; Van Soest, P. J. Feedbunk Management Evaluation Techniques. *Anim. Feed Sci. Technol.* **1996**, *57*, 347–358.

(18) Cao, Y.; Chen, S. S.; Zhang, S.; Ok, Y. S.; Matsagar, B. M.; Wu, K. C. W.; Tsang, D. C. W. Advances in Lignin Valorization towards Bio-Based Chemicals and Fuels: Lignin Biorefinery. *Bioresour. Technol.* **2019**, *291* (May). https://doi.org/10.1016/j.biortech.2019.121878.

(19) Pin, T. C.; Nascimento, V. M.; Costa, A. C.; Pu, Y.; Ragauskas, A. J.; Rabelo, S. C. Structural Characterization of Sugarcane Lignins Extracted from Different Protic Ionic Liquid Pretreatments. *Renew. Energy* **2020**, *161*, 579–592. https://doi.org/10.1016/j.renene.2020.07.078.

(20) Brandt, A.; Gräsvik, J.; Hallett, J. P.; Welton, T. Deconstruction of Lignocellulosic Biomass with Ionic Liquids. *Green Chem.* **2013**, *15* (3), 550–583. https://doi.org/10.1039/c2gc36364j.

(21) Espinoza-Acosta, J. L.; Torres-Chávez, P. I.; Olmedo-Martínez, J. L.; Vega-Rios, A.; Flores-Gallardo, S.; Zaragoza-Contreras, E. A. Lignin in Storage and Renewable Energy Applications: A Review. *J. Energy Chem.* **2018**, *27*, 1422–1438. https://doi.org/10.1016/j.jechem.2018.02.015.

(22) Montané, D.; Nabarlatz, D.; Martorell, A.; Torné-Fernández, V.; Fierro, V. Removal of Lignin and Associated Impurities from Xylo-Oligosaccharides by Activated Carbon Adsorption. *Ind. Eng. Chem. Res.* **2006**, *45* (7), 2294–2302. https://doi.org/10.1021/ie051051d.

(23) Francisco, M.; Mlinar, A. N.; Yoo, B.; Bell, A. T.; Prausnitz, J. M. Recovery of Glucose from an Aqueous Ionic Liquid by Adsorption onto a Zeolite-Based Solid. *Chem. Eng. J.* **2011**, *172* (1), 184–190. https://doi.org/10.1016/j.cej.2011.05.087.

(24) van der Wielen, L. A. M.; Mussatto, S. I.; van Breugel, J. Bioprocess Intensification: Cases That (Don't) Work. *N. Biotechnol.* **2020**, *61* (July 2020), 108–115. https://doi.org/10.1016/j.nbt.2020.11.007.

(25) Liu, Z.; Wang, K.; Chen, Y.; Tan, T.; Nielsen, J. Third-Generation Biorefineries as the Means to Produce Fuels and Chemicals from CO2. *Nat. Catal.* **2020**, *3* (March). https://doi.org/10.1038/s41929-019-0421-5.

(26) Bernal, A. P.; dos Santos, I. F. S.; Moni Silva, A. P.; Barros, R. M.; Ribeiro, E. M. Vinasse Biogas for Energy Generation in BrazilAn Assessment of Economic Feasibility, Energy Potential and Avoided CO2 Emissions. *J. Clean. Prod.* **2017**, *151*, 260–271. https://doi.org/10.1016/j.jclepro.2017.03.064.

(27) Santos, V. E. N.; Ely, R. N.; Szklo, A. S.; Magrini, A. Chemicals, Electricity and Fuels from Biorefineries Processing Brazil's Sugarcane Bagasse: Production Recipes and Minimum Selling Prices. *Renew. Sustain. Energy Rev.* **2016**, *53*, 1443–1458. https://doi.org/10.1016/j.rser.2015.09.069.

(28) Liu, E.; Li, M.; Das, L.; Pu, Y.; Frazier, T.; Zhao, B.; Crocker, M.; Ragauskas, A. J.; Shi, J. Understanding Lignin Fractionation and Characterization from Engineered Switchgrass Treated by an Aqueous Ionic Liquid. *ACS Sustain. Chem. Eng.* **2018**, *6* (5), 6612–6623. https://doi.org/10.1021/acssuschemeng.8b00384.

(29) Pindyck, R. S. Coase Lecture—Taxes, Targets and the Social Cost of Carbon. *Economica* **2017**, *84* (335), 345–364. https://doi.org/10.1111/ecca.12243.

(30) B3. Bolsa Brazil Balcao, Series Historicas http://www.b3.com.br/pt_br/market-data-e-indices/servicos-de-dados/market-data/historico/renda-fixa/ (accessed Aug 4, 2020).

Appendix A[4]

Physicochemical Characterization of Two Protic Hydroxyethylammonium Carboxylate Ionic Liquids in Water and their Mixtures

A systematic study, on the physicochemical properties characterization of two protic ionic liquids {2-hydroxyethylammonium acetate ([Mea][Ac]) and 2-hydroxuethylammonium hexanoate ([Mea][Hex])} and their mixture in water, was carried. The density and viscosity have been measured in the entire range of dilution between 278 K and 393 K. The conductivity, water activity and surface tension data were also studied and the influence of both anions, i.e $[Ac]^-$ and $[Hex]^-$, evaluated. The excess molar volume (V^E), molecular volume and thermal expansion coefficient were calculated from the experimental data, with negative values for V^E in the entire concentration range. Density data was fitted to a polynomial for density predictions as function of temperature and IL concentration with the average deviation percentage (ADP) not exceeding 0.63%. The viscosities of the binary systems (IL+water) were studied considering 6 different models. The resulting viscosity of binary systems, for both [Mea][Ac] and [Mea][Hex] in water, were better predicted by Herráez *et al* model when considering an IL concentration higher than 0.25 molar fraction. The systems containing $[Hex]^-$ exhibited higher water activities and lower conductivity and surface tension.

[4] This chapter is based in a prepared paper to be submitted in the Journal of *Chemistry and Engineering Data* as: Ferrari, F.A., Malaret, F., Eustace, S., Djanashvili. K., Hallett, J.P., Wielen, L.A.M, Witkamp, G.J, Forte, M.B.S.F. Physicochemical Characterization of Two Protic Hydroxyehtylammonium Carboxylate Ionic Liquids in Water and their Mixture

A.1 Introduction

Recently, much attention has been given to ionic liquids (ILs), which structure can be designed based on process needs, tuning distinct properties such as viscosity, density, conductivity and hydrogen bond potential. Therefore, physicochemical properties can be conveniently tuned optimizing the design of more efficient processes.

Ionic Liquids (ILs) molecules can be involved in different kinds of interaction, *e.g.* H bonding, Coulomb, van de Waals, solvophobic and dipole-dipole[1]. Studies involving ILs application are found in a wide range of fields, from catalysis to solvent applications[2,3], due to the vast number of possible cations and anions combinations. Protic ILs (PILs), which are characterized by a proton transfer between cation and anion, are an attractive sort of IL due to their lower cost and toxicity, and easier synthesis in comparison to aprotic ILs[4,5]. The fact that PILs contain both proton donor and acceptor sites lead to an increased contribution of the H-bond to the cation-anion interaction, defecting the electrostatic network, which gives distinct bulk properties for this class of ILs[1,6,7].

The presence of hydroxyl groups in de cation, such as those found in ethanolamine, will also affect the network formation. The additional H-bonding site hinders polar and a-polar segregation, increases the hydrophilicity and might favor cation-cation interaction[1,8]. Oxygen functionalized groups are also described to increase IL viscosity, and promote stronger H-bonding network, more pronounced in groups with higher electron densities, such as hydroxyl and ester groups [1,8–10]. Although the size of anion's alkyl chain has a direct influence on the molecular arrangement of ILs, it does not have a common effect on their properties, i.e. a longer molecule could potentially increase and decrease IL's viscosity, depending on the existence of a hydroxyl group in the cation[10–13].

Among PILs, ammonium based ILs, such as ethanolamine, have being reported as being an efficient class of solvents for the valorization of agricultural residues [14,15]. The physicochemical properties, such as density and viscosity of 2-hydroxyethylammonium acetate ([Mea][Ac]) and its aqueous mixtures were previous reported in literature [7,16,17], and it is found that even small variations in the IL's residual humidity can impact on the properties of the final system. The presence of water in some potential areas of ILs application is difficult to avoid. Moreover, water dilution can be used to decrease IL's viscosity and, therefore, improve the mass transfer within the system.

Besides cation-anion combination, the mixture of ILs can be used to fine-tune system properties towards a more efficient process[18–20]. In Chapter 2, the mixture of [Mea][Ac] and 2-hydroxyethylammonium hexanoate ([Mea][Hex]) was efficiently applied to improve lignin solubilization and enhance the saccharification of the carbohydrate portion of sugarcane straw. Later, the mixture of [Mea][Ac] and [Mea][Hex] was studied during IL recovery from aqueous streams (Chapter 3), where their distinct effect on water freezing point temperature was observed.

In this section, it is reported the experimental measurements of density, viscosity, conductivity, surface tension and water activity for [Mea][Ac], [Mea][Hex] and from their aqueous solutions. Temperature influence on density and viscosity is also explored. The mixture of [Mea][Ac] and [Mea][Hex] were investigate on regard the aforementioned properties.

A.2 Material & Methods

A.2.1 Synthesis and samples preparation

Acetic acid (99.7 %), hexanoic acid (99 %) and ethanolamine (99 %) were acquired from Sigma Aldrich. MilliQ water was used for dilutions. 2-Hydroxyethylammonium acetate ([Mea][Ac]) and 2-hydroxyethylammonium hexanoate ([Mea][Hex]), depicted in Figure 1, were synthesized in 100 mL Schott flasks by a one-step, acid–base exothermic neutralization. First, ethanolamine was weighed into a flask. The flask was closed with a silicone septum and placed in a cold-water bath. An equimolar quantity of either acetic acid or hexanoic acid was slowly added through the septum using a syringe. The reaction was carried out overnight at room temperature under agitation. The formation of [Mea][Ac] or [Mea][Hex] was confirmed by proton nuclear magnetic resonance (^{1}H NMR), and spectra are provided in Appendix B.

The humidity for [Mea][Ac] and [Mea][Hex] was 0.15 %(w/w) and 0.2 %(w/w), respectively, assessed through Karl Fisher titration. For the mixture samples, either water or ILs were weighted with a precision of 1 x10^{-4} g and, then, vigorously mixed for complete homogenization. Samples were sonicated for 2 h in sealed flasks at 45 °C, and kept in desiccator until analysis.

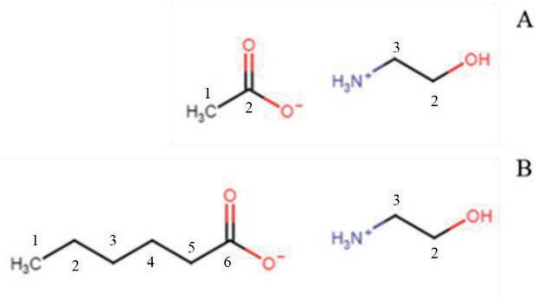

Fig 1: [Mea][Ac] (A) and [Mea][Hex] (B).

A.2.2 Volumetric Properties

Densities (ρ) of pure IL, mixtures and aqueous solutions were measured in the range of 298.15 – 396.15 K at atmosphere pressure, by means of vibrating tube densitometer DMA^{TM} 5000M Anton Paar (Austria), with precision of 1.0 x 10^{-6} g.cm^3 and 1.0 x 10^{-3} °C. Instrument was calibrated before each experimental run using dry air and water. At the end of each run, the density of MilliQ water was acquired for consistency purposes. Aqueous samples were measured in triplicate, and 5 times for the density of dry ILs.

The molar volume (V_m) was calculated according to eq 1, and the excess molar volumes (V^E) following equation 2:

$$V_m = \frac{(x_1 M_{1+} x_2 M_2)}{\rho_{mix}} \qquad \text{eq. 1}$$

$$V^E = V_m - \frac{x_1 M_1}{\rho_1} - \frac{x_2 M_2}{\rho_2} \qquad \text{eq. 2}$$

where, x_i denotes for the molar fraction of the component, M_i is the molar mass, ρ_i is the density. The correction of density due to viscosity is done automatically by the equipment.

The thermal expansion coefficient (α_p) indicates the volume dependence on temperature and was calculated according to equation 3.

$$\alpha_P = \frac{1}{V}\left(\frac{\partial V}{\partial T}\right)_P = -\left(\frac{\partial ln\rho}{\partial T}\right)_P \qquad \text{eq.3}$$

The molecular volume for a single IL pair was calculated using equation 4, where Na is the Avogadro constant (6.02214076×10^{23} mol^{-1})

$$V_m^f = \frac{Mw_{IL}}{N_a \cdot \rho_{IL}} \cdot \frac{10^{21} nm^3}{cm^3} = 1.6605 \cdot 10^{-3} \frac{Mw_{IL}}{\rho_{IL}} \quad \text{eq.4}$$

A.2.3 Viscosity

Viscosities (η) of pure IL, mixtures and aqueous solutions were measured in the range of 298.15 – 323.15 K at atmosphere pressure, by means of rolling ball tube Lovis^{TM} 2000M/ME Anton Paar (Austria), with accuracy of 0.5 % and 2.0 x 10^{-2} °C. Instrument was calibrated before each experimental run with MilliQ water and standard oil provided by the manufacturer. At the end of each run, the vicosity of MilliQ water and glycerol were acquired for consistency purposes. For samples without water addition at ambient temperature, viscosity was measured using Cone-plate model rheometer AR1500ex^{TM} TA Instruments (USA) due to their high viscosities. The shear rate used was $1s^{-1}$, from 0 to 300, with a cone diameter of 20 mm at 298.15 K. Aqueous samples were measured in triplicate, and 5 times for the dry ILs.

A.2.4 Conductivity

Conductivity was acquired through electrical potential measurements by means of self-made platinum probe at room temperature (293 K – 296 K). The conductivity was calculated through KCl calibration curve. Probe was exhaustively rinsed and dried between samples measurements.

A.2.5 Water Activity

Water activity (a_W) was measured through vapor sorption analysis using Q5000^{TM} SA TA Instruments (USA) with weight sensitivity of < 0.1 µg and accuracy of 0.01 %, isothermal stability of ± 0.1 °C and humidity accuracy in humidity chamber of ± 1 %RH. Aqueous IL samples were weighted in platinum pan, mass variations where acquired as the humidity inside the chamber was changed until constant weight. Then, the humidity was decreased, and the mass recorded after equilibrium, and on. After the desorption run, the humidity in chamber was increased at a constant level and mass variation due to water adsorption recorded. The a_W was assumed to be RH/ 100 at the equilibrium. Measurements were performed in triplicate.

A.2.6 Surface Tension

Surface tension was measured against air at room temperature (≈ 293 K) by means of the pendant drop method using DSA25S Krüss (Gemany). Samples were placed in a syringe, and the drop generated out the canula photographed. From the digital shape of the drop, surface tension was calculated by solving Laplace's equation for the curvature of the interface exposed to a gravitational field.

A.3 Results & Discussion

A.3.1 Volumetric Properties

The density of aqueous [Mea][Ac] and aqueous [Mea][Hex] are depicted in Figures 2-4 as function of temperature and water molar fraction. The complete data in Tables 1-10.

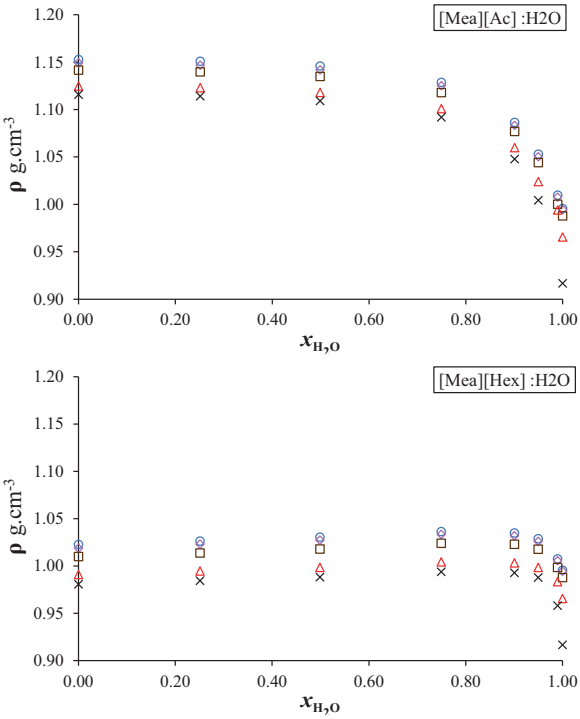

Fig 2: Density versus water molar fraction at different temperatures: 298.15 K (○), 303.15 K (◊), 318.15 K (□), 348.15 (Δ) and 363.15 (x).

Tab 1: Density of [Mea][Ac] as function of water mol fraction and temperature.

	[Mea][Ac] : [H2O]													
T K	**0.0104 : 0.9896**		**0.0503 : 0.9497**		**0.0993 : 0.9007**		**0.2506 : 0.7495**		**0.5011 : 0.4989**		**0.7489 : 0.2511**		**0.9810 : 0.0190**	
	ρ	**± σ**	**ρ**	**± σ**	**ρ**	**± σ**	**ρ**	**± σ**	**ρ**	**± σ**	**ρ**	**± σ**	**ρ**	**± σ**
298.15	1.00974	0.00118	1.05294	0.00118	1.08647	0.00132	1.12866	0.00028	1.14590	0.00027	1.15091	0.00022	1.15285	0.00015
303.15	1.00769	0.00115	1.05034	0.00140	1.08344	0.00207	1.12515	0.00152	1.14179	0.00110	1.14675	0.00117	1.14935	0.00112
318.15	1.00014	0.00109	1.04412	0.00125	1.07699	0.00129	1.11798	0.00027	1.13493	0.00024	1.13979	0.00021	1.14163	0.00013
323.15	0.99562	0.00207	1.04047	0.00107	1.07354	0.00215	1.11430	0.00158	1.13099	0.00112	1.13558	0.00119	1.13810	0.00114
348.15	0.99417	0.02923	1.02420	0.00300	1.05993	0.00158	1.10098	0.00026	1.11815	0.00028	1.12310	0.00022	1.12468	0.00024
363.15	0.88960	0.01460	1.00424	0.00372	1.04782	0.00231	1.09194	0.00026	1.10921	0.00028	1.11417	0.00023	1.11584	0.00027

Tab 2: Density of [Mea][Hex] as function of water mol fraction and temperature.

	[Mea][Hex] : [H2O]													
T K	**0.0100 : 0.9900**		**0.0501 : 0.9499**		**0.0998 : 0.9002**		**0.2499 : 0.7501**		**0.4999 : 0.5001**		**0.7529 : 0.2471**		**0.9715 : 0.0285**	
	ρ	**± σ**	**ρ**	**± σ**	**ρ**	**± σ**	**ρ**	**± σ**	**ρ**	**± σ**	**ρ**	**± σ**	**ρ**	**± σ**
298.15	1.00764	0.00026	1.02886	0.00043	1.03500	0.00001	1.03652	0.00098	1.03056	0.00098	1.02648	0.00122	1.02276	0.00120
303.15	1.00580	0.00044	1.02619	0.00042	1.03208	0.00001	1.03351	0.00142	1.02744	0.00100	1.02334	0.00109	1.01882	0.00119
318.15	0.99869	0.00117	1.01772	0.00039	1.02304	0.00002	1.02416	0.00099	1.01795	0.00110	1.01385	0.00099	1.01010	0.00121
323.15	0.99564	0.00168	1.01475	0.00038	1.01992	0.00002	1.02096	0.00110	1.01480	0.00132	1.01066	0.00128	1.00611	0.00120
348.15	0.98353	0.00000	0.99853	0.00000	1.00348	0.00000	1.00436	0.00085	0.99863	0.00088	0.99475	0.00108	0.99100	0.00132
363.15	0.95815	0.00000	0.98800	0.00000	0.99288	0.00000	0.99390	0.00070	0.98835	0.00117	0.98455	0.00100	0.98090	0.00133

Tab 3: Density of IL mixture as function of molar composition and temperature.

	[Mea][Ac] : [Mea][Hex]													
T K	**0.1433 : 0.8567**		**0.2500 : 0.7500**		**0.4000 : 0.6000**		**0.4999 : 0.5001**		**0.5994 : 0.4006**		**0.7651 : 0.2349**		**0.9003 : 0.0997**	
	ρ	**± σ**	**ρ**	**± σ**	**ρ**	**± σ**	**ρ**	**± σ**	**ρ**	**± σ**	**ρ**	**± σ**	**ρ**	**± σ**
298.15	1.03379	0.00034	1.04440	0.00093	1.05915	0.00003	1.07336	0.00196	1.08405	0.00000	1.10767	0.00085	1.13272	0.00025
303.15	1.03066	0.00034	1.04026	0.00060	1.05608	0.00003	1.06931	0.00241	1.08105	0.00000	1.10375	0.00099	1.12986	0.00001
318.15	1.02123	0.00035	1.03193	0.00094	1.04683	0.00003	1.06118	0.00198	1.07199	0.00001	1.09587	0.00084	1.12125	0.00002
323.15	1.01806	0.00035	1.02774	0.00060	1.04372	0.00004	1.05708	0.00243	1.06895	0.00001	1.09191	0.00100	1.11836	0.00002
348.15	1.00232	0.00035	1.01307	0.00110	1.02793	0.00004	1.04263	0.00201	1.05351	0.00001	1.07801	0.00097	1.10371	0.00004
363.15	0.99232	0.00036	1.00313	0.00109	1.01812	0.00004	1.03293	0.00202	1.04393	0.00001	1.06873	0.00103	1.09462	0.00004

Tab 4: Density of the IL mixture [Mea][Ac] 0.25:0.75 [Mea][Hex] as function of temperature and water molar fraction

	[Mea][Ac] 0.25:0.75 [Mea][Hex] : H2O (g.cm^{-3})											
T (K)	**0.15 : 0.85**		**0.2500 : 0.7500**		**0.30 : 0.70**		**0.50 : 0.50**		**0.75 : 0.25**		**1.00 : 0.00**	
	ρ	**± σ**	**ρ**	**± σ**	**ρ**	**± σ**	**ρ**	**± σ**	**ρ**	**± σ**	**ρ**	**± σ**
298.15			1.05271	0.00030	1.05214	0.00073	1.04910	0.00108	1.04572	0.00064	1.04440	0.00093
303.15			1.04969	0.00103	1.04908	0.00085	1.04602	0.00079	1.04262	0.00120	1.04026	0.00060
318.15			1.04047	0.00084	1.03982	0.00092	1.03666	0.00081	1.03326	0.00084	1.03193	0.00094
323.15			1.03734	0.00059	1.03667	0.00061	1.03353	0.00043	1.03012	0.00079	1.02774	0.00110
348.15			1.02114	0.00097	1.02050	0.00090	1.01744	0.00024	1.01407	0.00087	1.01307	0.00109
363.15			1.01091	0.00080	1.01032	0.00045	1.00740	0.00036	1.00412	0.00086	1.00313	0.00093

Tab 5: Density of the IL mixture [Mea][Ac] 0.75:0.25 [Mea][Hex] as function of temperature and water molar fraction

T K	[Mea][Ac] : [Mea][Hex] 0.75 : 0.25 : H2O											
	0.15 : 0.85		0.2500 : 0.7500		0.30 : 0.70		0.50 : 0.50		0.75 : 0.25		1.00 : 0.00	
	ρ	± σ	ρ	± σ	ρ	± σ	ρ	± σ	ρ	± σ	ρ	± σ
298.15	1.08630	0.00104	1.09870	0.00060	1.10169	0.00081	1.10836	0.00058	1.10919	0.00072	1.10767	0.00104
303.15	1.08361	0.00044	1.09589	0.00056	1.09885	0.00075	1.10548	0.00084	1.10628	0.00081	1.10375	0.00097
318.15	1.07529	0.00037	1.08729	0.00085	1.09020	0.00082	1.09672	0.00068	1.09748	0.00076	1.09587	0.00084
323.15	1.07242	0.00025	1.08436	0.00090	1.08726	0.00067	1.09377	0.00055	1.09452	0.00080	1.09191	0.00071
348.15			1.06921	0.00073	1.07212	0.00040	1.07874	0.00049	1.07947	0.00093	1.07801	0.00084
363.15			1.05962	0.00060	1.06256	0.00048	1.06934	0.00041	1.07013	0.00039	1.06873	0.00103

Tab 6: Viscosity of [Mea][Hex] as function of water mol fraction and temperature.

T (K)	[Mea][Hex] : [H2O]													
	0.0100 : 0.9900		0.0501 : 0.9499		0.0998 : 0.9002		0.2499 : 0.7501		0.4999 : 0.5001		0.7529 : 0.2471		0.9715 : 0.0285	
	η	± σ	η	± σ	η	± σ	η	± σ	η	± σ	η	± σ	η	± σ
298.15	1.35	0.12	3.93	0.14	12.14	0.46	59.74	0.00	280.26	14.23	828.70	80.54	1590.31	50.44
303.15			3.42	0.09	10.08	0.34	47.49	0.00	210.42	11.50	597.47	38.70	1099.90	80.18
318.15			2.30	0.06	5.93	0.12	25.80	0.00	97.72	2.60	249.08	11.22	475.11	30.17
323.15			2.01	0.07	5.14	0.10	21.55	0.00	77.82	3.40	191.69	10.93	354.74	25.79

Table 7: Viscosity of [Mea][Ac] as function of water mol fraction and temperature.

T (K)	[Mea][Ac] : [H2O]													
	0.0104 : 0.9896		0.0503 : 0.9497		0.0993 : 0.9007		0.2506 : 0.7495		0.5011 : 0.4989		0.7489 : 0.2511		0.9810 : 0.0190	
	η	± σ	η	± σ	η	± σ	η	± σ	η	± σ	η	± σ	η	± σ
298.15	0.89	0.04	2.08	0.05	4.39	0.32	27.23	0.36	221.43	13.76	872.99	90.30	2654.38	59.70
303.15			1.90	0.11	3.78	0.27	21.92	0.25	138.94	12.73	598.33	42.40	1282.60	84.30
318.15			1.33	0.05	2.54	0.17	12.56	0.25	70.40	3.38	223.05	12.40	606.16	115.07
323.15			1.27	0.00	2.25	0.15	10.46	0.28	49.80	3.25	155.38	10.07	413.89	79.96

Tab 8: Viscosity of IL mixture as function of molar composition and temperature.

T (K)	[Mea][Ac] : [Mea][Hex]													
	0.1433 : 0.8567		0.2500 : 0.7500		0.4000 : 0.6000		0.4999 : 0.5001		0.5994 : 0.4006		0.7651 : 0.2349		0.9003 : 0.0997	
	η	± σ	η	± σ	η	± σ	η	± σ	η	± σ	η	± σ	η	± σ
298.15	1661.94	71.56	1710.19	72.20	1714.00	69.82	1999.31	73.26	2096.25	80.13	2193.25	70.90	2153.81	72.45
303.15	1258.57	74.42	1292.70	94.30	1380.45	89.35	1410.80	89.75	1593.97	103.63	1536.35	234.45	1623.60	336.26
318.15	476.60	28.57	481.30	34.64	504.07	33.34	508.22	43.25	559.39	35.75	566.36	78.44	621.52	46.07
323.15	348.44	22.54	332.77	0.00	373.33	24.83	353.86	6.83	400.30	26.19	393.72	52.16	448.82	32.89

Tab 9: Viscosity of the IL mixture [Mea][Ac] 0.25:0.75 [Mea][Hex] as function of temperature and water molar fraction

T (K)	[Mea][Ac] : [Mea][Hex] 0.25 : 0.75 : H2O											
	0.15 : 0.85		0.2500 : 0.7500		0.30 : 0.70		0.50 : 0.50		0.75 : 0.25		1.00 : 0.00	
	η	± σ	η	± σ	η	± σ	η	± σ	η	± σ	η	± σ
298.15			46.75	0.42	73.47	0.51	263.57	13.76	826.82	75.27	1710.19	72.20
303.15			37.42	0.40	57.89	0.41	196.69	12.73	593.16	60.12	1292.70	94.30
318.15			20.92	0.23	30.71	0.46	90.96	3.38	243.02	22.47	481.30	34.64
323.15			17.79	0.18	25.47	0.17	72.51	3.25	186.34	20.02	332.77	0.00

Tab 10: Viscosity of the IL mixture [Mea][Ac] 0.75:0.25 [Mea][Hex] as function of temperature and water molar fraction

T (K)	[Mea][Ac] : [Mea][Hex] 0.75 : 0.25 : H2O											
	0.15 : 0.85		0.2500 : 0.7500		0.30 : 0.70		0.50 : 0.50		0.75 : 0.25		1.00 : 0.00	
	η	± σ	η	± σ	η	± σ	η	± σ	η	± σ	η	± σ
298.15	10.07	0.32	32.84	0.30	52.61	0.60	248.05	15.18	988.58	82.03	2193.25	70.90
303.15	8.41	0.15	26.41	0.27	41.38	0.52	182.05	14.20	683.22	70.04	1536.35	234.45
318.15	5.24	0.21	15.12	0.22	22.14	0.30	80.83	12.10	260.25	17.87	566.36	78.44
323.15	4.57	0.12	12.75	0.21	18.61	0.09	63.82	5.12	195.82	11.04	393.72	52.16

The increase in anion's alkyl chain length leads to a lower density of [Mea][Hex], as expected, which might be attributed to the bulkier chains, increasing steric hindrance. Alvarez *et al*[16] reported a low dependency on moisture for the density for [Mea][Ac], visible up to 0.5 water mol as shown in Figure 1, beyond which water has a significant influence on this property. Water content distinctly affects [Mea][Hex], the density slightly increases with increasing water up to a maximum at 0.9 molar fraction and, then, decreases towards the density of pure water. This trend is in agreement with a previous study for other ammonium alkanoate-based ILs [21].

In order to predict the mixture's density, the polynomial expressed in equation 5 was fitted to the experimental data as function of IL wt%(y) and temperature in K (x). The fitting parameters and the average percent deviation (APD) are summarized in Table 11, deviations from each experimental point are depicted in table 12. The APD was calculated following equation 6.

$$\rho = a.x + b.y + c.x^2 + d.y^2 + e.x.y + f \qquad \text{eq. 5}$$

$$APD = \frac{100}{n}\sum_{1}^{n}\left(\frac{\left|\rho_{experimental} - \rho_{model}\right|}{\rho_{experimental}}\right) \qquad \text{eq. 6}$$

Excess molar volumes (V^E) were considered to estimate the nonideality of the studied systems. V^E was calculated using equations 2. For both ILs, the V^E are negative within the entire range of dilution, with a minimum at water molar fraction near 0.75. The negative values indicate the attraction forces between the different molecules are greater than that from the same molecules in neat solvent. The longer carbonic chain from [Mea][Hex] had no evident effect on V^E, which is reasonable since water tend to bind to the H-bonding sites, i.e. COO^- (anion) and NH_3^+ and OH (cation) [22,23]. It was observed a greater temperature influence on V^E at 363.15 K, suggesting a lower thermal expansion by the mixture than that from pure components.

Table 11: Fitting parameters from eq. 4 for the ILs systems.

	a	b	c	d	e	f	APD
[Mea][Ac] and water	4.139 x 10^{-5}	2.864 x 10^{-1}	-1.020 x 10^{-5}	-1.459 x 10^{-1}	7.0 x 10^{-4}	9.93 x 10^{-1}	0.63 %
[Mea][Hex] and water	-4.0 x 10^{-4}	1.132 x 10^{-1}	-2.316 x 10^{-6}	-8.75 x 10^{-2}	3.431 x 10^{-5}	1.011	0.32 %
[Mea][Ac] and **[Mea][Hex]**	-6.0 x 10^{-4}	1.14 x 10^{-1}	-3.894 x 10^{-7}	1.42 x 10^{-2}	6.864 x 10^{-5}	1.037	0.07 %

Mixtures of [Mea][Ac] with [Mea][Hex] were considered to assess the effect of the anions combination on density. The anhydrous mixture exhibited a progressive change in density following the variation in the molar composition, with a slight deviation from linearity, as depicted in Figure 4. The higher deviations from linearity and, consequently, from ideality are found to be within the range of 0.4 to 0.6 molar fraction.

Two distinct molar compositions were selected to assess the influence of water on the mixtures, namely 0.25:0:75 and 0.75:0.25 [Mea][Ac]:[Mea][Hex] molar fraction, respectively. Density and V^E are depicted in Figure 5, the complete data is available in SI. As expected, the system richer in [Mea][Ac] exhibits higher density. Similarly to the dilution of pure [Mea][Hex], the density of mixtures exhibit a slight increase as the water content is increased. The V^E values for the mixtures are alike from pure ILs, being the minimum for 0.25:0.75 composition slightly dislocated towards the IL richer zone though.

Tab 12: Predicted values for density using equation 5 and parameter from Table 1, given in the main text.

[Mea][Ac] : H2O					[Mea][Hex] : H2O					[Mea][Ac] : [Mea][Hex]				
T (°C)	IL (w/w)	ρ experimental	ρ Predicted	Δ	T (°C)	IL (w/w)	ρ experimental	ρ Predicted	Δ	T (°C)	[Mea][Ac] (w/w)	ρ experimental	ρ Predicted	Δ
25	0.066	1.0097	1.0071	-0.3%	25	0.090	1.0076	1.0095	0.001894	25	0.10	1.03379	1.0340	0.000179
25	0.263	1.0529	1.0574	0.4%	25	0.342	1.0289	1.0287	-0.000153	25	0.19	1.04440	1.0439	-0.000462
25	0.426	1.0865	1.0906	0.4%	25	1.000	1.0350	1.0265	-0.008191	25	0.31	1.05915	1.0596	0.000391
25	0.692	1.1287	1.1281	0.0%	25	0.766	1.0365	1.0360	-0.000527	25	0.41	1.07336	1.0713	-0.001954
25	0.871	1.1459	1.1417	-0.4%	25	0.908	1.0306	1.0314	0.000803	25	0.51	1.08405	1.0841	3.66E-05
25	0.952	1.1509	1.1448	-0.5%	25	0.968	1.0265	1.0284	0.00186	25	0.69	1.10767	1.1086	0.000807
25	0.997	1.1528	1.1456	-0.6%	25	0.997	1.0228	1.0267	0.003847	25	0.86	1.13272	1.1321	-0.000593
30	0.066	1.0077	1.0047	-0.3%	30	0.090	1.0058	1.0069	0.00112	30	0.10	1.03066	1.0309	0.000235
30	0.263	1.0503	1.0557	0.5%	30	0.342	1.0262	1.0261	-6.09E-05	30	0.19	1.04026	1.0409	0.000592
30	0.426	1.0834	1.0895	0.6%	30	1.000	1.0321	1.0241	-0.007772	30	0.31	1.05608	1.0566	0.000459
30	0.692	1.1252	1.1279	0.2%	30	0.766	1.0335	1.0335	-3.57E-05	30	0.41	1.06931	1.0683	-0.000949
30	0.871	1.1418	1.1421	0.0%	30	0.908	1.0274	1.0289	0.001435	30	0.51	1.08105	1.0812	0.000102
30	0.952	1.1467	1.1455	-0.1%	30	0.968	1.0233	1.0259	0.002522	30	0.69	1.10375	1.1057	0.001765
30	0.997	1.1493	1.1465	-0.2%	30	0.997	1.0188	1.0242	0.005311	30	0.86	1.12986	1.1292	-0.000551
45	0.066	1.0001	0.9945	-0.6%	45	0.090	0.9987	0.9984	-0.000322	45	0.10	1.02123	1.0216	0.000335
45	0.263	1.0441	1.0476	0.3%	45	0.342	1.0177	1.0177	-2.84E-05	45	0.19	1.03193	1.0316	-0.000292
45	0.426	1.0770	1.0831	0.6%	45	1.000	1.0230	1.0160	-0.006912	45	0.31	1.04683	1.0475	0.000596
45	0.692	1.1180	1.1243	0.6%	45	0.766	1.0242	1.0253	0.00107	45	0.41	1.06118	1.0593	-0.001792
45	0.871	1.1349	1.1404	0.5%	45	0.908	1.0179	1.0208	0.002775	45	0.51	1.07199	1.0722	0.000233
45	0.952	1.1398	1.1446	0.4%	45	0.968	1.0139	1.0178	0.003904	45	0.69	1.09587	1.0970	0.001001
45	0.997	1.1416	1.1461	0.4%	45	0.997	1.0101	1.0161	0.005972	45	0.86	1.12125	1.1207	-0.000499
75	0.066	0.9942	0.9604	-3.4%	75	0.090	0.9835	0.9781	-0.005505	75	0.10	1.00232	1.0024	6.71E-05
75	0.263	1.0242	1.0176	-0.6%	75	0.342	0.9985	0.9977	-0.000825	75	0.19	1.01307	1.0126	-0.000463
75	0.426	1.0599	1.0565	-0.3%	75	1.000	1.0035	0.9967	-0.006803	75	0.31	1.02793	1.0287	0.000745
75	0.692	1.1010	1.1034	0.2%	75	0.766	1.0044	1.0057	0.001347	75	0.41	1.04263	1.0407	-0.001844
75	0.871	1.1181	1.1232	0.5%	75	0.908	0.9986	1.0014	0.002743	75	0.51	1.05351	1.0539	0.000352
75	0.952	1.1231	1.1291	0.5%	75	0.968	0.9947	0.9985	0.003738	75	0.69	1.07801	1.0790	0.000901
75	0.997	1.1247	1.1316	0.6%	75	0.997	0.9910	0.9968	0.005878	75	0.86	1.10371	1.1031	-0.000591
90	0.066	0.8896	0.9365	5.3%	90	0.090	0.9582	0.9664	0.008642	90	0.10	0.99232	0.9925	0.000204
90	0.263	1.0042	0.9958	-0.8%	90	0.342	0.9880	0.9861	-0.001871	90	0.19	1.00313	1.0028	-0.000292
90	0.426	1.0478	1.0364	-1.1%	90	1.000	0.9929	0.9854	-0.007495	90	0.31	1.01812	1.0191	0.000912
90	0.692	1.0919	1.0860	-0.5%	90	0.766	0.9939	0.9944	0.000471	90	0.41	1.03293	1.0312	-0.001712
90	0.871	1.1092	1.1077	-0.1%	90	0.908	0.9883	0.9901	0.001772	90	0.51	1.04393	1.0444	0.000489
90	0.952	1.1142	1.1145	0.0%	90	0.968	0.9846	0.9872	0.002721	90	0.69	1.06873	1.0697	0.000938
90	0.997	1.1158	1.1174	0.1%	90	0.997	0.9809	0.9856	0.004791	90	0.86	1.09462	1.0940	-0.000585
			APD =	0.63%				APD =	0.32%				APD =	0.07%

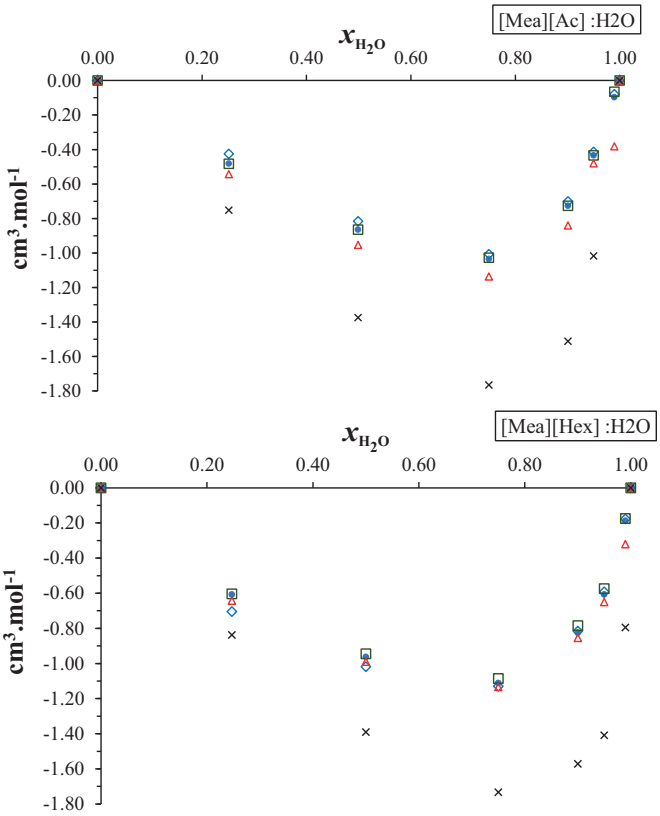

Fig 3: Excess molar volumes as function of water molar fraction at different temperatures: 298.15 K (○), 303.15 K (◊), 318.15 K (□), 348.15 (Δ) and 363.15 (x).

The calculated molecular volume for a single IL pair (eq. 4) are 0.17 nm^3 and 0.29 nm^3 for [Mea][Ac] and [Mea][Hex], respectively. These values were used to estimate the heat capacities using Volume Based Thermodynamics (VBT) correlations, equation 7 [24], which is believed to provide a result with a maximum mean absolute error of 24.5%. The calculated Cp values are 226 $J.mol^{-1}.K^{-1}$ (1.87 $J.g^{-1}.K^{-1}$) and 343 $J.mol^{-1}.K^{-1}$ (1.94 $J.g^{-1}.K^{-1}$) for [Mea][Ac] and [Mea][Hex], respectively.

$$C_p[\mathrm{J}.mol^{-1}.K^{-1}] = 1037V_m^f[\mathrm{nm}^3] + 45 \qquad \text{eq.7}$$

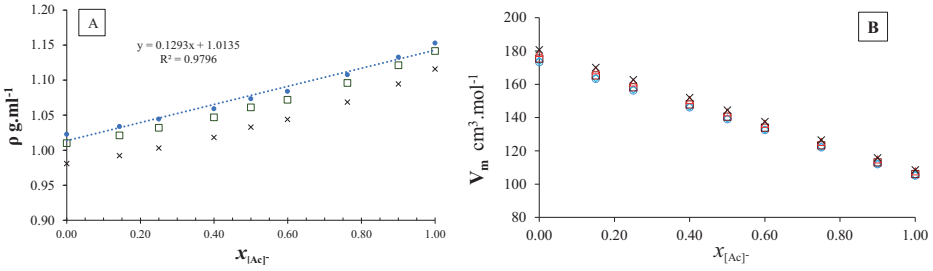

Fig 4: (A) Density and (B) molar volume of [Mea][Hex]:[Mea][Ac] mixture as function of mol fraction at different temperatures: 298.15 K (○), 303.15 K (◊), 318.15 K (□), 348.15 (Δ) and 363.15 (x).

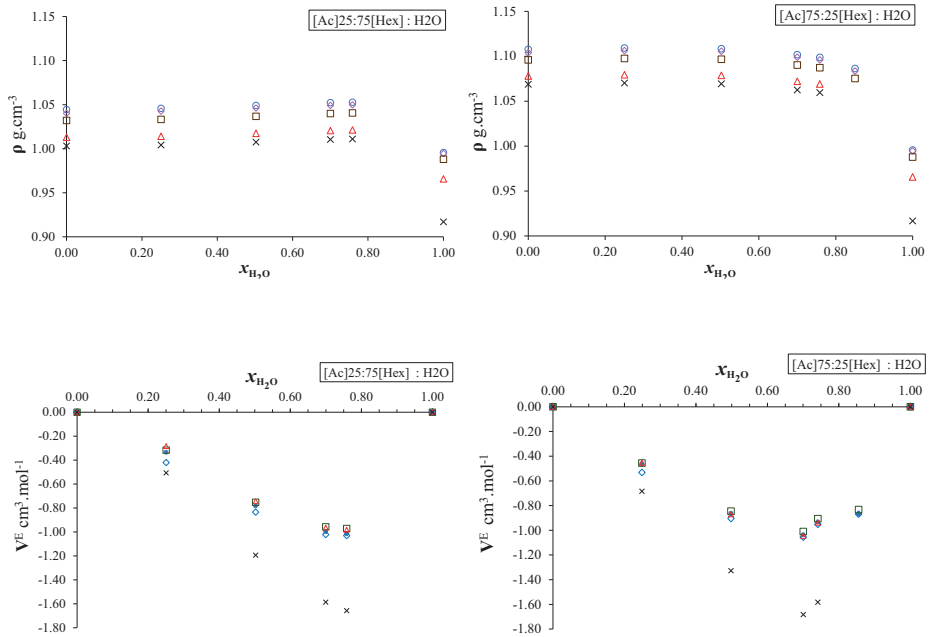

Fig 5: Density (ρ - top) and excess molar volume (V^E – bottom) of [Mea][Hex]:[Mea][Ac] mixtures as function of water molar fraction for two ILs composition at different temperatures: 298.15 K (○), 303.15 K (◊), 318.15 K (□), 348.15 (Δ) and 363.15 (x).

A.3.2 Viscosity and Conductivity

The generally high viscosities of ILs represent a major limitation in their use, due to poor heat and mass transfer and overall handling in process equipment. Therefore, the effect of temperature and water content on the viscosity of

[Mea][Ac], [Mea][Hex] and their mixtures were assessed. The data is provided in Tables 13-15.

The characteristics of the anions have a clear influence in the viscosity of resulting IL. Previous works reported both an increase and decrease in viscosity while increasing anion alkyl chain [7,11,12,25]. At 298 K (25 °C) [Mea][Ac] exhibits higher viscosity than [Mea][Hex], 2.7 and 1.6 Pa.s respectively. The difference reduces remarkably while increasing temperature, 1.3 and 1.1 Pa.s for [Mea][Ac] and [Mea][Hex], respectively, at 303 K.

Water addition had a great impact in IL viscosity, as shown in Figure 6, as expected due to water's viscosity be remarkable lower than IL. In the diluted region, up to 0.25 IL molar fraction, aqueous [Mea][Hex] exhibited higher viscosity than that from [Mea][Ac], which is unexpected since the dry [Mea][Ac] has higher viscosity.

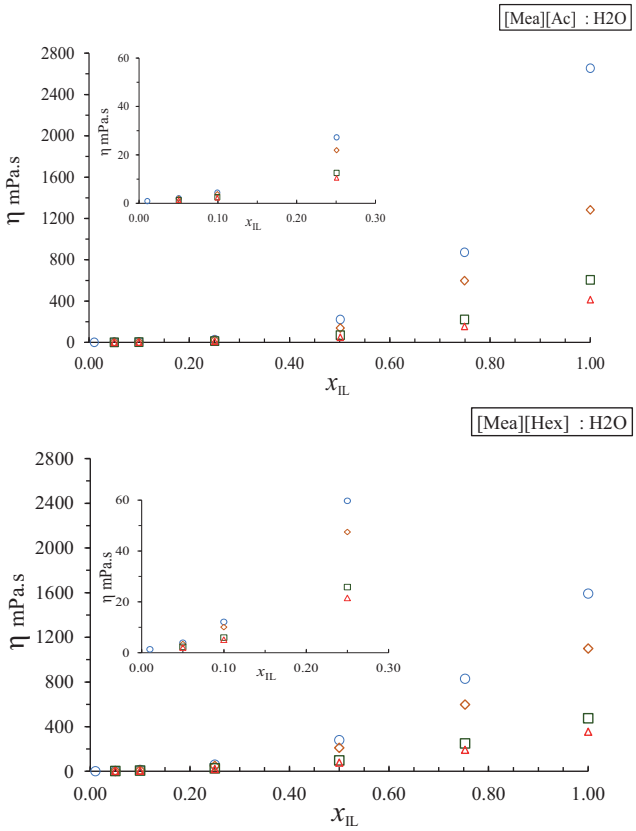

Fig 6: Viscosity as function of IL molar fraction in water at different temperatures: 298.15 K (○), 303.15 K (◊), 318.15 K (□) and 323.15 K (Δ). The region up to 0.3 IL molar fraction is depicted to illustrate the viscosity profile at lower IL concentrations

Tab 13: Aqueous [Mea][Ac] conductivity as function of concentration.

	[Mea][Ac] : H2O															
Molar Fraction	1.5E-08	7.4E-08	1.5E-07	7.4E-07	1.5E-06	1.5E-05	7.4E-05	0.0001	0.0015	0.0078	0.0163	0.0472	0.1295	0.3086	0.5724	1.0000
% w/w	0.00001	0.00005	0.0001	0.0005	0.001	0.01	0.05	0.1	1.0	5.0	10.0	25.0	50.0	75.0	90.0	100.0
Molarity	8.3E-07	4.1E-06	8.3E-06	4.1E-05	8.3E-05	8.26E-04	4.13E-03	8.26E-03	8.26E-02	4.17E-01	8.34E-01	2.2	4.5	7.0	8.5	8.3
Molality	1.7E-06	8.3E-06	1.7E-05	8.3E-05	1.65E-04	1.65E-03	8.26E-03	1.65E-02	1.67E-01	8.69E-01	1.83	5.5	16.5	49.5	148.6	
condutivity (mS)	0.00169	0.00173	0.00206	0.00522	0.00806	0.0652	0.317	0.542	5.35	23.1	35.3	56.4	37.5	8.06	1.188	0.1387

Tab14: Aqueous [Mea][Hex] conductivity as function of concentration.

	[Mea][Hex] : H2O															
Molar Fraction	1E-08	5.1E-08	1E-07	5.1E-07	1E-06	1E-05	0.00005	0.00010	0.0010	0.0053	0.0112	0.0328	0.0923	0.2337	0.4778	1.0000
% w/w	0.00001	0.00005	0.0001	0.0005	0.001	0.01	0.05	0.1	1.0	5.0	10.0	25.0	50.0	75.0	90.0	100.0
Molarity	5.6E-07	2.8E-06	5.6E-06	2.8E-05	5.6E-05	0.00056	0.00282	0.00564	0.05642	0.28436	0.56872	1.45283	2.93387	4.40081	5.2302	5.64207
Molality	1.1E-06	5.6E-06	1.1E-05	5.6E-05	0.00011	0.00113	0.00564	0.0113	0.11398	0.5939	1.25379	3.76138	11.2841	33.8524	101.557	
condutivity (mS)	0.00143	0.00132	0.00155	0.00318	0.00516	0.0379	0.22	0.368	3.23	13.96	21.5	29.4	25.6	7.73	1.09	0.1011

Tab 15: Aqueous mixture of [Mea][Ac] and [Mea][Hex] as function of IL concentration.

	[Mea][Ac] 0.25:0.75 [Mea][Hex] : H2O				[Mea][Ac]0.75 : 0.25[Mea][Hex] : H2O			
IL Molar Fraction	0.0008	0.0089	0.0623	0.2500	0.0010	0.0102	0.0690	0.2500
IL % w/w	0.7512	7.512	37.56	75.12	0.7143	7.143	35.715	71.43
Molarity	0.05	0.46	2.39	4.83	0.05	0.53	2.77	5.81
Molality	0.09	1.00	7.37	37.00	0.11	1.14	8.22	37.00
condutivity (mS)	4.05	25.39	40.73	11.203	3.09	19.221	32.985	8.727

The mixture of the ILs were also assessed regarding viscosity, as shown in Figure 7. It is possible to observe the existence of two distinct regions defined by the molar composition. The viscosity remains stable despite the increase in [Mea][Ac] concentration up to 0.4 molar fraction. The same holds true for [Mea][Hex], up to 0.4 molar fraction. The equimolar composition assumes a transition point between the lower viscosity region, [Mea][Hex]richer region, and the higher viscosity region, richer in [Mea][Ac]. The effect of temperature on viscosity was assessed in respect to the Vogel–Tammann–Fulcher (VTF) correlation[26], according to equation 8

$$\eta = \eta_o . e^{\frac{B}{T-T_0}} \qquad \text{eq. 8}$$

where the angular coefficient corresponds to η_0, T_0 and B are adjusted parameters. The "B" parameter can be taken as proportional to the Arrhenius' activation energy (E_a)[27,28], giving a good indication concerning the viscosity thermal sensitivity thus. The fitting parameters, determination coefficient (r^2) and the average percentual deviation (APD) of VTF equation are presented in Table 16. From the results in Table 16, it is possible to observe that [Mea][Ac] has a lower B than that obtained for [Mea][Hex], 35.24 and 205.26 respectively and, consequently, is more sensitive to temperature increase, in accordance with the experimental results. All ILs mixtures exhibited B values higher than those observed for the pure ILs, suggesting that the combination of ILs lead to higher thermal stability.

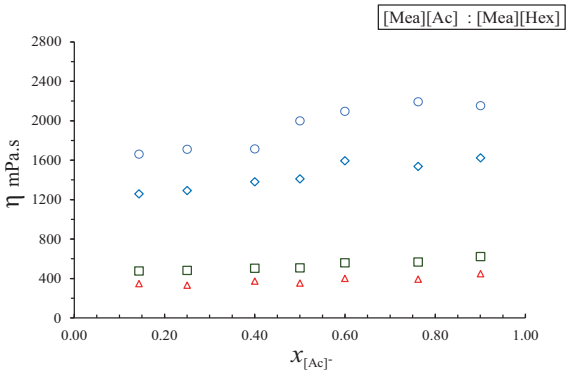

Fig 7: Viscosity of [Mea][Hex]:[Mea][Ac] mixture in different ionic molar composition at different temperatures: : 298.15 K (○), 303.15 K (◊), 318.15 K (□) and 323.15 K (Δ).

Tab 16: Fitting parameters for Vogel–Tammann–Fulcher correlation

Mixtures	η_0 (mPa.s)	T_0 (K)	B	r^2	APD* (%)
[Mea][Ac]	198.68	284.75	35.54	0.99878	6.3
[Mea][Hex]	195.03	249.535	205.26	0.99935	2.9
[Mea][Ac] 0.25 : 0.75 [Mea][Hex]	196.75	214.43	549.01	0.99547	18.7
[Mea][Ac] 0.50 : 0.50 [Mea][Hex]	203.03	203.34	746.35	0.99883	4.0
[Mea][Ac] 0.75 : 0.25 [Mea][Hex]	205.35	200.6	782.71	0.99922	3.3

*: $(100/N). \sum[(\eta_{pred.} - \eta_{exp.})/ \eta_{exp}]$

There are various equations to estimate the viscosity of mixtures in terms of pure component data. They may differ by whether taking adjustable parameters or not, which will be both considered to evaluate the mixtures from the present work. Those without adjustable parameters include the Arrhenius mixing law for viscosity, given in equation 9[29]. Kendall-Monroe proposed equation 10, from which the mixture viscosity is calculated the cubic-root average of the component viscosities [30]. Frenkel[31] considered Eyring's model [32] to take into consideration the interaction between components in a nonideal binary mixture, as demonstrated in equation 11, where, η_{12} is a constant attributed to the pair interaction and is calculated according to equation 12[33]. The further approaches assessed make use of adjustable parameters in other to account for nonidealities. Grunber and Nissan [29] correlated the natural logarithm of pure components' viscosities to that from the resulting mixture, including a so called "characteristic constant of the system" d_{12}, equation 13. Katti-Chaudhri [34] considered the volume of each component when correlating them to the viscosity of resulting mixture. In this work, we substituted the component volume (V) by the inverse of density ($1/\rho$) to contemplate the volumetric characteristic of each component, equation 14. Herraéz et al. [35] considered the Redlich-Kister polynomial, vastly used for excess properties calculations, to propose a model with the adjustable parameter B_0, equation 15. The APD calculated according to equation 6 and the fitting parameters, when applicable, are summarized in Table 17. We found that there is no unanimous model while predicting the viscosity of the studied mixtures. In general, the models presented smaller deviations for the viscosities of the mixtures between

[Mea][Ac] and [Mea][Hex], while larger deviations were found for the predictions of the aqueous mixtures. The smallest deviation for the [Mea][Ac]/[Mea]Hex] mixture was found using the Katti-Chaudhi model, while the best choice for the aqueous system was observed using Herraréz's model at IL concentrations higher than 0.25 molar fraction. For diluted systems, under 0.25 molar fraction, deviations were not smaller than 20 %.

$$\ln(\eta_{mix}) = x_1 \cdot \ln(\eta_{1)}) + x_2 \cdot \ln(\eta_2) \quad \text{eq.9}$$

$$\eta_{mix} = (x_1 {\eta_1}^{1/3} + x_2 {\eta_2}^{1/3})^3 \quad \text{eq.10}$$

$$\ln(\eta_{mix}) = x_1^2 \cdot \ln(\eta_1) + x_2^2 \cdot \ln(\eta_2) + 2x_1x_2 \ln(\eta_{12}) \quad \text{eq.11}$$

$$\eta_{12} = 0.5\eta_1 + 0.5\eta_2 \quad \text{eq.12}$$

$$\ln(\eta_{mix}) = x_1 \cdot \ln(\eta_1) + x_2 \cdot \ln(\eta_2) + x_1x_2d_{12} \quad \text{eq.13}$$

$$\ln\left(\eta_{mix}.\frac{1}{\rho}\right) = x_1 \cdot \ln\left(\eta_1\frac{1}{\rho_1}\right) + x_2 \cdot \ln\left(\eta_2\frac{1}{\rho_2}\right) + x_1x_2\left(\frac{W}{R.T}\right) \quad \text{eq.14}$$

$$\eta_{mix} = \eta_1 + (\eta_2 - \eta_1).x_2^{B_0} \quad \text{eq.15}$$

Besides the importance of conductivity data for its direct application, it also tells about the mass transfer since it can be used to assess the diffusivity of organic electrolytes in water[36]. Conductivity data was acquired at room temperature (20 °C – 23 °C) from aqueous solutions of [Mea][Ac], [Mea][Hex] and from their combination. In Figure 8, the conductivity is plotted versus solution molality. [Mea][Ac] exhibited the highest values among the assessed ionic systems. The conductivity increases in a higher rate up to 2 molal, reaching the maximum around 5 molal. The region of 5 molal is reported as a critical point where the ionic species form ions pair in [Mea][Ac], which corresponds to the observed maximum conductivity. The remaining systems seem to follow a similar trend of that described for [Mea][Ac], being the maximum point of [Mea][Hex] dislocated to more diluted regions though. Interestingly, the mixture with higher molar fraction of [Hex] (0.25:0.75) presented higher conductivity than that observed in the [Ac] richer mixture (0.75:0.25).

Tab 17: Average deviation percentage and fitting parameters for different models related to viscosity mixing prediction.

	Arrhenius mixing	Kendall-Monroe	Frenkel-Eyrin	Grunber and Nissan		Katti-Chaudhi		Herraéz et al	
	ADP (%)	ADP (%)	ADP (%)	d_{12}	ADP (%)	W/RT	ADP (%)	Bo	ADP (%)
[Mea][Ac] and H_2O	53.0	92.2	17.9	6.3021	16.6	5.9638	14.3	3.6905	29.7
[Mea][Hex] and H_2O	63.8	14.7	38.9	9.7184	44.9	9.5744	43.6	2.3484	18.7
[Mea][Ac] and **[Mea][Hex]**	7.6	8.3	19.4	-0.3157	92.5	-0.2615	5.1	1.8756	5.8

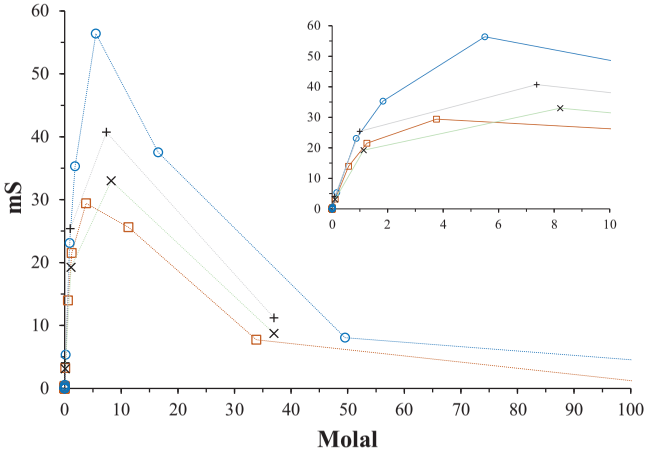

Fig 8: Conductivity as function of IL molality: (○)[Mea][Ac], (□)[Mea][Hex], (+)[Mea][Ac] 0.25:0.75 [Mea][Hex], (x)[Mea][Ac] 0.75:0.25 [Mea][Hex]. Lines plotted for guidance.

Walden plot has been widely applied to evaluate IL character regarding viscosity and conductivity. Generally, ILs can be classified as good, poor and nonionic depending on its position on the chart, having poor ionicity as they move away and to the right of the bisectrix and reference line[37]. The description of the studied ILs with respect to Walden plot is depicted in Figure 9. The ionic systems are distant to the reference line following the reported conductivities, i.e. [Mea][Ac] is the closest system to reference line. [Mea][Hex] samples exhibit a clear non-linear profile, not as apparent in [Mea][Ac], suggesting a possible aggregation, which might have a negative effect in the conductivity, in addition to viscosity. Walden plots are also used to investigate the ionicity of protic ILs [38] since a poor proton transfer from the acid to the base would entail in lower conductivity and, consequently, farther position from the reference line. However, both [Mea][Ac] and [Mea][Hex] exhibit good proton transfer, as discussed in Appendix B, thereby, their displacement to the right of reference line could be more to their high viscosity owing to extensive H-bonding.

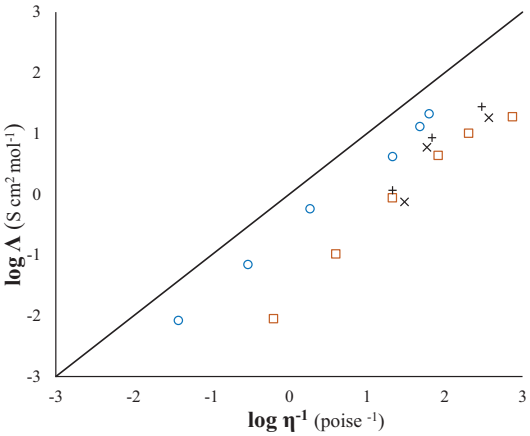

Fig 9: Walden plot for (○)[Mea][Ac], (□)[Mea][Hex], (+)[Mea][Ac] 0.25:0.75 [Mea][Hex], (x)[Mea][Ac] 0.75:0.25 [Mea][Hex].

A.3.3 Water Activity

Water activity (a_w) express the ratio between partial vapor pressure of water in a substance and the standard vapor pressure of pure water. In other words, how easy the water content may be utilized or separated. As expected, no hysteresis effect was observed during water adsorption and desorption experiments, as shown in

Figure 3 of the complementary data. Nevertheless, the values for a_w, shown in Table 18, are related to the adsorption experiments, where longer time lengths were given to reach the equilibrium. In Figure 10, a_w is depicted as function of IL concentration (A), and water activity coefficient (γ_{H2O}) is shown as function of water mass fraction (B) for both IL. An equimolar composition of [Mea][Ac] and [Mea][Hex] was also considered. All systems have similar values for a_w in the extreme regions of ionic and water concentration, distinct profiles are more evident after 5 molal though. The longer alkyl chain from $[Hex]^-$ leads to larger hydrophobic regions, which in turns increase a_w. Similar trend was observed for the a_w calculated from the freezing point depression of IL-water mixtures in Chapter 3. The a_w curve of the IL mixture lays in between those from the pure components; however, it exhibits higher a_w in the region of lower water concentration.

Tab 18: IL concentration and water activity (a_w) at 298.15 K (25 °C).

[Mea][Ac]				[Mea][Hex]				[Mea][Ac] 0.5 : 0.5 [Mea][Hex]			
IL %w	**± σ**	**Molal**	a_w	**IL %w**	**± σ**	**Molal**	a_w	**IL %w**	**± σ**	**Molal**	a_w
93.0	0.5	219	0.11	86.8	0.6	76	0.35	86.3	0.8	87	0.35
79.0	0.2	62	0.35	74.1	0.7	32	0.65	68.3	0.7	30	0.65
56.7	0.2	22	0.65	69.0	0.3	25	0.73	61.4	0.3	22	0.73
49.4	0.3	17	0.73	58.6	0.7	16	0.84	47.9	0.8	13	0.84
37.0	0.2	10	0.84	30.1	0.2	5	0.95	21.3	0.3	4	0.95
17.0	0.8	3	0.95	15.4	0.6	2	0.98	11.0	0.7	2	0.98
8.0	0.5	1	0.98								

A.3.4 Surface tension

Surface tension can be mechanically evaluated as the force acting along the edge of the fluid system and related to the border length. This force acts against the surface expansion since the increase in surface requires the investment of energy. Assuming the use of IL as a particular solvent, the surface tension would be the first force limiting solute-solvent interaction and, therefore, the initial, but not exclusive, constraint to mass transfer.

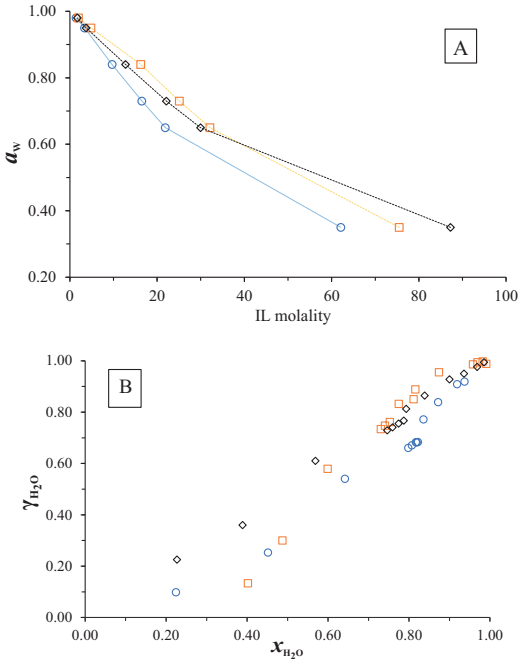

Fig 10: Water Isotherm equilibrium in the different systems, where "A" depicts water activity (a_W) as function of IL molality and "B" water activity coefficient (γ_{H2O}) as function of water mol fraction (x_{H2O}): (○)[Mea][Ac], (□)[Mea][Hex], (◊) equimolar [Mea][Ac]:[Mea][Hex]. Lines plotted for guidance purpose.

The measured surface tension for the pure ILs and for their mixture while anhydrous or in aqueous solution are available in Table 19. The molecular arrangement has a direct effect on the surface tension. For these ILs, it is considered that the charged group, i.e., NH_3^+ and COO^-, will be located toward the bulk of the liquid, while the alkyl chains exposed to the air, or void[17,38]. The higher surface of carbonic chain will decrease the surface tension, while the higher cohesiveness of the liquid due to H-bonding and Coulombic interaction will increase this property. [Mea]Hex] has a lower surface tension than [Mea][Ac], as expected based on the aforementioned. Although both ILs act decreasing water surface tension, [Mea][Hex] sows a better aptitude to act as surfactant, as depicted in Figure 11.

The presence of $[Hex]^-$, independent of concentration within the studied range, confers the system the same surface tension of that from the pure [Mea][Hex], supporting the assumption of alkyl chains being located toward the interface. The mixture of [Mea][Ac] and [Mea][Hex] acts predominantly on the molecular arrangement of the alkyl chains. The fact that the surface tension of the

aqueous systems is the same of that observed for the neat ILs suggests that, the H-bounding is the major responsible for fluid cohesiveness and, consequently, the major force against surface expansion in these ILs.

Tab 19: Surface tension for different water concentration and IL composition

	Molality	Molar Fraction	Surface Tension ($mN.m^{-1}$)
[Mea][Ac]			54.27
[Mea][Hex]			30.27
		0.25	31.60
[Mea][Ac]		0.50	32.73
:[Mea][Hex]		0.75	33.58
		0.90	35.56
	5.8	0.05	67.67
[Mea][Ac]:	37.0	0.25	57.61
H2O	111.0	0.50	52.93
	333.0	0.75	52.41
	5.8	0.05	34.35
[Mea][Hex]:	37.0	0.25	31.47
H2O	111.0	0.50	28.34
	333.0	0.75	30.67
[Mea][Ac]	6.0	0.05	29.43
0.75 : 0.25	38.0	0.25	32.26
[Mea][Hex]	114.0	0.50	33.54
: H2O	342.1	0.75	34.31
H2O			71.99

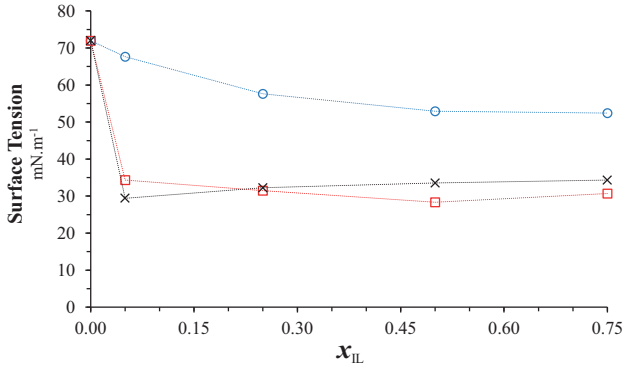

Fig 11: Surface tension as function of IL molar fraction: (○)[Mea][Ac], (□)[Mea][Hex], (x) [Mea][Ac] 0.75:0.25 [Mea][Hex]. Lines used as guidance.

A.4 Conclusions

Density and visosity data of the neat ILs [Mea][Ac] and [Mea][Hex], the binary system (IL + water) and the tertiary system (ILs mixture + water) have been measured in the range of 278 K – 363 K at atmospheric pressure. Properties, such as molar volume, excess molar volume, thermal expansion coefficient were also calculated. The observed V^E values were negative in the entire range of dilution and temperature for the binary and tertiary systems, considering both ILs. Density experimental data were fitted to a polynomial for density prediction as function of compositional and temperature for the binary systems, with [Mea][Ac] and water system presenting the maximum ADP, 0.63 %.

[Mea][Ac]'s viscosity is more sensitive to temperature change than [Mea][Hex], while their mixtures have lower sensitivity than the neat ILs. The resulting viscosity of binary systems, for both [Mea][Ac] and [Mea][Hex] in water, were better predicted by Herráez *et al* model when considering an IL concentration higher than 0.25 molar fraction. Under this concentration, none of the models considered exhibited an ADP inferior to 16 %. For the binary system [Mea][Ac] and [Mea][Hex] the lowest ADP (5.06 %) was obtained using the Catti-Chaudhi model.

[Mea][Hex] have a lower surface tension than [Mea][Ac]. The presence of [Mea][Hex] lead to a reduction in the surface tension of [Mea][Ac] and water systems. Moreover, systems with [Mea][Hex] exhibited higher water activities than those containing [Mea][Ac].

A.5 References

[1] D. Nagi, R. Thummuru, B.S. Mallik, Structure and Dynamics of Hydroxyl-Functionalized Protic Ammonium Carboxylate Ionic Liquids, (2017) 8097–8107. https://doi.org/10.1021/acs.jpca.7b05995.

[2] B. Wang, L. Qin, T. Mu, Z. Xue, G. Gao, Are Ionic Liquids Chemically Stable?, Chem. Rev. 117 (2017) 7113–7131. https://doi.org/10.1021/acs.chemrev.6b00594.

[3] A. Stark, Ionic liquids in the biorefinery: A critical assessment of their potential, Energy Environ. Sci. 4 (2011) 19–32. https://doi.org/10.1039/c0ee00246a.

[4] H. Baaqel, I. Díaz, V. Tulus, B. Chachuat, G. Guillén-Gosálbez, J.P. Hallett, Role of life-cycle externalities in the valuation of protic ionic liquids – a case study in biomass pretreatment solvents, Green Chem. (2020). https://doi.org/10.1039/d0gc00058b.

[5] A. Tzani, M. Elmaloglou, C. Kyriazis, D. Aravopoulou, I. Kleidas, A. Papadopoulos, E. Ioannou, A. Kyritsis, E. Voutsas, A. Detsi, Synthesis and structure-properties relationship studies of biodegradable hydroxylammonium-based protic ionic liquids, J. Mol. Liq. 224 (2016)

366–376. https://doi.org/10.1016/j.molliq.2016.09.086.

[6] K. Fumino, A. Wulf, R. Ludwig, The potential role of hydrogen bonding in aprotic and protic ionic liquids, Phys. Chem. Chem. Phys. 11 (2009) 8790–8794. https://doi.org/10.1039/b905634c.

[7] T.L. Greaves, K. Ha, B.W. Muir, S.C. Howard, A. Weerawardena, N. Kirby, C.J. Drummond, Protic ionic liquids (PILs) nanostructure and physicochemical properties: Development of high-throughput methodology for PIL creation and property screens, Phys. Chem. Chem. Phys. 17 (2015) 2357–2365. https://doi.org/10.1039/c4cp04241g.

[8] S.K. Das, D. Majhi, P.K. Sahu, M. Sarkar, Linking Diffusion–Viscosity Decoupling and Jump Dynamics in a Hydroxyl-Functionalized Ionic Liquid: Realization of Microheterogeneous Nature of the Medium, ChemPhysChem. 18 (2017) 198–207. https://doi.org/10.1002/cphc.201600983.

[9] Y. Deng, P. Husson, A.M. Delort, P. Besse-Hoggan, M. Sancelme, M.F. Costa Gomes, Influence of an oxygen functionalization on the physicochemical properties of ionic liquids: Density, viscosity, and carbon dioxide solubility as a function of temperature, J. Chem. Eng. Data. 56 (2011) 4194–4202. https://doi.org/10.1021/je2006743.

[10] T.L. Greaves, A. Weerawardena, I. Krodkiewska, C.J. Drummond, Protic ionic liquids: Physicochemical properties and behavior as amphiphile self-assembly solvents, J. Phys. Chem. B. 112 (2008) 896–905. https://doi.org/10.1021/jp0767819.

[11] D. Santos, É. Lourenço, M. Santos, J.P. Santos, E. Franceschi, A. Barison, S. Mattedi, Properties of aqueous solutions of ammonium-based ionic liquids and thermodynamic modelling using Flory theory, J. Mol. Liq. 229 (2017) 508–513. https://doi.org/10.1016/j.molliq.2016.12.084.

[12] P.K. Chhotaray, R.L. Gardas, Thermophysical properties of ammonium and hydroxylammonium protic ionic liquids, J. Chem. Thermodyn. 72 (2014) 117–124. https://doi.org/10.1016/j.jct.2014.01.004.

[13] A. Triolo, O. Russina, H.J. Bleif, E. Di Cola, Nanoscale segregation in room temperature ionic liquids, J. Phys. Chem. B. 111 (2007) 4641–4644. https://doi.org/10.1021/jp067705t.

[14] T.C. Pin, P.Y.S. Nakasu, S. Mattedi, S.C. Rabelo, A.C. Costa, Screening of protic ionic liquids for sugarcane bagasse pretreatment, Fuel. 235 (2019) 1506–1514. https://doi.org/10.1016/j.fuel.2018.08.122.

[15] R.M. Dias, A.M. da Costa Lopes, A.J.D. Silvestre, J.A.P. Coutinho, M.C. da Costa, Uncovering the potentialities of protic ionic liquids based on alkanolammonium and carboxylate ions and their aqueous solutions as non-derivatizing solvents of Kraft lignin, Ind. Crops Prod. 143 (2020) 111866. https://doi.org/10.1016/j.indcrop.2019.111866.

[16] V.H. Alvarez, S. Mattedi, M. Martin-Pastor, M. Aznar, M. Iglesias, Thermophysical properties of binary mixtures of {ionic liquid 2-hydroxy ethylammonium acetate + (water, methanol, or ethanol)}, J. Chem. Thermodyn. 43 (2011) 997–1010. https://doi.org/10.1016/J.JCT.2011.01.014.

[17] S.M. Hosseini, A. Hosseinian, S. Aparicio, An experimental and theoretical study on 2-hydroxyethylammonium acetate ionic liquid, J. Mol. Liq. 284 (2019) 271–281. https://doi.org/10.1016/J.MOLLIQ.2019.03.150.

[18] I.J. Villar-Garcia, K.R.J. Lovelock, S. Men, P. Licence, Tuning the electronic environment of cations and anions using ionic liquid mixtures, Chem. Sci. 5 (2014) 2573–2579. https://doi.org/10.1039/c4sc00106k.

[19] Y. Xiao, X. Huang, The physicochemical properties of a room-temperature liquidus binary ionic liquid mixture of [HNMP][CH3SO3]/[Bmim]Cl and its application for fructose conversion to 5-hydroxymethylfurfural, RSC Adv. 8 (2018) 18784–18791.

https://doi.org/10.1039/c8ra03604g.

[20] F.A. Ferrari, J.F.B. Pereira, G.J. Witkamp, M.B.S. Forte, Which variables matter for process design and scale-up? a study of sugar cane straw pretreatment using low-cost and easily synthesizable ionic liquids, ACS Sustain. Chem. Eng. 7 (2019) 12779–12788. https://doi.org/10.1021/acssuschemeng.9b01385.

[21] M. Usula, N. V. Plechkova, A. Piras, S. Porcedda, Ethylammonium alkanoate-based ionic liquid + water mixtures, J. Therm. Anal. Calorim. 121 (2015) 1129–1137. https://doi.org/10.1007/s10973-015-4753-3.

[22] P.B. Sánchez, J. García, A.A.H. Pádua, Structural effects on dynamic and energetic properties of mixtures of ionic liquids and water, J. Mol. Liq. 242 (2017) 204–212. https://doi.org/10.1016/j.molliq.2017.06.109.

[23] J. Shi, K. Balamurugan, R. Parthasarathi, N. Sathitsuksanoh, S. Zhang, V. Stavila, V. Subramanian, B.A. Simmons, S. Singh, Understanding the role of water during ionic liquid pretreatment of lignocellulose: Co-solvent or anti-solvent?, Green Chem. 16 (2014) 3830–3840. https://doi.org/10.1039/c4gc00373j.

[24] L. Glasser, H.D.B. Jenkins, Predictive thermodynamics for ionic solids and liquids, Phys. Chem. Chem. Phys. 18 (2016) 21226–21240. https://doi.org/10.1039/C6CP00235H.

[25] A.E. Latawiec, B.B.N. Strassburg, J.F. Valentim, F. Ramos, H.N. Alves-Pinto, Intensification of cattle ranching production systems: socioeconomic and environmental synergies and risks in Brazil, Animal. 8 (2014) 1255–1263. https://doi.org/10.1017/S1751731114001566.

[26] B.K. Chennuri, R.L. Gardas, Measurement and correlation for the thermophysical properties of hydroxyethyl ammonium based protic ionic liquids: Effect of temperature and alkyl chain length on anion, Fluid Phase Equilib. 427 (2016) 282–290. https://doi.org/10.1016/j.fluid.2016.07.022.

[27] J. Vila, P. Ginés, J.M. Pico, C. Franjo, E. Jiménez, L.M. Varela, O. Cabeza, Temperature dependence of the electrical conductivity in EMIM-based ionic liquids: Evidence of Vogel-Tamman-Fulcher behavior, Fluid Phase Equilib. 242 (2006) 141–146. https://doi.org/10.1016/j.fluid.2006.01.022.

[28] N. Metatla, A. Soldera, The Vogel-Fulcher-Tamman equation investigated by atomistic simulation with regard to the Adam-Gibbs model, Macromolecules. 40 (2007) 9680–9685. https://doi.org/10.1021/ma071788.

[29] L. Grunberg, A. Nissan, Mixture law for viscosity., Nature. 164 (1949) 799–800. https://doi.org/10.1038/164799b0.

[30] J. Kendall, K.P. Monroe, THE VISCOSITY OF LIQUIDS. II. THE VISCOSITY-COMPOSITION CURVE FOR IDEAL LIQUID MIXTURES. 1, J. Am. Chem. Soc. 39 (1917) 1787–1802. https://doi.org/10.1021/ja02254a001.

[31] Y.I. Frenkel, Kinetic theory of liquids, Dover, New York, 1955.

[32] H. Eyring, Examples of Absolute Reaction Rates, J. Chem. Phys. 283 (1936).

[33] O.E.A.A. Adam, A.M. Awwad, Estimation of excess molar volumes and theoretical viscosities of binary mixtures of benzene + n-alkanes at 298.15 K, Int. J. Ind. Chem. 7 (2016) 391–400. https://doi.org/10.1007/s40090-016-0100-1.

[34] P.K. Katti, M.M. Chaudhri, Viscosities of Binary Mixtures of Benzyl Acetatewith Dioxane, Aniline, and m-Cresol, J. Chem. Eng. Data. 9 (1964) 442–443. https://doi.org/10.1021/je60022a047.

[35] J. V. Herráez, R. Belda, O. Díez, M. Herráez, An equation for the correlation of viscosities of binary mixtures, J. Solution Chem. 37 (2008) 233–248. https://doi.org/10.1007/s10953-007-9226-2.

[36] L.A.M. Van Der Wielen, M. Zomerdijk, J. Houwers, K.C.A.M. Luyben, Diffusivities of organic electrolytes in water, Chem. Eng. J. 66 (1997) 111–121. https://doi.org/10.1016/S1385-8947(96)03167-1.

[37] W. Xu, L.M. Wang, R.A. Nieman, C.A. Angell, Ionic liquids of chelated orthoborates as model ionic glassformers, J. Phys. Chem. B. 107 (2003) 11749–11756. https://doi.org/10.1021/jp034548e.

[38] T.L. Greaves, A. Weerawardena, C. Fong, I. Krodkiewska, C.J. Drummond, Protic ionic liquids: Solvents with tunable phase behavior and physicochemical properties, J. Phys. Chem. B. 110 (2006) 22479–22487. https://doi.org/10.1021/jp0634048.

[39] N.J. Brooks, F. Castiglione, C.M. Doherty, A. Dolan, A.J. Hill, P.A. Hunt, R.P. Matthews, M. Mauri, A. Mele, R. Simonutti, I.J. Villar-Garcia, C.C. Weber, T. Welton, Linking the structures, free volumes, and properties of ionic liquid mixtures, Chem. Sci. 8 (2017) 6359–6374. https://doi.org/10.1039/C7SC01407D.

[40] C.A. Angell, The old problems of glass and the glass transition , and the many new twists, 92 (1995) 6675–6682.

[41] G. Richner, G. Puxty, Assessing the Chemical Speciation during CO 2 Absorption by Aqueous Amines Using in Situ FTIR, Ind. Eng. Chem. Res. 51 (2012) 14317–14324. https://doi.org/10.1021/ie302056f.

[42] B.A. Marekha, M. Bria, M. Moreau, I. De Waele, F.-A. Miannay, Y. Smortsova, T. Takamuku, O.N. Kalugin, M. Kiselev, A. Idrissi, Intermolecular interactions in mixtures of 1-n-butyl-3-methylimidazolium acetate and water: Insights from IR, Raman, NMR spectroscopy and quantum chemistry calculations, J. Mol. Liq. 210 (2015) 227–237. https://doi.org/10.1016/j.molliq.2015.05.015.

[43] Y. Chen, Y. Cao, Y. Zhang, T. Mu, Hydrogen bonding between acetate-based ionic liquids and water: Three types of IR absorption peaks and NMR chemical shifts change upon dilution, J. Mol. Struct. 1058 (2014) 244–251. https://doi.org/10.1016/j.molstruc.2013.11.010.

[44] S. Cha, M. Ao, W. Sung, B. Moon, B. Ahlström, P. Johansson, Y. Ouchi, D. Kim, Structures of ionic liquid–water mixtures investigated by IR and NMR spectroscopy, Phys. Chem. Chem. Phys. 16 (2014) 9591–9601. https://doi.org/10.1039/C4CP00589A.

[45] J. Umemura, D.G. Cameron, H.H. Mantsch, An FT-IR study of micelle formation in aqueous sodium n-hexanoate solutions, J. Phys. Chem. (1980). https://doi.org/10.1021/j100455a012.

[46] A.N. Campbell, J.I. Friesen, CONDUCTANCES OF AQUEOUS SOLUTIONS OF SODIUM HEXANOATE (SODIUM CAPROATE) AND THE LIMITING CONDUCTANCES OF THE HEXANOATE ION, AT 25 °C AND 35 °C, Can. J. Chem. (1960). https://doi.org/10.1139/v60-261.

[47] J. Umemura, H.H. Mantsch, D.G. Cameron, Micelle formation in aqueous n-alkanoate solutions: A fourier transform infrared study, J. Colloid Interface Sci. (1981). https://doi.org/10.1016/0021-9797(81)90350-7.

[48] S.M. Hosseini, A. Hosseinian, S. Aparicio, An experimental and theoretical study on 2-hydroxyethylammonium acetate ionic liquid, J. Mol. Liq. 284 (2019) 271–281. https://doi.org/10.1016/j.molliq.2019.03.150.

A.6 Complementary Data

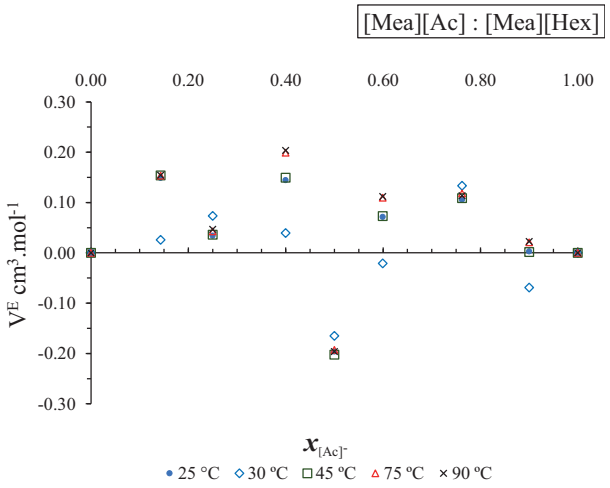

Fig 1: Excess molar volumes of [Mea][Hex]:[Mea][Ac] mixture as function of $[Ac]^-$ molar fraction at different temperatures: 278.15 K (○), 303.15 K (◊), 318.15 K (□), 348.15 (Δ) and 363.15 (x)

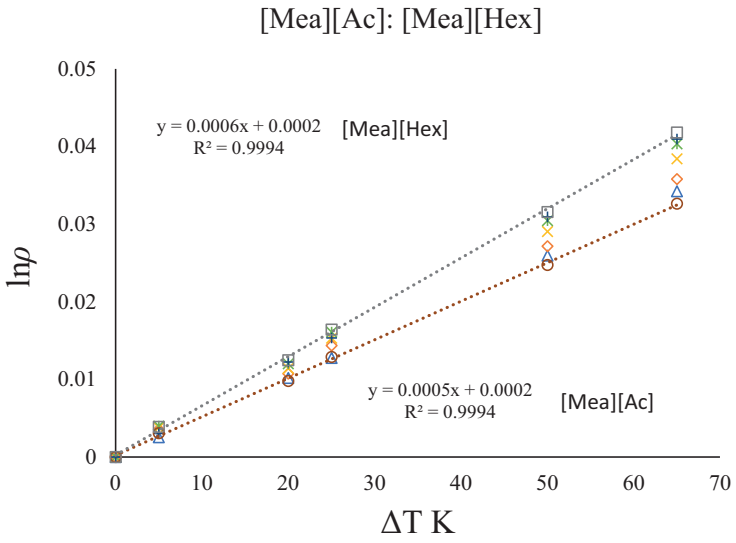

Fig 2: Graph of ln η versus variation in temperature (K) for the thermal expansion (α_p) determination of [Mea][Ac] and [Mea][Hex], and their molar mixtures: [Mea][Ac] (○), [Mea][Hex] (□),[Ac][Hex] – 0.15:0.85 (+) ,[Ac][Hex] – 0.25:0.75 (*),[Ac][Hex] – 0.50:0.50(x),[Ac][Hex] – 0.75:0.25(◊),[Ac][Hex] – 0.90:0.10(Δ).

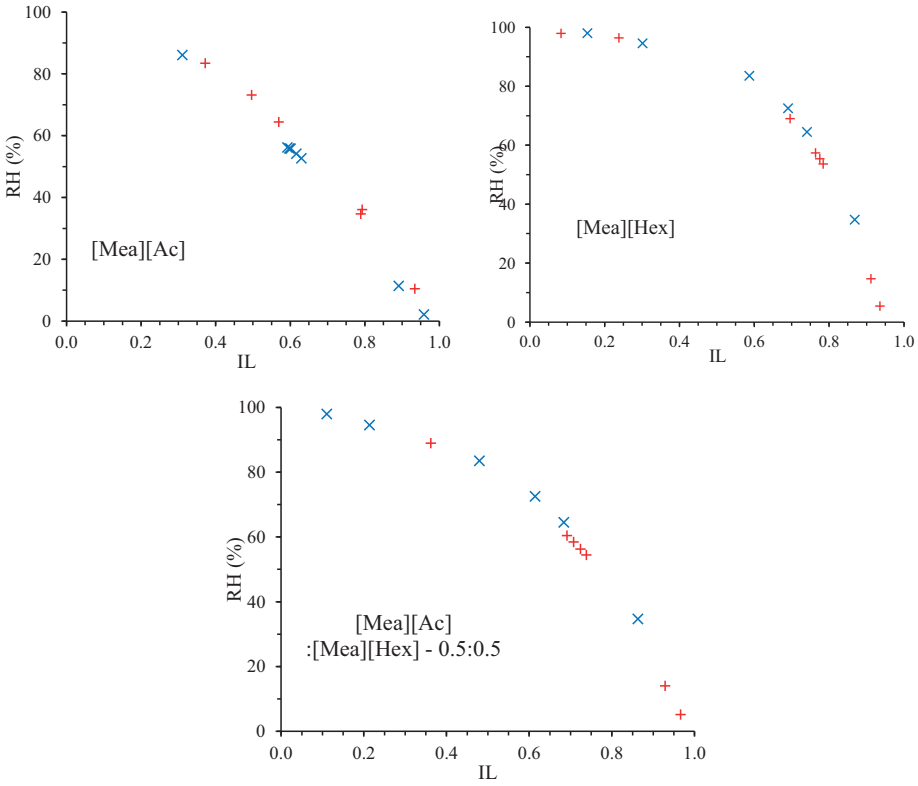

Fig 3: Water adsorption and desorption profiles as function of relative humidity (RH) and IL mass fraction in the different IL systems: (x) Adsorption, (+) Desorption

Appendix B[5]

Insights in the molecular ion interactions of 2-hydroxyethylammonium acetate and 2-hydroxyethylammonium hexanoate and their mixture in water using DSC, FTIR and NMR techniques

The understand of how ILs' molecules interact, or change, in the presence of other components, whether ions or water, can provide valuable information for a better comprehension of this class of solvents. Differential scanning calorimetry, FTIR and H^1 and C^{13} NMR techniques were used to study the 2-hydroxyethylammonium acetate ([Mea][Ac]) and 2-hydroxyethylammonium hexanoate ([Mea][Hex]) at different compositions both anhydrous and in aqueous solution. It was found that [Mea][Ac], as opposed to [Mea][Hex], did not go under crystallization, what was observed for the latter at 245 K. All studied systems exhibited a glass transition event, which varied according to the IL composition. The FTIR and NMR analysis provided evidence of the distinct molecular behave of [Mea][Ac] and [Mea][Hex]. The cation-anion interaction of both ILs were greatly affected by water presence, as observed by the chemical shifts from the FTIR and NMR analysis.

[5] This chapter is based in a prepared paper to be submitted in the Journal of *Chemistry and Engineering Data* as: Ferrari, F.A., Malaret, F., Eustace, S., Djanashvili. K., Hallett, J.P., Wielen, L.A.M, Witkamp, G.J, Forte, M.B.S.F. Physicochemical Characterization of Two Protic Hydroxyehtylammonium Carboxylate Ionic Liquids in Water and their Mixture.

B.1 Introduction

The knowledge of the physicochemical characteristics of Ionic Liquids (ILs) is essential for process design and modeling. Within the ionic structure, there are other molecular interaction, such as h-bonding and hydrophobic, stabilizing a preferred conformation at the molecular level, which will affect the bulk property. The understand of how ILs' molecules interact, or change, in the presence of other components, whether other IL or water, can provide valuable information for a better comprehension of this class of solvents.

NMR spectroscopy provides a powerful tool for investigation of physical properties in material science. NMR spectroscopy has been traditionally used as a tool for structural determination or confirmation of 3D structures of both small molecules and even large biomolecules such as enzymes. Many other spectroscopic tools are available in NMR which are often overlooked by organic chemists and biochemists alike. For example, Spin-lattice relaxation or longitudinal, more commonly reported as T1 relaxation, and spin-spin relaxation, more commonly reported as T2 relaxation, times can be explored to assess molecular dynamics in solutions[1]. Pulsed field gradients (PFGs) not only allows for increased performance in routine spectroscopy, it also permits chemists to identify individual compounds in mixtures based on differences in diffusion coefficients[2]. NMR spectroscopy is a valuable tool to investigate the behavior of individual molecules[3,4]

The thermal characterization, for instance by means of differential scanning calorimetry (DSC) technique, can provide valuable information about ILs, such as melting point and glass transition temperatures. This assessment is especially useful while trying to recover ILs from aqueous streams by means of freeze concentration.

IR spectroscopy has been widely used in analytical chemistry identifying intra-molecular vibrational modes, which assigns specific spectrum for substances. Because IR technique can be used to assess the strength of H-bounds between species in solutions[5], it became a valuable tool to evaluate the h-bonding between cation and anion in ILs, since the variation in this interaction is sensitively reflected in the spectrum and chemical shifts[6].

In this work, DSC, ^{1}H and ^{13}C NMR, and IR techniques were used to assess the influence of water in neat IL and mixtures at the molecular level.

B.2 Material & Methods

B.2.1 Synthesis and samples preparation

Acetic acid (99.7 %), hexanoic acid (99 %) and ethanolamine (99 %) were acquired from Sigma Aldrich. MilliQ water was used for dilutions. 2-Hydroxyethylammonium acetate ([Mea][Ac]) and 2-hydroxyethylammonium hexanoate ([Mea][Hex]), depicted in Figure 1, were synthesized in 100 mL Schott flasks by a one-step, acid–base exothermic neutralization. First, ethanolamine was weighed into a flask. The flask was closed with a silicone septum and placed in a cold-water bath. An equimolar quantity of either acetic acid or hexanoic acid was slowly added through the septum using a syringe. The reaction was carried out overnight at room temperature under agitation. The formation of [Mea][Ac] or [Mea][Hex] was confirmed by proton nuclear magnetic resonance (^{1}H NMR), and spectra are provided in complementary data.

The humidity for [Mea][Ac] and [Mea][Hex] was 0.15 %(w/w) and 0.2 %(w/w), respectively, assessed through Karl Fisher titration. For the mixture samples, either water or ILs were weighted with a precision of 1 x10^{-4} g and, then, vigorously mixed for complete homogenization. Samples were sonicated for 2 h in sealed flasks at 45 °C and kept in desiccator until analysis.

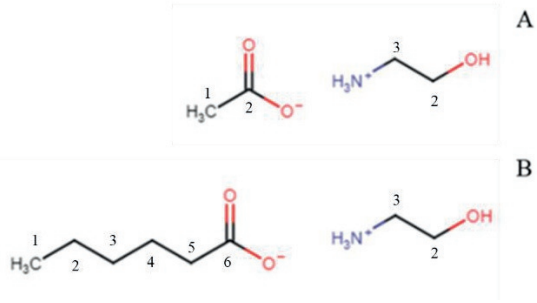

Fig 1: [Mea][Ac] (A) and [Mea][Hex] (B). Numbers assign atoms discussed in NMR section

B.2.2 Differential Scanning Calorimetry (DSC)

The glass transition (T_g) of the ILs was determined using a calorimeter DSC8500 PerkinElmer (USA) in a cooling−heating cycle at 10 K min^{-1}. The ILs were first heated from 163.15 K to 396.15 K, to remove the previous thermal

history. Then the sample was cooled down to 153.15 K, kept for 20 min. and heated again to 323.15 K.

B.2.3 FTIR

The PerkinElmer Spectrum 100 FT-IR spectrometer with a diamond germanium ATR single reflection crystal was used. The spectra were recorded between 500 cm^{-1} and 4000 cm^{-1} with a resolution of 2 cm^{-1} and each sample was scanned 16 times.

B.2.4 NMR

All measurements were performed at 298.15 K in a 5 mm borosilicate NMR tube containing a sealed 3 mm capillary containing deuterated benzene used for locking and shimming. All spectra were referenced to C_6D_5H at 7.15 ppm in the proton spectra and 127.00 ppm for carbon-13 for C_6D_6. The proton spectra were recorded using 8 scans, a relaxation delay of 1.0 seconds and an acquistion time or 2.56 seconds at a 45° hard pulse width at 399.67 MHz. The carbon spectra were recorded using 256 scans, a relaxation delay of 1.0 seconds and an aquistion time of 1.31 seconds at a 45° hard pulse width at 100.51 MHz. The spectra were processed using MestReNova version 12.01 with no apodization applied. All measurements were performed using an Agilnet 400MR fitted with a OneNMR probe.

B.3 Results and Discussion

B.3.1 Differential Scanning Calorimetry (DSC)

Samples of the pure ILs and their mixtures were submitted to DSC analysis in order to assess their thermal profile. The DSC graphs and data are available in complementary data. Pure [Mea][Hex] was the only one to exhibit a crystallization peak, at – 28 °C. All samples presented well defined glass transition temperatures (T_g). T_g gives an indication about the cohesiveness of sample's molecules. Less cohesive the molecules are, lower is the T_g[7]. In IL, the cohesive energy is mainly attributed to Coulomb and H-bounding interactions[3,8]. In Figure 2 T_g is plotted against the molar fraction of [Mea][Ac] in the ionic mixture. [Mea][Ac] has a marginally higher T_g than that observed for $[Hex]^-$, 198.68 K and 195.03 K

respectively. Among the mixtures, the composition of 0.75 [Mea][Ac] presented the highest T_g, suggesting a higher molecular cohesiveness at this point, which agrees to the thermal sensibility assessed through VTF equation for viscosity dependence of temperature in Appendix A.

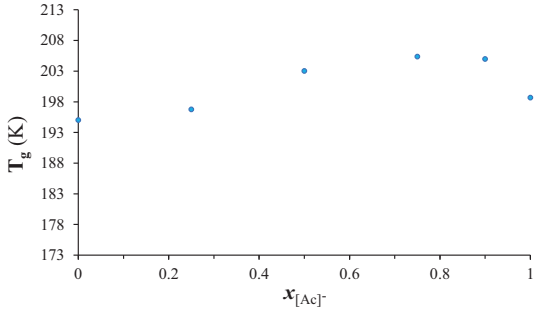

Fig 2: T_g values for [Mea][Ac]:[Mea][Hex] mixtures as function of [Mea][Ac] molar fraction

Glass-forming fluids can be classified as fragile or strong, based on how sensitive to temperature are their viscosity[7,9]. This analysis can be performed through the T_g-scaled Arrhenius plot, as depicted in Figure 3, which correlates the logarithm of viscosity (Pa.s) against T_g/T. The studied ILs, whether the pure ILs or their combination, occupy the same spot on the chart. Moreover, the similar activation energy observed in the viscosity assessment (Appendix A) suggests that the higher T_g observed for the mixtures might be related to a more effective molecular packing, and not due to formation of additional chemical bounding.

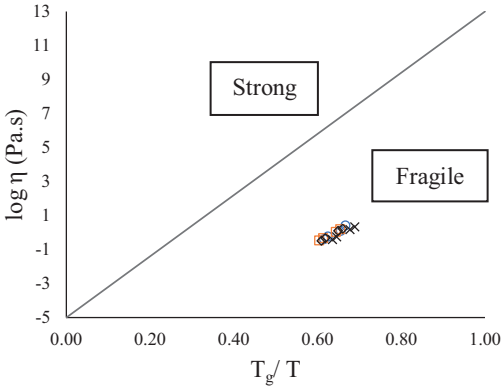

Fig 3: T_g-scaled Arrhenius Plot relating the viscosity to the T_g. Compounds over the line have the viscosity less impacted by temperature, and the opposite for those under the reference line, namely strong and fragile, respectively. (○)[Mea][Ac], (□)[Mea][Hex], (◊) [Mea][Ac] 0.25:0.75 [Mea][Hex], (x) [Mea][Ac] 0.75:0.25 [Mea][Hex]. Viscosity values from Appendix A.

Solutions at water composition of 0.75 molar fraction were used to assess the influence of water presence on T_g, for the pure ILs and also for the mixture containing [Mea][Ac] 0.75 mol. Water strongly interacts with IL's molecules, hindering cation-anion interaction, decreasing overall cohesiveness, thus lowering the T_g to 177 K for the pure ILs and to 178 K for the mixture at 0.75.

B.3.2 Infra-Red

The ILs used in this study are completely miscible with water. To investigate the interactions between these ILs and water, the FTIR spectra were recorded as a function of water concentration for binary and tertiary mixtures (Figure 4). To the best of our knowledge, the TFIR spectra for these systems have not been reported so far, therefore, the spectral assignment is based on previous work involving the different moieties in these systems. The strong C=O stretching signal at 1707 cm^{-1} in the acetic acid and hexanoic acid FTIR spectra cannot be seen in any of the spectrum shown in Figure 3, indicating a complete proton transfer from the acid to the amine.

There is a broad band from 2400 cm^{-1} to 3700 cm^{-1} , kwon as the "the hydrogen stretching region", which results from the overlapping of the N−H, C−H, and O−H stretching modes of aminoalcohol with the O−H stretching modes of H_2O, which strongly absorbs int his region[10]. It is difficult to distinguish between the individual contributions, and in consequence, the wavenumber region from 2400 cm^{-1} to 4000 cm^{-1} did not provide useful information. However, a small signal of known origin can be seen at 3556 cm^{-1} when the ILs are mixed, both in aqueous and anhydrous conditions.

Upon water dilution of the neat ILs, as shown in Figures 4 A and 3B, some signals experienced a water-induced shift. Figure 5 summarizes the magnitude of the water-induced shift of the absorption maximum as a function of IL/water concentration.

The wavenumber shifts observed upon dilution for [Mea][Ac] are: 1530 cm^{-1} attributed to a combination of the symmetric rocking from the cation $\delta s(NH_3^+)$ and asymmetric stretching from the anion $\nu_{as}(COO^-)$, 1394 cm^{-1} $\nu_s(COO^-)$, 1335 cm^{-1} (CH_3 deformation - anion), 1071 cm^{-1} ν(C-N), 1012 cm^{-1} ν(C-OH), and 920 cm^{-1} (C-C stretching - anion). For [Mea][Hex] are: 1532 cm^{-1} attributed to a combination of the symmetric rocking from the cation $\delta s(NH_3^+)$ and asymmetric

stretching from the anion $\nu_{as}(COO^-)$, 1399 cm^{-1} $\nu_s(COO^-)$, 1225 cm^{-1} (CH_2 anion), 1100 cm^{-1} (CH_2 anion), 1071 cm^{-1} ν(C-N) and 1023 cm^{-1} ν(C-OH).

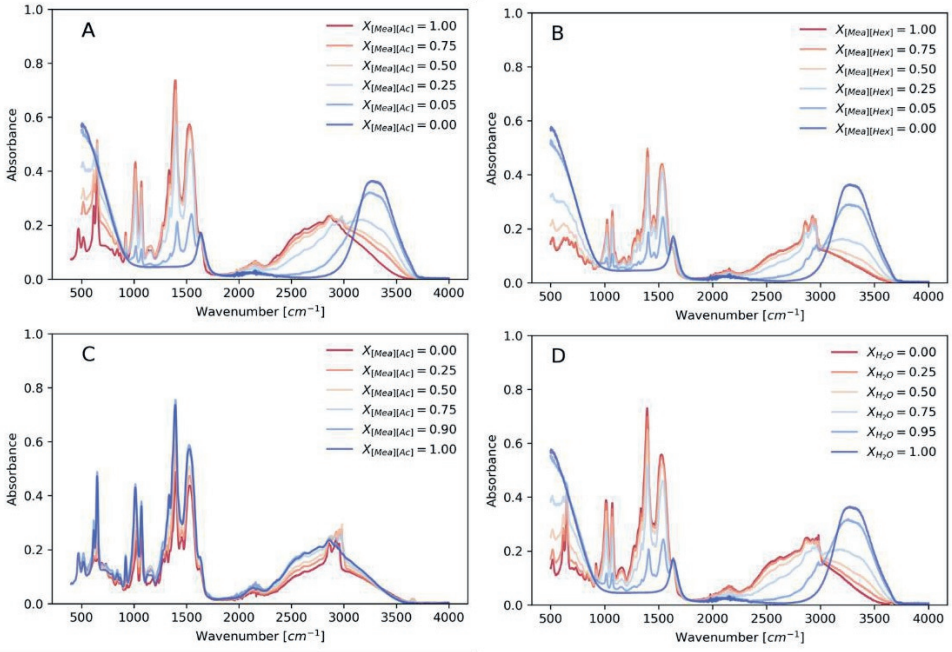

Fig 4: FTIR spectrum for different systems as a function of concentration in molar basis. [A] [Mea][Ac] and water mixtures. [B] [Mea][Hex] and water mixture. [C] Binary system [Mea][Ac] and [Mea][Hex]. [D] Tertiary system: [Mea][Ac]:[Mea][Hex] (0.75:0.25 molar fraction) system diluted with water.

For both ILs, the signals involving (COO^-) vibrations modes (~1530 cm^{-1}, ~1394 cm^{-1}) experiment a water-induced blue shift, indicating that, with respect to the interactions involving this group and their direct environment in pure ILs, *i.e.* anion-cation, adding water induces a weakening of these interactions, as a result of the higher affinity of the water molecules towards the carboxylic groups. A similar behavior have been observed for other [Ac]-based ILs[11,12] . In both systems, the ν(C-N) signal at 1071 cm^{-1} experienced a slight water-induced red shift. A similar phenomena have been reported for imidazolium based ILs, for which upon water dilution, there is a red shift of some vibrational modes of the cation concurrently with the strengthening of the hydrogen bond interaction with the proton acceptors [126]. An interesting result is the band attributed to the ν(C-OH) vibration, 1023 cm^{-1} for [Mea][Hex] and 1012 cm^{-1} for [Mea][Ac], which experiments a water-induce red shift for the [Mea][Hex] and a blue shift in the [Mea][Ac]. The blue shift is due to the weaking of the hydrogen bonding between the cation and anion due to the hydration of the carboxylic group in the [Ac] anion as previously discussed. The

reason for the extreme red shift of the absorption band at 1023 cm^{-1} for [Mea]Hex] is not clear, and should be further investigated with spectroscopic and computational methods. This strengthening upon dilution of that interactions between the cation-anion in [Mea][Hex] might be the cause of the density maxima shown in Figure 4.

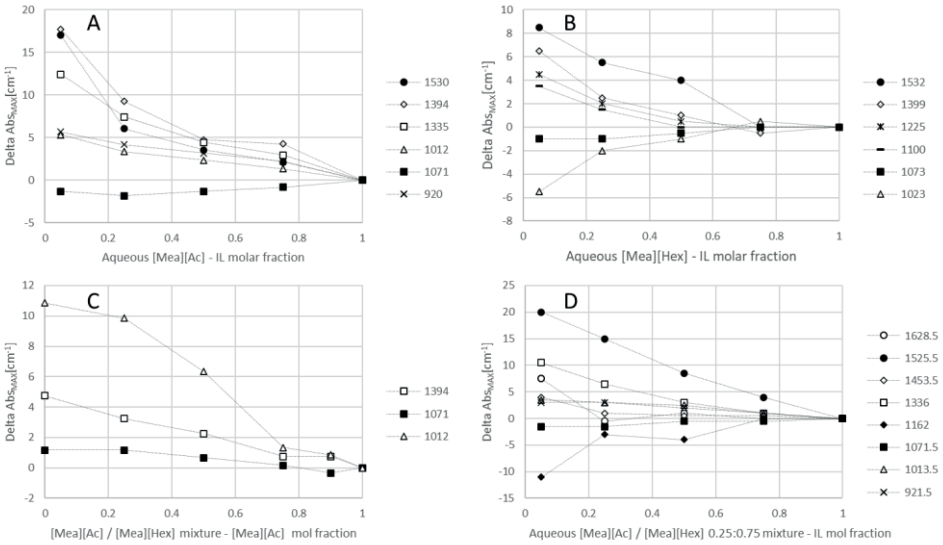

Fig 5: Water-induce shift for the binary mixture of ILs and water. [A] [Mea][Ac] and water mixtures. [B] [Mea][Hex] and water mixture. [C] Binary system [Mea][Ac] and [Mea][Hex]. [D] Tertiary system: [Mea][Ac]:[Mea][Hex] (0.75: 0.25 mol) system diluted with water.

The 1335 cm^{-1} signal attributed to the CH_3 deformation in the anion shows a water-induced blue shift in the case of the [Ac] anion while it is not observed for the [Hex] moiety. This might be explained by the inability of the [Ac] anions to aggregate to form micelles, therefore, the addition of water influences the chemical environment around the -CH_3. For the [Hex] anions in aqueous sodium of n-hexanoate, FTIR data have shown the formation of micelles that takes places in three stages. Firstly, below ~0.75 M (X_{H2O}=0.986) the solution is essentially monomeric. At a concentration of ~0.75 M the onset of progressive aggregation can be seen with counterion binding. At a concentration of ~1.75 M (X_{H2O}=0.963) there is a transition from a state of heterogeneous aggregation to a homogeneous micellar state [13–15]. By analogy, in the experiments performed in this study, all the

[Hex] systems should be in a homogeneous micellar state as (X_{H2O}<0.963), which corresponds to the region of maximum conductivity (Appendix A).

B.3.3 NMR

In terms of NMR spectroscopy the most obvious variables that can be investigated are the chemical shifts of the signals in the proton and carbon-13 spectra. Secondary to the chemical shifts, both T1 and T2 relaxation reveals a lot of information about the physical composition of the sample.

The most obvious trend from this system is the change in both the intensity and the chemical shift in the water signal. In the most dilute system, the water signal appears at the expected 4.8 ppm. As the concentration of water is decreased a downfield shift in the signal is observed in combination with a reduction in the signal. It should also be noted that the signal assigned to water is actually an average signal for all exchangeable protons from each species in solution. On decreasing the concentration of water, the relative contribution from these protons increases until the water concentration becomes negligible. While this result is not entirely surprising the results of the change in the chemical shifts of the non-exchangeable protons is more remarkable.

While it is perhaps no revelation that a reduction in solvation due to waning water concentrations which may be expected to be linear or almost linear, a maximum change in chemical shift is observed in the region 0.10 – 0.25 molar for [Mea][Ac], as depicted in Figure 6. In fact, this is most pronounced for the signals corresponding to protons 1 acetate and 2 and 3 from ethanolamine. This overall upfield shift of the signals can be attributed to an overall net increase in hydrogen bonding and in increase in structure resulting in a net increase in local electron density, especially for the signals attributed to ethanolamine which has both hydrogen bond acceptor and donor sites. As the water concentration is decreased an overall loss on solvation due to hydrogen bonding causes a downfield shift in all peaks. Furthermore, there is also a steady increase in line-width on decreasing water concentrations. A similar trend can be seen from the ^{13}C spectra assessment, as shown in Figure 6. Surprisingly, for the signals attribute to carbon 2 of acetate an overall continued upfield shift is observed which would indicate an overall increase in electron density, possibly attributed to a loss in ionic character, this rate of change in chemical shift inflects at 50% mole fraction.

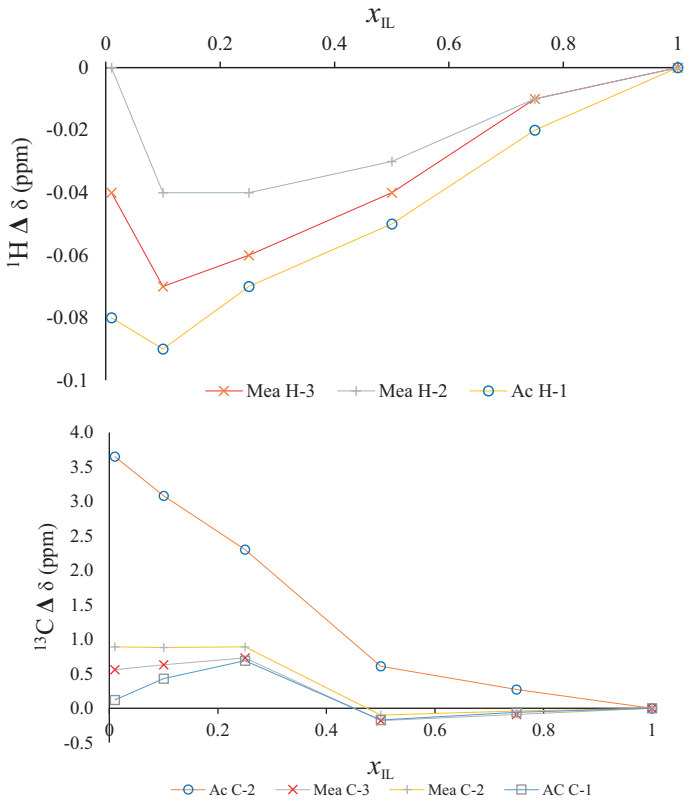

Fig 6: ^{1}H and ^{13}C delta chemical shifts for [Mea][Ac] aqueous solution as function of IL mol fraction

In contrast to the acetate system, the hexanoate ^{1}H δ signals do not show an overall maximum or minimum. It is overserved an upfield shift at 0.75 molar fraction for protons 2 and 5 for hexanoate and 3 for ethanolamine, and a constant upfield for proton 1 from hexanoate, as depicted in Figure 7. The protons [Hex]-5 and [Mea]-3 seem to follow the same trend as water concentration increases, possibly due to water close interaction to the charged sites from the IL, in accordance with what is observed from FTIR data. Likewise the acetate counterpart, line broadening is seen on increasing concentrations of ionic liquids. The signals for the ^{13}C show a downfield maximum at 0.75 mole fraction ionic liquid, followed by an overall upfield, as shown in Figure 6. The exception relies on [Hex]-6 carbon, which experiences a constant downfield after 0.5 IL mol fraction, likewise to observed in [Ac]-1 carbon. This indicates the intense water interaction with the carboxylic site from both ILs, which is in accordance to reported literature [16,17] and FTIR data.

Spin-lattice relaxation or longitudinal, more commonly reported as T1 relaxation, may be described as the decay constant for the recovery of the magnetic moment towards equilibrium in the Z axis, this is typical measured by observing the decay in signal in the XY plane using inversion recovery experiments. Quantitatively these results are report as R1 ($1.T1^{-1}$).

The rates of R1 relaxation, as shown in Figure 8, of all signals also show a similar trend to the change in ^{1}H and ^{13}C chemical shifts. All relaxation rates reach a maximum at 0.25 IL mole fraction for [Mea][Ac], which can also be attributed to an increase in hydrogen bonding efficiency. The rates of longitudinal relaxation reach a maxim at around 0.75 [Mea][Hex] mole fraction, which also agrees with the ^{13}C data.

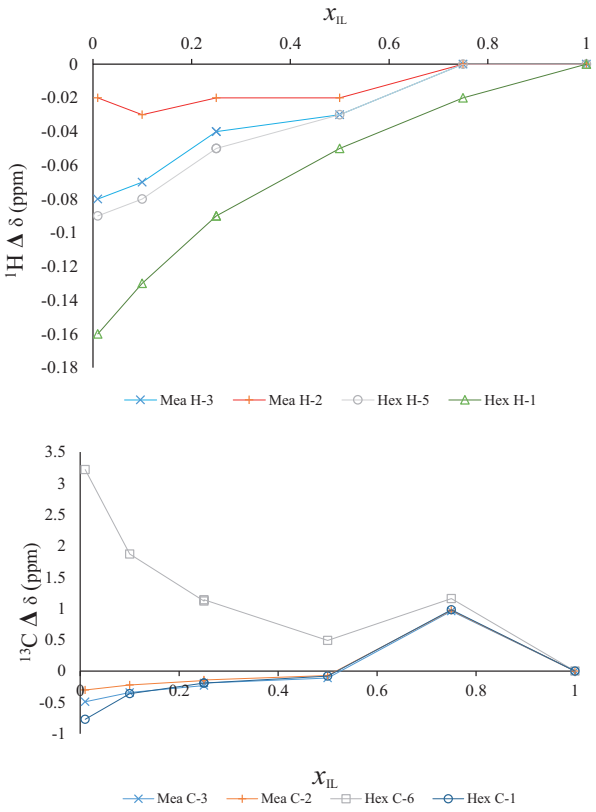

Fig 7: ^{1}H and ^{13}C delta chemical shifts for [Mea][Hex] aqueous solution as function of IL mol fraction

Transverse or spin-spin relaxation more commonly reported as T2 relaxation, may be described as the loss of vector due to dephasing of the spins, and is qualitatively reported as R2 ($1.T2^{-1}$). The R2 relaxation rates were determined using the CPMG sequence.

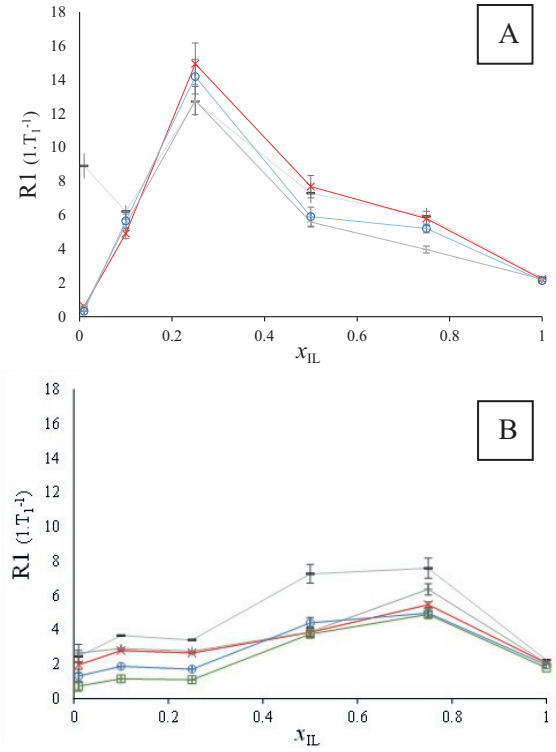

Fig 8: R1 relaxation for [Mea][Ac] (A) and [Mea][Hex] as function of IL molar fraction.

As can be expected due to an overall decrease in mobility and subsequent increase in anisotropy the R2 relaxation rates increase steadily. The increase in R2 relaxation rates concurs with the increased line widths observed for the proton signals. However, close examination of the results reveals an inflection also in the range 0.10 – 0.25 IL, figure 6 (complementary data). Similar to the acetate analogue there is a net increase in spin-spin relaxation. However, it is clear from the trends that there is a sharper increase at 0.75 IL, which is in accord with the other data.

The diffusion rates for each signal are summarized in Table 1. As expected, an overall decrease in diffusion coefficients is seen on increasing mole fraction of ionic liquid. There is, however, a steady region between 0.10 – 0.25 mole fraction [Mea][Ac]. This follows the same trends seen for changes in chemical shift and

relaxation rates. For [Mea][Hex], a pronounced decrease in diffusion on increasing ionic liquid content as seen for the acetate counterpart. When comparing the diffusivities of the cation in disrespect to the anion for both ILs, [Mea] exhibits a close diffusion rate of that from acetate in the entire range of dilution. Conversely, in [Mea][Hex] the proximity is only observed above 0.75 IL molar fraction, suggesting that, for the latter, the cation mobility foes not follow that from the anion [Hex] in the diluted regions, under 0.75 IL molar fraction.

Tab 1 Diffusion rates measured by NMR, as function of component molar fraction.

		Diffusion Rates							
		[Mea]		[Ac]		[Hex]		H_2O	
	x	D ($cm^2.s^{-1}$)	Error	D ($cm^2.s^{-1}$)	Error	D ($cm^2.s^{-1}$)	Error	D ($cm^2.s^{-1}$)	Error
Molar Fraction [Mea][Ac] in H_2O	**0.01**	1.5E-05	1.5E-07	1.5E-05	4.6E-08	-		1.8E-05	4.7E-08
	0.10	2.6E-06	1.4E-08	2.5E-06	3.0E-09	-		4.9E-06	3.3E-08
	0.25	2.6E-06	1.3E-08	2.5E-06	4.5E-09	-		4.9E-06	3.5E-08
	0.50	7.2E-08	1.1E-09	7.5E-08	2.8E-10	-		1.1E-07	4.7E-09
	0.75	2.3E-08	1.3E-10	2.3E-08	1.0E-10	-		2.6E-08	2.3E-10
	1.00	5.5E-09	9.6E-10	5.9E-09	3.5E-10	-			
Molar Fraction [Mea][Hex] in H_2O	**0.01**	1.8E-04	6.0E-07	-		1.5E-05	2.9E-07	1.7E-05	9.2E-08
	0.10	2.2E-06	2.9E-08	-		1.9E-06	1.9E-08	4.5E-06	4.0E-09
	0.25	3.0E-07	2.5E-09	-		2.1E-07	1.3E-09	9.1E-07	1.0E-08
	0.50	5.1E-08	2.0E-10	-		4.6E-08	6.0E-11	6.9E-08	7.1E-10
	0.75	1.8E-08	9.3E-11	-		1.7E-08	3.8E-11	2.0E-08	1.1E-10
	1.00	9.5E-09	3.7E-10	-		9.7E-09	1.9E-10		
Molar Fraction [Mea][Ac] in [Mea][Hex]	**0.15**	1.0E-08	4.4E-10	1.0E-08	2.9E-10	9.8E-09	2.8E-10	-	
	0.25	8.8E-09	3.6E-10	9.1E-09	2.1E-10	8.9E-09	2.8E-10	-	
	0.40	9.3E-09	3.6E-10	8.8E-09	1.3E-10	9.1E-09	3.3E-10	-	
	0.50	7.9E-09	2.3E-10	8.3E-09	4.3E-11	7.8E-09	2.4E-10	-	
	0.60	9.2E-09	4.3E-10	8.2E-09	1.2E-10	9.1E-09	3.4E-10	-	
	0.75	7.1E-09	1.1E-09	7.0E-09	2.3E-10	7.7E-09	1.3E-09	-	
	0.90	5.7E-09	7.4E-10	5.3E-09	2.9E-10	3.0E-09	2.0E-09	-	
[Ac] 0.25: 0.75 [Hex] in H_2O	**0.25**	2.0E-07	1.8E-08	2.9E-07	3.6E-09	1.6E-07	3.5E-09	6.9E-07	7.5E-09
	0.50	5.5E-08	3.9E-10	6.2E-08	1.5E-10	4.8E-08	1.4E-10	8.0E-08	1.3E-09
	0.75	2.7E-08	1.8E-10	2.8E-08	1.3E-10	2.5E-08	7.2E-11	3.3E-08	3.4E-10
[Ac] 0.50: 0.50 [Hex] in H_2O	**0.25**	3.3E-07	4.2E-09	4.0E-07	9.9E-10	2.2E-07	1.6E-09	1.0E-06	1.0E-08
	0.50	5.7E-08	3.9E-10	6.1E-08	1.2E-10	4.7E-10	1.3E-10	8.7E-08	1.3E-09
	0.75	1.8E-08	9.5E-11	1.8E-08	7.1E-11	1.7E-08	5.6E-11	2.1E-08	1.2E-10
[Ac] 0.75: 0.25 [Hex] in H_2O	**0.25**	2.7E-07	1.8E-09	3.1E-07	5.6E-10	2.0E-07	1.6E-09	7.4E-07	6.8E-09
	0.50	2.7E-07	1.8E-09	3.1E-07	5.6E-10	2.0E-07	1.6E-09	7.4E-07	6.8E-09
	0.75	2.4E-08	1.3E-10	2.4E-08	1.0E-10	2.3E-08	1.5E-10	2.9E-08	2.6E-10

From the NMR assessment of the dry ILs mixture, no significant trends are observed going from pure acetate to pure hexaonate in the anhydrous mixtures, although it is probably noteworthy to mention a perhaps counterintuitive slightly higher diffusion constants for the pure hexanoate compared to the pure acetate based on molecular weights. This would indicate stronger ionic binding for the more compact acetate system.

The IL proportion between [Ac] and [Hex] has distinct effect of diffusion rate depending on water concentration. At the diluted region (0.75 water fraction), acetate/hexanoate proportion, whether 0.25 or 0.75 molar fraction, have a negative effect on diffusion. Conversely, at concentrated regions (0.25 water fraction) the same proportion (0.25 and 0.75) have a positive effect on species diffusion rate. [Ac] tend to diffuse faster than [Mea] and [Hex] as water concentration increases, with the lowest diffusion rate for the latter.

Differently from what is observed for aqueous [Mea][Hex] alone, the ^{13}C chemical shift from COO^- exhibits a progressive and continuous downshift as water concentration increases, for both anions. A progressive upfield is observed for both C in [Mea], opposed to the downfield observed at 0.25 and 0.75 IL fraction in the single ionic aqueous solutions, [Mea][Ac] and [Mea][Hex] respectively. Intriguingly, [Mea] presents the minimum R1 relaxation times at the concentrated IL fraction (0.75 IL) in all [Ac]:[Hex] mixtures, while anions have their R1 maximum at this point.

B.4 Conclusion

The mixtures of both ILs exhibited higher T_g than those for neat ILs, suggesting a higher cohesiveness by the mixtures than pure ILs. Neat [Mea][Hex] was the only system to exhibit a crystallization event (245 K).

It was observed that water has influence in the cation-anion interaction for both ILs. Results also suggest a possible aggregation for [Mea][Hex] in aqueous solution.

Although FTIR and NMR assessment suggest the occurrence of molecular events at 0.05, 0.25, 0.50 and 0.75 IL molar fractions, further investigation is required to elucidate the nature of such trials.

B.5 References

(1) Clop, E. M.; Perillo, M. A.; Chattah, A. K. 1 H and 2 H NMR Spin–Lattice Relaxation Probing Water: PEG Molecular Dynamics in Solution. *J. Phys. Chem. B* **2012**, *116* (39), 11953–11958. https://doi.org/10.1021/jp304569a.

(2) Menjoge, A.; Dixon, J.; Brennecke, J. F.; Maginn, E. J.; Vasenkov, S. Influence of Water on Diffusion in Imidazolium-Based Ionic Liquids : A Pulsed Field Gradient NMR Study. **2009**, 6353–6359.

(3) Brooks, N. J.; Castiglione, F.; Doherty, C. M.; Dolan, A.; Hill, A. J.; Hunt, P. A.; Matthews, R. P.; Mauri, M.; Mele, A.; Simonutti, R.; Villar-Garcia, I. J.; Weber, C. C.; Welton, T. Linking the Structures, Free Volumes, and Properties of Ionic Liquid Mixtures. *Chem. Sci.*

2017, *8* (9), 6359–6374. https://doi.org/10.1039/C7SC01407D.

(4) Hansen, P. E.; Spanget-larsen, J. NMR and IR Investigations of Strong Intramolecular Hydrogen Bonds. **2017**. https://doi.org/10.3390/molecules22040552.

(5) Mizuno, K.; Miyashita, Y.; Shindo, Y.; Ogawa, H. NMR and FT-IR Studies of Hydrogen Bonds in Ethanol-Water Mixtures *. **1995**, 3225–3228. https://doi.org/10.1021/j100010a037.

(6) Cha, S.; Ao, M.; Sung, W.; Moon, B.; Ahlström, B.; Johansson, P.; Ouchi, Y.; Kim, D. Structures of Ionic Liquid–Water Mixtures Investigated by IR and NMR Spectroscopy. *Phys. Chem. Chem. Phys.* **2014**, *16* (20), 9591–9601. https://doi.org/10.1039/C4CP00589A.

(7) Greaves, T. L.; Weerawardena, A.; Fong, C.; Krodkiewska, I.; Drummond, C. J. Protic Ionic Liquids: Solvents with Tunable Phase Behavior and Physicochemical Properties. *J. Phys. Chem. B* **2006**, *110* (45), 22479–22487. https://doi.org/10.1021/jp0634048.

(8) Greaves, T. L.; Ha, K.; Muir, B. W.; Howard, S. C.; Weerawardena, A.; Kirby, N.; Drummond, C. J. Protic Ionic Liquids (PILs) Nanostructure and Physicochemical Properties: Development of High-Throughput Methodology for PIL Creation and Property Screens. *Phys. Chem. Chem. Phys.* **2015**, *17* (4), 2357–2365. https://doi.org/10.1039/c4cp04241g.

(9) Angell, C. A. The Old Problems of Glass and the Glass Transition , and the Many New Twists. **1995**, *92* (July), 6675–6682.

(10) Richner, G.; Puxty, G. Assessing the Chemical Speciation during CO 2 Absorption by Aqueous Amines Using in Situ FTIR. *Ind. Eng. Chem. Res.* **2012**, *51* (44), 14317–14324. https://doi.org/10.1021/ie302056f.

(11) Marekha, B. A.; Bria, M.; Moreau, M.; De Waele, I.; Miannay, F.-A.; Smortsova, Y.; Takamuku, T.; Kalugin, O. N.; Kiselev, M.; Idrissi, A. Intermolecular Interactions in Mixtures of 1-n-Butyl-3-Methylimidazolium Acetate and Water: Insights from IR, Raman, NMR Spectroscopy and Quantum Chemistry Calculations. *J. Mol. Liq.* **2015**, *210*, 227–237. https://doi.org/10.1016/j.molliq.2015.05.015.

(12) Chen, Y.; Cao, Y.; Zhang, Y.; Mu, T. Hydrogen Bonding between Acetate-Based Ionic Liquids and Water: Three Types of IR Absorption Peaks and NMR Chemical Shifts Change upon Dilution. *J. Mol. Struct.* **2014**, *1058*, 244–251. https://doi.org/10.1016/j.molstruc.2013.11.010.

(13) Umemura, J.; Cameron, D. G.; Mantsch, H. H. An FT-IR Study of Micelle Formation in Aqueous Sodium n-Hexanoate Solutions. *J. Phys. Chem.* **1980**. https://doi.org/10.1021/j100455a012.

(14) Campbell, A. N.; Friesen, J. I. CONDUCTANCES OF AQUEOUS SOLUTIONS OF SODIUM HEXANOATE (SODIUM CAPROATE) AND THE LIMITING CONDUCTANCES OF THE HEXANOATE ION, AT 25 °C AND 35 °C. *Can. J. Chem.* **1960**. https://doi.org/10.1139/v60-261.

(15) Umemura, J.; Mantsch, H. H.; Cameron, D. G. Micelle Formation in Aqueous N-Alkanoate Solutions: A Fourier Transform Infrared Study. *J. Colloid Interface Sci.* **1981**. https://doi.org/10.1016/0021-9797(81)90350-7.

(16) Hosseini, S. M.; Hosseinian, A.; Aparicio, S. An Experimental and Theoretical Study on 2-Hydroxyethylammonium Acetate Ionic Liquid. *J. Mol. Liq.* **2019**, *284*, 271–281. https://doi.org/10.1016/j.molliq.2019.03.150.

(17) Nagi, D.; Thummuru, R.; Mallik, B. S. Structure and Dynamics of Hydroxyl-Functionalized Protic Ammonium Carboxylate Ionic Liquids. **2017**, 8097–8107. https://doi.org/10.1021/acs.jpca.7b05995.

B.6 Complementary Data

Tab 1: Glass Transition (Tg) Temperature

x [Mea][Ac]	***x*** [Mea][Hex]	**Tg** (K)
0.00	1.00	195.03
0.25	0.75	196.75
0.50	0.50	203.03
0.75	0.25	205.35
0.90	0.90	204.97
1.00	0.00	198.68

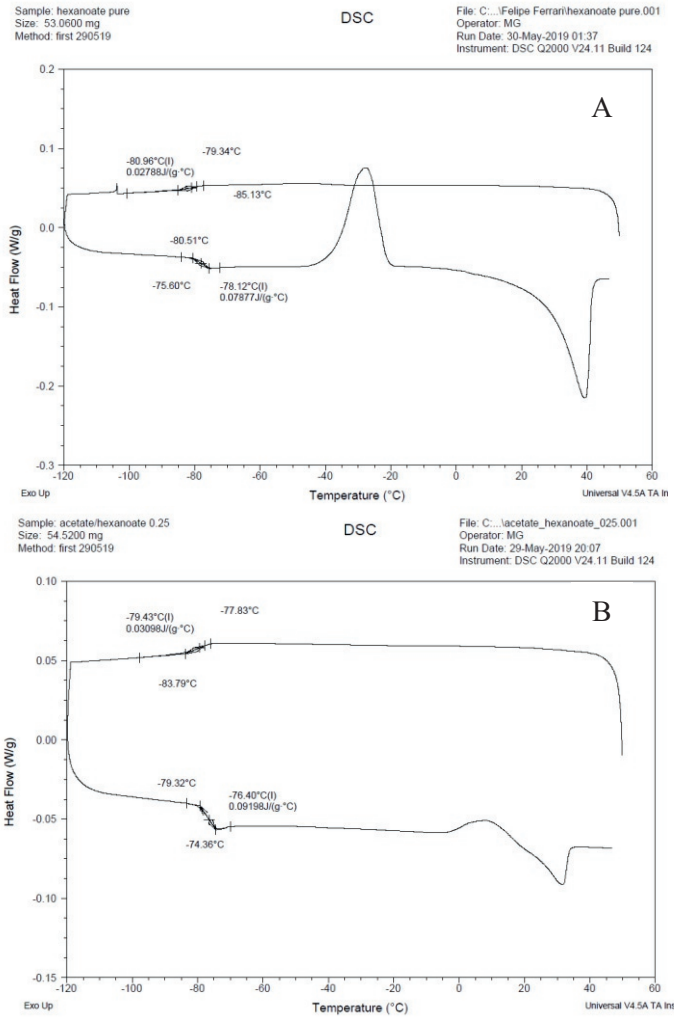

Fig 1: DSC for (A) [Mea][Hex], (B) [Ac][Hex] – 0.25:0.75

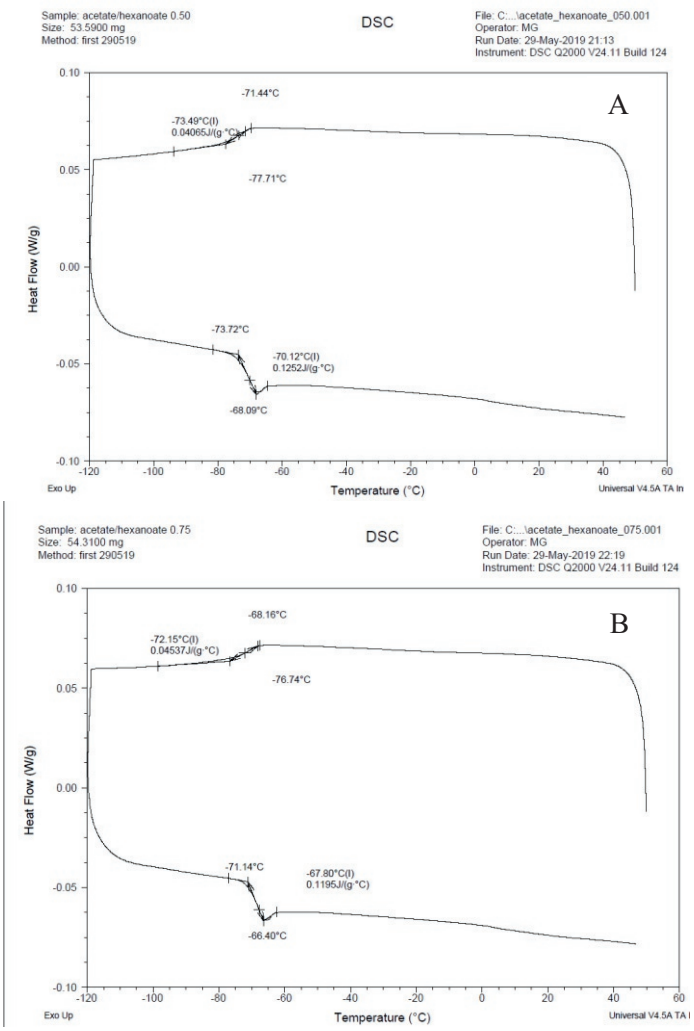

Fig 2: DSC for (A) [Ac][Hex] – 0.50:0. 50, (B) [Ac][Hex] – 0.75:0.2 5

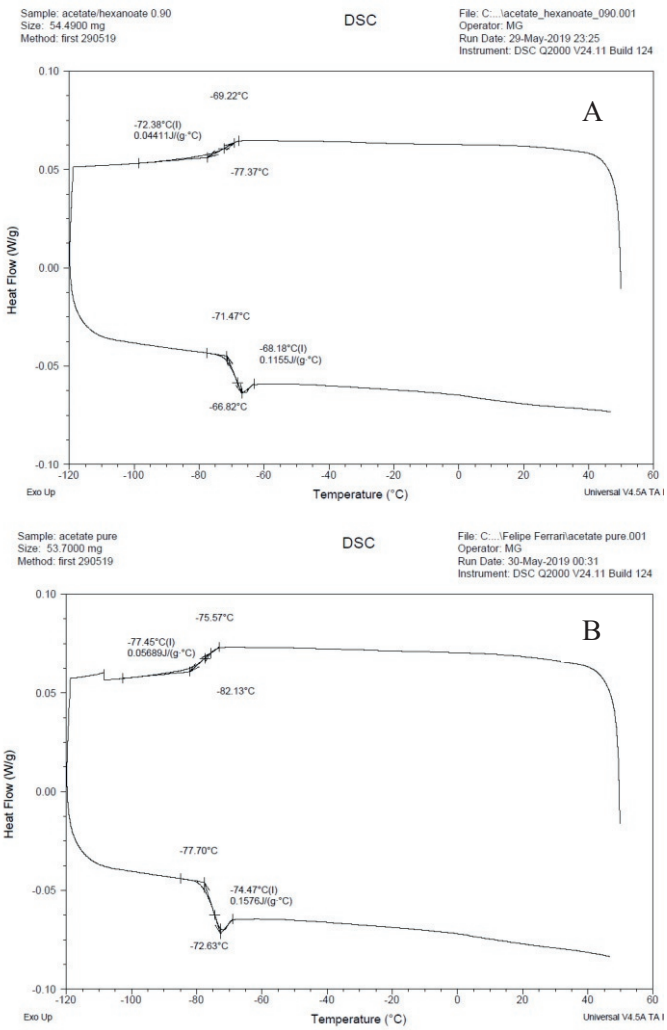

Fig 3: DSC for (A) [Ac][Hex] – 0.90:0.10, (B) [Mea][Ac].

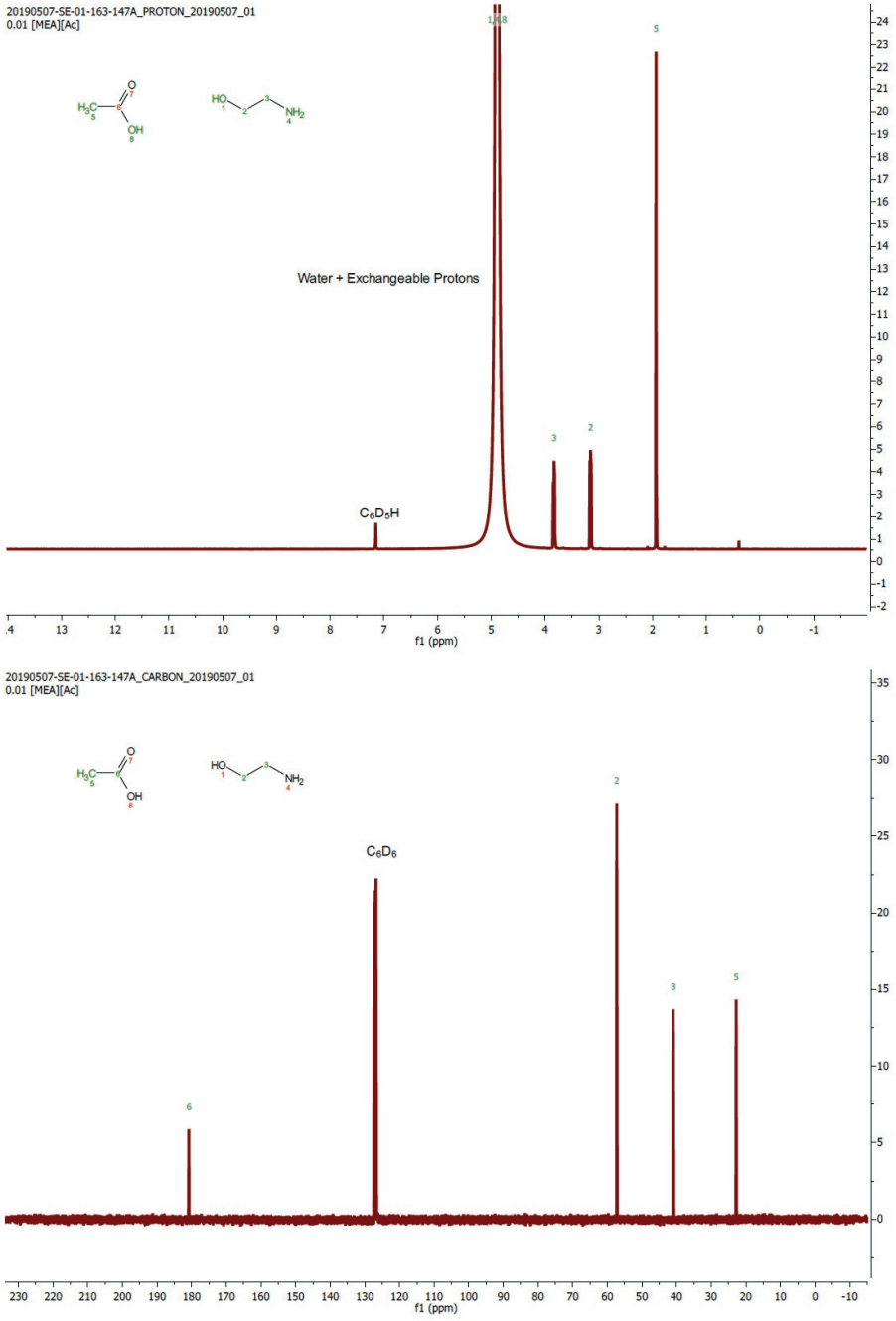

Fig 4: ^{1}H and ^{13}C NMR [Mea][Ac].

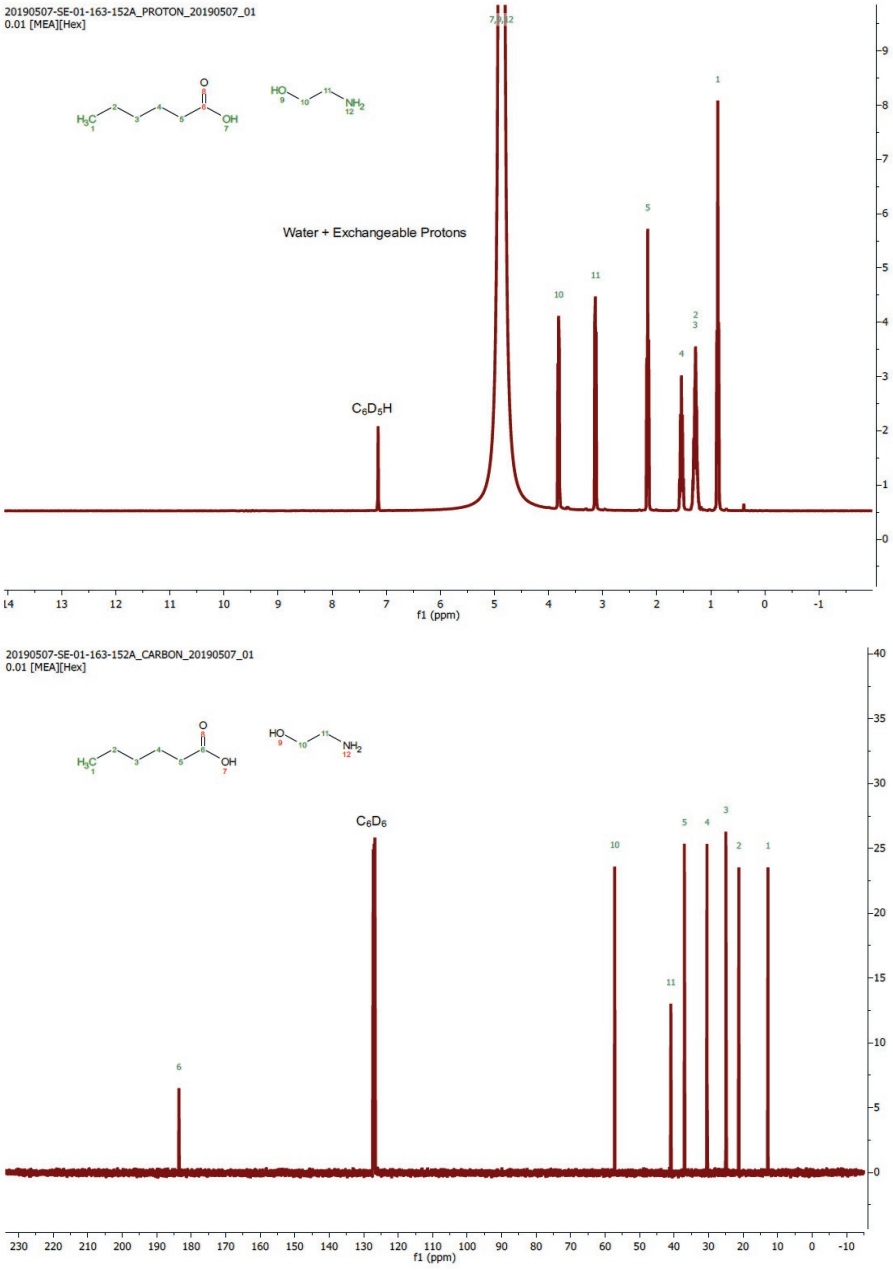

Fig 5: ^{1}H and ^{13}C NMR [Mea][Hex].

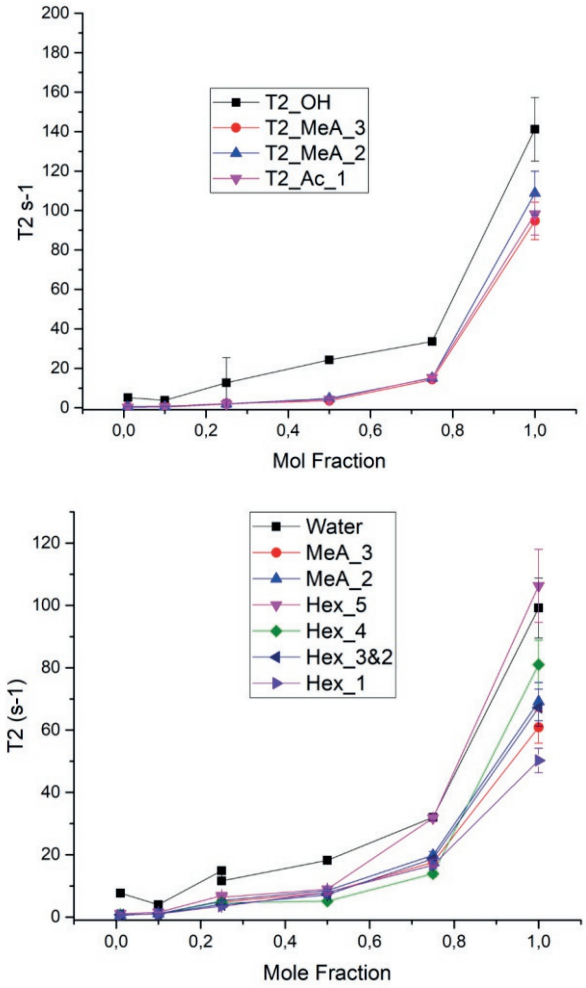

Fig 6: T2 relaxation for [Mea][Ac] and [Mea][Hex] as function of IL molar fraction.

Acknowledgments

Marcus, I remember our first talk about how would sound if I chose the PhD as my next professional step. From that point on it became a plan, not an intention anymore. That was the second time you have put me onboard. Thanks for all time invested in our relationship, as friend, supervisor and now co-worker. I have learned from you not only how to be a better professional, but also how to be a better person. There is a bright future ahead, I admire you for always challenge academia responsibility towards society, we should have more of that. Geert-Jan, thanks for taking part of this journey, at the same time that your personal boat was also sailing to further seas. You have always brought me on the same level, with kindness and respect, softening the natural self-criticism, which is present when one is filling the emptiness of incomprehension with knowledge. Thanks for our talks, not so often due to circumstances, but always productive and pleasant. Luuk, I have a great respect and admiration for you. You are a bright and responsible scientist, who assumes the burden of diplomacy towards a better society. Your guidance was especially important, making me reflect about the matters of our field, knowledge that goes beyond the pages of this book. I have learned a lot from you, and I am very thankful for that. Professors, it was a pleasure and honor to be under your supervision and to engage in discussions. I wish we share the same felling for each other. Thank you for always questioning my work, helping me to improve it and exercising science with me. You have my gratitude and respect.

Thanks, Prof Mark, for making me part of the group and for a valuable teaching "There is no trick question, it is all a matter of self-esteem". You are a reference for me. Thanks Prof Patricia to put so much effort in the dual degree program. The modern development is only possible when international borders are crossed. It is a hard task but, luckily, we have a professional like you committed to that. Thanks a lot Yi Song, Max, Ben, Stef and Apileina, you made my experimental work easier and funnier. Ben Norder, it was a pleasure to meet you and I enjoyed every minute we shared. Special thanks to Kawieta, my life could have been much harder if you were not there, always helping, solving and advising.

Thanks, EBT and BPE teams who were always supportive: Michele, Marissa, Chris, Shengle, Leonor, Jules, Dana, Hugo, Monica and Debora. Specially, Florence, Ingrid, Sergio, David (el cantor), Marta, Simon (best mustache) and Chema, for making it a funnier and warmer place. Danny, you have always been a lovely person to me, friendly and prompt to help me whenever

needed, you can always count on me. Thanks to my last office mates, Michael, Jelmer and Gerben, +Jure, for the sharp and funny discussions. Special thanks to my big office mates: Sanna, Mariek, Yacintha, Jeffrey, Charllote, Nina, Maxim, Britt, Shupan and Ale. You have added colors even to the grayest days, without you my memories would not be so shine. Stephen, thanks for being such a good and nice colleague. EBT and BPE, you will always have a special spot in my heart and within my memories.

Prof Jason, besides being part of my committee, twice, I would like to thank you and your group for receiving me so well. You are an example of leadership by admiration, inside and outside your group. Special thanks to Clementine, Francisco, Raul and Anton for turning my time at London a special memory.

Elisa, Andreia, Bianca, Ana Maria e Carlita, you were my Brazilian piece at TU. Thanks for our coffee and talks, sometimes likely a big breath before a dive. I hope we keep holding high and proudly our flag, wherever our feet take us.

Prof Jorge, thanks for guiding me on my first steps into the word of Ionic Liquids. Ariel, thanks for all the support with this difficult task that is to understand Ionic Liquids, and for the insightful talks. Aureliano, it was always a pleasure to meet you in FEA, specially at the coffee place.

Henrique (Cindy), thanks for all partnership during the time in Delft. I already miss our conversations, jokes and time expended together. Henrique (Facis), I have lots of colleagues, but just few friends, and you are among them for sure. You should be in the Portuguese part, it would be easier to thank you. My "brother", thanks for everything!! Specially for the Bebop! Athila, you have been my friend since childhood, and maybe, alongside my father, was the person who the most incentived me to pursue my PhD. You have your share of responsibility in these pages and direct contribution in the cover.

Most Special Thanks to LEMEB, the group that brought me back to science. A place where I shared ideas, jokes, thoughts, knowledge, work, feelings and a lot of coffee. I taught and learned with you. Many thanks Rô, Fifa, Chico, Andreas, Priscila, Labate, Bernardo, Fernando, Luciano, Welão, Fernando, Paty, Lucas, Robson, Marcos, Ederson. Guta, Glei, Bia, Pame, Su, Igor, Capone, Laurinha, Dani e Zé, my English lacks vocabulary to express my gratitude. Vijay, you have my greatest admiration, some of my deepest reflections were triggered by our conversations.

Terei aqui a maior dificuldade dentre meus agradecimentos pois, a falta de vocabulário não mais é cabida. Aqui, a dificuldade se deve a incapacidade de expressar a mais honesta gratidão em palavras.

Tia Rosana e tio Norair, vocês foram minhas primeiras referências de ciência. Sempre os admirei muito e espero que, ao longo da minha vida, eu consiga retribuir esse brilho. Tio, sua cultura sempre me fascinou e inspirou. Tia, lembro-me de caminhadas pela praia em Peruíbe, de conversas na cozinha, quintal ou à mesa em que suas palavras guiavam uma cabeça ainda perdida sobre a vida. Obrigado.

Nano, você sempre foi meu herói e melhor amigo. Aprendi contigo que precisamos "dizer o que queremos da maneira que consigam ouvir". Isso diz muito sobre a relação humana. Talvez não tivesse sido essa sua pretensão naquele momento, mas o fato é que representa uma mensagem muito valiosa para mim.

Pai e Mãe, não existem palavras, em qualquer que seja o idioma, capazes de expressar fielmente o que vocês significam para mim. Pai, você sempre alimentou minha curiosidade e me ensina ao longo de toda a vida. Do manejo de ferramentas à fabricação dos bens mais variados ao nosso redor. Como tratar um animal à definição de que um prisma é um sólido geométrico cujas faces são retangulares e a base um polígono qualquer. Você foi o primeiro inventor que conheci e, para mim, o maior deles. Aprendi contigo que todas as pessoas são dignas de respeito e atenção, e eu sempre carregarei isso.

Mãe, você me ensinou a maior verdade sobre a vida profissional, " não importa o que você faça, mas o faça em seu melhor". Você é de uma dedicação incondicional aos seus filhos que, se eu for capaz de exercê-la em sua fração com meu rebento, estarei seguro de ser um ótimo pai. Você é um exemplo de perseverança e de que sempre podemos recomeçar se for preciso. Você é umas das pessoas mais justas e a mais honesta que eu conheci. Espero que tenha orgulho do seu filho, como tenho em tê-la como mãe.

Agradeço vocês dois pelo suporte incondicional em minhas escolhas! Por sempre me dar uma resposta seguida de explicação, e incentivarem que o contrário assim o fosse.

Finalmente, não poderia terminar essas linhas sem agradecer minha fiel companheira, melhor amiga e esposa. Marina, você me apoiou em todas as escolhas, e lidou com todas as dificuldades que as seguiram. Não há pessoa que me conheça mais, justamente porque esteve ao meu lado partilhando de todos os

sentimentos humanos, sejam eles agradáveis ou não. Obrigado por ser meu porto, em meio a qualquer tempestade. Obrigado por não aceitar minhas respostas caso ausentes de seus cabíveis argumentos. Obrigado por me acompanhar e fazer parte dos meus sonhos.

Curriculum Vitae

Felipe Ferrari was born on March 8, 1987 in Campinas, São Paulo, Brazil. Before university (2002-2004), Felipe took secondary education classes together with Chemistry course at the Technical State School (ETECAP) in Campinas. In 2006, Felipe entered the Federal University of São Carlos (UFSCar) to study Biotechnology. From 2007 to 2009, Felipe studied alternative forms to control bacterial contamination in ethanol fermentation using natural extracts. In 2009 he conducted his undergraduation research on microbial production of Hyaluronic Acid under the supervision of Prof.dr. Reinaldo Bastos. Felipe started his masters course in Chemical Engineering (Bioprocess Engineering) at the University of Campinas (UNICAMP) under the supervision of Prof.dr. Maria Helena Santanna. The topic of his masters was the microbial production of Hyaluronic Acid, and during his thesis a novel reactor design was proposed for solid state microbial cultivation. In 2012, Felipe joined AMBEV, working there for 4 years, where he ended up occupying a manager position in the commercial area. In 2016, Felipe started his PhD in the context of an agreement on joint doctoral supervision between University of Campinas, Brazil and Delft University of Technology, The Netherlands, under the supervision of Prof.dr. Marcus Forte (Faculty of Food Engineering – UNICAMP), Prof. dr. Geert-Jan Witkamp (KAUST – Saudi Arabia) and Prof.dr.ir. Luuk van der Wielen (TNW – TUDelft). In parallel to his PhD activities Felipe engaged in social activities at UNICAMP in 2016 and as student representative at the Bioenergy PhD program (2019-2020).

List of Publication

Part of the research conducted in this project led to the following:

Scientific Paper

Published

César, F.; Martins, M.; Beatriz, L.; **Ferrari, F**.; Bruno, M.; Forte, S.; Cândida, S.; Teixeira, T.; Goldbeck, R. *Screening of Potential Endoglucanases, Hydrolysis Conditions and Different Sugarcane Straws Pretreatments for Cello-Oligosaccharides Production*. Bioresour. Technol, 2020.

Ferrari, F. A., Pereira, J. F. B., Witkamp, G. J., & Forte, M. B. S. *Which variables matter for process design and scale-up? A study of sugar cane straw pretreatment using low-cost and easily synthesizable ionic liquids*. ACS Sustainable Chemistry and Engineering, 2019.

Submitted

Ferrari, F. A., Wielen, L. A. M., Forte, M. B. S., Witkamp, G. J. *Complete Continuous Ionic Liquid Recycle From Aqueous Streams through Freeze Concentration*. – Separation and Purification Technology

Prepared for Submission

Ferrari, F.A., Pessoa, G., Franco, T.T., C.K., Witkamp, G.J., Dias, M., Cavaliero, van der Wielen, L.A.M., Forte, M.B.S. *The Role of Ionic Liquid Pretreatment and Recycle Design in the Sustainability of a Biorefinery: a Sugarcane to Ethanol Example* – Green Chemistry

Ferrari, F.A., Malaret, F., Eustace, S., Djanashvili. K., Hallett, J.P., Wielen, L.A.M, Witkamp, G.J, Forte, M.B.S.F. *Physicochemical Characterization of Two Protic Hydroxyehtylammonium Carboxylate Ionic Liquids in Water and their Mixture.* - Journal of Chemical & Engineering Data

Published Book Chapter

Antunes F.A.F., Chandel A.K., Terán-Hilares R., Milessi T.S.S., Travalia B.M., **Ferrari F. A.**, Hernandez-Pérez A.F, Ramos L., Marcelino P.F., Brumano L.P., Silva G.M., Forte M.B.S., Santos J.C., Felipe M.G.A., da Silva S.S. **Biofuel Production from Sugarcane in Brazil**. In: Khan M., Khan I. (eds) Sugarcane Biofuels. Springer, Cham., 2019

Works Presented in Conferences

BBEST 2020-21/BIOFUTURE SUMMIT II (2020)

- *Increasing sugarcane straw pre-treatment efficiency using ionic liquid mixtures at low temperature* – BBEST AWARD (2nd place Doctorate)

European Congress on Applied Biotechnology (ECAB 2019)

- *The influence of water addition in Pre-Treatment of Sugarcane Straw Using Three Different Ionic Liquids*
- *Phase Behavior of Bio-based Ionic Liquid Crystal Mixtures based on Choline and Fatty Acids – co-author*

Nacional Bioprocess Symposium (Sinaferm 2019)

- *Increasing Sugarcane Straw Pretreatment Efficiency Using Ionic Liquid Mixtures at Low Temperature*

5th Iberoamerican Meeting on Ionic Liquids (IMIL 2017)

- *Impacts on sugar and inhibitors concentrations after pretreatment of sugarcane straw using ionic liquids and diluted acid strategies*

Brazilian Bioenergy Science and Technology Conference (BEBEST 2017)

Sugarcane Straw Pre-treatment by Softer Conditions Using Low-Cost Protic Ionic Liquids: impact on enzymatic hydrolysis